

# **A Study on Microstructures of Homogenization for Topology Optimization**

**By**

**Yulu Wang, BEngSc, MEngSc**

**A thesis submitted in fulfillment of the requirement of  
the degree of Doctor of Philosophy  
to Victoria University of Technology**

School of Architectural, Civil and Mechanical Engineering  
Victoria University of Technology  
Melbourne, Australia

October, 2003

## **DECLARATION**

This thesis does not contain any material, which has been previously submitted for a degree or diploma at any university. Except where due reference is made in the text, the work described in this thesis is the result of candidate's own investigations.

---

Candidate

---

Supervisor

---

Co-Supervisor

# ACKNOWLEDGEMENTS

I wish to express my sincere gratitude to my supervisor, Dr. Danh Tran and co-supervisor, Prof. Mike Xie. They have been offering unfailing support in my PhD study. Their advice on technical matters, constant encouragement and motivation, ready accessibility and constructive criticism are greatly acknowledged. They made every effort to ensure that I was provided with excellent equipment and a comfortable working environment.

I would like to take this opportunity to express my appreciation to the School of Architectural, Civil and Mechanical Engineering, Victoria University of Technology which has provided research resources and facilities and a stimulating and positive study environment.

I am also grateful to the Victoria University of Technology in providing financial support through the Victoria University Postgraduate Research Scholarship, throughout my PhD study.

I wish to thank the academic and administrative staff of the School of Architectural, Civil and Mechanical Engineering for their encouragement, support and friendship throughout my study. I would also like to express my appreciation to the technical staff of the School in particular to Mr. Tien Do for their help.

Finally, I would like to express my heartfelt gratitude to my parents and my wife for their love, tireless support and encouragement throughout this study and during the many years of study that preceded it. Without their support this thesis would not have been possible. It is to them I dedicate this thesis.

## SUMMARY

This thesis studies topology optimization method employing the homogenization method, with a focus on different microstructures and their effects on the topology optimization solutions. The method is based on considering the design domain as a composite having an infinite number of infinitely small holes which are periodically distributed. As a result of introducing a material density function to represent the microstructure, the complex nature of the topology optimization problem can be converted to a problem of sizing optimization of determining the values of the parameters describing the microstructures. The main task for the homogenization method is to model and formulate these microstructures.

In the thesis, different microstructure models were investigated. The strengths and weaknesses of each type of microstructures were discussed. Homogenization method was employed to formulate the homogenized properties of the material. The optimality criteria and schemes of updating the design variables in the topology optimization process were derived for the newly developed microstructures and existing microstructures for which the information is not available in the literature. New microstructure models of one-material and bi-material were established. Based on these studies, a computer software package called *Homogenization with Different Microstructures* (HDM) incorporating fifteen existing and the new microstructure models was developed. By using the software, a series of problems were studied and solutions given by different microstructure models

were compared.

Firstly, the effects of the various one-material microstructure models were investigated. A number of examples of topological optimization problems with different loading cases were solved. The loading cases considered were single loading, surface loading, multiple loading and gravity loading.

For bi-material microstructure models, both cases of material without void and materials with void under different loading cases were studied. Benchmark topological optimization problems were investigated by using six different bi-material microstructure models that have been developed and programmed in the Chapter 4 and Chapter 5.

In the thesis, we proposed a new method to define microstructures to permit using shape optimization method to find optimal microstructures or using simple boundary shapes to describe a microstructure, hence to avoid the use of the complicated topology optimization method. Two types of microstructures, circular and cross shape were developed under this definition. Three multi-void microstructures and four new bi-material models are developed.

Our research shows that the cross shape and power-law models with  $\mu = 3$ , for both one-material and bi-material models, perform the best in terms of convergence and ease of implementation of the optimum layouts. The ranked layered model gives more complicated layouts in most cases. Triangular, circular and hexagon microstructure models using HDM produced similar

optimization solutions to those of the rectangular microstructure model developed by Hassani and Hinton (1998).

Comparing solutions of benchmark problems given by the HDM software incorporating all the fifteen microstructure models to those given by other software package demonstrates that the HDM program is effective for a range of structural topology optimization problems.

# Table of Contents

---

<b>DECLARATION</b>	<b>ii</b>
<b>ACKNOWLEDGEMENTS</b>	<b>iii</b>
<b>SUMMARY</b>	<b>iv</b>
<b>TABLE OF CONTENTS</b>	<b>vii</b>
<b>LIST OF FIGURES</b>	<b>xii</b>
<b>LIST OF TABLES</b>	<b>xix</b>
<b>NOTATIONS</b>	<b>xx</b>
<b>CHAPTER 1 INTRODUCTION</b>	
1.1 General	1-1
1.2 Aims of the Research	1-4
1.3 Contribution of the Research	1-4
1.4 Significance of the Research	1-5
1.5 Layout of the Thesis	1-5
<b>CHAPTER 2 OVERVIEW OF STRUCTURAL OPTIMIZATION</b>	
2.1 Structural Optimization Method	2-1
2.2 Mathematical Description of an Optimization Problem	2-2
2.3 Classification of a Structural Optimization Problem	2-3
2.4 Solution methods for Structural Optimization	2-5
2.4.1 Calculus methods	2-6
2.4.2 Numerical methods	2-8
2.5 Structural Topology Optimization	2-13

2.5.1	Topology optimization for discrete structures	2-14
2.5.2	Topology optimization for continuous structures	2-16
2.6	Summary	2-18

## **CHAPTER 3 HOMOGENIZATION AND MICROSTRUCTURES**

### **REVIEW**

3.1	Homogenization Method	3-2
3.1.1	Introduction	3-2
3.1.2	A brief review of periodic structure	3-4
3.1.3	The homogenization formulas in elastic composite materials with a periodic structure	3-7
3.1.4	Application of homogenization for topology optimization in minimum compliance problems	3-11
3.2	Microstructures Review	3-14
3.2.1	One-material microstructure	3-15
3.2.2	Bi-material microstructure	3-29
3.3	Summary	3-32

## **CHAPTER 4 MICROSTRUCTURES STUDY**

4.1	Development of New Microstructures	4-1
4.1.1	Simple internal boundary (SIB) microstructures	4-2
4.1.2	Multi-void microstructures	4-8
4.1.3	Bi-material microstructures	4-9
4.2	Development of Material Properties for the New Microstructures	4-11

4.2.1	Material properties development	4-11
4.2.2	Boundary condition	4-19
4.2.3	Computer Program Implementation	4-21
4.3	Summary	4-23

## **CHAPTER 5 OPTIMIZATION APPROACH**

5.1	Optimality Conditions for Different Microstructure Models	5-2
5.1.1	Kuhn-Tucker conditions	5-4
5.1.2	Updating design variables	5-7
5.1.3	Optimality conditions for new microstructure models	5-9
5.1.4	Optimality conditions for existing microstructure models	5-21
5.2	Principal Stress Based Optimal Orientation	5-30
5.3	Convergence Criterion	5-31
5.4	Measures to Control Checkerboard Pattern	5-32
5.5	Computer Program Implementation	5-34
5.6	Summary	5-38

## **CHAPTER 6 COMPARISONS BETWEEN ALGORITHMS USING BENCHMARK TOPOLOGY OPTIMIZATION PROBLEMS**

6.1	Algorithm Test by Deep Cantilever Beam Optimization	6-1
6.2	Comparing Algorithms for One-material Microstructure Models with Algorithm Found in Literature	6-14
6.2.1	Results of topology optimization available in literature	6-14
6.2.2	Results of HDM algorithm with different material models	6-19

6.2.3	Optimization layouts of the power-law model and the artificial model	6-21
6.2.4	Iteration history for different material models	6-23
6.3	Comparisons Between Algorithms for Bi-material Microstructure Models	6-26
6.4	Effect of finite element discretization	6-34
6.5	Conclusions	6-36

**CHAPTER 7 STUDY ON THE EFFECT OF VARIOUS ONE-MATERIAL MICROSTRUCTURES ON TOPOLOGY OPTIMIZATION RESULTS**

7.1	Topology Optimizations with Single Load	7-2
7.2	Topology Optimizations with Surface Load	7-32
7.3	Topology Optimizations with Multiple Loads	7-53
7.4	Topology Optimizations with Gravity Load	7-57
7.5	Effect of Microstructures on Topology Optimization	7-60
7.6	Conclusions	7-62

**CHAPTER 8 STUDY ON THE EFFECT OF BI-MATERIAL MICROSTRUCTURES ON TOPOLOGY OPTIMIZATION**

8.1	Topology Optimization Using Bi-material Models with Void	8-2
8.2	Topology Optimization Using Bi-material Models without Void	8-14
8.3	Effects of Different Models on Topology Optimization	8-27
8.4	Conclusions	8-28

## **CHAPTER 9 CONCLUSIONS AND RECOMMENDATIONS**

9.1	Conclusions	9-2
9.1.1	Comparison of microstructure models	9-2
9.1.2	Optimization results given by HDM	9-5
9.1.3	Optimal layout criteria	9-6
9.1.4	Checkerboard control	9-7
9.2	Recommendations for further investigations	9-7

### **Appendix A**

### **Appendix B**

### **Appendix C**

## **REFERENCES**

# List of Figures

---

Figure 2.1	Three categories of structural optimization	2-5
Figure 3.1	Homogenization limit	3-3
Figure 3.2	(a) A oscillating function	3-5
Figure 3.2	(b) One of oscillations in the expended scale	3-6
Figure 3.5	A periodic structure of composites and an enlargement of a basic cell	3-6
Figure 3.4	A structure with cellar microstructures	3-8
Figure 3.5	A base cell	3-9
Figure 3.6	Ranked layered microstructure	3-16
Figure 3.7	Rectangular microstructure	3-20
Figure 3.8	Triangular microstructure	3-22
Figure 3.9	Hexagon microstructure	3-23
Figure 3.10	Minimum weight microstructure	3-26
Figure 3.11	Four microstructures with extremal bulk modules	3-27
Figure 3.12	Topology optimized microstructures	3-28
Figure 3.13	Parameterized microstructures	3-29
Figure 3.14	Ranked layered bi-material cells	3-30
Figure 4.1	Definition of base cell	4-3
Figure 4.2	New coordinate system	4-3
Figure 4.3	A quarter of unit cell	4-3
Figure 4.4	The area occupied by hard and soft materials of circular model for $0 \leq r \leq \frac{1}{\sqrt{2}}$	4-5

Figure 4.5	The area occupied by hard and soft materials of circular model in $\frac{1}{\sqrt{2}} < r \leq 1$	4-5
Figure 4.6	The area occupied by hard and soft materials of circular model for $0 \leq r \leq \frac{1-\delta}{\sqrt{2}}$	4-6
Figure 4.7	The area occupied by hard and soft materials of circular model for $\frac{1-\delta}{\sqrt{2}} < r \leq 1-\delta$	4-6
Figure 4.8	The area occupied by hard and soft materials of circular model for $1-\delta < r \leq 1$	4-7
Figure 4.9	Cross shape boundary	4-8
Figure 4.10	Multi-void microstructures	4-9
Figure 4.11	Bi-material microstructures	4-10
Figure 4.12	Boundary conditions for <i>case a, b and c</i>	4-20
Figure 4.13	Boundary conditions for <i>case d</i>	4-21
Figure 4.14	Algorithm for one-material model	4-23
Figure 4.15	Algorithm for bi-material model	4-24
Figure 4.16	Polynomials for cross shape model	4-25
Figure 5.1	Geometrical interpretation of Kuhn-Tucker condition	5-5
Figure 5.2	Checkerboard problem	5-32
Figure 5.3	Topology optimization procedure using homogenization method	5-40
Figure 6.1	A deep cantilever beam	6-2
Figure 6.2	Optimum feature of the deep cantilever beam	6-2
Figure 6.3	Optimum layout of deep cantilever beam for power-law	

one-material model	6-3
Figure 6.4 Optimum layout of deep cantilever beam for ranked layered material model	6-3
Figure 6.5 Optimum layout of deep cantilever beam for triangular material model	6-4
Figure 6.6 Optimum layout of deep cantilever beam for hexagon material model	6-4
Figure 6.7 Optimum layout of deep cantilever beam for cross shape material model	6-4
Figure 6.8 Optimum layout of deep cantilever beam for circular material model	6-5
Figure 6.9 Optimum layout of deep cantilever beam for triangular multi-void material model	6-5
Figure 6.10 Optimum layout of deep cantilever beam for rectangular multi-void material model	6-5
Figure 6.11 Optimum layout of deep cantilever beam for square multi-void material model	6-6
Figure 6.12 Optimization layouts of <i>case a</i>	6-8~10
Figure 6.13 Optimization layouts of <i>case b</i>	6-11~13
Figure 6.14 A short cantilever beam	6-15
Figure 6.15 Discretized design domain from Min etc.	6-15
Figure 6.16 Optimal structure layouts from Min etc.	6-16
Figure 6.17 Convergence histories in the case of volume constraint 40% from Min etc.?	6-16

Figure 6.18 Optimal layout and iteration history from Hassani and Hinton	6-17
Figure 6.19 Optimal layouts of using artificial model with different penalty from Hassani and Hinton	6-18
Figure 6.20 The iteration history of using artificial model with different penalty from Hassani and Hinton	6-18
Figure 6.21 The optimization results of using ranked layered material model from Hassani and Hinton	6-18
Figure 6.22 The iteration history of using ranked layered model from Hassani and Hinton	6-19
Figure 6.23 Optimization result with different microstructures	6-20~21
Figure 6.24 Optimization results for different power values	6-22~23
Figure 6.25 Iteration histories for different material models	6-24~25
Figure 6.26 Iteration histories for different power values	6-27~28
Figure 6.27 A cantilever beam problem	6-29
Figure 6.28 Optimal layout from Thomsen	6-30
Figure 6.29 Optimization layouts of using HDM	6-31~33
Figure 6.30 The optimum layouts for different finite element discretizations.	6-34
Figure 6.31 Iteration histories for different finite element discretizations.	6-35
Figure 7.1 A simply supported beam	7-3
Figure 7.2 Optimization layout by PLATO software for the simply supported beam problem	7-3

Figure 7.3 Optimization results with different microstructures by HDM for the simply supported beam problem	7-3~5
Figure 7.4 Iteration histories with different models for the simply supported beam problem	7-7~8
Figure 7.5 Comparison iteration histories	7-9
Figure 7.6 Optimization results with different power values for the simply supported beam optimization	7-10~12
Figure 7.7 Iteration histories with different power values for the simply supported beam problem	7-13~14
Figure 7.8 A square domain with a point load	7-16
Figure 7.9 Optimum layouts of using the PLATO software for the square domain with a point load problem	7-17
Figure 7.10 Optimization result for different microstructures for <i>case a</i>	7-17~19
Figure 7.11 Optimum layout of using PLATO with rectangular model	7-20
Figure 7.12 Optimization layouts for different models for <i>case b</i>	7-20~21
Figure 7.13 Optimization results with different power values for the volume fraction $V_s / V = 40\%$ .	7-22~23
Figure 7.14 A domain with two sides' boundary constraints	7-24
Figure 7.15 Optimum layout of using PLATO software for the domain with two sides' boundary constraints problem	7-25
Figure 7.16 Optimization layouts of different microstructures for the domain with the two sides' boundary constraints problem	7-25~28

Figure 7.17 Results of different power values for the domain with the two sides' boundary constraints problem	7-29~32
Figure 7.18 Design domain of a bridge model	7-33
Figure 7.19 Result of using PLATO software for the bridge model	7-33
Figure 7.20 Optimization layouts of different microstructures for the bridge model	7-34~36
Figure 7.21 Sydney Harbor Bridge	7-36
Figure 7.22 Iteration histories of different material models for the bridge model problem	7-37~38
Figure 7.23 Optimization layouts of different power values for the bridge model problem	7-39~42
Figure 7.24 Iteration histories of different power values for the bridge model problem	7-42~44
Figure 7.25 A square domain with pressure load	7-46
Figure 7.26 Result of using PLATO software for the square domain with pressure load problem	7-46
Figure 7.27 Optimization layouts of different microstructures for the square domain with pressure load problem	7-47~48
Figure 7.28 Optimization results with different power values for the square domain with pressure load problem	7-49~50
Figure 7.29 Optimization layouts of different microstructures for the square domain with pressure load problem in <i>case b</i>	7-51~52
Figure 7.30 A simply supported beam with three points load problem	7-54

Figure 7.31 Optimization results for different microstructures for simply supported beam with multiple load	7-54~56
Figure 7.32 Design domain under gravity loads	7-57
Figure 7.33 Optimization layouts for different microstructures models with gravity load	7-58~59
Figure 8.1 Optimization layouts of bi-material models	8-3~4
Figure 8.2 Iteration history for ranked layered bi-material model	8-4
Figure 8.3 Iteration histories for the rest of bi-material models	8-5
Figure 8.4 Optimization layouts for different power values	8-6~7
Figure 8.5 Layouts of six bi-material models	8-7~8
Figure 8.6 Result layouts of six bi-material models	8-10~11
Figure 8.7 Design domain of a bridge model	8-12
Figure 8.8 Optimization layouts of six bi-material models	8-12~13
Figure 8.9 A short cantilever beam	8-15
Figure 8.10 Result layouts of six bi-material models	8-15~17
Figure 8.11 A supported beam	8-18
Figure 8.12 Optimization layouts of six bi-material models	8-18~19
Figure 8.13 A two side's supported beam	8-20
Figure 8.14 Optimization layouts of six bi-material models	8-20~22
Figure 8.15 Press machine frame model	8-23
Figure 8.16 Optimization layouts of six bi-material models	8-23~26

# List of Tables

---

Table 4.1	Parameters of the bi-material models	4-10
Table 6.1	Iteration numbers for different convergence tolerance	6-6
Table 6.2	The initial and final strain energy for different power values for short cantilever beam problem	6-28
Table 6.3	Strain energies for the different finite element discretizations	6-35
Table 7.1	Iteration numbers and final strain energies at convergence tolerance for the microstructures using HDM	7-9
Table 7.2	The initial and final strain energy with different power values for single supported beam optimization	7-15
Table 7.3	Iteration numbers and final strain energies at convergence tolerance for the microstructures using HDM	7-39
Table 7.4	The initial and final strain energy for different power values for the bridge model problem	7-44
Table 8.1	Iteration numbers and final strain energies at convergence tolerance for the microstructures using HDM	8-5
Table 8.2	Iteration numbers and final strain energies at convergence tolerance for the microstructures using HDM	8-9

---

## NOTATIONS

---

### Acronyms:

CATO	Constrained adaptive topology optimization software developed by Bulman, Siens and Hinton.
ESO	Evolutionary structural optimization
HDM	Homogenization with different microstructures program
PLATO	Topology optimization software developed by Hassani and Hinton
SIB	Simple internal boundary
SIMP	Solid Isotropic Microstructures with Penalization
Strand7	Finite element software developed by G+D Computing Limited

### Tensors, Scalars and Functions

$a(u, v)$	Energy bilinear form for internal work
$a$	Design variables
$b$	Design variables
$e$	as a superscript indicates dependency to the cell of periodicity
$f(x)$	Objective function
$\bar{f}$	Average body forces within the cell
$g_k(x)$	Inequality constraint function
$g$	Number of element

$h_j$	Equality constraint function
$p$	Function of the position vector $x$
$q$	Function of the position vector $x$
$r$	Design variable
$s$	Boundary of the hole in base cell
$t$	Slack variables
$\vartheta_i^y$	Arbitrary constants of integration in $y$
$u_i$	Displacement associate with $i$
$x_m^l$	Lower bounds of design variable
$x_m^u$	Upper bounds of design variable
$x, y$	Global Cartesian coordinates
$x_i, y_i$	Cartesian coordinate of node $i$
$E$	Young's modulus of solid material
$E_{ad}$	Admissible elasticity tensors
$E_{ijkl}$	Elasticity tensor
$E_{ijkl}^G$	General elasticity tensor
$E_{ijkl}^H$	Homogenized elasticity tensor
$E_{ijkl}^e$	Coefficients of elasticity of an inhomogeneous body
$F$	Objective function
$G$	Base cell body
$H$	Hole of the base cell
$H^1$	Sobolev space

$L(u)$	Load bilinear form for external work
$L_2$	Hilbert space
$L$	Lagrangian function
$N^g$	Global shape function.
$Y_i$	Dimension of periodic base cell

### **Greek symbols**

$\alpha$	Solid part shape function
$\beta$	Y- periodic function
$\zeta$	Lagrangian multiplier
$\delta_{ij}$	Kronecker delta symbol
$\lambda$	Lagrangian multiplier
$\varepsilon_{ij}$	Second order strain
$\varepsilon^0$	Initial strain loading
$\delta$	A small value to define solid size
$\varsigma$	Small parameter indicating the characteristic of non-homogeneity dimension
$\sigma_{ij}$	Second order stress
$\bar{\sigma}_{ij}$	Average residual stress within the cell
$\theta$	Orientation angle
$\mu$	Intermediate values as a penalization
$\varrho$	Design variable in ranked layered model
$\gamma$	Design variable

$\nu$	Poisson's ratio
$\eta$	Moving limit
$\rho$	Density
$\chi$	Discrete function
$(\chi)_{kl}$	Y- Periodic function
$\Delta$	Convergence tolerance
$\xi(x)$	Continuous approximation function
$\Psi$	Solid part of cell
$\Pi$	Total potential energy
$\Omega$	Design domain
$\Omega_s$	Solid part of design domain
$\Gamma_t$	Boundary on which the surface force applied
$\Gamma_d$	Boundary on which displacements are prescribed

### Special Symbols

$\ \mathfrak{g}\ $	Norm
$\in$	Belongs to
$\sum$	Summation
$\cap$	Intersection of sets
$\forall$	For all
$\partial$	Partial differentiation
$\nabla$	Gradient operator

## Vectors and Matrixes

<b>f</b>	Vector of structure load
<b>p</b>	Vector of surface force in the hole
<b>t</b>	Vector of traction force
<b>u</b>	Displacement vector
<b>v</b>	Vector of virtual displacement
<b>x</b>	Vector of design variables
<b>y</b>	Position vector in microscopic coordinate
<b>Y<sub>p</sub></b>	Vector of periodicity, $\mathbf{Y}_p = [Y_1, Y_2, Y_3]^T$
<b>f<sub>i</sub><sup>e</sup></b>	Force vector for element e associated with node i
<b>R<sup>n</sup></b>	n dimensional space
<b>V</b>	Space of admissible displacement
<b>V<sub>Ω×Ψ</sub></b>	Space of admissible displacements defined in $\Omega \times \Psi$
<b>W(Y)</b>	Space of periodic function
<b>B</b>	Strain-displacement matrix
<b>D</b>	Element of constitutive matrix
<b>D<sup>G</sup></b>	Element of general constitutive matrix of
<b>D<sup>H</sup></b>	Element of homogenized constitutive matrix
<b>K</b>	Symmetric, banded stiffness matrix
<b>N</b>	Matrix of arbitrary integers $\mathbf{N} = \begin{bmatrix} n_1 & 0 & 0 \\ 0 & n_2 & 0 \\ 0 & 0 & n_3 \end{bmatrix}$
<b>O</b>	Matrix of linear differential operators
<b>T</b>	Transformation matrix

## **Chapter 1**

---

# **INTRODUCTION**

### **1.1 General**

The natural resources available to human beings are very limited, which means we should use these resources as efficiently as possible. Optimization is a tool for finding the best possible solution to an engineering problem. In this respect, optimization plays a very important role in the engineering field.

The concept of an optimum in an engineering problem is intriguing and has been under intensive investigation for decades. Earlier, engineering design was conceived as a kind of art that demanded great ingenuity and experience of the designer, and the development of the field was characterised by gradual improvement of existing types of engineering design. The design process was a sequential trial and error. It started from an initial design based on the knowledge and experience of the designer, then followed by an analysis to the performance of the design. Based on the information obtained, a new design was developed. Nowadays, intense technological competition requires reduction of design time and costs of the products while ensuring high quality

and functionality. The current concept of design places greater emphasis on efficient use of energy, environmental problems, saving as much natural resources as possible, Therefore it often involves creative activity for which prior engineering experience is totally lacking. Such creativity must naturally resorts to application of scientific methods. In recent decades, the development of computer technology has provided the opportunity to revolutionize the traditional design process. The engineering design has been changing from trial and error to scientifically based methods of rational design and optimization. This has already occurred with structural optimization.

Structural optimization is a part of an optimal design field dealing with structural elements or structural systems and is employed in several engineering fields. The main task of structural optimization is to find the ‘best possible solution’ to a structure that meets all the multidisciplinary requirements imposed by functionality and manufacturing conditions. A structural optimization design is a rational establishment of a structure which is the best of all possible solutions within a prescribed objective and a set of constraints. Structural optimization has become a multidisciplinary subject with applications in many fields, such as automotive, aeronautical, mechanical, civil, nuclear, naval and off-shore engineering. As a result of rapidly growing applications of structural optimization, the importance of the research in structural optimization methods is realized by more and more scientists and engineers.

Topological structural optimization is regarded as one of the most challenging topics in structural mechanics, in which one needs to change the topology as well as the shape during the process of optimization. This significantly increases the complexity of the optimization problem.

In order to overcome the difficulty of topology optimization problems, various optimization design techniques have been developed in recent decades. Among these, the homogenization method proves to be one of the general approaches to shape and topology optimization. This method is based on the theory of homogenization. The main idea of the homogenization method is to consider the design domain as a composite material consisting of an infinite number of periodically distributed small holes. By introducing a material density function, the complex nature of the topological optimization problem can be converted to a sizing optimization problem by treating the sizes of the small holes as the design variables. The very important task of homogenization method for topology optimization is to create and formulate a microstructure model for the design domain.

Although there has been considerable work done in the field of the homogenization method for structural topology optimization, the studies and comparisons of the existing microstructures and exploration for new microstructures are comparatively modest and limited. More studies on different microstructures for homogenization method need to be carried out.

## **1.2 Aim of the Research**

The general aim of the research is to develop simple, general, and more computationally efficient microstructures to improve the homogenization method so that it can be put for practical use and to examine the effect of these different microstructures on different kinds of topology optimization problems.

The specific aims of the proposed project are:

- a. Investigating the properties of existing microstructures.
- b. Identifying the strengths and weaknesses of each type of microstructures.
- c. Establishing new microstructures for shape and topology optimization.
- d. Deriving an efficient algorithm of optimization procedure for different microstructure models.
- e. Developing a general computer software package incorporating all the existing and new microstructures.
- f. Solving different types of optimization problems by using different microstructures and comparing the optimization results.

## **1.3 Contribution of the Research**

In this thesis, a study on the microstructures has been carried out and new microstructures including one-material and bi-material microstructures have been proposed. These microstructures help to overcome the inherent difficulties of some existing microstructures and make structural topology optimization

design more accurate. A computer software package for topology optimization catering for all microstructures, existing and newly studied here, was developed. All these will reduce the gap between the mathematical complexity of topological optimization and its practical application in engineering design.

#### **1.4 Significance of the Research**

In the topology optimization field, the homogenization method can be used to solve a wide range of practical problems. In this respect, this study is significant in that it contributes to the development of homogenization to a comprehensive and practical tool in engineering. The finding from this research will provide useful information for researchers and design engineers in choosing microstructures suitable for their tasks. The computer software package can be used for practical applications as well as for future research and development. Consequently, more efficient designs using less material and energy can be obtained for engineering structures.

#### **1.5 Layout of the Thesis**

The thesis consists of nine chapters. An outline is given as follows:

**Chapter 1** outlines the general background and basic concept of structural optimization and the homogenization method as well as the aims, contribution and significance of the thesis.

**Chapter 2** presents a comprehensive review of the development history and status of structural optimization. Different optimization methods are described and their advantages and limitations are discussed, topological optimization methods are emphasized.

**Chapter 3** describes the theoretical basis of the homogenization method and its application in topological optimization. In this chapter, the concept of periodic structure is first described. It is followed by the homogenization formulas in elastic composite materials with a periodic structure and the application of homogenization method in topology optimization. Next is a review on microstructures. In this section, different models of microstructures are studied. The advantages and disadvantages of current microstructures model are described. Finally, a brief summary is presented.

**Chapter 4** In this chapter, a new definition for developing microstructures is given. Nine new microstructure models are developed. The method for deriving material properties of the new microstructures is studied.

**Chapter 5** mainly deals with computer program implementation for different microstructure models, followed by the treatment of the technique of principal-stress based optimal orientation and checkerboard control technique.

**Chapter 6** In this chapter, structural topology optimization of a number of benchmark problems is studied. The algorithms for new microstructure models

are tested and compared with other methods.

**Chapter 7** deals with different loading cases (single load, surface load, multiple load, and gravity load cases). A series of structural topological optimization problems are carried out. The results and their accuracy for different microstructures are compared. Advantages and disadvantages of different microstructures are summarized.

**Chapter 8** conducts numerical tests on bi-material models. The two types investigated are: one is a model of bi-material without void and the other is bi-material with void. Examples of structural topological optimization under different loading cases are presented. Their solutions are compared. Advantages and disadvantages of different bi-material microstructures are summarized.

**Chapter 9** presents general conclusions regarding the effectiveness and efficiency of microstructures studied. Suggestions for further investigations were given.

**Appendix A** presents the homogenization formulas in elastic composite materials with a periodic structure.

**Appendix B** presents a typical run of the HDM software.

**Appendix C** presents Optimality criteria for deep cantilever beam with a single load

Finally, a list of references is given in alphabetical order of the first authors.

## **Chapter 2**

---

# **OVERVIEW OF STRUCTURAL OPTIMIZATION**

This chapter reviews the development of the theory of structural optimization and its applications. The background of structural optimization method is first described, followed by mathematical description for general optimization problems. Approaches for structural optimization including classical calculus methods and numerical methods are reviewed and their algorithms are presented. Topology optimization is introduced in more details. The current situation and future directions of structural optimization are summarized.

### **2.1 Structural Optimization Method**

A structural optimization design problem is described by the objectives of the problem, the constraints involved and the design variables. A general structural optimization problem is formulated as: “*Minimise (or maximise) an objective function subject to behavioural and geometrical constraints.*”

The objective function or behavioral constraints are usually described as follows:

- structural volume or weight, storage capacity.
- cost of material or manufacturing.
- global measure of the structural performance such as stiffness, buckling load, plastic collapse load, natural vibration frequency, dynamic response, etc.
- local structural responses such as stress, strain or displacement at prescribed points; maximum stress, strain or displacement in the whole structure, stress intensity factor, etc.

Geometrical constraints are usually described as follows:

- manufacturing limitations.
- availability of member sizes.
- fabrication.
- physical limitations.

The design variables are to be determined during the optimization process.

Design variables can be continuous or discrete.

## **2.2 Mathematical Description of an Optimization Problem**

An optimization problem can be mathematically stated as searching for the minimum (or maximum) value of a function  $f(\mathbf{x})$  and the related variable vector  $\mathbf{x} = (x_1, x_2, \dots, x_n) \in \mathbf{R}^n$ ,  $\mathbf{R}^n$  is  $n$  dimensional space, which yields the optimal

solution subject to some constraints. The optimization problem in its most general form may be expressed as follows (Haftka and Gurdal, 1992):

$$\begin{aligned} & \text{Minimize} && f(\mathbf{x}) \\ & \text{Such that} && h_j(\mathbf{x}) = 0 \quad j = 1, 2, \dots, n_h \\ & && g_k(\mathbf{x}) \leq 0 \quad k = 1, 2, \dots, n_g \end{aligned} \quad (2.1)$$

where  $h_j$  and  $g_k$  are constraints,  $j$  and  $k$  are the number of equality of constraints and inequality constraints, respectively.

The sets of design variables which satisfy all the constraints constitute the feasible domain. The infeasible domain is the collection of all design points that violate at least one of the constraints. If the objective function and both equality and inequality constraints are linear functions of the design variables, then the problem is a linear optimization problem. In a non-linear optimization problem, either the objective function or at least one of the constraints is a non-linear function of the design variables. From the engineering point of view, the objective function  $f(\mathbf{x})$  is usually chosen as the structural volume, weight, cost, performance, serviceability or their combination. Structural optimization problems are usually non-linear optimization problems (Chu, 1997).

### **2.3 Classifications of Structural Optimization**

According to the design variables to be optimised, the structural optimization in engineering field can be classified into the following three types:

**Sizing optimization:** In this type of optimization problems, the domain of the structure is fixed during the optimization process. Design variables for sizing can be discrete or continuous. Sizing optimization can usually be considered as the implementation of optimization at details design stage.

**Shape optimization:** In shape optimization problems, the domain is not fixed but the topology is. Shape optimization is always used in the selection of the optimum shape of external boundary surfaces or curve. Examples of this type of problem include finding the boundaries of a structure, finding the location of joints of a skeletal structure, finding the optimal values for parameters, which define the middle surface of a shell structure. This may be seen as the implementation of the optimization techniques at the preliminary design stage.

**Topology optimization:** In some cases, sizing and shape optimization methods may lead to sub-optimal results. To overcome this deficiency topology optimization must be considered. Topology optimization is to find the optimal layout of a structure within a defined design domain. Different from shape or sizing optimization method, the initial design domain in topology optimization is a grand or universal structural, for example, a rectangular plate, in some two dimensional design problems. The only known quantities in the problem are the applied loads, the possible support conditions, the volume of the structure to be constructed and maybe some additional design restrictions defined by the designer. The physical size, shape, and connectivity of the structure are not known. The topology, shape, and size of the structure are not represented by

standard parametric functions but by a set of distributed functions defined over the fixed design domain. These functions in turn represent a parameterization of the stiffness tensor of the continuum and a suitable choice of this parameterization, which would lead to the proper design formulation for topology optimization (Bendsøe and Sigmund, 2002). Topology optimization is the most difficult and challenging task among the three types of structural optimization problems.

Figure 2.1, which is extracted from Bendsøe and Sigmund (2002) shows the three categories of structural optimization, a) sizing optimization problem of a truss structure, b) shape optimization and c) topology structural optimization.

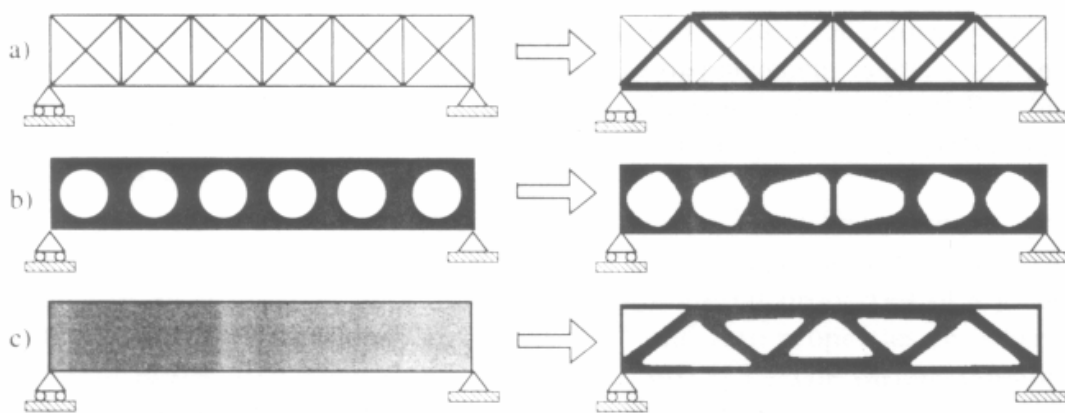


Figure 2.1 Three categories of structural optimization.

*(From Bendsøe and Sigmund, 2002, page 2)*

## **2.4 Solution Methods for Structural Optimization**

Different approaches to solve the structural optimization problems can be broadly classified into classical calculus methods and numerical methods.

### **2.4.1 Calculus methods**

The differential calculus was introduced into optimization problem in the 17th century. The first use of the calculus methods to structural design can be attributed to Maxwell (1895) in designing the least weight layout of frameworks. The later research on the optimal topology of trusses by Michell (1904) resulted in the well known Michell type structures. The typical calculus methods are differential calculus and calculus of variations

#### *Differential Calculus*

The method of differential calculus stated that the conditions for existence of extreme values are the first order partial derivatives of the objective function with respect to the design variable to be zero.

The formula of differential calculus is as follows:

$$\nabla F(x_i) = 0, i = 1, 2, \dots, n. \quad (2.2)$$

Where the vector  $\mathbf{x} = \{x_1, x_2, \dots, x_n\}$  is the extreme points.

The differential calculus usually can only be applied to very simple cases such as unconstrained optimization problems.

#### *Calculus of Variations*

Calculus of variations is a generalization of the differentiation theory. It deals with optimization problems having an objective function  $F$  expressed as a

definite integral of a functional  $Q$ ,  $Q$  is defined by an unknown function  $y$  and some of its derivatives (Haftka and Gurdal 1992):

$$F = \int_a^b Q(\mathbf{x}, \mathbf{y}, \frac{d\mathbf{y}}{d\mathbf{x}}, \dots, \frac{d^n \mathbf{y}}{d\mathbf{x}^n}) d\mathbf{x} \quad (2.3)$$

Where  $\mathbf{y} = \mathbf{y}(\mathbf{x})$  is directly related to the design variable  $\mathbf{x}$ . Optimization is to find the form of function  $\mathbf{y} = \mathbf{y}(\mathbf{x})$  instead of individual extreme values of design variables.

The necessary condition for an extremum is the first order of variation equal to zero.

$$\delta F = \int_a^b \left( \frac{\partial Q}{\partial \mathbf{y}} \delta \mathbf{y} + \frac{\partial Q}{\partial \mathbf{y}'} \delta \mathbf{y}' + \dots \right) d\mathbf{x} = 0 \quad (2.4)$$

Where  $\mathbf{y}' = d\mathbf{y} / d\mathbf{x}$

Taking into account of boundary conditions at fixed  $\mathbf{y}(a)$  and  $\mathbf{y}(b)$  (Haftka and Gurdal 1992), Equation (2.4) can be expressed as

$$\frac{\partial Q}{\partial \mathbf{y}} - \frac{d}{d\mathbf{x}} \left( \frac{\partial Q}{\partial \mathbf{y}'} \right) = 0 \quad (2.5)$$

This is the well known Euler-Lagrange equation.

Although the application of calculus method is very limited, it is a very important stage in the development of optimization methods. Calculus methods have the fundamental importance in exploring mathematical nature of optimization and in providing the lower bound optimum against which the results by alternative methods can be checked (Haftka and Gurdal 1992).

### ***2.4.2 Numerical methods***

In general structural optimization problems are highly non-linear. In the design of real structural systems, the use of numerical methods is unavoidable. Nowadays the numerical methods of structural optimization generally fall into the following categories:

- Direct minimization techniques (e.g. mathematical programming, MP)
- Indirect methods (e.g. optimality criteria, OC)
- Genetic Algorithms method

#### *Mathematical Programming*

Mathematical programming (MP) was one of the most popular optimum search techniques formulated in 1950s (Heyman 1951). It is a step-by-step search approach involving iterative processes. Each iteration consists of two basic steps:

- a) differentiating the value of the objective function and its gradients with respect to all design variables,
- b) calculation of a change of the design variable that would result in a reduction of the objective function.

Steps a) and b) are repeated until a local minimum of the objective function is reached.

In the early stages, the mathematical programming method was only limited to linear problems where the objective functions and constraints are linear functions of design variables. Since 1960, numerous algorithms of nonlinear programming techniques have been developed such as: nonlinear programming (NLP) (Schmit, 1960), feasible direction (Zoutendijk 1960), gradient projection (Rosen 1961) and penalty function method (Fiacco and McCormick 1968). At the same time, approximation techniques using the standard linear programming to address nonlinear problems, such as sequential linear programming (Arora 1993) have been studied.

The main advantage of MP methods is that they can be applied to most problems within and outside the field of structural optimization. The main disadvantage of MP methods is that as the number of design variables and constraints increases, the cost of computing derivatives becomes expensive.

### *Optimality Criteria*

Optimality criteria are necessary conditions for minimality of the objective function and these can be derived by using either variational methods or extremum principles of mechanics. Optimality criteria (OC) method was analytically formulated by Prager and co-workers in 1960s (Prager and Shield 1968; Prager and Taylor 1968). It was later developed numerically and become a widely accepted structural optimization method (Venkayya et al. 1968).

OC methods can be divided into two types. One type is rigorous mathematical statements such as the Kuhn-Tucker conditions. The other is algorithms used to resize the structure for satisfying the optimality criterion. Different optimization problems require different forms of the optimality criterion.

In Kuhn-Tucker conditions (Haftka and Gurdal 1992), the inequality constraints can be transformed into equality constraints by adding slack variables. In this case, the inequality constraints in Equation (2.1) can be written as

$$\mathbf{g}_k(\mathbf{x}) + t_k^2 = 0, \quad k = 1, 2, 3, \dots, n_g \quad (2.6)$$

$t_k^2$  is slack variables

The Lagrangian function of the optimization can be defined as

$$L(\mathbf{x}, t, \lambda, \zeta) = f(\mathbf{x}) + \sum_{j=1}^{n_h} \zeta_j h_j(\mathbf{x}) + \sum_{k=1}^{n_g} \lambda_k (\mathbf{g}_k(\mathbf{x}) + t_k^2) \quad (2.7)$$

where  $\zeta_j$  and  $\lambda_k$  are Lagrangian multipliers.

Differentiating the Lagrangian function (2.7) with respect to  $\mathbf{x}$ ,  $t$ ,  $\lambda$ , and  $\zeta_j$  we obtain

$$\frac{\partial L}{\partial x_i} = \frac{\partial f}{\partial x_i} + \sum_{j=1}^{n_h} \zeta_j \frac{h_j(x)}{\partial x_i} + \sum_{k=1}^{n_g} \lambda_k \frac{\mathbf{g}_k(x)}{\partial x_i} = 0, \quad i = 1, 2, \dots, n \quad (2.8)$$

$$\frac{\partial L}{\partial \zeta_j} = h_j = 0 \quad j = 1, 2, \dots, n_h \quad (2.9)$$

$$\frac{\partial L}{\partial \lambda_k} = \mathbf{g}_k + t_k^2 = 0 \quad k = 1, 2, \dots, n_g \quad (2.10)$$

$$\frac{\partial L}{\partial t_k} = 2\lambda_k t_k = 0 \quad k = 1, 2, \dots, n_g \quad (2.11)$$

From (2.10) and (2.11) we can get

$$\begin{aligned} g_k(x) &\leq 0, & k = 1, 2, \dots, n_g \\ \lambda_k g_k &= 0, & k = 1, 2, \dots, n_g \end{aligned} \quad (2.12)$$

This implies that when an inequality constraint is not active, the Lagrangian multiplier associated with the constraint is zero.

By using Kuhn-Tucker conditions, the optimality conditions for the optimization problem can be stated as

$$\begin{aligned} \frac{\partial L}{\partial x_i} &= \frac{\partial f}{\partial x_i} + \sum_{j=1}^{n_h} \zeta_j \frac{h_j(x)}{\partial x_i} + \sum_{k=1}^{n_g} \lambda_k \frac{g_k(x)}{\partial x_i} = 0, & i = 1, 2, \dots, n \\ \frac{\partial L}{\partial \zeta_j} &= h_j = 0 & j = 1, 2, \dots, n_h \\ g_k(x) &\leq 0, & k = 1, 2, \dots, n_g \\ \lambda_k g_k &= 0, & k = 1, 2, \dots, n_g \\ \lambda_k &\geq 0, & k = 1, 2, \dots, n_g \end{aligned} \quad (2.13)$$

The optimal criteria method is one of the best-established and widely accepted optimization techniques.

It should be mentioned here the attempt to combine both the mathematical programming method and optimal criteria method by dual MP methods. As

dual methods search the optimum direction in the space of Lagrangian multipliers instead of that of the initial design variables, it can save considerable computing efforts when the number of constraints is smaller than that of design variables (Fleury, 1979).

### *Genetic Algorithms*

Genetic Algorithms (GA) were first developed in 1970s (Holland, 1975). The GA method uses genetic processes of reproduction, crossover and mutation. The procedures are summarized as follows:

- a) An initial population of designs is randomly created.
- b) The fitness of each individual is evaluated according to a fitness function.
- c) The fittest members are reproduced and allowed to cross among themselves.
- d) A new generation is developed with member having higher degree of desirable characteristics than the parent generation.
- e) This procedure is repeated until a near optimum solution has been reached.

Although the GA method may not yet be as popular as MP or OC method, this method has merits of being reliable and robust (Nagendra, Haftka and Gurdal, 1993).

## **2.5 Structural Topological Optimization**

With the exception of a few early landmark results (Maxwell 1895; Michell 1904), the historical development of the field of structural optimization seems to have followed an opposite route to the actual structural design process (Haftka and Gurdal 1992; Kirsch 1993). Since its inception, research in numerical optimal structural design went from element stiffness design, through geometric and shape optimization to topology optimization design. It is also clear that the major impact on the structural efficiency, in the sense of stiffness/volume or stress/volume ratio, is determined at the conceptual stage by the topology and shape of the structure. No amount of fine-tuning of the cross-sections and thicknesses of the elements will compensate for a conceptual error in the topology or the structural shape (Olhoff *et al.* 1991).

With the development of high-speed computer, the topology optimization method using numerical approach has been growing quickly (Haftka and Grandhi (1986), Kirsch (1989) and Rozvany *et al.* (1995)). A numerical approach to topological design starts with a domain of material to which the external loads and boundary conditions apply. The optimization algorithm then proceeds with removing out ineffectual material to generate best structural solutions. In most cases, the objective function for topology optimization problems is often the compliance (Taylor 1977).

Generally speaking, structural topology optimization can be considered as a material distribution problem. Two classes of structural domains have been used in topology optimization problems. One is called the ‘Discrete’ structure. Early solutions can be seen in the papers of Don *et al.* (1964); Dobbs and Felton (1969), examples of applying the concept to large-scale structures have been given by Zhou and Rozvany (1991). The other domain is continuous structures. The continuum is typically divided into appropriate finite elements where every element has intrinsic structural properties. They are reviewed in the following sections.

### ***2.5.1 Topology optimization for discrete structures***

According to the survey by Topping (Topping, 1993), topology optimization method for discrete structures can be classified into three categories:

#### *Geometric Approach*

In the geometric approach, the properties of cross-section and the coordinates of joints are design variables. During the optimization process, the number of joints and connecting members are fixed while some joints are permitted to coalesce.

#### *Hybrid Approach*

In the hybrid approach, the design variables are divided into size design variables and geometrical design variables and are separated in the design

space. During the optimization process, the element size is firstly changed while keeping the topology unchanged; next, optimum position of the element nodes is searched.

### *Ground Structure Approach Method*

Combined with the MP and OC method, the ground approach method is now widely used in topology optimization problems. In the ground structure approach, a ground structure is considered as a dense set of nodes and a number of potential connections between the nodes. During the optimization process, the number and size of connecting elements are changed, but the nodes numbers and position are fixed. If the section area of elements are reduced to zero during the optimization process, the elements are considered as non-existent and the topology is changed accordingly.

A remarkable advantage of the ground structure approach method is that the design domain is fixed thus the problem of mesh regeneration can be avoided.

## **2.5.2 Topology optimization for continuous structures**

### *Heuristic Methods*

Heuristic methods are those addressing structural optimization problems in a less mathematical but more intuitive way. Instead of complex mathematical

formulation, the heuristic methods are based on simple concepts or natural laws. These methods fall into two categories.

#### *Evolutionary structural method (ESO)*

The evolutionary structural method was first proposed by Xie and Steven (1993, 1994a). This method is based on the concept of slowly removing the inefficient material from the structure and/or gradually shifting the material from the strongest part of the structure to the weakest part until the structure evolves to the desired optimum. The ESO method offers a simple way to obtain optimum designs using standard finite element analysis codes. Compared to other structural optimisation methods, the ESO method is overwhelmingly attractive due to its simplicity and effectiveness. During the last ten years, ESO has been demonstrated to be capable of solving many problems of size, shape and topology optimum designs for static and dynamic problems (Rong *et al*, 2001).

#### *Homogenisation Method*

Compared to the methods discussed above, the homogenization method is more complex. This method is based on the mathematical theory of homogenization, which has been developed since 1970's (Babuska, 1976, Cioranescu and Paulin 1979). The homogenization method can be used to find the effective properties of the equivalent homogenized material and can be applied to many areas of physics and engineering. Since being firstly proposed for topology optimization

in 1988 by Bendsøe and Kikuchi (1988), homogenization method has attracted the attention of many researchers and design engineers and has been used by industrial companies around the world for product development, particularly in the automobile industry.

The homogenisation method has been successfully applied to both static and dynamic problems with weight constraint (Tenek and Hagiwara 1993, Ma et al. 1995). With regard to the algorithm aspect, the homogenisation method uses traditional mathematical programming or optimality criteria as search techniques. The advantages of homogenization method are rigorous theoretical basis and good convergence behaviour. The disadvantage of homogenization method is that difficulties associated with those traditional methods are magnified in the homogenisation method.

#### *H/e-method*

The h/e-method is a hybrid method. It is an abbreviation of the combination of homogenization and evolutionary methods in various degrees. Bulman, Sienz and Hinton (2001) developed the CATO (constrained adaptive topology optimization) algorithm combines idea from the two procedures: the more mathematically rigorous homogenization method and more intuitive evolutionary methods. They systematically investigated the performance of the algorithm for topology optimization using a series of benchmark problems and their study results show that in general cases, the h/e CATO algorithms compared well with the homogenization method.

## **2.6 Summary**

With the development of computer technology, structural optimization has become a very important design tool in engineering. The applications of structural optimization designs have been widely extended to various fields such as aerospace, transportation, mechanical and civil engineering.

Numerical methods have been developed very rapidly and have been widely used in the structural optimization problems. With the advance of high-speed computers and the relatively inexpensive computational power, numerical methods play more and more important role in structural optimization.

In structural optimization problems, topological structural optimization has the complex features of both sizing, and shape optimization problems. In the optimization process, trying to change the topology as well as the shape during the optimization processes makes the problem more complex. This class of problems is still regarded as one of the most challenging in structural mechanics.

Homogenization method is very useful tool in solving topology structural optimization problems. It is regarded as the one of the most general approach to finding optimum shapes and topology of structures. Details of this method will be presented in next chapter.

## **Chapter 3**

---

# **HOMOGENIZATION AND MICROSTRUCTURES REVIEW**

By using the concept of the composite microstructures distribution, the homogenization method can be used to solve structural topology optimization problems. The results obtained have good agreements with the experimental data available in literature.

In general, the mathematical theory of homogenization does not provide analytical formulas or numerical algorithms directly suited to obtaining answers to engineering problems. Thus, a 'gap' exists between the mathematical theory of homogenization and the mechanics of composites. This gap acts as the principal obstacle to a wide application of the methods of the mathematical theory of homogenization in practical work. To solve this problem, microstructure model of homogenization and its formulation must be well established.

In the last ten years, researchers and engineers have done a lot of work on microstructures development. Up to now, various types of microstructures have

been proposed and used for shape and topology optimization. In this chapter, the detailed homogenization formulas and different microstructures are reviewed.

## **3.1 Homogenization Method**

### ***3.1.1 Introduction***

Homogenization is a mathematical method. It considers problems which are parameterized by a scale parameter  $\zeta$  and represented by a family of functions  $\mathbf{w}(\zeta)$ . It allows us to "upscale" the governing differential equations and transforms the initial problem to a problem for a homogeneous body, where  $\zeta > 0$  is a spatial (length) scale parameter, the typical size of a pore in a basic cell.

The essential step for homogenization is to determine the limit

$$\mathbf{w} = \lim_{\zeta \rightarrow 0} \mathbf{w}(\zeta) \quad (3.1)$$

This limit can be considered as the result of the "up scaling" procedure (Figure 3.1), followed by finding differential equations that the limit  $\mathbf{w}$  satisfies and proving that formula (3.1) holds (Hornung, 1997).

This method not only offers formulas for upscaling but also provides tools for producing rigorous mathematical convergence proofs (Hornung, 1997).

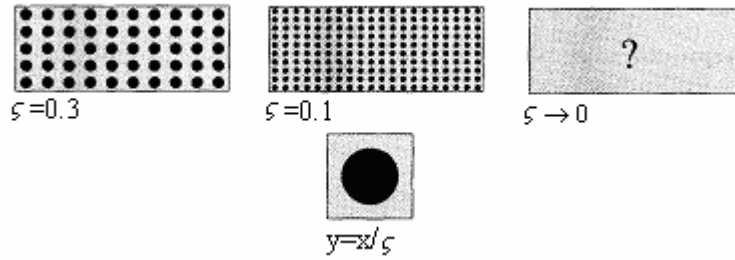


Figure 3.1 Homogenization limit (Hornung, 1997)

From a mathematical point of view, the theory of homogenization uses the asymptotic expansion and the assumption of periodicity to substitute the differential equations with rapidly oscillating coefficients with differential equations whose coefficients are constant or slowly varying in such a way that the solutions are close to the initial equations (Oleinik, 1984).

Homogenization theory, a rigorous mathematical theory, can be used as an alternative approach to find the properties of composites and advanced materials with microstructures. This theory can be applied in many areas of physics and engineering having finely heterogeneous continuous media such as heat transfer or fluid flow in porous media or, for example, electromagnetism in composites. In fact the basic assumption of continuous media in mechanics and physics can be thought of as sort of homogenization, as the materials are composed of atoms or molecules.

The essential steps to solve problems by the homogenization method are assuming a periodic structure for a design domain, defining shapes of microstructure for the small-scale  $\zeta$  and finding homogenized material properties.

### 3.1.2 A brief review of periodic structure

In the homogenization theory, the composite structure is supposed to be made of sets of basic cells that have a regular periodicity. For general boundary condition  $\Gamma_d \cap \Gamma_t = \emptyset$ , they have the following properties.

$$q(\mathbf{x} + \mathbf{N}\mathbf{Y}_p) = q(\mathbf{x}) \quad (3.2)$$

Where:  $\mathbf{x} = [x_1, x_2, x_3]^T$  is a position vector of a point.

$q$  is a function of the position vector  $x$ .

$\mathbf{Y}_p = [Y_1, Y_2, Y_3]^T$  is a constant vector

$\mathbf{N}$  is a 3x3 diagonal matrix

$$\mathbf{N} = \begin{bmatrix} n_1 & 0 & 0 \\ 0 & n_2 & 0 \\ 0 & 0 & n_3 \end{bmatrix},$$

Where  $n_1, n_2, n_3$  are arbitrary integer numbers.

Most of the natural and artificial materials are heterogeneous at a micro-scale level. Periodic materials and structures are widely found in engineering practice. They are also found in nature, with various small deviations from periodicity.

The dimension of cell or microstructure is very small compared to that of the structural body, the scale, of order  $\zeta$  ( $0 < \zeta \ll 1$ ). Due to high level of heterogeneity of material, quantities such as displacements and stresses vary

rapidly within a very small neighborhood  $\zeta$  of a given point  $\mathbf{x}$ . Thus, all quantities have two explicit dependences. One is on the macroscopic level  $x$ , which indicates slow variations. The other is on the microscopic level  $\mathbf{y} = \mathbf{x}/\zeta$ , which describes rapid oscillations. We also assume that the form and composition of the base cell varies in a smooth way with the macroscopic variable  $x$ . For example, let a property be represented by a general function,  $\phi = \phi(\mathbf{x}, \mathbf{y})$ , where the dependence of the function on the microscopic variable  $\mathbf{y} = \mathbf{x}/\zeta$  is periodic,  $\phi = \phi(\mathbf{x}, \mathbf{y} + Y)$ . The functions having this nature are called  $Y$ -periodic functions. If we assume that  $\phi(\mathbf{x})$  is a physical quantity of a heterogeneous medium. Then  $\phi(\mathbf{x})$  will have the oscillation as shown in Figure 3.2 (a). An enlargement of one of the oscillations in the expanded scale is shown in Figure 3.2(b). The characteristic dimension of in-homogeneity and scale enlargement is shown in Figure 3.3.

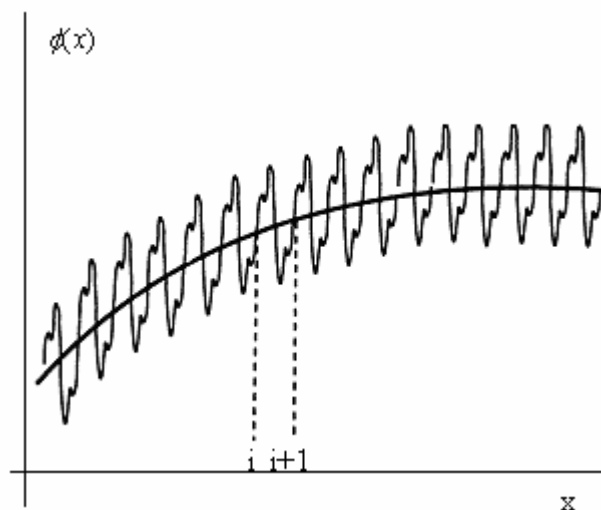


Figure 3.2 (a) A oscillating function (Hassani and Hinton, 1998)

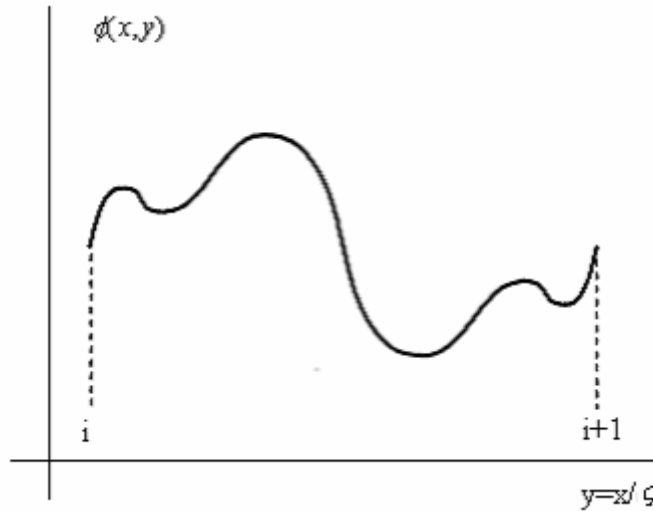


Figure 3.2 (b) One of the oscillations in the expanded scale, magnifying the section in (a) (Hassani and Hinton, 1998)

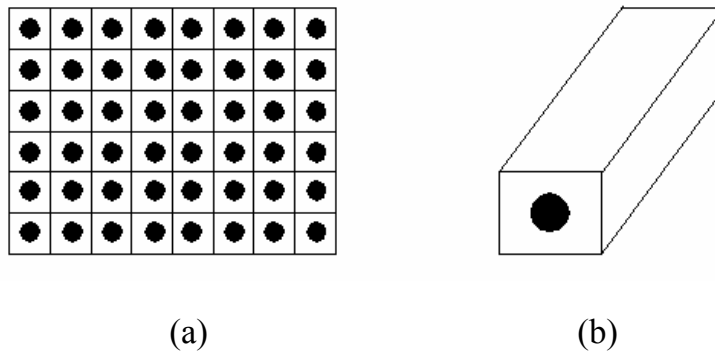


Figure 3.3 (a) The periodic structure of composites and (b) an enlargement of a base cell

If we assign a coordinate system  $\mathbf{x} = (x_1, x_2, x_3)$  in  $\mathbf{R}^3$  (where  $\mathbf{R}^3$  is a three dimensional space) to define  $\Omega$ , a periodic domain of the composite material problem. The domain can be regarded as a collection of parallelepiped cells of identical dimensions  $\zeta Y_1, \zeta Y_2, \zeta Y_3$ , which  $Y_1, Y_2$  and  $Y_3$  are the sides of the base cell  $Y$  in a local microscopic coordinate system.

$$\mathbf{y} = (y_1, y_2, y_3) = \mathbf{x} / \zeta = \left( \frac{x_1}{\zeta}, \frac{x_2}{\zeta}, \frac{x_3}{\zeta} \right).$$

Therefore for a fixed  $\mathbf{x}$  on the macroscopic level, any dependency on  $\mathbf{y}$  is considered  $Y$ -periodic. For different points, the structure of the composite may vary, but if we look through a microscope at a point at  $\mathbf{x}$ , the pattern is periodic.

The behavior of the composite can be expressed by a function of scale  $\zeta$

$$\phi^\zeta(\mathbf{x}) = \phi^0(\mathbf{x}, \mathbf{y}) + \zeta \phi^1(\mathbf{x}, \mathbf{y}) + \zeta^2 \phi^2(\mathbf{x}, \mathbf{y}) + \dots = \sum_{i=1}^{\infty} \zeta^i \phi^i(\mathbf{x}, \mathbf{y}) \quad (3.3)$$

To illustrate the application of the asymptotic expansion method, a problem of the linear elasticity for a non-homogeneous solid with a periodic structure is given by homogenization method in the following section.

### ***3.1.3 The homogenization formulas in elastic composite materials with a periodic structure***

The homogenization formulas in elastic composite materials with a periodic structure can be found in Hassani and Hinton (1998). Following is a brief review.

Let us consider a non-homogeneous, elastic solid, which occupies a domain  $\Omega$  in the space  $\mathbf{R}^3$  with a smooth boundary  $\Gamma$  comprising  $\Gamma_d$  (where displacements are prescribed) and  $\Gamma_t$  (the traction boundary, where body force  $\mathbf{f}$  and traction  $\mathbf{t}$  are applied) (Figure 3.4).

Let  $\mathbf{f}$  be the body force,  $\mathbf{u}$  the displacement field that defines equilibrium of elastic structure and  $\mathbf{v}$  the kinematically admissible virtual displacement field.

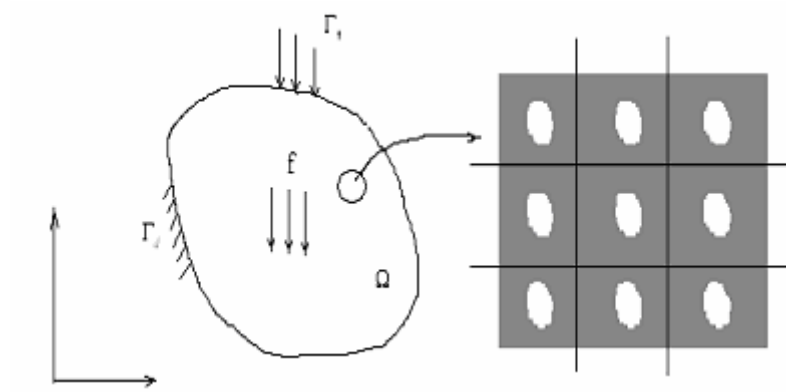


Figure 3.4 A structure with cellular microstructures

Let  $a(\mathbf{u}, \mathbf{v})$  be the energy bilinear form

$$a(\mathbf{u}, \mathbf{v}) = \int_{\Omega} E_{ijkl}(\mathbf{x}) \varepsilon_{ij}(\mathbf{u}) \varepsilon_{kl}(\mathbf{v}) d\Omega \quad (3.4)$$

with strain-displacement relations

$$\varepsilon_{ij}(\mathbf{u}) = \frac{1}{2} \left( \frac{\partial u_i}{\partial x_j} + \frac{\partial u_j}{\partial x_i} \right) \quad (3.5)$$

and the load bilinear form for external work

$$L(\mathbf{v}) = \int_{\Omega} \mathbf{f} \cdot \mathbf{v} d\Omega + \int_{\Gamma_t} \mathbf{t} \cdot \mathbf{v} ds \quad (3.6)$$

The linear problem of elasticity for such a body can be formulated in the following way:

- equilibrium equations  $\frac{\partial \sigma_{ij}}{\partial x_j} + f_i = 0$  in  $\Omega$  (3.7)

- loading conditions  $\sigma_{ij} n_j = p_i$  on  $\Gamma_t$ ,  $u_i = 0$  on  $\Gamma_d$  (3.8)

- linear elasticity relationship  $\sigma_{ij} = E_{ijkl} \varepsilon_{kl}$  (3.9)

The coefficients of elasticity  $\{E_{ijkl}\}$  of a non-homogeneous body are functions of the spatial coordinates  $\mathbf{x} = (x_1, x_2, x_3)$ , and are assumed to satisfy the following conditions (Kalamkarov and Kolpakov 1997, Bendsøe 1995):

$$\mathbf{C1.} \quad E_{ijkl} = E_{jikl} = E_{ijlk} = E_{klij}, \quad (3.10)$$

$$\mathbf{C2.} \quad E_{ijkl}(\mathbf{x}) \in E_{ad}(\Omega) \text{ and } \|E_{ijkl}\|_{E_{ad}(\Omega)} \leq M, \quad (3.11)$$

$$\mathbf{C3.} \quad E_{ijkl}(\mathbf{x})\varepsilon_{ij}\varepsilon_{kl} \geq m\varepsilon_{ij}\varepsilon_{kl} \quad (3.12)$$

where the constants  $0 < m$  and  $M < \infty$  do not depend on  $\mathbf{x}$ ,  $E_{ad}(\Omega)$  is admissible elasticity tensors which are allowed to vary over the domain of the body.

Let us consider the case when a non-homogeneous elastic material has a periodic structure in the coordinates  $x_1, x_2, x_3$ . The rectangular base cell of the cellular body  $Y$  is illustrated in Figure 3.5. The boundary of the hole  $H$  is defined by  $S$  ( $\partial H = S$ ) and is assumed to be smooth and the tractions  $\mathbf{p}$  may exist inside the holes.

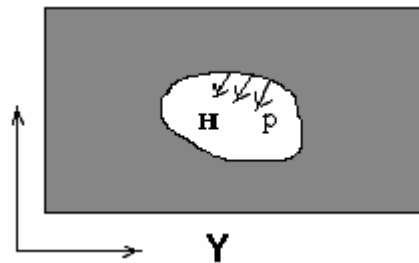


Figure 3.5 A base cell

The virtual displacement equation can be constructed as:

$$\int_{\Omega^e} E_{ijkl} \frac{\partial u_k^e}{\partial x_l} \frac{\partial v_i}{\partial x_j} d\Omega = \int_{\Omega^e} f_i^e v_i d\Omega + \int_{\Gamma_t} t_i v_i d\Gamma + \int_{S^e} p_i^e v_i dS \quad \forall \mathbf{v} \in \mathbf{V}^e, \mathbf{u}^e \in \mathbf{V}^e \quad (3.13)$$

where  $e$  is a superscript indicates dependency to the cell of periodicity and  $\mathbf{V}^e$  is a space of admissible displacement.  $t_i$  and  $p_i$  are components of traction  $\mathbf{t}$  and pressure  $\mathbf{p}$ .

By using the asymptotic expansion method, the following equation for the problem of the linear elasticity for a non-homogeneous solid with a periodic structure can be derived (see details in Appendix A).

$$\begin{aligned} \int_{\Omega} \left[ \frac{1}{|Y|} \int_{\Psi} \left( E_{ijkl} - E_{ijpq} \frac{\partial (\chi_p)_{kl}}{\partial y_q} \right) dY \right] \frac{\partial u_k^0(\mathbf{x})}{\partial x_l} \frac{\partial v_i(\mathbf{x})}{\partial x_j} d\Omega &= \int_{\Omega} \left( \frac{1}{|Y|} \int_{\Psi} E_{ijkl} \frac{\partial \beta_k}{\partial y_l} dY \right) \frac{\partial v_i(\mathbf{x})}{\partial x_j} d\Omega \\ + \int_{\Omega} \left( \frac{1}{|Y|} \int_{\Psi} f_i dY \right) v_i(\mathbf{x}) d\Omega + \int_{\Gamma_t} t_i v_i(\mathbf{x}) d\Gamma &\quad \forall \mathbf{v} \in \mathbf{V}_{\Psi} \end{aligned} \quad (3.14)$$

Where  $(\chi)_{kl} \in V_{\Psi}$  is a Y- periodic function being the solution of

$$\int_{\Psi} E_{ijkl} \frac{\partial (\chi_p)_{kl}}{\partial y_q} \frac{\partial v_i(\mathbf{y})}{\partial y_j} dY = \int_{\Psi} E_{ijkl} \frac{\partial v_i(\mathbf{y})}{\partial y_j} dY \quad \forall \mathbf{v} \in \mathbf{V}_{\Psi} \quad (3.15)$$

and  $\beta \in V_{\Psi}$ ,  $\beta$  is a Y- periodic function being the solution of

$$\int_{\Psi} E_{ijkl} \frac{\partial \beta_k}{\partial y_l} \frac{\partial v_i(\mathbf{y})}{\partial y_j} dY = \int_{S^e} p_i v_i(\mathbf{y}) dY \quad \forall \mathbf{v} \in \mathbf{V}_{\Psi} \quad (3.16)$$

and  $\Psi$  indicates the solid part of the cell.

Now, if we define that

$$E_{ijkl}^H = \frac{1}{|Y|} \int_{\Psi} \left( E_{ijkl} - E_{ijpq} \frac{\partial (\chi_p)_{kl}}{\partial y_q} \right) dY \quad (3.17)$$

$$\bar{\sigma}_{ij}(\mathbf{x}) = \int_{\Psi} E_{ijkl} \frac{\partial \beta_k}{\partial y_l} dY \quad (3.18)$$

$$\bar{f}_i(x) = \frac{1}{|Y|} \int_{\Psi} f_i dY \quad (3.19)$$

(3.14) can be written as

$$\begin{aligned} \int_{\Omega} E_{ijkl}^H \frac{\partial u_k^0(\mathbf{x})}{\partial x_l} \frac{\partial v_i(\mathbf{x})}{\partial x_j} d\Omega &= \int_{\Omega} \bar{\sigma}_{ij}(\mathbf{x}) \frac{\partial v_i(\mathbf{x})}{\partial x_j} d\Omega \\ + \int_{\Omega} \bar{f}_i(\mathbf{x}) v_i(\mathbf{x}) d\Omega + \int_{\Gamma_i} t_i v_i(\mathbf{x}) d\Gamma &\quad \forall \mathbf{v} \in \mathbf{V}_{\Psi} \end{aligned} \quad (3.20)$$

It is noticed that the formula above is very similar to the equation of virtual displacement (3.13).  $E_{ijkl}^H$  defined by (3.17) is the homogenized elastic tensor.  $\bar{\sigma}$  are average ‘residual’ stresses within the cell due to the tractions  $p$  inside the holes and  $\bar{f}$  are the average body forces.

The solution of the elastic composite material with a periodic structure problem by homogenization method can be summarized as:

- a. Solving the integral equations (3.15) and (3.16) in the base cell and get  $\chi$  and  $\beta$ .
- b. Using (3.17), (3.18) and (3.19) get  $E_{ijkl}^H$ ,  $\bar{\sigma}$  and  $\bar{f}$
- c. In macroscopic coordinates  $x$ , construct and solve the equation (3.20).

### ***3.1.4 Application of homogenization for topology optimization in minimum compliance problems***

A problem in topology optimization can be formulated as finding the optimal spatial distribution of material for a given set of loads and boundary conditions to minimize certain objective function. The solution usually involves three

classes of regions: solid, porous and empty. By using of the concept of a composite periodic microstructures distribution, the problem can be converted into a sizing optimization problem with parameters defining the microstructure taken as design variables.

In optimal design for minimum compliance problem, we seek the optimal choice of elasticity tensor  $E_{ijkl}$  in some given set of admissible elasticity tensors  $E_{ad}$ . The admissible tensors will usually be allowed to vary over the domain of the body, so that  $E_{ijkl}$  will be a function of the spatial variable  $\mathbf{x} \in \Omega$ .

The topology optimization problem can be described as (Bendsøe, 1995):

$$\begin{aligned} & \underset{\mathbf{u} \in \mathbf{V}, M}{\text{minimize}} \quad L(\mathbf{u}) \\ & \text{such that: } a(\mathbf{u}, \mathbf{v}) = L(\mathbf{v}), \text{ for all } \mathbf{v} \in \mathbf{V} \\ & E_{ijkl} \in E_{ad} \end{aligned} \tag{3.21}$$

where  $a(\mathbf{u}, \mathbf{v})$  and  $L(\mathbf{v})$  are the energy bilinear form for the internal work and the load linear form described before,  $L(\mathbf{u})$  is the mean compliance,  $\mathbf{V}$  denoting the space of kinematically admissible displacement field, the index  $M$  indicates that the energy bilinear form  $a_E$  depends on the design variables.

The topology optimization procedure consists of the following steps:

- Step 1* Choose a suitable reference domain that allows surface tractions, fixed boundaries, etc. to be defined
- Step 2* Choose a composite, constructed by periodic repetition of a unit cell consisting of the given material with one or more holes.

*Step 3* Solving the integral equations in the base cell and using (3.17), (3.18) and (3.19) get  $E_{ijkl}^H$ ,  $\bar{\sigma}$  and  $\bar{f}$ . In macroscopic coordinates  $x$ , solving the equation (3.20).

*Step 4* Using structural optimization method described in Chapter 2, compute (3.21) for the optimal distribution of this composite material in the reference domain, treat the problem as a sizing problem.

In general, we cannot use homogenization theory to solve engineering problems directly. To solve engineering problems by homogenization method, microstructure model and its formulation must be established first. The finding of equivalent homogeneous solid instead of the original non-homogeneous composite solid, is one of the principal applications of the mathematical theory of homogenization.

With the advance in sciences and high technologies, a number of new materials and special structures have been developed. Particular material properties can be obtained by the design of composition and microstructures. Some man-made materials have special microstructure properties and are composed of multi-phase materials. Composites technology creates the opportunity to implement specific physical properties into the individual regions of the structure. By changing the material microstructure, such as the composition and/or the fiber orientation, composites can exhibit desirable mechanical and thermal properties. Optimization of material selection and material composition provides a new era for structural engineering. The research of advanced materials can also be

extended to the research of homogenization microstructures design. In the next section, we will review these microstructures.

### **3.2 Microstructures Review**

The fact that material with microstructure is an integral part of problem of optimal structural design was first clearly demonstrated by Cheng and Olhoff (Cheng, 1981) on optimal thickness distribution for elastic plates. The work by Cheng and Olhoff led to a series of works on optimal design problems, such as microstructures formulation of the problem, plate models and optimal design problems (Bendsøe, 1986), design of composite plates of extremal rigidity (Gibiansky, 1984), regularization of optimal design problems for bars and plates (Lurie, Fedorov and Cherkaev, 1982 a and b), least-weight design of perforated plates (Rozvany, Ong, Szeto, Olhoff and Bendsøe, 1987), and so on. These studies concluded that laminated structures give more efficient designs and thus microstructures were built up in order to obtain the strongest structures. This requires a consistent way for computing effective material properties for materials with microstructures and this can conveniently be carried out using the method of homogenization. Thus, optimal design of structures is closely connected with studies of microstructures and the very important problem of finding the effective homogenized material properties for composite microstructures (Bendsøe, 1988).

Up to now, various types of microstructures have been proposed and used for shape and topology optimization. From the material structure point of view, these microstructures can be broadly classified into one-material microstructure and bi-material microstructures.

### ***3.2.1. One-material microstructures***

In one-material microstructures the material model contains one material with one or more voids. If a portion of the medium consists only of voids, material is not placed over that area. On the other hand, if there is no porosity at some portion, a solid structure needs to be placed at that location. There are many different types of one-material models used at present. These material models are:

#### *Ranked Layered Microstructures*

The basic idea of this type of microstructures is to find extremal microstructures, which has maximum rigidity or equivalently minimum compliance. These types of microstructures are also called optimal microstructures in the sense that they achieve optimality in the well-known Hashin-Shtrikman bounds (Bendsøe and Sigmund, 2002) on the effective properties of composite materials.

Figure 3.6 shows an example of the rank layered microstructures. Each cell of this periodic microstructure is constructed from layers of solid material and

void. The so-called rank-1 material consists of alternating layers of solid material and void.

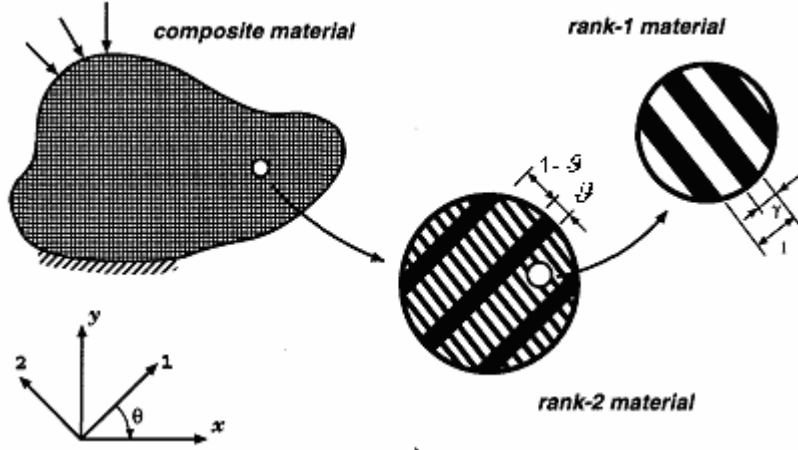


Figure 3.6 Ranked layered microstructure (Hassani and Hinton, 1998)

The rank-2 material is constructed in a similar manner, with layers of different ranks being orthogonal to each other. In the topology optimization problems, rank-2 layered material model is the most commonly used in ranked layered microstructures. For rank-2 layered material model, the elements of the matrix of elasticity coefficients are functions of three parameters:  $\vartheta, \gamma$ ,  $0 \leq \gamma \leq 1, 0 \leq \vartheta \leq 1$ , and orientation angle  $\theta$  (shown on Figure 3.6). So that the volume occupied by the solid  $\Omega_s$  is:

$$\Omega_s = \int_{\Omega} (\vartheta + \gamma - \vartheta\gamma) d\Omega \quad (3.21)$$

and the density of the composite can be written as

$$\rho = \rho(\vartheta, \gamma) = (\vartheta + \gamma - \vartheta\gamma) \rho_s \quad (3.22)$$

where  $\rho_s$  is the density of solid.

It is noted that by changing the value of  $\gamma$  and  $\varrho$  it is possible to cover the complete range of cell relative density from zero to one.

Many scientists and engineers have carried out a lot of research on ranked layered microstructures, i.e., Gibianski and Cherkaev (1987) derived the minimum complementary energy density for the class of matrix layered composites of any rank, and applied this as an upper bound on the energy density. At the same time they also applied the theory of quasiconvexity to construct a lower bound on the complementary energy density of a composite which is valid for any microstructure. Optimum composites are characterized by having a complementary energy density which lies between these two bounds. For the limiting case of perforated composites, these bounds coalesce and yield analytical expressions for the energy density of the optimum perforated laminate microstructure. Olhoff (1998), continued to study the topology optimization of linearly elastic three-dimensional continuum structures subjected to a single case of static loading. Several examples of optimum topology designs of three-dimensional structures were presented, including illustrative full three-dimensional layout and topology optimization problems for plate-like structures. They remarked that:

- The dependence of effective macroscopic properties on the microstructure geometry can be expressed by an explicit analytic form for the optimum three-dimensional material microstructures.
- The optimum microstructures provide a full relaxation of the three-dimensional generalized shape optimization problem. This means that the

problem is well-posed and that the optimum solution is convergent with respect to finite element mesh refinement.

- The use of optimum microstructures renders the topology optimization problem convex such that local optimum solutions are avoided. This implies that a usual sensitivity based procedure of mathematical programming can be applied for the solution of the complete optimization problem.

Allaire and Aubry (1999) studied optimal microstructures for plane shape optimization problems and pointed out that in two dimensional spaces, when the eigenvalues of the average stress have opposite signs, there is no optimal periodic microstructure. In this case, any optimal microstructure is degenerated, to the rank-2 layered material, i.e. it cannot sustain a non-aligned shear stress. When the eigenvalues of the average stress have the same sign, the higher order layered material is optimal and does not degenerate.

The advantage of the rank layered material model is that the effective material properties of the microstructures can be derived by analytical method. By using analytical method, Allaire and Aubry achieve optimality in the well-known Hashin-Shtrikman bounds on the effective properties of composite materials. Therefore, ranked layered microstructures are also called optimal microstructures.

The disadvantage of the rank layered material model is that the rank layered material cells provide no resistance to shear stress in between the layers. This

will result in the stiffness matrix of the structure becoming singular. One-way of “avoiding” the singularity problem is to use a very soft material instead of the voids. However, in this case, the strain energy calculated during optimization process (commonly used for objective function) is modified energy. On the other hand, the combination of a very soft material with a solid material will cause numerical problems due to ill conditioning of the global stiffness matrix. For some different loading cases or different design domains, the structure might be unstable.

At present, this type of microstructures has been studied only for compliance design (Rozvany, 2001), in which the total amount of external work is either minimized or constrained.

### *Rectangular Microstructure*

Rectangular microstructure was first proposed by Bendsøe and Kikuchi (1988). This microstructure is a square cell with centrally placed rectangular hole (Figure 3.7). In three-dimensional spaces, this micro-cell will be a cubic cell with a rectangular parallelepiped hole.

Rectangular microstructure is one of the most commonly used microstructure model for topology optimization using homogenization method. The area occupied by the solid material  $\Omega_c$  in the base cell is given by

$$\Omega_c = (1 - x_a \cdot x_b) \quad (3.23)$$

The area occupied by the solid material  $\Omega_s$  in the design domain is given by

$$\Omega_s = \int_{\Omega} (1 - x_a \cdot x_b) d\Omega \quad (3.24)$$

Where  $x_a, x_b$  are shown in Figure 3.7  $0 \leq x_a \leq 1, 0 \leq x_b \leq 1$ ,  $\Omega$  is the design domain and  $\Omega_s$  denotes the solid part of it.

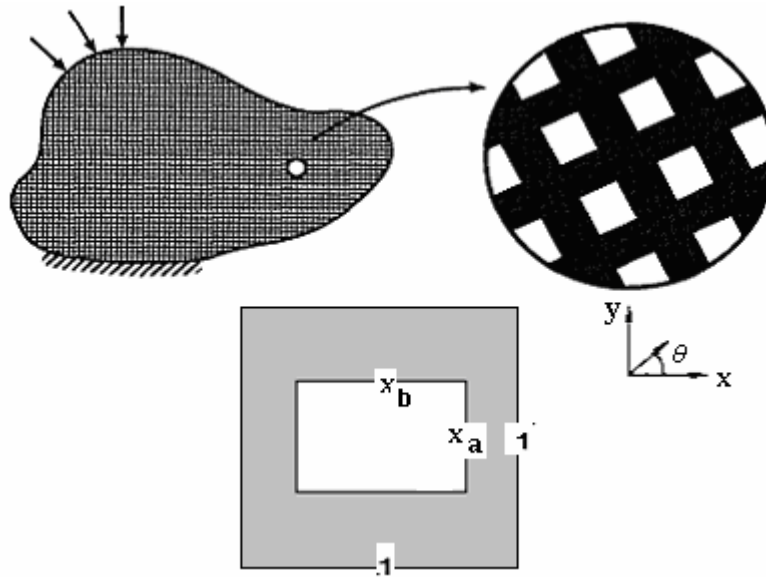


Figure 3.7 Rectangular microstructure.

In general, the microscopic perforations in the cellular body, with respect to the coordinate axes, can have different orientations and this orientation  $\theta$  will affect the properties of the elastic constitutive matrix. So orientation  $\theta$  is considered as a design variable in the formulation. The elastic module  $E_{ijkl}$  is the function of  $x_a, x_b$  and  $\theta$ . Generally, the effective material properties of such a structure are derived by a series of finite element analyses for voids of different sizes of voids.

Hassani and Hinton (1998) studied the rectangular microstructure systematically. In their book “*Homogenization and Structural Topology Optimization*”, the effective material properties obtained by the finite element solution of the homogenization equation for square unit cells with Young’s modulus  $E=0.91$  and the Poisson’s ratio  $\nu=0.3$ . Two polynomials were given. Several benchmark problems were studied. Computer software with rectangular and artificial microstructures named PLATO has been developed and successfully used in topology optimization problems.

The advantage of rectangular microstructures is the smaller number of variables required if square void is chosen. The rectangular microstructure model gives calculated true strain energy. Therefore, a solution of minimal compliance can be judged based on the value of strain energy.

The disadvantages of rectangular microstructure are:

- The homogenization equation has to be solved by numerical techniques. But with high speed computer developed, this problem is easy to be overcome.
- The optimization results often have “grey” region. The “grey” means it does not give a clear black and white image as power-law model does (discussed later).

*Triangular Microstructure*

Triangular microstructure is less used for solving topological structural optimization problems. Folgado *et al* (1995) calculated layout optimization problems of plate reinforcements with buckling load (Figure 3.8). But no details of microstructure modelling and calculation were given.

The advantage of the triangular microstructure models is that the true strain energy can be calculated by numerical techniques. The disadvantage of triangular microstructures is more complicated shape than rectangular microstructure and this will increase computation time and cost.

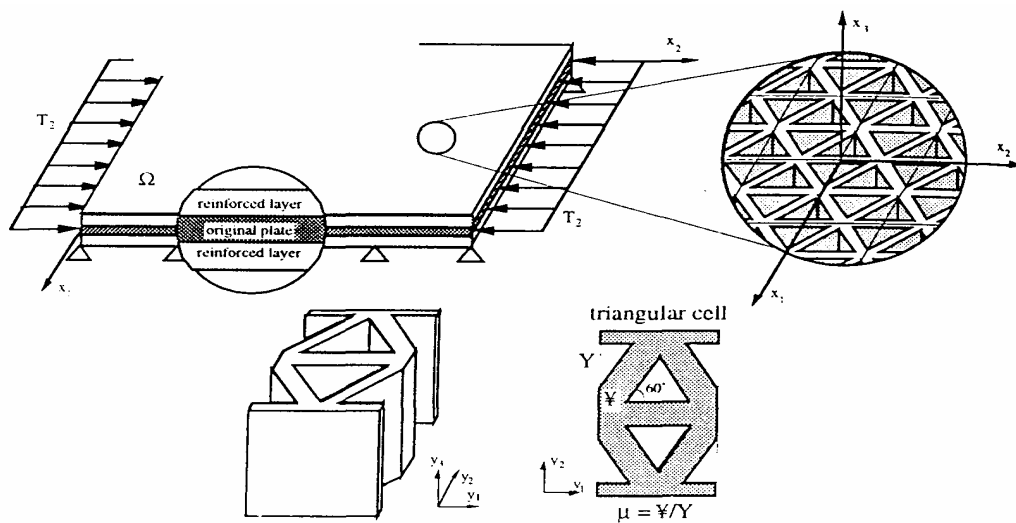


Figure 3.8 Triangular microstructure (Folgado *et al* 1995)

*Hexagon Microstructure*

Hexagon microstructure model is shown in Figure 3.9. Hassani and Hinton (1998) showed this shape of microstructure called honeycomb base cell as an example of microstructures development. Up to now, this model has not been

seen used in solving topology optimization problems. In this research project, this microstructure is developed and used to solve a series of benchmark topology optimization problems.

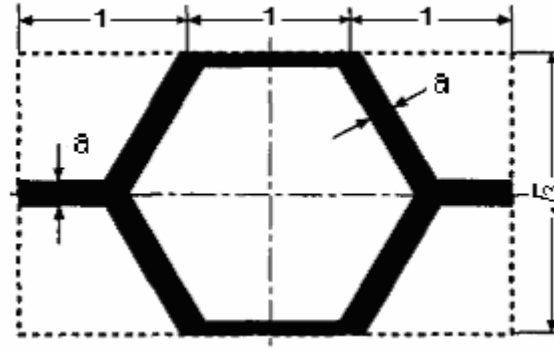


Figure 3.9. Hexagon microstructure

The advantages and disadvantages are the same as the triangular microstructure model.

### *Microstructures with Penalization*

#### *(a) SIMP Model*

The term "SIMP" was introduced by Rozvany in 1992. It is an acronym for Solid Isotropic Microstructures with Penalization. The method was proposed under the terms "direct approach" or "artificial material model" by Bendsøe in 1989. The geometrical shape of this model is the same as the rectangular model (Figure 3.7). By applying a penalization  $\mu$  to equation (3.23), the porous areas can be suppressed. This makes the solution only consist of solid and void regions. From a theoretical point of view, this microstructure model does not need homogenization (Rozvany, 2001). In SIMP model, the penalization  $\mu > 1$  is usually between 3 and 9 suggested by Hassani and Hinton (Hassani and

Hinton, 1998).

*(b) Power-law Model*

Power-law is a similar method to SIMP. The characteristic of power-law is that the material properties between solid and void are interpolated with a smooth continuous function which only depends on the material density. The Young's modulus  $E$  is written as

$$E(\rho) = (\rho)^\mu \cdot E^0 \quad (3.25)$$

where  $E^0$  is the Young's modulus of solid material and  $\mu$  is a penalization power. High values of  $\mu$  decreases the stiffness of intermediate density elements and makes "black and white" pattern in the results.

Bendsøe and Sigmund (1999, 2002) did a systematic study on this microstructure model and suggest that the power  $\mu$  should be selected according to the rule:

$$\mu \geq \max\left(\frac{2}{1-\nu}, \frac{4}{1+\nu}\right) \quad (3.26)$$

where the  $\nu$  is Poison's ratio.

The advantages of SIMP or Power-law models are: these types of models do not require homogenization of the microstructure. Therefore, the algorithm does not require higher mathematics for derivations and is easily understood.

Due to the penalty power used, the optimization solutions are clearer than other microstructures. These make the optimal solution easy to be implemented in practice.

The disadvantages of SIMP (Power-law) are:

- The solution depends on the value of penalization.
- The strain energy calculated in the optimization process is not real; it does not necessarily converge to the true value of the optimal solution.
- The optimal layout is dependent on the mesh.

### *Optimum Topology Microstructures*

The so-called optimum topology microstructure is a microstructure developed by using topology optimization method. Sigmund treats the problem numerically as an inverse homogenization problem of generating the topology of a unit cell of a periodic medium (Sigmund, 1994). The method for the generating microstructures is as follows:

Consider a given positive semi-definite rigidity tensor and consider the problem of finding the minimum weight truss or continuum topology for a unit cell  $Y$  in a periodic medium. This is an optimal design problem of generating an optimum topology for materials. Using standard notation for homogenization, this problem can be written as a topology design problem for a unit cell.

$$\begin{aligned} & \underset{D \in E_{ad} \cdot \mathcal{X}}{\text{minimize}} \{ \text{Volume of cell } Y \} \\ & \text{Subject to: } E_{ijkl}^H = E_{ijkl}^{\text{given}} \end{aligned}$$

Notice that the condition on the homogenized coefficients in the problem is a strain energy criterion, making it equivalent to a multiple load minimum compliance problem. The volume of material is to be minimized under conditions of specified compliance, for a number of independent load cases (in the form of pre-strains).

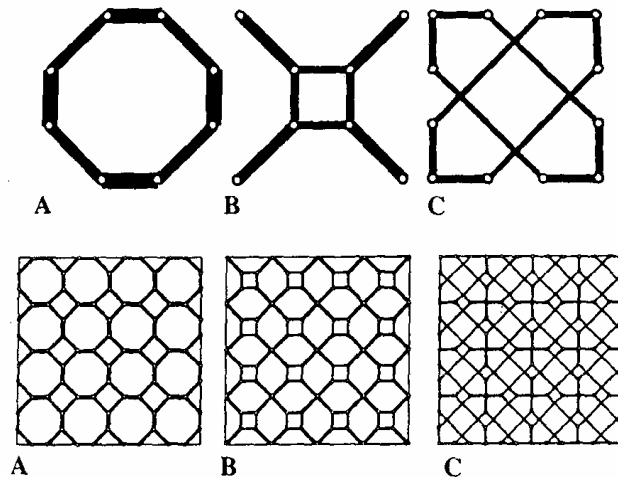


Figure 3.10 Minimum weight microstructures (Bendsøe, 1995).

Figure 3.10 shows minimum weight 2-D microstructures (upper row shows the unit cells, lower row an assemblage of cells) for obtaining materials with the indicated rigidity in the axis of the cell, corresponding to the optimal material for a single strain field  $\varepsilon = (1, 1, 0)$ . This is an isotropic material with Poisson's ratio 1.0 (Bendsøe, 1995). The three designs all have the same weight and are obtained using a 4 by 4 equidistant nodal lay-out in a square cell. All 120

possible connections between the nodal points are considered as potential members.

Sigmund (2000) gave the optimum topology microstructures as shown in Figure 3.11, 3.12, and 3.13.

In Figure 3.11, four microstructures obtained by a numerical inverse homogenization procedure, (a) isotropic hexagonal microstructure, (b) isotropic triangular microstructure, (c) isotropic octagonal microstructure and (d) symmetric square microstructure.

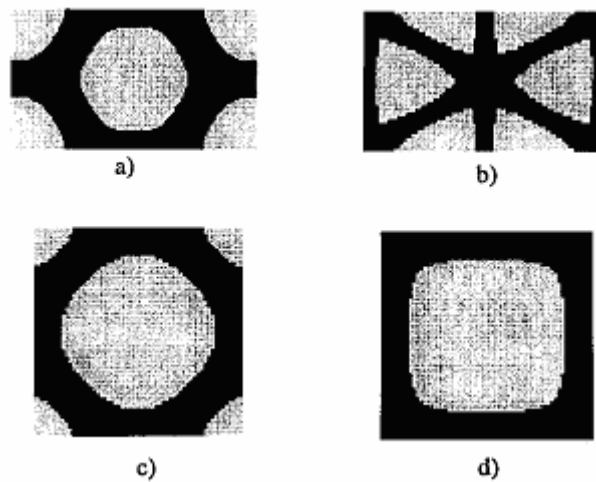


Figure 3.11 Four microstructures with extremal bulk moduli

In Figure 3.12, three by three arrays of topology optimized microstructures for maximum and minimum shear moduli and volume fraction  $p = 0.5$ . Microstructures 1 and 5-7 are obtained from a rectangular base-cell discretized with  $80 \times 40$  finite elements. Microstructures 2 and 3 are obtained using a square base-cell discretized with  $60 \times 60$  elements. Microstructure 1 has high bulk and shear modulus and is seen to have a triangular geometry.

Microstructure 3 is a one-length-scale version of the negative Poisson's ratio herringbone structure by Milton (1992). Microstructure 5 has close to minimum bulk and shear modulus and is the inversion of micro structure 1. Microstructures 6 and 7 are hexagon-like cells, where the bulk modulus of microstructure 7 is close to the upper bulk bound. By gradually allowing more local variation in the microstructure by increasing the value of the filter parameter, first microstructure 8 and then microstructure 9 are obtained.

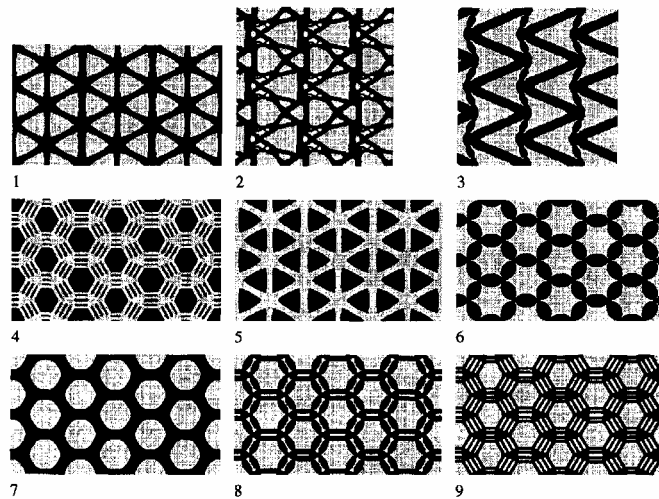


Figure 3.12 Topology optimized microstructures for maximum and minimum shear moduli and volume fraction  $p = 0.5$ .

Figure 3.13 shows some parameterized microstructures. The top left consists of triangular regions with pure phase 2 material, hexagonal regions with pure phase 1 material and laminated beams consisting of layers of phase 1 and phase 2 material. The laminated region consists of infinitely fine layering of phase 1 and 2.

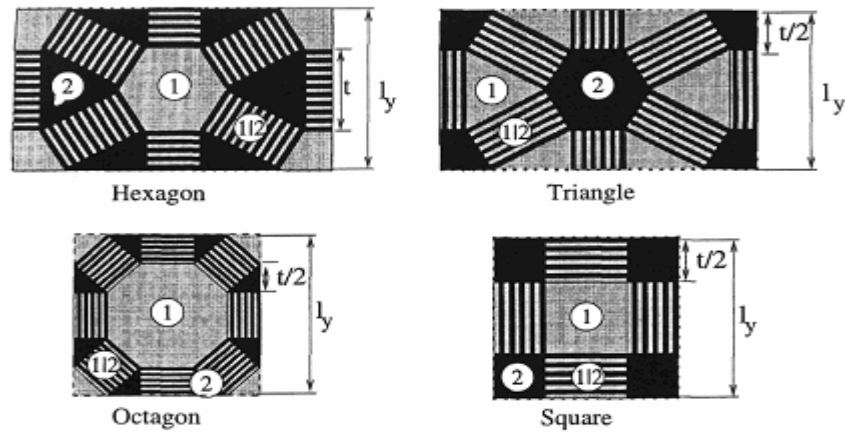


Figure 3.13 Parameterized microstructures

Up to now, many such microstructures have been developed by topology optimization method. Because of its complicated geometrical shapes, such techniques are only used in the optimal material design of microstructures. The microstructures developed have not been used for solving structural topology optimization problems.

### 3.2.2. *Bi-material microstructures*

The so-called bi-material microstructures contain two materials with or without voids. The optimization problem is defined in such a way that the geometry parameters of the hard, the soft materials and the void are the design variables. If a portion of the medium consists only of voids, material is not placed over that area. On the other hand, if there is no porosity at some position, a solid structure needs to be placed at that location.

The current models used in topology optimization problems are: ranked layered bi-material model and power-law bi-material model:

*Ranked layered bi-material model*

Rank layered bi-material model is one type of microstructure that can be applied in order to produce a relaxed form of the topology structural optimization problem. Figure 3.14 shows two types of rank layered bi-material models. Each cell of this periodic microstructure is constructed from layers of different materials and voids.

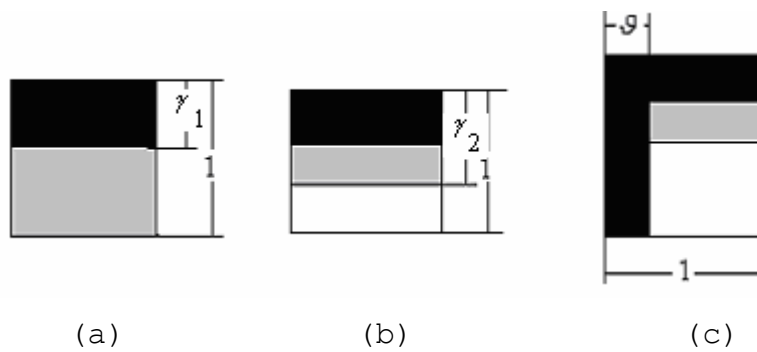


Figure 3.14 Rank layered bi-material cell

where  $0 \leq \gamma_1 \leq 1$ ,  $0 \leq \gamma_2 \leq 1$ ,  $0 \leq \vartheta \leq 1$ .

For ranked layered material microstructures, the effective material properties generally can be derived analytically. In such an analytical approach, explicit expressions for the effective elastic tensor can be obtained by establishing the optimal upper and lower bounds for the complementary elastic energy density of the perforated material. These microstructures are known as “extremal” microstructures in the sense that they achieve optimality in the Hashin-Shtrikman bounds on the effective properties of composite materials. This method can be applied to both two-dimensional and three-dimension layered material cell of finite rank.

In rank-2 bi-material model shown in Figure 3.14 (c), the volume occupied by hard material  $\Omega_s$  and soft material  $\Omega_l$  can be written as

$$\Omega_s = \int_{\Omega} \left[ (\mathcal{G}^g + (1 - \mathcal{G}^g) \gamma_1^g \gamma_2^g) \right] d\Omega \quad (3.27)$$

$$\Omega_l = \int_{\Omega} \left[ (1 - \mathcal{G}^g) (1 - \gamma_1^g) \gamma_2^g \right] d\Omega \quad (3.28)$$

Olhoff *et al* (1992) and Thomsen (1992) used bi-material rank-2 composite for topology optimization problems. Their studies showed that the structures of optimum topology obtained within the initial formulation are mainly composites. As this may be undesirable in certain cases, a formulation was presented that penalizes formation of composite and yields structures which entirely consist of isotropic base materials without small-scale mixing. Some numerical examples pertaining to generation of optimum topologies of joints and assemblies of sandwich panels and beams, and optimum reinforcement against concentrated loads, were presented.

#### *Power-law bi-material model*

For power-law bi-material microstructure model, the Young's modulus  $E$  can be written as:

$$E(\rho) = (\rho_1)^\mu ((\rho_2)^\mu E_1 + (1 - \rho_2)^\mu E_2) \quad (3.29)$$

where  $E_1, E_2$  are Young's modulus of harder and softer materials,  $\rho_1, \rho_2$  are design variables which represented densities of harder and softer materials,  $\mu$  is value of penalization power.

Sigmund (2001) designed of multi-physics actuators using power-law bi-material mode and suggested invoking each property independently and writing the constraint as:  $\sum_{g=1}^N \rho_1^g \rho_2^g V^g \leq V_1$  ,  $\sum_{g=1}^N \rho_1^g (1 - \rho_2^g) V^g \leq V_2$  . Where  $g$  is element number,  $V^g$  is element volume,  $V_1, V_2$  are the constraint of material volumes,  $N$  is number of elements.

Bi-material optimization has significant practical importance and can be used in many engineering field, for example, the optimal design of steel reinforcement in concrete or metal fibre reinforcement in ceramics. At present there has been very little work done on the topology optimization problems using bi-material microstructures. More studies on different bi-material models need to be carried out.

### **3.3 Summary**

The homogenization method can be used to solve structural topology optimization problems. The results obtained have good agreements with the experimental data available in literature. However, the mathematical theory of homogenization does not provide analytical formulas or numerical algorithms

directly suited to obtaining answers to engineering problems. Thus, a 'gap' exists between the mathematical theory of homogenization and the mechanics of composites. To solve this problem, microstructure model of homogenization and its formulation must be well established.

In the last ten years, researchers and engineers have done a lot of work on microstructures development. From the material point of view, they can be classified as one-material microstructures and bi-material microstructures. From the geometrical shape point of view, these microstructures can be divided into rank layered material microstructures, rectangular microstructure, triangular microstructure, penalization microstructures (power-law) and optimum topology microstructure.

Microstructures play a very important role in topology structural optimization when using homogenization method and more studies on microstructures need to be carried out. In the next chapter, new models of microstructures of one-material and bi-material are developed.

## **Chapter 4**

---

# **MICROSTRUCTURES STUDY**

From the previous chapter of microstructures review, we can see that many different microstructures have been developed by various researches and used in structural topology optimization problems. Each microstructure has its strength and weakness. More studies on different microstructures and development of new ones are needed in enhancing the homogenization method to solve practical engineering problems of topology optimization. In this chapter, new microstructures are defined first and then the algorithm to obtain their homogenized properties is presented. More benchmark studies on all existing and new microstructures are carried out and will be presented in later chapters.

### **4.1 Development of New Microstructures**

In the development of microstructures here, emphasis is put on defining hole or void of different geometrical shapes, taking into account the following points:

- The microstructures should allow material covering the whole range of void, density of composite could be changed from zero (void) to one (solid).
- They should satisfy the periodicity assumption. This is essential for using the

homogenization equations.

- The parameters of geometry should be defined as simple as possible.

In this research, two simple internal boundary microstructures, three multi-void microstructures and four bi-material microstructures were developed.

#### ***4.1.1 Simple internal boundary (SIB) microstructures***

##### *Definition of SIB microstructures*

Assume that there are two materials filling the whole area of the cell: hard and soft material. The boundary line between the hard and soft materials is defined by  $z(x,y)$  with following properties:

- The boundary  $z(x,y)$  is sufficiently smooth or sectionally smooth.
- $z(x,y)$  is symmetric with respect to the axes of symmetry  $\bar{x}$  and  $\bar{y}$  as illustrated in Figure 4.1. Hence, only a quarter of the domain of the unit cell needs to be analyzed (Figure 4.3).
- In order to make the problem simpler, variables are changed from coordinate  $x, y$  to  $\bar{x}, \bar{y}$ , and the boundary  $z(x,y)$  can be described by a function as (Figure 4.2):

$$\bar{y} = \begin{cases} 1 & \text{if } f(\bar{x}) \geq 1 \\ f(\bar{x}) & \text{if } f(\bar{x}) < 1 \end{cases} \quad (4.1)$$

where  $0 \leq \bar{x} \leq 1$ ,  $\bar{x}, \bar{y}$  are dimensionless parameters.

If the area taken by hard material of the cell is denoted by  $\Omega_s$ , then

$$\Omega_s = 4 \cdot \left(1 - \int_0^1 \bar{y} d\bar{x}\right) \quad (4.2)$$

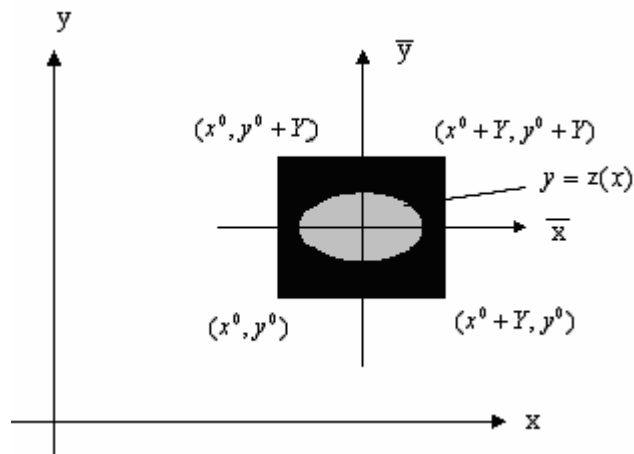


Figure 4.1 Definition of base cell

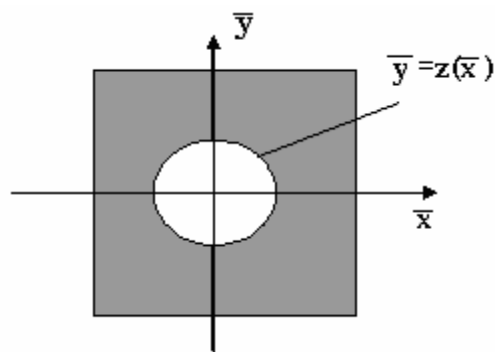


Figure 4.2 New coordinate system

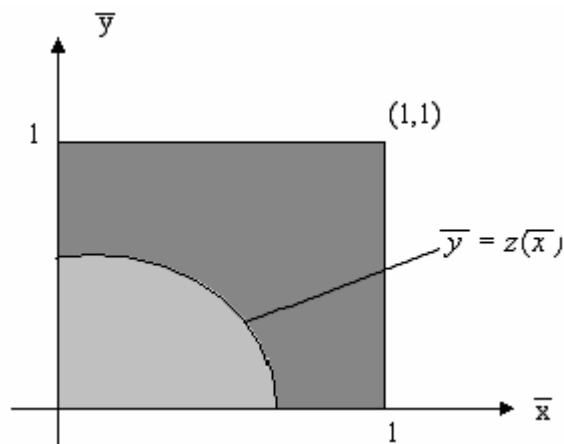


Figure 4.3 A quarter of the domain of the unit cell

In the case of a void instead of soft material, to avoid singularity of the

microstructure, a simple scheme to define the function  $\bar{y}$  in (4.1) is presented as follows. Let  $h$  be the hard material fraction defined as  $h = \Omega_s / \Omega$ , where  $\Omega_s$  is area taken by hard material and  $\Omega$  is the area of full cell, and  $\delta$  is a small value.

The function (4.1) is defined as:

- if  $h \geq 2\delta - \delta^2$ ,

$$\bar{y} = \begin{cases} 1 - \delta & \text{for } \bar{x} \leq 1 - \delta \text{ if } z(\bar{x}) \geq 1 - \delta \\ z(\bar{x}) & \text{for } \bar{x} \leq 1 - \delta \text{ if } z(\bar{x}) < 1 - \delta \\ 0 & \text{for } \bar{x} > 1 - \delta \end{cases} \quad (4.3)$$

- if  $h \leq 2\delta - \delta^2$ ,

$$\bar{y} = \begin{cases} 1 - a, & \text{for } \bar{x} \leq 1 - \delta \\ 0, & \text{for } \bar{x} > 1 - \delta, \end{cases} \quad (4.4)$$

where  $a$  is design variable,  $0 \leq a \leq \delta$

There are two ways for choosing the internal shape function:

- One is using shape optimization method. In this way, the fraction of hard and soft materials are fixed,  $\bar{y} = z(\bar{x})$  is obtained by using shape optimization method.
- The other is developing the microstructure with a simple shape function and the parameters of geometry as simple as possible.

In order to make the microstructure geometry simpler, the second way is used in this project and the following microstructures are developed:

*Circular boundary microstructure*

For circular microstructure,  $\bar{y} = f(\bar{x})$  defined by  $\bar{x}^2 + \bar{y}^2 = 2 \cdot r^2$ , where  $0 \leq r \leq 1$  is a design variable for topology optimization. The areas occupied by hard material (black region) and soft material (grey region) for two cases are:

- For  $0 \leq r \leq \frac{1}{\sqrt{2}}$ ,  $\Omega_s = 4 - \pi r^2$ , as shown in Figure 4.4

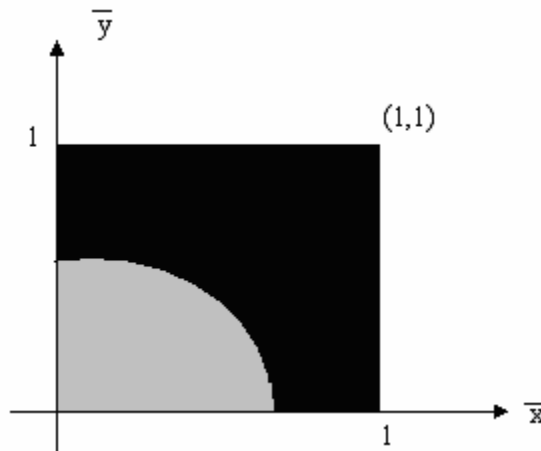


Figure 4.4 The area occupied by hard and soft material for  $0 \leq r \leq \frac{1}{\sqrt{2}}$

- for  $\frac{1}{\sqrt{2}} < r \leq 1$ ,  $\Omega_s = 4(1 - (\sqrt{2r^2 - 1} + \int_{\sqrt{2r^2 - 1}}^1 \sqrt{2r^2 - x^2} d\bar{x}))$ , as shown in Figure 4.5

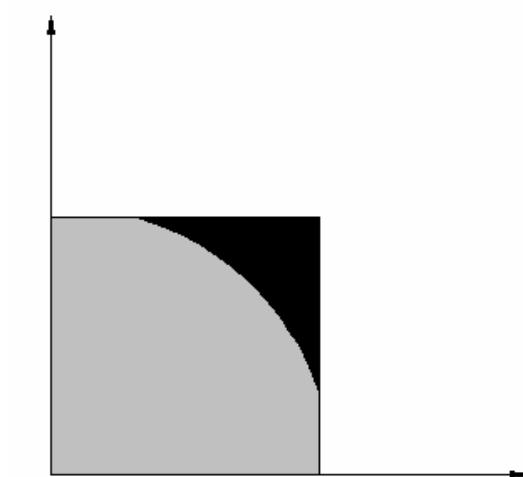


Figure 4.5 The area occupied by hard and soft material for  $\frac{1}{\sqrt{2}} < r \leq 1$

If we consider the soft material to be a void, then the area occupied by the hard material  $\Omega_s$  is defined as:

- when  $0 \leq r \leq \frac{1-\delta}{\sqrt{2}}$ ,  $\Omega_s = 4 - \pi r^2$ , as shown in Figure 4.6

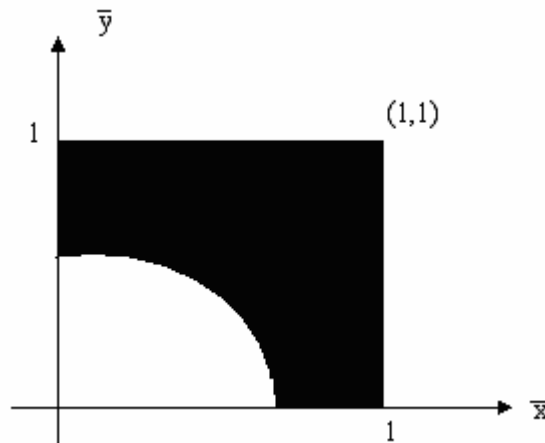


Figure 4.6 The area occupied by hard material for  $0 \leq r \leq \frac{1-\delta}{\sqrt{2}}$

- When  $\frac{1-\delta}{\sqrt{2}} < r \leq 1-\delta$ , as shown in Figure 4.7

$$\Omega_s = 4(1 - (\int_0^{\sqrt{2r^2 - (1-\delta)^2}} (1-\delta) d\bar{x} + \int_{\sqrt{2r^2 - (1-\delta)^2}}^{1-\delta} \sqrt{2r^2 - \bar{x}^2} d\bar{x}))$$

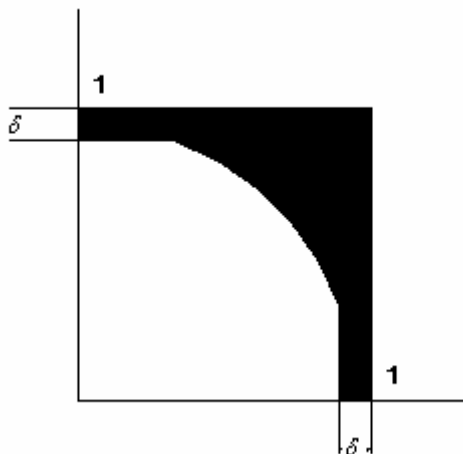


Figure 4.7 The area occupied by hard material for  $\frac{1-\delta}{\sqrt{2}} < r \leq 1-\delta$

- when  $1-\delta < r \leq 1$ ,  $\Omega_s = 4(1-r^2)$ , as shown in Figure 4.8

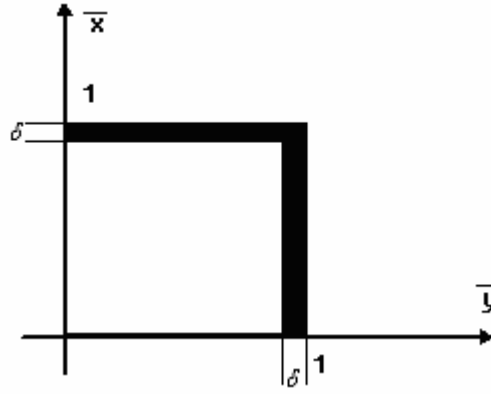


Figure 4.8 The area occupied by hard material for  $1 - \delta < r \leq 1$

*Cross-shape boundary microstructure*

In this type of microstructure, the boundary shape is found by noting that:

$$\bar{y} = \begin{cases} 1, & \bar{x} \leq r \\ r, & \bar{x} > r, \end{cases} \text{ and } \bar{x} = \begin{cases} 1, & \bar{y} \leq r \\ r, & \bar{y} > r \end{cases}$$

where  $0 \leq r \leq 1$  is design variable and  $0 \leq \bar{x} \leq 1, 0 \leq \bar{y} \leq 1$ .

The formula for area calculation is defined as

$$\bar{y} = \begin{cases} 1, & \bar{x} \leq r \\ r, & \bar{x} > r, \end{cases} \tag{4.5}$$

The area occupied by hard material  $\Omega_s$  (black region) and soft material  $\Omega_t$  (grey region) is shown in Figure 4.9.

$$\Omega_s = 4 \left( \int_0^r 1 d\bar{x} + \int_r^1 r d\bar{x} \right) = 4(r + r - r^2) = 4(2r - r^2) \tag{4.6}$$

$$\Omega_t = 4(1 - 2r + r^2)$$

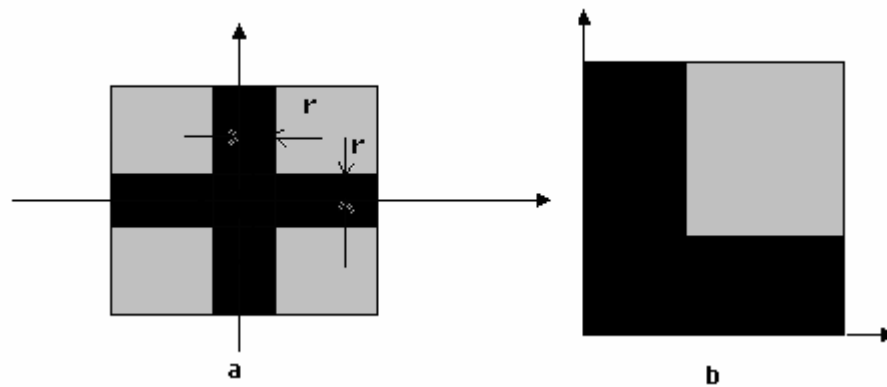


Figure 4.9 Cross-shape boundary, *a*) a full cell, *b*) is a quarter

For the SIB microstructure models, the homogenization equation is solved by finite element method. A computer code for calculating the effective material property is developed and will be used together with topology optimization program.

#### 4.1.2 Multi-void microstructures

For the so-called multi-void microstructure is more than one void in a microstructure. In the multi-void microstructure development, a symmetric geometrical shape with respect to the two axes of symmetry is retained. The difference between the single void microstructures and multi-void microstructures is that for the same area of solid material, the multi-void microstructures have more internal boundaries. This will result in different stiffness. Three types of multi-void microstructures are proposed. These microstructure models are: (a) triangular multi-void model, (b) rectangular multi-void model and (c) square multi-void model all shown in Figure 4.10.

For multi-void microstructure model, the homogenization equation is solved by finite element method. A general computer code for calculating the effective material property is also developed and used together with topology optimization program. A series of benchmark problems are provided in later chapters.

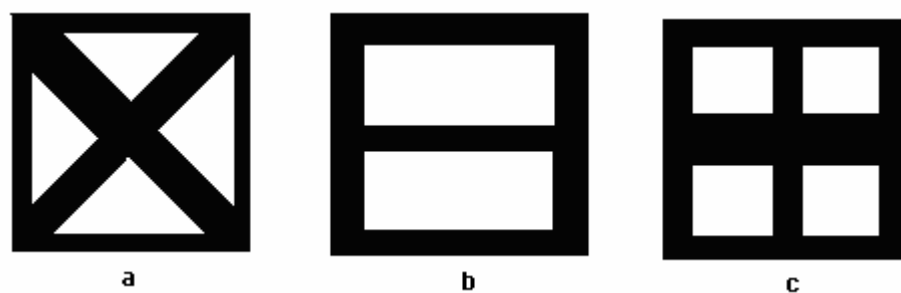


Figure 4.10 Multi-void microstructures

### ***4.1.3 Bi-material microstructures***

In this research, the following new bi-material microstructures have been developed: cross shape bi-material microstructure, square bi-material microstructure, double rectangular bi-material microstructure and triangular bi-material microstructure (shown in Figure 4.11). The areas occupied by hard and soft materials are shown in Table 4.1.

It can be seen that all new microstructures can be geometrically defined with a few parameters and their effective material property can be derived by a series of finite element analyses as shown in the following section.

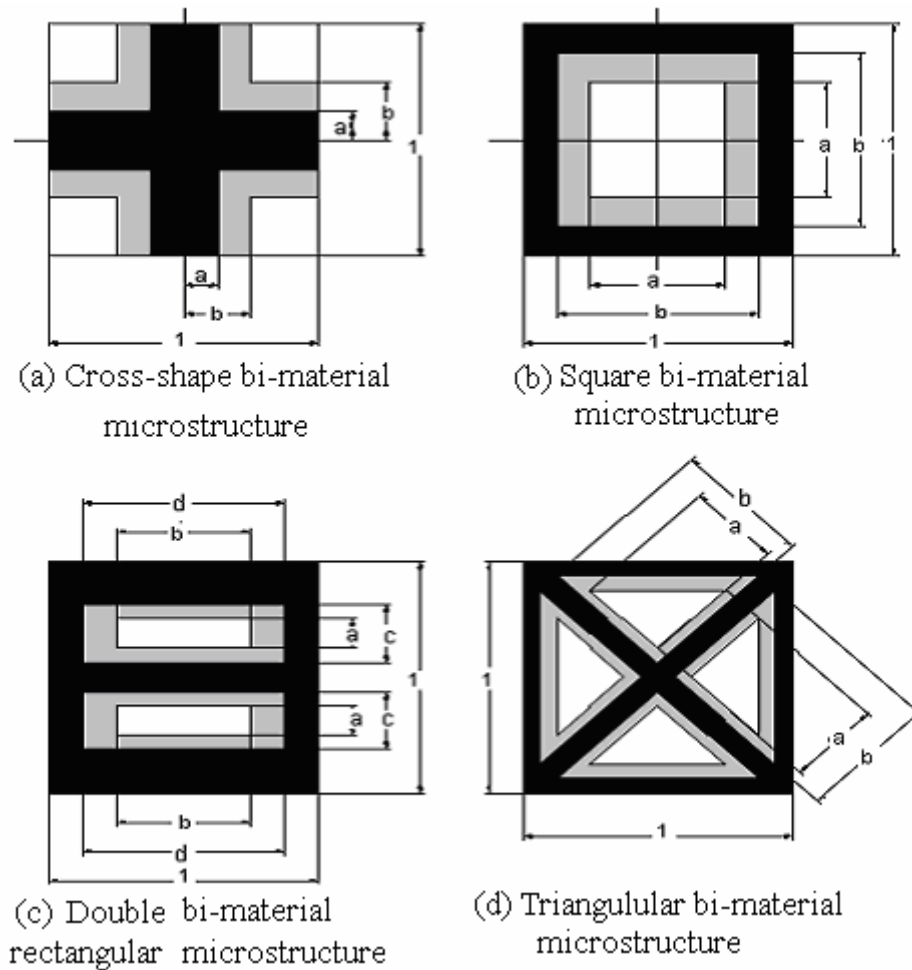


Figure 4.11 Bi-material microstructures

Model name	No of parameters	Area of hard material	Area of soft material	Design variable limitation
Cross-shape	2	$4 \cdot (a - a^2)$	$4(b - a)(1 - a - b)$	$0 \leq 2a \leq 2b \leq 1$
Square	2	$1 - b^2$	$b^2 - a^2$	$0 \leq a \leq b \leq 1$
Double rectangular	4	$1 - 2c \cdot d$	$2 \cdot (c \cdot d - a \cdot b)$	$0 \leq 2a \leq 2c \leq 1,$ $0 \leq b \leq d \leq 1$
Triangular	2	$1 - 2 \cdot b^2$	$2 \cdot b^2 - 2 \cdot a^2$	$0 \leq a \leq b \leq \frac{\sqrt{2}}{2}$

Table 4.1 Parameters of bi-material models

## 4.2 Development of Material Properties for the New Microstructures

Once the geometrical shape of microstructures is defined, the homogenization theory is used to determine the macroscopic mechanical properties of the materials.

In the following sections, the finite element formulae and boundary conditions are used to develop the formulation of homogenized material properties of microstructures. It is followed by the algorithm development for computer implementation.

### 4.2.1 Material properties development

From the homogenization Equations (3.15) and (3.17) in Section 3.13, the homogenized elasticity tensor  $E_{ijkl}^H$  can be expressed as (Hassani and Hinton, 1998; Bendsøe, 1995; and Bendsøe and Sigmund, 2002)

$$E_{ijkl}^H = \frac{1}{|Y|} \int_{\Psi} \left( E_{ijkl} - E_{ijpq} \frac{\partial(\chi_p)_{kl}}{\partial y_q} \right) dY \quad (4.7)$$

with the cell problem given by:

$$\int_{\Psi} E_{ijkl} \frac{\partial(\chi_p)_{kl}}{\partial y_q} \frac{\partial v_i(\mathbf{y})}{\partial y_j} dY = \int_{\Psi} E_{ijkl} \frac{\partial v_i(\mathbf{y})}{\partial y_j} dY \quad \forall \mathbf{v}_i \in \mathbf{V}_{\Psi} \quad (4.8)$$

For a general orthotropic material in two-dimensional problems, the homogenized elasticity tensor  $E_{ijkl}^H$  can be reduced to be  $E_{1111}^H, E_{1122}^H, E_{2222}^H, E_{1212}^H$ . In this case, the values of  $i, j, p, q, k, l$  only need to be set to 1 or 2. The homogenized elasticity tensor  $E_{ijkl}^H$  can be found by investigating four cases:

- **a:**  $i, j, k, l = 1$ , in which we can get  $E_{1111}^H$
- **b:**  $i = j = 1, k = l = 2$ , in which we can get  $E_{1122}^H$
- **c:**  $i, j, k, l = 2$ , in which we can get  $E_{2222}^H$
- **d:**  $i = j = 1, k = 1, l = 2$ , in which we can get  $E_{1212}^H$

**Case a:** ( $i, j, k, l = 1$ )

From Equation (4.7) we have

$$E_{1111}^H = \frac{1}{|Y|} \int_{\Psi} \left( E_{1111} - E_{1111} \frac{\partial(\chi_1)_{11}}{\partial y_1} - E_{1122} \frac{\partial(\chi_2)_{11}}{\partial y_2} \right) dY \quad (4.9)$$

Expanding (4.8) we have

$$\int_Y \left[ \left( E_{1111} \frac{\partial(\chi_1)_{11}}{\partial y_1} + E_{1122} \frac{\partial(\chi_2)_{11}}{\partial y_2} \right) \frac{\partial v_1}{\partial y_1} + E_{1212} \left( \frac{\partial(\chi_1)_{11}}{\partial y_1} + \frac{\partial(\chi_2)_{11}}{\partial y_2} \right) \left( \frac{\partial v_1}{\partial y_2} + \frac{\partial v_2}{\partial y_1} \right) + \left( E_{1122} \frac{\partial(\chi_1)_{11}}{\partial y_1} + E_{2222} \frac{\partial(\chi_2)_{11}}{\partial y_2} \right) \frac{\partial v_2}{\partial y_2} \right] dY = \int_Y \left( E_{1111} \frac{\partial v_1}{\partial y_1} + E_{1122} \frac{\partial v_2}{\partial y_2} \right) dY \quad (4.10)$$

(4.10) can also be written as

$$\int_Y \begin{pmatrix} \frac{\partial v_1}{\partial y_1} \\ \frac{\partial v_2}{\partial y_2} \\ \frac{\partial v_1}{\partial y_2} + \frac{\partial v_2}{\partial y_1} \end{pmatrix}^T \begin{bmatrix} E_{1111} & E_{1122} & 0 \\ E_{1122} & E_{2222} & 0 \\ 0 & 0 & E_{1212} \end{bmatrix} \begin{pmatrix} \frac{\partial(\chi_1)_{11}}{\partial y_1} \\ \frac{\partial(\chi_2)_{11}}{\partial y_2} \\ \frac{\partial(\chi_1)_{11}}{\partial y_1} + \frac{\partial(\chi_2)_{11}}{\partial y_2} \end{pmatrix} dY \quad (4.10)$$

$$= \int_Y \begin{pmatrix} \frac{\partial v_1}{\partial y_1} \\ \frac{\partial v_2}{\partial y_2} \\ \frac{\partial v_1}{\partial y_2} + \frac{\partial v_2}{\partial y_1} \end{pmatrix}^T \begin{pmatrix} E_{1111} \\ E_{1122} \\ 0 \end{pmatrix} dY$$

To make the formulae simpler, defining the function in (4.10) as:

$$\boldsymbol{\varepsilon}(\mathbf{v}) = \begin{pmatrix} \frac{\partial v_1}{\partial y_1} \\ \frac{\partial v_2}{\partial y_2} \\ \frac{\partial v_1}{\partial y_2} + \frac{\partial v_2}{\partial y_1} \end{pmatrix}, \mathbf{D} = (\mathbf{D}_1, \mathbf{D}_2, \mathbf{D}_3) = \begin{bmatrix} E_{1111} & E_{1122} & 0 \\ E_{1122} & E_{2222} & 0 \\ 0 & 0 & E_{1212} \end{bmatrix}, \boldsymbol{\varepsilon}(\boldsymbol{\chi})_{11} = \begin{pmatrix} \frac{\partial(\chi_1)_{11}}{\partial y_1} \\ \frac{\partial(\chi_2)_{11}}{\partial y_2} \\ \frac{\partial(\chi_1)_{11}}{\partial y_1} + \frac{\partial(\chi_2)_{11}}{\partial y_2} \end{pmatrix} \quad (4.11)$$

Then (4.10) can be written as

$$\int_Y \boldsymbol{\varepsilon}^T(\mathbf{v}) \cdot \mathbf{D} \cdot \boldsymbol{\varepsilon}(\boldsymbol{\chi})_{11} dY = \int_Y \boldsymbol{\varepsilon}^T(\mathbf{v}) \cdot \mathbf{D}_1 dY \quad \forall \mathbf{v} \in \mathbf{V}_\Psi \quad (4.12)$$

(4.9) can be expressed as

$$E_{1111}^H = \frac{1}{|Y|} \int_Y \left( E_{1111} - \begin{pmatrix} E_{1111} \\ E_{1122} \\ 0 \end{pmatrix}^T \begin{pmatrix} \frac{\partial(\chi_1)_{11}}{\partial y_1} \\ \frac{\partial(\chi_2)_{11}}{\partial y_2} \\ 0 \end{pmatrix} \right) dY = \frac{1}{|Y|} \int_Y (E_{1111} - \mathbf{D}_1^T \boldsymbol{\varepsilon}(\boldsymbol{\chi})_{11}) dY \quad \forall \mathbf{v} \in \mathbf{V}_\Psi \quad (4.13)$$

In order to solve the Equation (4.13) and get  $E_{1111}^H$ , discretizing the base cell by using the finite element method (Rao, 1999), (4.12) can be expressed as

$$\left( \int_Y \mathbf{B}^T \cdot \mathbf{D} \cdot \mathbf{B} dY \right) \cdot \langle \boldsymbol{\chi} \rangle_{11} = \int_Y \mathbf{B}^T \cdot \mathbf{D}_1 dY \quad (4.14)$$

where  $\mathbf{B} = \mathbf{O} \cdot \mathbf{N}^g$  is the global strain matrix,  $\mathbf{O}$  is the matrix of linear differential operators and  $\mathbf{N}^g$  is global shape function and  $\langle \boldsymbol{\chi} \rangle_{11}$  is discretized function of  $(\boldsymbol{\chi})_{11}$ .

$$\mathbf{O} = \begin{bmatrix} \frac{\partial}{\partial y_1} & 0 \\ 0 & \frac{\partial}{\partial y_2} \\ \frac{\partial}{\partial y_2} & \frac{\partial}{\partial y_1} \end{bmatrix}, \text{ and } \boldsymbol{\varepsilon}(\boldsymbol{\chi})_{11} = \mathbf{O} \cdot \mathbf{N}^g \cdot \langle \boldsymbol{\chi} \rangle_{11} = \mathbf{B} \cdot \langle \boldsymbol{\chi} \rangle_{11},$$

Defining the cell stiffness matrix and force vector as:

$$\mathbf{K} = \int_Y \mathbf{B}^T \cdot \mathbf{D} \cdot \mathbf{B} dY \text{ and } \mathbf{f} = \int_Y \mathbf{B}^T \cdot \mathbf{D}_1 dY \quad (4.15)$$

We can see that (4.15) leads to the well known stiffness equation

$$\mathbf{K}(\chi)_{11} = \mathbf{f} \quad (4.16)$$

If loading is an initial strain  $\varepsilon^0$  in  $x$  direction ( $\varepsilon_{11}^0 = 1, \varepsilon_{12}^0 = 0, \varepsilon_{11}^0 = 0$ ),  $\mathbf{f}$  can be expressed as

$$\mathbf{f} = \int_Y \mathbf{B}^T \cdot \mathbf{D} \cdot \varepsilon^0 dY = \int_Y \mathbf{B}^T \cdot \mathbf{D}_1 dY \quad (4.17)$$

This is exactly equal to the  $\mathbf{f}$  in (4.15). So we can calculate (4.15), (4.16) and (4.11) by giving an initial strain in  $x$  direction and get the  $(\chi)_{11}$  and  $\varepsilon(\chi)_{11}$ . According to (4.13), the first element of the homogenized elasticity tensor  $E_{1111}^H$  can thus be obtained.

**Case b** ( $i = j = 1, k = l = 2$ ):

From (4.7) we can get

$$E_{1122}^H = \frac{1}{|Y|} \int_Y \left( E_{1122} - E_{1111} \frac{\partial(\chi_1)_{22}}{\partial y_1} - E_{1122} \frac{\partial(\chi_2)_{22}}{\partial y_2} \right) dY \quad (4.18)$$

Expanding (4.8), we have

$$\int_Y \left[ \left( E_{1111} \frac{\partial(\chi_1)_{22}}{\partial y_1} + E_{1122} \frac{\partial(\chi_2)_{22}}{\partial y_2} \right) \frac{\partial v_1}{\partial y_1} + E_{1212} \left( \frac{\partial(\chi_1)_{22}}{\partial y_1} + \frac{\partial(\chi_2)_{22}}{\partial y_2} \right) \left( \frac{\partial v_1}{\partial y_2} + \frac{\partial v_2}{\partial y_1} \right) + \left( E_{2211} \frac{\partial(\chi_1)_{22}}{\partial y_1} + E_{2222} \frac{\partial(\chi_2)_{22}}{\partial y_2} \right) \frac{\partial v_2}{\partial y_2} \right] dY = \int_Y \left( E_{1122} \frac{\partial v_1}{\partial y_1} + E_{2222} \frac{\partial v_2}{\partial y_2} \right) dY \quad (4.19)$$

Rearranging (4.19) we can get

$$\begin{aligned}
 & \int_Y \begin{pmatrix} \frac{\partial v_1}{\partial y_1} \\ \frac{\partial v_2}{\partial y_2} \\ \frac{\partial v_1}{\partial y_2} + \frac{\partial v_2}{\partial y_1} \end{pmatrix}^T \begin{bmatrix} E_{1111} & E_{1122} & 0 \\ E_{1122} & E_{2222} & 0 \\ 0 & 0 & E_{1212} \end{bmatrix} \begin{pmatrix} \frac{\partial(\chi_1)_{22}}{\partial y_1} \\ \frac{\partial(\chi_2)_{22}}{\partial y_2} \\ \frac{\partial(\chi_1)_{22}}{\partial y_1} + \frac{\partial(\chi_2)_{22}}{\partial y_2} \end{pmatrix} dY \\
 & = \int_Y \begin{pmatrix} \frac{\partial v_1}{\partial y_1} \\ \frac{\partial v_2}{\partial y_2} \\ \frac{\partial v_1}{\partial y_2} + \frac{\partial v_2}{\partial y_1} \end{pmatrix}^T \begin{pmatrix} E_{1122} \\ E_{2222} \\ 0 \end{pmatrix} dY
 \end{aligned} \tag{4.20}$$

Similarly considering

$$\boldsymbol{\varepsilon}(\mathbf{v}) = \begin{pmatrix} \frac{\partial v_1}{\partial y_1} \\ \frac{\partial v_2}{\partial y_2} \\ \frac{\partial v_1}{\partial y_2} + \frac{\partial v_2}{\partial y_1} \end{pmatrix}, \boldsymbol{\varepsilon}(\boldsymbol{\chi})_{22} = \begin{pmatrix} \frac{\partial(\chi_1)_{22}}{\partial y_1} \\ \frac{\partial(\chi_2)_{22}}{\partial y_2} \\ \frac{\partial(\chi_1)_{22}}{\partial y_1} + \frac{\partial(\chi_2)_{22}}{\partial y_2} \end{pmatrix}, \mathbf{D} = [\mathbf{D}_1 \quad \mathbf{D}_2 \quad \mathbf{D}_3] = \begin{bmatrix} E_{1111} & E_{1122} & 0 \\ E_{1122} & E_{2222} & 0 \\ 0 & 0 & E_{1212} \end{bmatrix} \tag{4.21}$$

Then (4.20) can be written as

$$\int_Y \boldsymbol{\varepsilon}^T(\mathbf{v}) \cdot \mathbf{D} \cdot \boldsymbol{\varepsilon}(\boldsymbol{\chi})_{22} dY = \int_Y \boldsymbol{\varepsilon}^T(\mathbf{v}) \cdot \mathbf{D}_2 dY \quad \forall \mathbf{v} \in \mathbf{V}_\Psi \tag{4.22}$$

(4.18) can be written as

$$E_{1122}^H = \frac{1}{|Y|} \int_Y \left( E_{1122} - \begin{pmatrix} E_{1111} \\ E_{1122} \\ 0 \end{pmatrix}^T \begin{pmatrix} \frac{\partial \chi_1^{22}}{\partial y_1} \\ \frac{\partial(\chi_2)_{22}}{\partial y_2} \\ 0 \end{pmatrix} \right) dY = \frac{1}{|Y|} \int_Y (E_{1122} - \mathbf{D}_1^T \boldsymbol{\varepsilon}(\boldsymbol{\chi})_{22}) dY \quad \forall \mathbf{v} \in \mathbf{V}_\Psi \tag{4.23}$$

By using the finite element method to discretize the base cell, (4.22) can be written

as

$$\int_Y \mathbf{B}^T \cdot \mathbf{D} \cdot \mathbf{B} dY(\boldsymbol{\chi})_{22} = \int_Y \mathbf{B}^T \cdot \mathbf{D}_2 dY \tag{4.24}$$

Where the  $(\chi)_{22}$  is the discretized function of  $(\chi)_{22}$

If we define the stiffness and force vector as

$$\mathbf{K} = \int_Y \mathbf{B}^T \cdot \mathbf{D} \cdot \mathbf{B} dY \text{ and } \mathbf{f} = \int_Y \mathbf{B}^T \cdot \mathbf{D}_2 dY \quad (4.25)$$

We have

$$\mathbf{K}(\chi)_{22} = \mathbf{f} \quad (4.26)$$

Considering an initial strain  $\boldsymbol{\varepsilon}^0$  loading in  $y$  direction ( $\varepsilon_{11}^0 = 0, \varepsilon_{12}^0 = 0, \varepsilon_{22}^0 = 1$ ),  $\mathbf{f}$  can be written as

$$\mathbf{f} = \int_Y \mathbf{B}^T \cdot \mathbf{D} \cdot \boldsymbol{\varepsilon}^0 dY = \int_Y \mathbf{B}^T \cdot \mathbf{D}_2 dY \quad (4.27)$$

This is exactly equal to the  $\mathbf{f}$  in (4.25). Calculating (4.25), (4.26) and (4.21) by given an initial strain in  $y$  direction, the  $(\chi)_{22}$  and  $\boldsymbol{\varepsilon}(\chi)_{22}$  can be obtained. According to (4.18), the elements of the homogenized elasticity tensor  $E_{1122}^H$  can be calculated.

**Case c** ( $i, j, k, l = 2$ ):

In this case, from Equation (4.7), we have:

$$E_{2222}^H = \frac{1}{|Y|} \int_Y \left( E_{2222} - E_{2211} \frac{\partial(\chi_1)_{22}}{\partial y_1} - E_{2222} \frac{\partial(\chi_2)_{22}}{\partial y_2} \right) dY \quad (4.28)$$

This can also be written as:

$$E_{2222}^H = \frac{1}{|Y|} \int_Y \left( E_{2222} - \begin{pmatrix} E_{1122} \\ E_{2222} \\ 0 \end{pmatrix}^T \begin{pmatrix} \frac{\partial(\chi_1)_{22}}{\partial y_1} \\ \frac{\partial(\chi_2)_{22}}{\partial y_2} \\ 0 \end{pmatrix} \right) dY = \frac{1}{|Y|} \int_Y (E_{2222} - \mathbf{D}_2^T \boldsymbol{\varepsilon}(\chi)_{22}) dY \quad \forall \mathbf{v} \in \mathbf{V}_\Psi \quad (4.29)$$

Similar to the case **b**,  $(\chi)_{22}$  and  $\boldsymbol{\varepsilon}(\chi)_{22}$  can be obtained by calculating (4.25), (4.26)

(4.21),. According to (4.29), the elements of the homogenized elasticity tensor  $E_{222}^H$  can be calculated.

**Case d** ( $i = j = 1, k = 1, l = 2$ ):

Expanding (4.8), we have

$$\int_Y \left[ \left( E_{1111} \frac{\partial(\chi_1)_{12}}{\partial y_1} + E_{1122} \frac{\partial(\chi_2)_{12}}{\partial y_2} \right) \frac{\partial v_1}{\partial y_1} + E_{1212} \left( \frac{\partial(\chi_1)_{12}}{\partial y_1} + \frac{\partial(\chi_2)_{12}}{\partial y_2} \right) \left( \frac{\partial v_1}{\partial y_2} + \frac{\partial v_2}{\partial y_1} \right) + \left( E_{1122} \frac{\partial(\chi_1)_{12}}{\partial y_1} + E_{2222} \frac{\partial(\chi_2)_{12}}{\partial y_2} \right) \frac{\partial v_2}{\partial y_2} \right] dY = \int_Y \left( E_{1212} \left( \frac{\partial v_1}{\partial y_1} + \frac{\partial v_2}{\partial y_2} \right) \right) dY \quad (4.30)$$

Considering the Equation (4.7), we can get

$$E_{1212}^H = \frac{1}{|Y|} \int_Y \left( E_{1212} - E_{1212} \frac{\partial(\chi_1)_{12}}{\partial y_2} - E_{1212} \frac{\partial(\chi_2)_{12}}{\partial y_1} \right) dY \quad (4.31)$$

Then Equation (4.30) can be written as

$$\begin{aligned} & \int_Y \begin{pmatrix} \frac{\partial v_1}{\partial y_1} \\ \frac{\partial v_2}{\partial y_2} \\ \frac{\partial v_1}{\partial y_2} + \frac{\partial v_2}{\partial y_1} \end{pmatrix}^T \begin{bmatrix} E_{1111} & E_{1122} & 0 \\ E_{1122} & E_{2222} & 0 \\ 0 & 0 & E_{1212} \end{bmatrix} \begin{pmatrix} \frac{\partial(\chi_1)_{12}}{\partial y_1} \\ \frac{\partial(\chi_2)_{12}}{\partial y_2} \\ \frac{\partial(\chi_1)_{12}}{\partial y_1} + \frac{\partial(\chi_2)_{12}}{\partial y_2} \end{pmatrix} dY \\ &= \int_Y \begin{pmatrix} \frac{\partial v_1}{\partial y_1} \\ \frac{\partial v_2}{\partial y_2} \\ \frac{\partial v_1}{\partial y_2} + \frac{\partial v_2}{\partial y_1} \end{pmatrix}^T \begin{pmatrix} 0 \\ 0 \\ E_{1212} \end{pmatrix} dY \end{aligned} \quad (4.32)$$

Considering

$$\boldsymbol{\varepsilon}(\mathbf{v}) = \begin{pmatrix} \frac{\partial v_1}{\partial y_1} \\ \frac{\partial v_2}{\partial y_2} \\ \frac{\partial v_1}{\partial y_2} + \frac{\partial v_2}{\partial y_1} \end{pmatrix}, \quad \boldsymbol{\varepsilon}(\boldsymbol{\chi})_{12} = \begin{pmatrix} \frac{\partial(\chi_1)_{12}}{\partial y_1} \\ \frac{\partial(\chi_2)_{12}}{\partial y_2} \\ \frac{\partial(\chi_1)_{12}}{\partial y_1} + \frac{\partial(\chi_2)_{12}}{\partial y_2} \end{pmatrix}, \quad \mathbf{D} = [\mathbf{D}_1 \quad \mathbf{D}_2 \quad \mathbf{D}_3] = \begin{bmatrix} E_{1111} & E_{1122} & 0 \\ E_{1122} & E_{2222} & 0 \\ 0 & 0 & E_{1212} \end{bmatrix} \quad (4.33)$$

Then (4.33) can be written as

$$\int_Y \boldsymbol{\varepsilon}^T(\mathbf{v}) \cdot \mathbf{D} \cdot \boldsymbol{\varepsilon}(\boldsymbol{\chi})_{12} dY = \int_Y \boldsymbol{\varepsilon}^T(\mathbf{v}) \cdot \mathbf{D}_3 dY \quad \forall \mathbf{v} \in \mathbf{V}_\Psi \quad (4.34)$$

(4.31) can be written as

$$E_{1212}^H = \frac{1}{|Y|} \int_Y \left( E_{1212} - \begin{pmatrix} 0 \\ 0 \\ E_{1212} \end{pmatrix}^T \begin{pmatrix} 0 \\ 0 \\ \frac{\partial(\chi_1)_{12}}{\partial y_1} + \frac{\partial(\chi_2)_{12}}{\partial y_2} \end{pmatrix} \right) dY = \frac{1}{|Y|} \int_Y (E_{1212} - \mathbf{D}_3^T \boldsymbol{\varepsilon}(\boldsymbol{\chi})_{12}) dY \quad \forall \mathbf{v} \in \mathbf{V}_\Psi \quad (4.35)$$

By using the finite element method to discretize the base cell, (4.34) can be written as

$$\int_Y \mathbf{B}^T \cdot \mathbf{D} \cdot \mathbf{B} dY (\boldsymbol{\chi})_{12} = \int_Y \mathbf{B}^T \cdot \mathbf{D}_3 dY \quad (4.36)$$

Similarly as above, by defining

$$\mathbf{K} = \int_Y \mathbf{B}^T \cdot \mathbf{D} \cdot \mathbf{B} dY \quad \text{and} \quad \mathbf{f} = \int_Y \mathbf{B}^T \cdot \mathbf{D}_3 dY \quad (4.37)$$

We have the stiffness equation as following

$$\mathbf{K} (\boldsymbol{\chi})_{12} = \mathbf{f} \quad (4.38)$$

If we exert an unit initial shear strain  $\boldsymbol{\varepsilon}^0$  loading ( $\varepsilon_{11}^0 = 0, \varepsilon_{22}^0 = 0, \varepsilon_{12}^0 = \frac{1}{2}$ ),

$\mathbf{f}$  can be written as

$$\mathbf{f} = \int_Y \mathbf{B}^T \cdot \mathbf{D} \cdot \boldsymbol{\varepsilon}^0 dY = \int_Y \mathbf{B}^T \cdot \mathbf{D}_3 dY \quad (4.39)$$

This is the same with the Equation (4.37), by calculating (4.37), (4.38) and (4.33) with implying an unit initial shear strain  $\boldsymbol{\varepsilon}^0$  loading and give the displacement  $(\boldsymbol{\chi})_{12}$  and  $\boldsymbol{\varepsilon}(\boldsymbol{\chi})_{12}$ . According to (4.35), the element of the homogenized elasticity tensor  $E_{1212}^H$  can be obtained.

#### 4.2.2 Boundary condition

##### Case a:

In unit cells, the geometry of the cell is symmetric with respect to the axes of symmetry  $x'$  and  $y'$  as illustrated in Figure 4.1. The loading to be imposed in this case is a unit initial strain in the x direction ( $\varepsilon_{11}^0=1$ ,  $\varepsilon_{22}^0=0$ ,  $\varepsilon_{12}^0=0$ ). From the geometry and loading symmetry with respect to  $y'$ , we have

$$u(x^0, y) = -u(x^0 + Y_1, y), \quad (4.40)$$

$$v(x^0, y) = v(x^0 + Y_1, y) \quad (4.41)$$

Similarly with respect to  $x'$ , we have

$$u(x, y^0) = u(x, y^0 + Y_2), \quad (4.42)$$

$$v(x, y^0) = -v(x, y^0 + Y_2) \quad (4.43)$$

From the definition of periodicity, we can get

$$u(x^0, y) = u(x^0 + Y_1, y) = 0, \quad (4.44)$$

$$v(x, y^0) = v(x, y^0 + Y_2) = 0 \quad (4.45)$$

The boundary conditions according to (4.44) and (4.45), are shown in Figure 4.12.

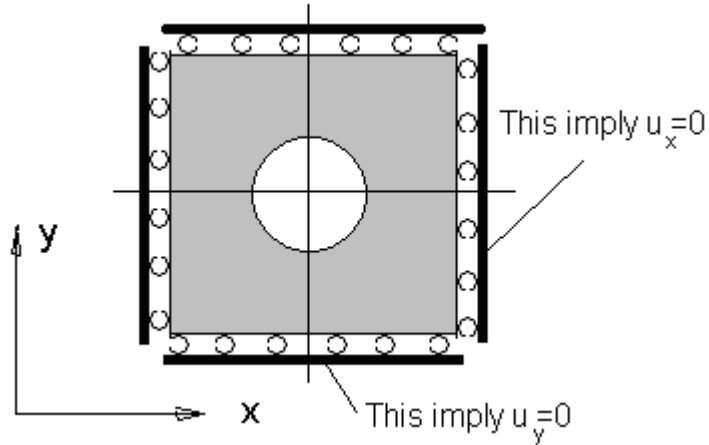


Figure 4.12 Boundary conditions for case a, b and c

**Case b:**

The boundary conditions are the same as Case a. The loading to be imposed in this case is a unit initial strain in the y direction ( $\varepsilon_{11}^0 = 0$ ,  $\varepsilon_{22}^0 = 1$ ,  $\varepsilon_{12}^0 = 0$ ).

**Case c:**

The boundary conditions are the same as Case a. The loading to be imposed in this case is a unit initial strain in the y direction ( $\varepsilon_{11}^0 = 0$ ,  $\varepsilon_{22}^0 = 1$ ,  $\varepsilon_{12}^0 = 0$ ).

**Case d:**

We apply a unit initial shear strain ( $\varepsilon_{11}^0 = 0$ ,  $\varepsilon_{22}^0 = 0$ ,  $2\varepsilon_{12}^0 = 1$ ) with respect to the axes of symmetry  $x'$  and  $y'$  (Figure 4.1). From the anti-symmetry condition, the displacement may be written as

$$u(x^0, y) = u(x^0 + Y_1, y), \quad (4.46)$$

$$v(x^0, y) = -v(x^0 + Y_1, y) \quad (4.47)$$

$$u(x, y^0) = -u(x, y^0 + Y_2), \quad (4.48)$$

$$v(x, y^0) = v(x, y^0 + Y_2) \quad (4.49)$$

Because of periodicity, we can get

$$v(x^0, y) = v(x^0 + Y_1, y) = 0, \quad (4.50)$$

$$u(x, y^0) = u(x, y^0 + Y_2) = 0 \quad (4.51)$$

From (4.50) we can see that for the points located on the left and right hand side edges of the base cell, the vertical displacement is zero. According to (4.51) the nodes located on the bottom and top edges have zero horizontal displacement. These boundary conditions are shown in Figure 4.13.

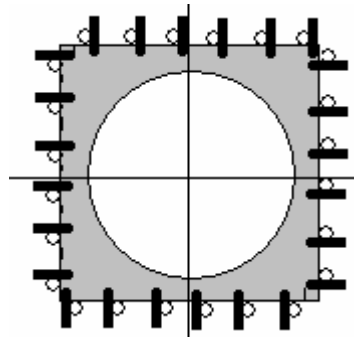


Figure 4.13 Boundary conditions for case d

### 4.2.3 Computer program implementation

A general computer code based on the Strand7 program was written to calculate all new microstructure properties. This computer program can also be applied to existing microstructure models such as triangular microstructure and hexagon microstructure can be calculated. The procedure is shown as following:

*Step 1.* Draw a square or rectangular outside line of the microstructure.

*Step 2.* Draw internal line of the microstructure.

*Step 3.* Apply initial strain loading and boundary constraint in  $x$  direction.

*Step 4.* Discretize the reference domain, and calculate displacement and strain

field by using Strand7 program

- Step 5.* Compute the homogenized values of  $E_{1111}^H$  by formula (4.13)
- Step 6.* Apply initial strain loading and boundary constraint in  $y$  direction.
- Step 7.* Calculate displacement and strain field by using Strand7 program
- Step 8.* Compute the homogenized values of  $E_{1122}^H, E_{2222}^H$  by formula (4.23),(4.29)
- Step 9.* Apply initial shear strain loading and anti-symmetry boundary constraint.
- Step 10.* Calculate displacement and strain field by using Strand7 program
- Step 11.* Compute the homogenized values of  $E_{1212}^H$  by formula (4.35)
- Step 12* Output the all values of homogenization matrix
- Step 13* Check the number of the times of internal size changing, if it is not active, continue, otherwise stop.
- Step 14* Resize the internal boundary line of the microstructure, go to step 3

The algorithm for one-material model and bi-material model are shown in Figure 4.14 and Figure 4.15 respectively.

By using the finite element analysis and boundary conditions defined above, the element of the elasticity matrix can be expressed as polynomials of the homogenized values with different void sizes of microstructures for given material properties. The Figure 4.16 shows polynomials of  $E_{1111}^H, E_{1122}^H, E_{2222}^H$  and  $E_{1212}^H$  for cross shape model with material properties of  $\nu = 0.3, \frac{E}{1-\nu^2} = 1$ . It should be noted that different material properties would result in different polynomials at microstructure level.

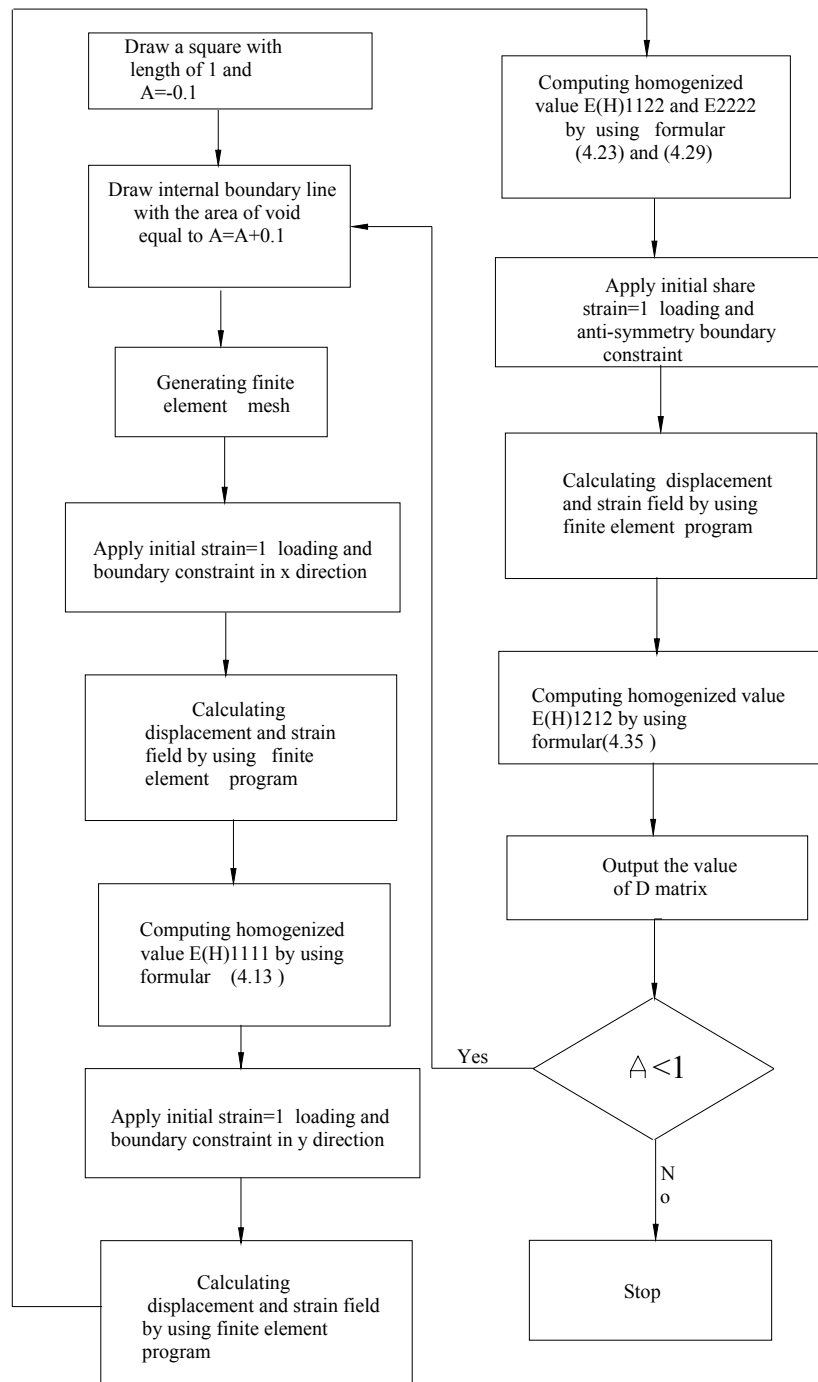


Figure 4.14 Algorithm for one-material model

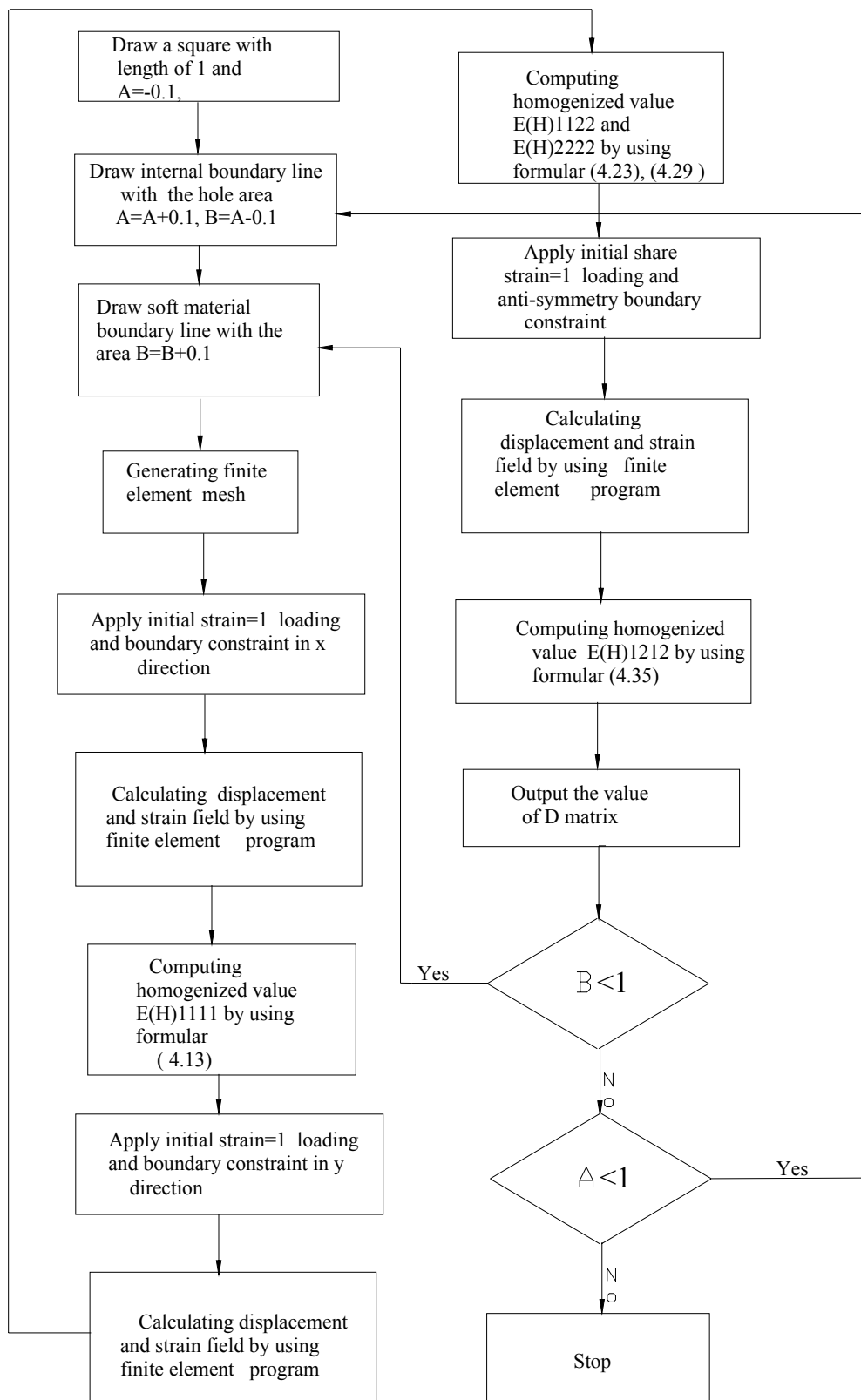


Figure 4.15 Algorithm for bi-material model

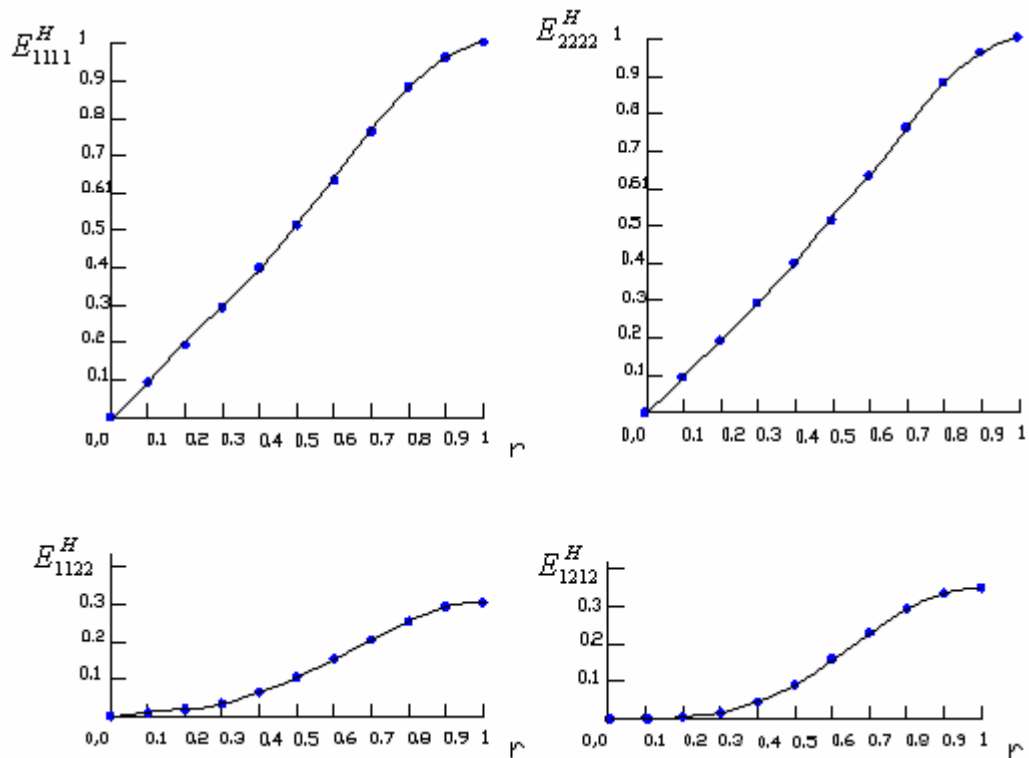


Figure 4.16 Polynomials for homogenized elasticity tensors in terms of void sizes for Cross shape model.

### 4.3 Summary

In this section, a new class of microstructure has been defined. By using the new concept, circular and cross shape microstructures were studied. Two new types of microstructures, multi-void microstructures and bi-material microstructures have been developed. The homogenization theory is used to determine the macroscopic mechanical properties of the materials. Finite element formulae and boundary conditions for the new microstructure models are given. All new microstructures will be used for structural topology optimization problems as presented in later chapters.

## **Chapter 5**

---

# **OPTIMIZATION APPROACH**

This chapter presents the implementation of the topology optimization procedures by using homogenization method. The theoretical aspect for the problem statement is described, the optimality criteria using Kuhn-Tucker conditions are formulated for new microstructures and some existing microstructures for which the microstructure formulation and optimization program have not been available in literature. These criteria are very essential in formulating scheme of updating the design variables in the process of optimization. As mentioned previously it is these criteria that make the optimization approach vigorous and ensure its convergence. The determination of the optimal orientation by using the principal stress method is presented. A measure for checkerboard pattern control is developed. The topology optimization computer program for new microstructures and existing microstructures including homogenization and finite element solver is written and a software named HDM (Homogenization with Different Microstructures) is developed to implement the topology optimization by homogenization method.

## 5.1 Optimality Conditions for Different Microstructure Models

A very important task for structural topology optimization is to find a structure with maximum stiffness for a fixed amount of material. In the general linear elasticity problems, the structure should have minimum mean compliance with respect to displacements or design variables. From Section 3.14, we know that in optimal design for minimum compliance problem, the topology optimization problem can be described as (Bendsøe, 1995):

$$\begin{aligned} & \underset{\mathbf{u} \in \mathbf{V}}{\text{minimize}} \quad L(\mathbf{u}) \\ & \text{such that: } a(\mathbf{u}, \mathbf{v}) = L(\mathbf{v}), \text{ for all } \mathbf{v} \in \mathbf{V} \\ & E_{ijkl} \in E_{ad} \end{aligned} \quad (5.1)$$

where  $a(\mathbf{u}, \mathbf{v})$  and  $L(\mathbf{v})$  are respectively the energy bilinear form for the internal work and the load linear form described before,  $L(\mathbf{u})$  is the mean compliance,  $\mathbf{V}$  denoting the space of kinematically admissible displacement field.

If the structure is fixed on the boundary  $\Gamma_d$ , by choosing  $\mathbf{u} \in \mathbf{V}$  instead of  $\mathbf{v}$  in (5.1), the following equation is obtained.

$$a(\mathbf{u}, \mathbf{u}) = L(\mathbf{u})$$

As the strain energy is equal to  $\frac{1}{2}a(\mathbf{u}, \mathbf{u})$ , the structure with minimum mean compliance with respect to displacements or design variables is equivalent to that with minimum strain energy.

As we know that the total potential energy with respect to displacements or design variables is defined as:

$$\Pi(\mathbf{u}) = \frac{1}{2} a(\mathbf{u}, \mathbf{u}) - L(\mathbf{u})$$

where  $\frac{1}{2} a(\mathbf{u}, \mathbf{u})$  is the strain energy and  $L(\mathbf{u})$  is the mean compliance.

The total potential energy is also equivalent to the maximum total potential energy with respect to displacements or design variables (Hassani and Hinton, 1998).

In the general linear elasticity problems, the structure should have maximum total potential energy with respect to displacements or design variables.

By discretizing the reference domain using a finite element mesh, the optimality conditions for optimization problems can be stated as

$$\begin{aligned} \text{Maximize}_{x_i^g, \theta^g (g=1, \dots, m)} \quad \Pi(u) &= \frac{1}{2} \sum_{g=1}^m \int_{\Omega^g} \boldsymbol{\varepsilon}^T(\mathbf{u}) \mathbf{D}^g \boldsymbol{\varepsilon}(\mathbf{u}) d\Omega - \sum_{g=1}^m \int_{\Omega^g} \mathbf{u}^T \mathbf{f} d\Omega - \sum_{g=1}^m \int_{\Omega^g} \mathbf{u}^T \mathbf{t} d\Gamma \\ \text{Such that} \quad \sum_{g=1}^m (\alpha(x_i^g) \Omega^g) - \Omega_u &\leq 0 \\ x_i^l &\leq x_i^g \leq x_i^u, \quad i = 1, 2, 3, \dots, n, \quad g = 1, 2, \dots, m \end{aligned} \quad (5.2)$$

where  $x_i^g$  is design variable,  $n$  is the number of design variables,  $x_i^l$  and  $x_i^u$  are lower and upper limit of  $x_i^g$ ,  $\theta^g$  is orientation variable,  $\alpha(x_i^g)$  is solid part shape function,  $\Omega^g$  is the volume of the element  $g$ ,  $m$  is the number of elements,  $\sum_{g=1}^m (\alpha(x_i^g) \Omega^g)$  is the volume of the solid part and  $\Omega_u$  is the upper

limit on volume of solid material.

The tool for searching for the optimum of a structure here is using Kuhn-Tucker conditions. As described in Chapter 2, the Kuhn-Tucker conditions is a rigorous mathematical statement. It is one of the basic theories for non-linear optimization programming. For a convex minimization problem, the necessary Kuhn-tucker conditions are also sufficient. A local minimum is also the global one (Hassani and Hinton, 1998). In the following section, we will detail the formulae.

### **5.1.1 Kuhn-Tucker conditions**

From Chapter 2, we know that in Kuhn-Tucker conditions, the inequality constraints are transformed into equality constraints by adding slack variables  $t_k^2$ . In this case, the inequality constraints in Equation (2.1) can be written as

$$g_k(\mathbf{x}) + t_k^2 = 0, \quad k = 1, 2, 3, \dots, n_g \quad (5.3)$$

Here, we use  $F(x)$  to indicate the objective function in the formulation (5.2), in which

$$F(\mathbf{x}) = \Pi(\mathbf{u}) = \frac{1}{2} \sum_{g=1}^m \int_{\Omega^g} \boldsymbol{\varepsilon}^T(\mathbf{u}) \mathbf{D}^g \boldsymbol{\varepsilon}(\mathbf{u}) d\Omega - \sum_{g=1}^m \int_{\Omega^g} \mathbf{u}^T \mathbf{f} d\Omega - \sum_{g=1}^m \int_{\Omega^g} \mathbf{u}^T \mathbf{t} d\Gamma \quad (5.4)$$

and  $g_k(x_i)$  indicate all the inequality constraints in the formulation (5.2).

Then we can define the new Lagrangian function as

$$L(\mathbf{x}, s, \boldsymbol{\lambda}) = F(\mathbf{x}) + \sum_{k=1}^{n_g} \lambda_k (g_k(x_i) + t_k^2) \quad (5.5)$$

Differentiating the Lagrangian function (5.5) with respect to  $\mathbf{x}$ ,  $t$ , and  $\boldsymbol{\lambda}$ , we obtain,

$$\frac{\partial L}{\partial x_i^*} = \frac{\partial F}{\partial x_i^*} + \sum_{k=1}^{n_g} \lambda_k \frac{g_k(x_i^*)}{\partial x_i^*} = 0, \quad i = 1, 2, \dots, n \quad (5.6)$$

$$g_k(x_i^*) + t_k^2 = 0 \quad k = 1, 2, \dots, n_g \quad (5.7)$$

$$\frac{\partial L}{\partial \lambda_k} = \frac{\partial L}{\partial t_k} = 2\lambda_k t_k = 0 \quad k = 1, 2, \dots, n_g \quad (5.8)$$

From (5.7) and (5.8) we can get

$$\begin{aligned} g_k(x_i^*) &\leq 0, & k = 1, 2, \dots, n_g \\ \lambda_k g_k(x_i^*) &= 0, & k = 1, 2, \dots, n_g \end{aligned} \quad (5.9)$$

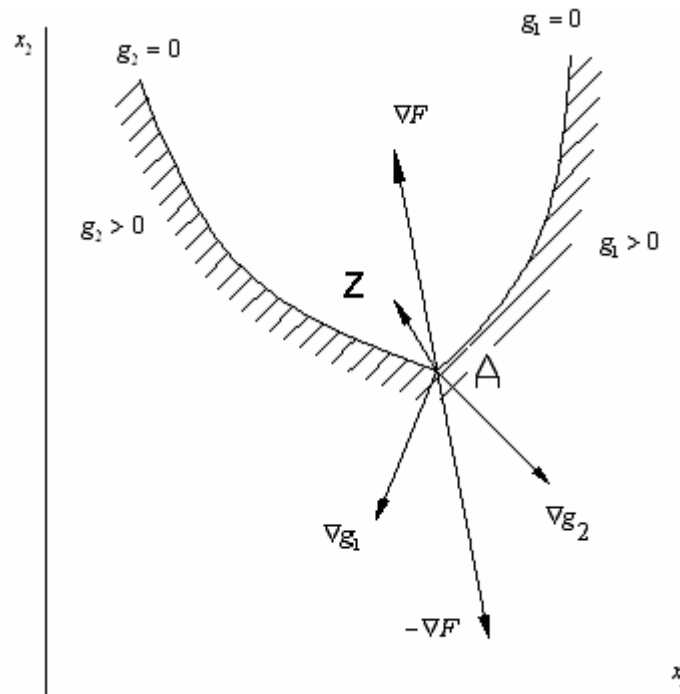


Figure 5.1 Geometrical interpretation of Kuhn-Tucker condition

A geometrical interpretation of the Kuhn-Tucker conditions is illustrated in Figure 5.1 for the case of two constraints.  $\nabla g_1$  and  $\nabla g_2$  denote the gradients of the two constraints, for example, which are orthogonal to the respective constraint surfaces. The vector  $s$  shows a typical feasible direction which does

not lead immediately to any constraint violation. Equation (5.6) can be written as

$$\nabla F = -(\lambda_1 \nabla g_1 + \lambda_2 \nabla g_2) \quad (5.10)$$

Assume that we want to determine whether point A is a minimum or not. To improve the design we need to proceed from point A in a direction  $s$  that is usable and feasible. For the direction to be usable, a small move along this direction should decrease the objective function. To be feasible,  $s$  should form an obtuse angle with  $\nabla g_1$  and  $\nabla g_2$ . To be a direction of decreasing  $F$  it must form an acute angle with  $\nabla F$ . Clearly from Figure 5.1, any vector which forms an acute angle with  $\nabla F$  will also form an obtuse angle with either  $\nabla g_1$  or  $\nabla g_2$ . Thus, the Kuhn-Tucker conditions mean that no feasible design with reduced objective function is to be found in the neighbourhood of A. Mathematically, the condition that a direction  $z$  be feasible is written as

$$z^T \nabla g_k(x_i^*) \leq 0 \quad (5.11)$$

The condition for a usable direction (one that decreases the objective function) is

$$z^T (-\nabla F) > 0 \quad (5.12)$$

Multiplying the equation (5.10) by  $s_k$  and summing over  $k$  we obtain

$$z^T (-\nabla F) = \sum_{k=1}^{n_g} \lambda_k z^T \nabla g_k(x_i^*) \quad (5.13)$$

Consider (5.11), (5.12) and (5.13), it is impossible if  $\lambda_k \geq 0$ .

For general optimization problems with inequality constraints, the Kuhn-Tucker conditions are a necessary condition. In these cases, we need to compare the entire set of local minimum and find the global one. For a convex minimum problem, the necessary Kuhn-tucker conditions are also sufficient, any local minimum is also the global one.

### 5.1.2 Updating design variables

Introducing multiplier  $\lambda_{i1}^g, \lambda_{i2}^g$  and  $\lambda$  ( $g=1,2,\dots,m$ ), the Lagrangian function L to the problem (5.2) may be expressed as

$$L = \frac{1}{2} \sum_{g=1}^m \int_{\Omega^g} \boldsymbol{\varepsilon}^T(\mathbf{u}) \mathbf{D}^g \boldsymbol{\varepsilon}(\mathbf{u}) d\Omega - \sum_{g=1}^m \int_{\Omega^g} \mathbf{u}^T \mathbf{f} d\Omega - \sum_{g=1}^m \int_{\Omega^g} \mathbf{u}^T \mathbf{t} d\Gamma - \lambda \left( \sum_{g=1}^m (\alpha(x_i^g) \Omega^g) - \Omega_u \right) - \sum_{g=1}^m \lambda_{i1}^g (x_i^l - x_i^g) - \sum_{g=1}^m \lambda_{i2}^g (x_i^g - x_i^u) \quad i=1,2,3,\dots,n, \quad g=1,2,\dots,m \quad (5.14)$$

Differentiating the Lagrangian function (5.14) with respect to  $x_i^g$ , we can get

$$\frac{1}{2} \sum_{g=1}^m \int_{\Omega^g} \boldsymbol{\varepsilon}^T(\mathbf{u}) \frac{\partial \mathbf{D}^g}{\partial x_i^g} \boldsymbol{\varepsilon}(\mathbf{u}) d\Omega - \sum_{g=1}^m \int_{\Omega^g} \mathbf{u}^T \frac{\partial \mathbf{f}}{\partial x_i^g} d\Omega - \lambda \frac{\partial \alpha(x_i^g)}{\partial x_i^g} \Omega^g + \lambda_{i1}^g - \lambda_{i2}^g = 0 \quad (5.15)$$

Let:

$$\varphi = \frac{\frac{1}{2} \sum_{g=1}^m \int_{\Omega^g} \boldsymbol{\varepsilon}^T(\mathbf{u}) \frac{\partial \mathbf{D}^g}{\partial x_i^g} \boldsymbol{\varepsilon}(\mathbf{u}) d\Omega - \sum_{g=1}^m \int_{\Omega^g} \mathbf{u}^T \frac{\partial \mathbf{f}}{\partial x_i^g} d\Omega}{\lambda \frac{\partial \alpha(x_i^g)}{\partial x_i^g} \Omega^g} \quad (5.16)$$

According to equation (5.15)

$$\varphi = 1 + \frac{\lambda_{i2}^g - \lambda_{i1}^g}{\lambda \frac{\partial \alpha(x_i^g)}{\partial x_i^g} \Omega^g} \quad (5.17)$$

- If  $\lambda \frac{\partial \alpha(x_i^g)}{\partial x_i^g} \Omega^g > 0$ , in the  $k$ th iteration, the design variable  $x_i^g$  has

been increased towards the optimum point, here  $x_i^g > x_i^l$  and lower side limit is not active, therefore,  $\lambda_{i1}^g = 0$ . Because of  $\lambda_{i2}^g \geq 0$ , from (5.17) it follows that  $\varphi \geq 1$ . On the other hand, when we decrease  $x_i^g$ , we will get  $\varphi \leq 1$ .

It follows that if  $\varphi > 1$ , then we let  $x_i^g$  increase by a small value  $\eta$ . If  $\varphi \leq 1$ , then we let  $x_i^g$  decrease by a small value  $\eta$ . Based on this conclusion, we calculate the value  $\varphi$  by using (5.17). We update design variables using following formulae (Bendsøe, 1995):

$$(x_i^g)_{k+1} = \begin{cases} \max \{ (1-\eta)(x_i^g)_k, x_{\min} \} & \text{if } \varphi_i \leq \max \{ 1-\eta, x_{\min} \} \\ \min \{ (1+\eta)(x_i^g)_k, 1 \}, & \text{if } \varphi_i \geq \min \{ 1+\eta, 1 \} \\ (x_i^g)_k \cdot \varphi_i & \text{otherwise} \end{cases} \quad (5.18)$$

- If  $\lambda \frac{\partial \alpha(x_i^g)}{\partial x_i^g} \Omega^g < 0$ , in an iteration  $k$ , the design variable  $x_i^g$  has been decreased towards the optimum point. In this case  $x_i^g < x_i^u$  and upper limit is not active, therefore,  $\lambda_{i2}^g = 0$ . Because of  $\lambda_{i1}^g \geq 0$ , from (5.17) it follows that  $\varphi \geq 1$ . On the other hand, when we increase  $x_i^g$ , we will get  $\varphi \leq 1$ .

It follows that If  $\varphi > 1$ , then we let  $x_i^g$  decrease by a small value  $\eta$ . If  $\varphi \leq 1$ , then we let  $x_i^g$  increase by a small value  $\eta$ . We then update design variables using following formulae:

$$x_{i+1}^g = \begin{cases} \min \{ (1+\eta)x_i^g, 1 \} & \text{if } \varphi_i \leq \max \{ 1-\eta, x_{\min} \} \\ \max \{ (1-\eta)x_i^g, x_{\min} \}, & \text{if } \varphi_i \geq \min \{ 1+\eta, 1 \} \\ r_i^g \cdot \varphi_i & \text{otherwise} \end{cases} \quad (5.19)$$

### 5.1.3 Optimality conditions for new microstructure models

#### 5.1.3.1 One-material models

##### Cross shape microstructure

For cross shape (Figure 4.9) model, the optimality conditions can be expressed as

$$\begin{aligned} \text{Maximize}_{\gamma^g, \theta^g (g=1, \dots, m)} \quad & \Pi(\mathbf{u}) = \frac{1}{2} \sum_{g=1}^m \int_{\Omega^g} \boldsymbol{\varepsilon}^T(\mathbf{u}) \mathbf{D}^g \boldsymbol{\varepsilon}(\mathbf{u}) d\Omega - \sum_{g=1}^m \int_{\Omega^g} \mathbf{u}^T \mathbf{f} d\Omega - \sum_{g=1}^m \int_{\Omega^g} \mathbf{u}^T \mathbf{t} d\Gamma \\ \text{Such that} \quad & \sum_{g=1}^m 4(2r^g - r^{g2}) \Omega^g - \Omega_s \leq 0 \\ & r^g - 1 \leq 0 \quad \quad \quad g = 1, 2, \dots, m \\ & -r^g \leq 0 \quad \quad \quad g = 1, 2, \dots, m \end{aligned} \quad (5.20)$$

Introducing multipliers  $\lambda$  and  $\lambda_1^g, \lambda_2^g$  ( $g = 1, 2, \dots, m$ ), the Lagrangian function L to the problem (5.20) may be expressed as

$$\begin{aligned} L = \Pi(\mathbf{u}) = & \frac{1}{2} \sum_{g=1}^m \int_{\Omega^g} \boldsymbol{\varepsilon}^T(\mathbf{u}) \mathbf{D}^g \boldsymbol{\varepsilon}(\mathbf{u}) d\Omega - \sum_{g=1}^m \int_{\Omega^g} \mathbf{u}^T \mathbf{f} d\Omega - \sum_{g=1}^m \int_{\Omega^g} \mathbf{u}^T \mathbf{t} d\Gamma \\ & - \lambda \left( \sum_{g=1}^m 4(2r^g - r^{g2}) \Omega^g - \Omega_s \right) - \sum_{g=1}^m \lambda_1^g (-r^g) - \sum_{g=1}^m \lambda_2^g (r^g - 1) \end{aligned} \quad (5.21)$$

Differentiating the Lagrangian function (5.21) with respect to  $r^g$ , we can get

$$\begin{aligned} & \frac{1}{2} \int_{\Omega^g} \boldsymbol{\varepsilon}^T(\mathbf{u}) \frac{\partial \mathbf{D}^g}{\partial r^g} \boldsymbol{\varepsilon}(\mathbf{u}) d\Omega - \int_{\Omega^g} \mathbf{u}^T \frac{\partial \mathbf{f}}{\partial r^g} d\Omega \\ & - 8\lambda(1-r^g)\Omega^g + \lambda_1^g - \lambda_2^g = 0, \quad (g = 1, 2, \dots, m) \end{aligned} \quad (5.22)$$

Using Kuhn-Tucker conditions, we have

$$\sum_{g=1}^m 4(2r^g - r^{g^2})\Omega^g - \Omega_s \leq 0 \quad (5.23)$$

$$-r^g \leq 0 \quad (5.24)$$

$$r^g - 1 \leq 0 \quad (5.25)$$

$$\lambda \left( \sum_{g=1}^m 4(2r^g - r^{g^2})\Omega^g - \Omega_s \right) = 0 \quad (5.26)$$

$$\lambda_1^g (-r^g) = 0 \quad (5.27)$$

$$\lambda_2^g (r^g - 1) = 0 \quad (5.28)$$

$$\lambda \geq 0 \quad (5.29)$$

$$\lambda_1^g \geq 0 \quad g = 1, 2, \dots, m \quad (5.30)$$

$$\lambda_2^g \geq 0 \quad g = 1, 2, \dots, m \quad (5.31)$$

If defining

$$\varphi = \frac{\frac{1}{2} \int_{\Omega^g} \boldsymbol{\varepsilon}^T(\mathbf{u}) \frac{\partial \mathbf{D}^g}{\partial r^g} \boldsymbol{\varepsilon}(\mathbf{u}) d\Omega - \int_{\Omega^g} \mathbf{u}^T \frac{\partial \mathbf{f}}{\partial r^g} d\Omega}{8\lambda(1-r^g)\Omega^g} \quad (5.32)$$

According to (5.22), we have

$$\varphi = 1 + \frac{1}{8\lambda(1-r^g)\Omega^g} (\lambda_2^g - \lambda_1^g) \quad (5.33)$$

Update the design variable as follows:

$$r_{i+1}^g = \begin{cases} \max \left\{ (1-\eta)r_i^g, x_{\min} \right\} & \text{if } \varphi_i \leq \max \{1-\eta, x_{\min}\} \\ \min \left\{ (1+\eta)r_i^g, 1 \right\}, & \text{if } \varphi_i \geq \min \{1+\eta, 1\} \\ r_i^g \cdot \varphi_i & \text{otherwise} \end{cases} \quad (5.34)$$

### Circular microstructure

For circular model (Figure 4.6-4.8), the optimality conditions can be expressed as follows:

$$\begin{aligned} \text{Maximize}_{\gamma^g, \theta^g (g=1, \dots, m)} \quad & \Pi(\mathbf{u}) = \frac{1}{2} \sum_{g=1}^m \int_{\Omega^g} \boldsymbol{\varepsilon}^T(\mathbf{u}) \mathbf{D}^g \boldsymbol{\varepsilon}(\mathbf{u}) d\Omega - \sum_{g=1}^m \int_{\Omega^g} \mathbf{u}^T \mathbf{f} d\Omega - \sum_{g=1}^m \int_{\Omega^g} \mathbf{u}^T \mathbf{t} d\Gamma \\ \text{Such that} \quad & \sum_{g=1}^m (4 - \pi r^{g2}) \Omega^g - \Omega_s \leq 0 && \text{if } 0 \leq r \leq \frac{1-\delta}{\sqrt{2}} \\ & \sum_{g=1}^m \left( 1 - \left( \int_0^{\sqrt{2r^2-(1-\delta)^2}} (1-\delta) dx + \int_{\sqrt{2r^2-(1-\delta)^2}}^{1-\delta} \sqrt{2r^2-x^2} dx \right) \right) \Omega^g - \Omega_s \leq 0 && \text{if } \frac{1-\delta}{\sqrt{2}} < r < 1-\delta \\ & \sum_{g=1}^m (1 - r^{g2}) \Omega^g - \Omega_s \leq 0 && \text{if } 1-\delta \leq r \leq 1 \\ & r^g - 1 \leq 0 && g = 1, 2, \dots, m \\ & -r^g \leq 0 && g = 1, 2, \dots, m \end{aligned} \quad (5.35)$$

Defining

$$\varpi = \int_0^{\sqrt{2r^2-(1-\delta)^2}} (1-\delta) dx + \int_{\sqrt{2r^2-(1-\delta)^2}}^{1-\delta} \sqrt{2r^2-x^2} dx \quad (5.36)$$

Introducing multipliers  $\lambda_1^g, \lambda_2^g$  and  $\lambda$  ( $g = 1, 2, \dots, m$ ), the Lagrangian function L to the problem (5.35) can be conducted as

$$\begin{aligned}
 L = \Pi(\mathbf{u}) &= \frac{1}{2} \sum_{g=1}^m \int_{\Omega^g} \boldsymbol{\varepsilon}^T(\mathbf{u}) \mathbf{D}^g \boldsymbol{\varepsilon}(\mathbf{u}) d\Omega - \sum_{g=1}^m \int_{\Omega^g} \mathbf{u}^T \mathbf{f} d\Omega - \sum_{g=1}^m \int_{\Omega^g} \mathbf{u}^T \mathbf{t} d\Gamma \\
 &- \lambda \left( \sum_{e=1}^m (4 - \pi r^{e2}) \Omega^e - \Omega_s \right) - \sum_{g=1}^m \lambda_1^g (-r^g) - \sum_{g=1}^m \lambda_2^g (r^g - 1) \quad \text{if } 0 \leq r \leq \frac{1-\delta}{\sqrt{2}}
 \end{aligned} \tag{5.37}$$

$$\begin{aligned}
 L = \Pi(\mathbf{u}) &= \frac{1}{2} \sum_{g=1}^m \int_{\Omega^g} \boldsymbol{\varepsilon}^T(\mathbf{u}) \mathbf{D}^g \boldsymbol{\varepsilon}(\mathbf{u}) d\Omega - \sum_{g=1}^m \int_{\Omega^g} \mathbf{u}^T \mathbf{f} d\Omega - \sum_{g=1}^m \int_{\Omega^g} \mathbf{u}^T \mathbf{t} d\Gamma \\
 &- \lambda \left( \sum_{g=1}^m (1 - \varpi) \Omega^g - \Omega_s \right) - \sum_{g=1}^m \lambda_1^g (-r^g) - \sum_{g=1}^m \lambda_2^g (r^g - 1) \quad \text{if } \frac{1-\delta}{\sqrt{2}} < r < 1 - \delta
 \end{aligned} \tag{5.38}$$

$$\begin{aligned}
 L = \Pi(\mathbf{u}) &= \frac{1}{2} \sum_{g=1}^m \int_{\Omega^g} \boldsymbol{\varepsilon}^T(\mathbf{u}) \mathbf{D}^g \boldsymbol{\varepsilon}(\mathbf{u}) d\Omega - \sum_{g=1}^m \int_{\Omega^g} \mathbf{u}^T \mathbf{f} d\Omega - \sum_{g=1}^m \int_{\Omega^g} \mathbf{u}^T \mathbf{t} d\Gamma \\
 &- \lambda \left( \sum_{g=1}^m (1 - r^{g2}) \Omega^g - \Omega_s \right) - \sum_{g=1}^m \lambda_1^g (-r^g) - \sum_{e=1}^m \lambda_2^e (r^e - 1) \quad \text{if } 1 - \delta \leq r \leq 1
 \end{aligned} \tag{5.39}$$

In the equation (5.37),  $0 \leq r \leq \frac{1-\delta}{\sqrt{2}}$ , the upper side constraint for  $r^g$  are not active, then  $\lambda_2^g = 0$ . In the equation (5.38),  $\frac{1-\delta}{\sqrt{2}} < r < 1 - \delta$ , the lower and upper side constraint for  $r^g$  are not active, then  $\lambda_1^g = \lambda_2^g = 0$ . In the equation (5.39),  $1 - \delta \leq r \leq 1$ , the lower side constraint for  $r^g$  are not active, then  $\lambda_1^g = 0$ .

Differentiating the Lagrangian function (5.37) with respect to  $r^g$ , we can get

$$\begin{aligned}
 &\frac{1}{2} \int_{\Omega^g} \boldsymbol{\varepsilon}^T(\mathbf{u}) \frac{\partial \mathbf{D}^g}{\partial r^g} \boldsymbol{\varepsilon}(\mathbf{u}) d\Omega - \int_{\Omega^g} \mathbf{u}^T \frac{\partial \mathbf{f}}{\partial r^g} d\Omega \\
 &+ 2\lambda\pi r^{g2} \Omega^g + \lambda_1^g = 0, \quad (g = 1, 2, \dots, m)
 \end{aligned} \tag{5.40}$$

Differentiating the Lagrangian function (5.38) with respect to  $r^g$ , we can get

$$\begin{aligned} & \frac{1}{2} \int_{\Omega^g} \boldsymbol{\varepsilon}^T(\mathbf{u}) \frac{\partial \mathbf{D}^g}{\partial r^g} \boldsymbol{\varepsilon}(\mathbf{u}) d\Omega - \int_{\Omega^g} \mathbf{u}^T \frac{\partial \mathbf{f}}{\partial r^g} d\Omega \\ & + \lambda \Omega^g \frac{\partial \bar{\varpi}}{\partial r^g} = 0, \quad (g = 1, 2, \dots, m) \end{aligned} \quad (5.41)$$

Differentiating the Lagrangian function (5.39) with respect to  $r^g$ , we can get

$$\begin{aligned} & \frac{1}{2} \int_{\Omega^g} \boldsymbol{\varepsilon}^T(\mathbf{u}) \frac{\partial \mathbf{D}^g}{\partial r^g} \boldsymbol{\varepsilon}(\mathbf{u}) d\Omega - \int_{\Omega^g} \mathbf{u}^T \frac{\partial \mathbf{f}}{\partial r^g} d\Omega \\ & + 2\lambda r^g \Omega^g - \lambda_2^g = 0, \quad (g = 1, 2, \dots, m) \end{aligned} \quad (5.42)$$

By defining

$$\begin{aligned} \varphi &= \frac{\frac{1}{2} \int_{\Omega^g} \boldsymbol{\varepsilon}^T(\mathbf{u}) \frac{\partial \mathbf{D}^g}{\partial r^g} \boldsymbol{\varepsilon}(\mathbf{u}) d\Omega - \int_{\Omega^g} \mathbf{u}^T \frac{\partial \mathbf{f}}{\partial r^g} d\Omega}{-2\pi\lambda r^g \Omega^g} \quad \text{when } 1 < r \leq \frac{1-\delta}{\sqrt{2}} \\ \varphi &= \frac{\frac{1}{2} \int_{\Omega^g} \boldsymbol{\varepsilon}^T(\mathbf{u}) \frac{\partial \mathbf{D}^g}{\partial r^g} \boldsymbol{\varepsilon}(\mathbf{u}) d\Omega - \int_{\Omega^g} \mathbf{u}^T \frac{\partial \mathbf{f}}{\partial r^g} d\Omega}{-\lambda \Omega^g \frac{\partial \bar{\varpi}}{\partial r^g}} \quad \text{when } \frac{1-\delta}{\sqrt{2}} < r < 1-\delta \\ \varphi &= \frac{\frac{1}{2} \int_{\Omega^g} \boldsymbol{\varepsilon}^T(\mathbf{u}) \frac{\partial \mathbf{D}^g}{\partial r^g} \boldsymbol{\varepsilon}(\mathbf{u}) d\Omega - \int_{\Omega^g} \mathbf{u}^T \frac{\partial \mathbf{f}}{\partial r^g} d\Omega}{-2\lambda r^g \Omega^g} \quad \text{when } 1-\delta \leq r \leq 1 \end{aligned} \quad (5.43)$$

We can update design variables by the following formula:

$$r_{i+1}^g = \begin{cases} \min\{(1+\eta)r_i^g, 1\} & \text{if } \varphi_i \leq \max\{1-\eta, x_{\min}\} \\ \max\{(1-\eta)r_i^g, x_{\min}\}, & \text{if } \varphi_i \geq \min\{1+\eta, 1\} \\ r_i^g \cdot \varphi_i & \text{otherwise} \end{cases} \quad (5.44)$$

### Multi-void microstructures

*Triangular multi-void microstructure* (Figure 4.10 (a)):

The optimality conditions can be expressed as

$$\begin{aligned}
 & \underset{a^g, \theta^g (g=1, \dots, m)}{\text{Maximize}} \quad \Pi(\mathbf{u}) = \frac{1}{2} \sum_{g=1}^m \int_{\Omega^g} \boldsymbol{\varepsilon}^T(\mathbf{u}) \mathbf{D}^g \boldsymbol{\varepsilon}(\mathbf{u}) d\Omega - \sum_{g=1}^m \int_{\Omega^g} \mathbf{u}^T \mathbf{f} d\Omega - \sum_{g=1}^m \int_{\Omega^g} \mathbf{u}^T \mathbf{t} d\Gamma \\
 & \text{Such that} \quad \sum_{g=1}^m (1 - 2a^{g^2}) \Omega^g - \Omega_s \leq 0 \\
 & \quad a^g - \frac{\sqrt{2}}{2} \leq 0 \quad g = 1, 2, \dots, m \\
 & \quad -a^g \leq 0 \quad g = 1, 2, \dots, m
 \end{aligned} \tag{5.45}$$

Introducing multipliers  $\lambda_{a1}^g, \lambda_{a2}^g$  and  $\lambda$  ( $g = 1, 2, \dots, m$ ), using Lagrangian function and defining

$$\varphi = \frac{\frac{1}{2} \int_{\Omega^g} \boldsymbol{\varepsilon}^T(\mathbf{u}) \frac{\partial \mathbf{D}^g}{\partial a^g} \boldsymbol{\varepsilon}(\mathbf{u}) d\Omega - \int_{\Omega^g} \mathbf{u}^T \frac{\partial \mathbf{f}}{\partial a^g} d\Omega}{-4\lambda a^g \Omega^g} \tag{5.46}$$

Design variables are updated by:

$$a_{i+1}^g = \begin{cases} \min \{ (1 + \eta) a_i^g, 1 \} & \text{if } \varphi_i \leq \max \{ 1 - \eta, 0 \} \\ \max \{ (1 - \eta) a_i^g, 0 \}, & \text{if } \varphi_i \geq \min \{ 1 + \eta, 1 \} \\ a_i^g \cdot \varphi_i & \text{otherwise} \end{cases} \tag{5.47}$$

*Rectangular multi-void microstructure* (Figure 4.10 (b)):

The optimality conditions can be expressed as

$$\begin{aligned}
 & \underset{a^g, b^g, \theta^g (g=1, \dots, m)}{\text{Maximize}} \quad \Pi(\mathbf{u}) = \frac{1}{2} \sum_{g=1}^m \int_{\Omega^g} \boldsymbol{\varepsilon}^T(\mathbf{u}) \mathbf{D}^g \boldsymbol{\varepsilon}(\mathbf{u}) d\Omega - \sum_{g=1}^m \int_{\Omega^g} \mathbf{u}^T \mathbf{f} d\Omega - \sum_{g=1}^m \int_{\Omega^g} \mathbf{u}^T \mathbf{t} d\Gamma \\
 & \text{Such that} \quad \sum_{g=1}^m (1 - 2a^g b^g) \Omega^g - \Omega_s \leq 0 \\
 & \quad a^g - 1 \leq 0 \quad g = 1, 2, \dots, m \\
 & \quad -a^g \leq 0 \quad g = 1, 2, \dots, m \\
 & \quad b^g - \frac{1}{2} \leq 0 \quad g = 1, 2, \dots, m \\
 & \quad -b^g \leq 0 \quad g = 1, 2, \dots, m
 \end{aligned} \tag{5.48}$$

Introducing multipliers  $\lambda_{a1}^g, \lambda_{a2}^g, \lambda_{b1}^g, \lambda_{b2}^g$  and  $\lambda$  ( $g = 1, 2, \dots, m$ ), using Lagrangian function and defining

$$\begin{aligned} \varphi &= \frac{\frac{1}{2} \int_{\Omega^g} \boldsymbol{\varepsilon}^T(\mathbf{u}) \frac{\partial \mathbf{D}^g}{\partial a^g} \boldsymbol{\varepsilon}(\mathbf{u}) d\Omega - \int_{\Omega^g} \mathbf{u}^T \frac{\partial \mathbf{f}}{\partial a^g} d\Omega}{-2\lambda b^g \Omega^g} \\ \psi &= \frac{\frac{1}{2} \int_{\Omega^g} \boldsymbol{\varepsilon}^T(\mathbf{u}) \frac{\partial \mathbf{D}^g}{\partial b^g} \boldsymbol{\varepsilon}(\mathbf{u}) d\Omega - \int_{\Omega^g} \mathbf{u}^T \frac{\partial \mathbf{f}}{\partial b^g} d\Omega}{-2\lambda a^g \Omega^g} \end{aligned} \quad (5.49)$$

Design variables are updated by

$$\begin{aligned} a_{i+1}^g &= \begin{cases} \min\{(1+\eta)a_i^g, 1\} & \text{if } \varphi_i \leq \max\{1-\eta, x_{\min}\} \\ \max\{(1-\eta)a_i^g, x_{\min}\}, & \text{if } \varphi_i \geq \min\{1+\eta, 1\} \\ a_i^g \cdot \varphi_i & \text{otherwise} \end{cases} \\ b_{i+1}^g &= \begin{cases} \min\{(1+\eta)b_i^g, 1\} & \text{if } \psi_i \leq \max\{1-\eta, x_{\min}\} \\ \max\{(1-\eta)b_i^g, x_{\min}\}, & \text{if } \psi_i \geq \min\{1+\eta, 1\} \\ b_i^g \cdot \psi_i & \text{otherwise} \end{cases} \end{aligned} \quad (5.50)$$

*Square multi-void microstructure* (Figure 4.10 (c)):

The optimality conditions can be expressed as

$$\begin{aligned} \text{Maximize}_{a^g, \theta^g (g=1, \dots, m)} \quad \Pi(\mathbf{u}) &= \frac{1}{2} \sum_{g=1}^m \int_{\Omega^g} \boldsymbol{\varepsilon}^T(\mathbf{u}) \mathbf{D}^g \boldsymbol{\varepsilon}(\mathbf{u}) d\Omega - \sum_{g=1}^m \int_{\Omega^g} \mathbf{u}^T \mathbf{f} d\Omega - \sum_{g=1}^m \int_{\Omega^g} \mathbf{u}^T \mathbf{t} d\Gamma \\ \text{Such that} \quad \sum_{g=1}^m (1-4a^{g^2})\Omega^g - \Omega_s &\leq 0 \\ a^g - \frac{1}{2} &\leq 0 & g = 1, 2, \dots, m \\ -a^g &\leq 0 & g = 1, 2, \dots, m \end{aligned} \quad (5.51)$$

Introducing multipliers  $\lambda_{a1}^g, \lambda_{a2}^g$  and  $\lambda$  ( $g = 1, 2, \dots, m$ ), using Lagrangian

function and defining

$$\varphi = \frac{\frac{1}{2} \int_{\Omega^g} \boldsymbol{\varepsilon}^T(\mathbf{u}) \frac{\partial \mathbf{D}^g}{\partial a^g} \boldsymbol{\varepsilon}(\mathbf{u}) d\Omega - \int_{\Omega^g} \mathbf{u}^T \frac{\partial \mathbf{f}}{\partial a^g} d\Omega}{-8\lambda a^g \Omega^g} \quad (5.52)$$

Design variables are updated by:

$$a_{i+1}^g = \begin{cases} \min \{ (1+\eta)a_i^g, 1 \} & \text{if } \varphi_i \leq \max \{ 1-\eta, x_{\min} \} \\ \max \{ (1-\eta)a_i^g, x_{\min} \}, & \text{if } \varphi_i \geq \min \{ 1+\eta, 1 \} \\ a_i^g \cdot \varphi_i & \text{otherwise} \end{cases} \quad (5.53)$$

### 5.1.3.2 Bi-material Models

*Cross shape bi-material microstructure*

In the model of cross-shape bi-material microstructure (Figure 4.10 (a)), the optimality conditions can be expressed as

$$\begin{aligned} \text{Maximize}_{a^g, b^g, \theta^g (g=1, \dots, m)} \quad & \Pi(\mathbf{u}) = \frac{1}{2} \sum_{g=1}^m \int_{\Omega^g} \boldsymbol{\varepsilon}^T(\mathbf{u}) \mathbf{D}^g \boldsymbol{\varepsilon}(\mathbf{u}) d\Omega - \sum_{g=1}^m \int_{\Omega^g} \mathbf{u}^T \mathbf{f} d\Omega - \sum_{g=1}^m \int_{\Omega^g} \mathbf{u}^T \mathbf{t} d\Gamma \\ \text{Such that} \quad & \sum_{g=1}^m 4 \cdot (2a^g - a^{g^2}) \Omega^g - \Omega_{s1} \leq 0 \\ & \sum_{g=1}^m 4 \cdot (b^g - a^g)(2 - a^g - b^g) \Omega^e - \Omega_{s2} \leq 0 \\ & -a^g \leq 0 \quad g = 1, 2, \dots, m \\ & b^g - 1 \leq 0 \quad g = 1, 2, \dots, m \\ & a^g - b^g \leq 0 \quad g = 1, 2, \dots, m \end{aligned} \quad (5.54)$$

Introducing multipliers  $\lambda_a^g, \lambda_{ab}^g, \lambda_b^g$  and  $\lambda_1, \lambda_2$  ( $g = 1, 2, \dots, m$ ), the Lagrangian function L to the problem (5.54) can be expressed as

$$\begin{aligned}
 L = \Pi(\mathbf{u}) = & \frac{1}{2} \sum_{g=1}^m \int_{\Omega^g} \boldsymbol{\varepsilon}^T(\mathbf{u}) \mathbf{D}^g \boldsymbol{\varepsilon}(\mathbf{u}) d\Omega - \sum_{g=1}^m \int_{\Omega^g} \mathbf{u}^T \mathbf{f} d\Omega - \sum_{g=1}^m \int_{\Omega^g} \mathbf{u}^T \mathbf{t} d\Gamma \\
 & - \lambda_1 \left( \sum_{g=1}^m 4 \cdot (2a^g - a^{g2}) \Omega^g - \Omega_{s1} \right) \\
 & - \lambda_2 \left( \sum_{g=1}^m 4 \cdot (b^g - a^g)(2 - a^g - b^g) \Omega^g - \Omega_{s2} \right) \\
 & - \sum_{g=1}^m \lambda_a^g (-a^g) - \sum_{g=1}^m \lambda_{ab}^g (a^g - b^g) - \sum_{g=1}^m \lambda_b^g (b^g - 1)
 \end{aligned} \tag{5.55}$$

Differentiating the Lagrangian function (5.55) with respect to  $a^g, b^g$ , and defining

$$\begin{aligned}
 \varphi &= \frac{\frac{1}{2} \int_{\Omega^g} \boldsymbol{\varepsilon}^T(\mathbf{u}) \frac{\partial \mathbf{D}^g}{\partial a^g} \boldsymbol{\varepsilon}(\mathbf{u}) d\Omega - \int_{\Omega^g} \mathbf{u}^T \frac{\partial \mathbf{f}}{\partial a^g} d\Omega}{8(1 - a^g)(\lambda_1 - \lambda_2) \Omega^g} \\
 \psi &= \frac{\frac{1}{2} \int_{\Omega^g} \boldsymbol{\varepsilon}^T(\mathbf{u}) \frac{\partial \mathbf{D}^g}{\partial b^g} \boldsymbol{\varepsilon}(\mathbf{u}) d\Omega - \int_{\Omega^g} \mathbf{u}^T \frac{\partial \mathbf{f}}{\partial b^g} d\Omega}{8\lambda_2(1 - b^g) \Omega^g}
 \end{aligned} \tag{5.56}$$

It follows that

$$\begin{aligned}
 a_{i+1}^g &= \begin{cases} \max \{ (1 - \eta) a_i^g, x_{\min} \}, & \text{if } \varphi_i \leq \max \{ 1 - \eta, x_{\min} \} \\ \min \{ (1 + \eta) a_i^g, 1 \}, & \text{if } \varphi_i \geq \min \{ 1 + \eta, 1 \} \\ a_i^g \cdot \varphi_i & \text{otherwise} \end{cases} \\
 b_{i+1}^g &= \begin{cases} \max \{ (1 - \eta) b_i^g, x_{\min} \} & \text{if } \psi_i \leq \max \{ 1 - \eta, x_{\min} \} \\ \min \{ (1 + \eta) b_i^g, 1 \}, & \text{if } \psi_i \geq \min \{ 1 + \eta, 1 \} \\ b_i^g \cdot \psi_i & \text{otherwise} \end{cases}
 \end{aligned} \tag{5.57}$$

### Square bi-materials microstructures

In the model of square hole bi-material microstructures (Figure 4.11 (b)), the optimality conditions can be expressed as

$$\text{Maximize}_{a^g, b^g, \theta^g (g=1, \dots, m)} \quad \Pi(\mathbf{u}) = \frac{1}{2} \sum_{g=1}^m \int_{\Omega^g} \boldsymbol{\varepsilon}^T(\mathbf{u}) \mathbf{D}^g \boldsymbol{\varepsilon}(\mathbf{u}) d\Omega - \sum_{g=1}^m \int_{\Omega^g} \mathbf{u}^T \mathbf{f} d\Omega - \sum_{g=1}^m \int_{\Omega^g} \mathbf{u}^T \mathbf{t} d\Gamma$$

$$\text{Such that} \quad \sum_{g=1}^m (1 - b^{g2}) \Omega^g - \Omega_{s1} \leq 0$$

$$\sum_{g=1}^m (b^{g2} - a^{g2}) \Omega^g - \Omega_{s2} \leq 0 \quad (5.58)$$

$$-a^g \leq 0 \quad g = 1, 2, \dots, m$$

$$b^g - 1 \leq 0 \quad g = 1, 2, \dots, m$$

$$a^g - b^g \leq 0 \quad g = 1, 2, \dots, m$$

Introducing multipliers  $\lambda_a^g, \lambda_{ab}^g, \lambda_b^g$  and  $\lambda_1, \lambda_2$  ( $g = 1, 2, \dots, m$ ), using

Lagrangian function and defining

$$\varphi = \frac{\frac{1}{2} \int_{\Omega^g} \boldsymbol{\varepsilon}^T(\mathbf{u}) \frac{\partial \mathbf{D}^g}{\partial a^g} \boldsymbol{\varepsilon}(\mathbf{u}) d\Omega - \int_{\Omega^g} \mathbf{u}^T \frac{\partial \mathbf{f}}{\partial a^g} d\Omega}{-2a^g \lambda_2 \Omega^g} \quad (5.59)$$

$$\psi = \frac{\frac{1}{2} \int_{\Omega^g} \boldsymbol{\varepsilon}^T(\mathbf{u}) \frac{\partial \mathbf{D}^g}{\partial b^g} \boldsymbol{\varepsilon}(\mathbf{u}) d\Omega - \int_{\Omega^g} \mathbf{u}^T \frac{\partial \mathbf{f}}{\partial b^g} d\Omega}{-2(\lambda_1 - \lambda_2) b^g \Omega^g}$$

It follows that

$$a_{i+1}^g = \begin{cases} \min \{ (1 + \eta) a_i^g, 1 \} & \text{if } \varphi_i \leq \max \{ 1 - \eta, x_{\min} \} \\ \max \{ (1 - \eta) a_i^g, x_{\min} \}, & \text{if } \varphi_i \geq \min \{ 1 + \eta, 1 \} \\ a_i^g \cdot \varphi_i & \text{otherwise} \end{cases} \quad (5.60)$$

$$b_{i+1}^g = \begin{cases} \min \{ (1 + \eta) b_i^g, 1 \} & \text{if } \psi_i \leq \max \{ 1 - \eta, x_{\min} \} \\ \max \{ (1 - \eta) b_i^g, x_{\min} \}, & \text{if } \psi_i \geq \min \{ 1 + \eta, 1 \} \\ b_i^g \cdot \psi_i & \text{otherwise} \end{cases}$$

### Rectangular bi-material microstructures

In the model of double rectangular bi-material microstructure (Figure 4.11 (c)),

the optimality conditions can be expressed as

$$\text{Maximize}_{a^g, b^g, c^g, d^g, \theta^g (g=1, \dots, m)} \Pi(\mathbf{u}) = \frac{1}{2} \sum_{g=1}^m \int_{\Omega^g} \boldsymbol{\varepsilon}^T(\mathbf{u}) \mathbf{D}^g \boldsymbol{\varepsilon}(\mathbf{u}) d\Omega - \sum_{g=1}^m \int_{\Omega^g} \mathbf{u}^T \mathbf{f} d\Omega - \sum_{g=1}^m \int_{\Omega^g} \mathbf{u}^T \mathbf{t} d\Gamma$$

$$\text{Such that } \sum_{g=1}^m (1 - 2c^g d^g) \Omega^g - \Omega_s \leq 0$$

$$\sum_{g=1}^m 2(c^g d^g - a^g b^g) \Omega^g - \Omega_s \leq 0$$

$$a^g - c^g \leq 0 \quad g = 1, 2, \dots, m$$

$$-a^g \leq 0 \quad g = 1, 2, \dots, m \quad (5.61)$$

$$b^g - d^g \leq 0 \quad g = 1, 2, \dots, m$$

$$-b^g \leq 0 \quad g = 1, 2, \dots, m$$

$$c^g - \frac{1}{2} \leq 0 \quad g = 1, 2, \dots, m$$

$$d^g - 1 \leq 0 \quad g = 1, 2, \dots, m$$

Introducing multipliers  $\lambda_a^g, \lambda_b^g, \lambda_{ac}^g, \lambda_c^g, \lambda_{bd}^g, \lambda_d^g$  and  $\lambda_1, \lambda_2$  ( $g = 1, 2, \dots, m$ ), using

Lagrangian function and defining

$$\begin{aligned} \varphi &= \frac{\frac{1}{2} \int_{\Omega^g} \boldsymbol{\varepsilon}^T(\mathbf{u}) \frac{\partial \mathbf{D}^g}{\partial a^g} \boldsymbol{\varepsilon}(\mathbf{u}) d\Omega - \int_{\Omega^g} \mathbf{u}^T \frac{\partial \mathbf{f}}{\partial a^g} d\Omega}{-2b^g \lambda_2 \Omega^g} \\ \psi &= \frac{\frac{1}{2} \int_{\Omega^g} \boldsymbol{\varepsilon}^T(\mathbf{u}) \frac{\partial \mathbf{D}^g}{\partial b^g} \boldsymbol{\varepsilon}(\mathbf{u}) d\Omega - \int_{\Omega^g} \mathbf{u}^T \frac{\partial \mathbf{f}}{\partial b^g} d\Omega}{-2a^g \lambda_2 \Omega^g} \\ \omega &= \frac{\frac{1}{2} \int_{\Omega^g} \boldsymbol{\varepsilon}^T(\mathbf{u}) \frac{\partial \mathbf{D}^g}{\partial c^g} \boldsymbol{\varepsilon}(\mathbf{u}) d\Omega - \int_{\Omega^g} \mathbf{u}^T \frac{\partial \mathbf{f}}{\partial c^g} d\Omega}{-2(\lambda_1 - \lambda_2) d^g \Omega^g} \\ \phi &= \frac{\frac{1}{2} \int_{\Omega^g} \boldsymbol{\varepsilon}^T(\mathbf{u}) \frac{\partial \mathbf{D}^g}{\partial d^g} \boldsymbol{\varepsilon}(\mathbf{u}) d\Omega - \int_{\Omega^g} \mathbf{u}^T \frac{\partial \mathbf{f}}{\partial d^g} d\Omega}{-2(\lambda_1 - \lambda_2) c^g \Omega^g} \end{aligned} \quad (5.62)$$

The design variables can be updated by

$$\begin{aligned}
 a_{i+1}^g &= \begin{cases} \min \{(1+\eta)a_i^g, 1\} & \text{if } \varphi_i \leq \max \{1-\eta, x_{\min}\} \\ \max \{(1-\eta)a_i^g, x_{\min}\}, & \text{if } \varphi_i \geq \min \{1+\eta, 1\} \\ a_i^g \cdot \varphi_i & \text{otherwise} \end{cases} \\
 b_{i+1}^g &= \begin{cases} \min \{(1+\eta)b_i^g, 1\} & \text{if } \psi_i \leq \max \{1-\eta, x_{\min}\} \\ \max \{(1-\eta)b_i^g, x_{\min}\}, & \text{if } \psi_i \geq \min \{1+\eta, 1\} \\ b_i^g \cdot \psi_i & \text{otherwise} \end{cases} \\
 c_{i+1}^g &= \begin{cases} \min \{(1+\eta)c_i^g, 1\} & \text{if } \omega_i \leq \max \{1-\eta, x_{\min}\} \\ \max \{(1-\eta)c_i^g, x_{\min}\}, & \text{if } \omega_i \geq \min \{1+\eta, 1\} \\ a_i^g \cdot \omega_i & \text{otherwise} \end{cases} \\
 d_{i+1}^g &= \begin{cases} \min \{(1+\eta)d_i^g, 1\} & \text{if } \phi_i \leq \max \{1-\eta, x_{\min}\} \\ \max \{(1-\eta)d_i^g, x_{\min}\}, & \text{if } \phi_i \geq \min \{1+\eta, 1\} \\ b_i^g \cdot \phi_i & \text{otherwise} \end{cases}
 \end{aligned} \tag{5.63}$$

### Triangular bi-material microstructure

In the model (d) of Figure 4.10, the optimality conditions can be expressed as

$$\begin{aligned}
 \text{Maximize}_{a^g, b^g, \theta^g (g=1, \dots, m)} \quad & \Pi(\mathbf{u}) = \frac{1}{2} \sum_{g=1}^m \int_{\Omega^g} \boldsymbol{\varepsilon}^T(\mathbf{u}) \mathbf{D}^g \boldsymbol{\varepsilon}(\mathbf{u}) d\Omega - \sum_{g=1}^m \int_{\Omega^g} \mathbf{u}^T \mathbf{f} d\Omega - \sum_{g=1}^m \int_{\Omega^g} \mathbf{u}^T \mathbf{t} d\Gamma \\
 \text{Such that} \quad & \sum_{g=1}^m (1-2b^{g2})\Omega^g - \Omega_s \leq 0 \\
 & \sum_{g=1}^m 2(b^{g2} - a^{g2})\Omega^g - \Omega_s \leq 0 \\
 & b^g - \frac{\sqrt{2}}{2} \leq 0 \quad g = 1, 2, \dots, m \\
 & a^g - b^g \leq 0 \quad g = 1, 2, \dots, m \\
 & -a^g \leq 0 \quad g = 1, 2, \dots, m
 \end{aligned} \tag{5.64}$$

Introducing multipliers  $\lambda_a^g, \lambda_{ab}^g, \lambda_b^g$  and  $\lambda_1, \lambda_2$  ( $g = 1, 2, \dots, m$ ), using Lagrangian function and defining

$$\begin{aligned} \varphi &= \frac{\frac{1}{2} \int_{\Omega^g} \boldsymbol{\varepsilon}^T(\mathbf{u}) \frac{\partial \mathbf{D}^g}{\partial a^g} \boldsymbol{\varepsilon}(\mathbf{u}) d\Omega - \int_{\Omega^g} \mathbf{u}^T \frac{\partial \mathbf{f}}{\partial a^g} d\Omega}{-4a^g \lambda_2 \Omega^g} \\ \psi &= \frac{\frac{1}{2} \int_{\Omega^g} \boldsymbol{\varepsilon}^T(\mathbf{u}) \frac{\partial \mathbf{D}^g}{\partial b^g} \boldsymbol{\varepsilon}(\mathbf{u}) d\Omega - \int_{\Omega^g} \mathbf{u}^T \frac{\partial \mathbf{f}}{\partial b^g} d\Omega}{-4(\lambda_1 - \lambda_2) b^g \Omega^g} \end{aligned} \quad (5.65)$$

The design variables can be updated by:

$$\begin{aligned} a_{i+1}^g &= \begin{cases} \min \{ (1+\eta) a_i^g, 1 \} & \text{if } \varphi_i \leq \max \{ 1-\eta, x_{\min} \} \\ \max \{ (1-\eta) a_i^g, x_{\min} \}, & \text{if } \varphi_i \geq \min \{ 1+\eta, 1 \} \\ a_i^g \cdot \varphi_i & \text{otherwise} \end{cases} \\ b_{i+1}^g &= \begin{cases} \min \{ (1+\eta) b_i^g, 1 \} & \text{if } \psi_i \leq \max \{ 1-\eta, x_{\min} \} \\ \max \{ (1-\eta) b_i^g, x_{\min} \}, & \text{if } \psi_i \geq \min \{ 1+\eta, 1 \} \\ b_i^g \cdot \psi_i & \text{otherwise} \end{cases} \end{aligned} \quad (5.66)$$

#### 5.1.4 Optimality conditions for existing microstructure models

Some microstructure models were developed, but the computer program codes for optimization have not been given in literature. In order to compare effects of microstructures used and the newly developed, a program code of structural topology optimization catering for the following microstructures is developed in this research. These microstructure models considered are:

*Ranked layered model*

According to the discussion in Chapter 3, for ranked-2 layered model, the optimality conditions can be expressed as

$$\begin{aligned}
 \text{Maximize}_{\mathcal{G}^g, \gamma^g, \theta^g (g=1, \dots, m)} \quad & \Pi(\mathbf{u}) = \frac{1}{2} \sum_{g=1}^m \int_{\Omega^g} \boldsymbol{\varepsilon}^T(\mathbf{u}) \mathbf{D}^g \boldsymbol{\varepsilon}(\mathbf{u}) d\Omega - \sum_{g=1}^m \int_{\Omega^g} \mathbf{u}^T \mathbf{f} d\Omega - \sum_{g=1}^m \int_{\Omega^g} \mathbf{u}^T \mathbf{t} d\Gamma \\
 \text{Such that} \quad & \sum_{g=1}^m (\mathcal{G}^g + \gamma^g - \mathcal{G}^g \gamma^g) \Omega^g - \Omega_s \leq 0 \\
 & \mathcal{G}^g - 1 \leq 0 \quad \quad \quad g = 1, 2, \dots, m \\
 & -\mathcal{G}^g \leq 0 \quad \quad \quad g = 1, 2, \dots, m \\
 & \gamma^g - 1 \leq 0 \quad \quad \quad g = 1, 2, \dots, m \\
 & -\gamma^g \leq 0 \quad \quad \quad g = 1, 2, \dots, m
 \end{aligned} \tag{5.67}$$

Introducing multipliers  $\lambda_{g1}^g, \lambda_{g2}^g, \lambda_{\gamma 1}^g, \lambda_{\gamma 2}^g$  and  $\lambda$  ( $g = 1, 2, \dots, m$ ), the Lagrangian function  $L$  to the problem (5.67) can be expressed as

$$\begin{aligned}
 L = \Pi(\mathbf{u}) = & \frac{1}{2} \sum_{g=1}^m \int_{\Omega^g} \boldsymbol{\varepsilon}^T(\mathbf{u}) \mathbf{D}^g \boldsymbol{\varepsilon}(\mathbf{u}) d\Omega - \sum_{g=1}^m \int_{\Omega^g} \mathbf{u}^T \mathbf{f} d\Omega - \sum_{g=1}^m \int_{\Omega^g} \mathbf{u}^T \mathbf{t} d\Gamma \\
 & - \lambda \left( \sum_{g=1}^m (\mathcal{G}^g + \gamma^g - \mathcal{G}^g \gamma^g) \Omega^g - \Omega_s \right) - \sum_{g=1}^m \lambda_{g1}^g (-\mathcal{G}^g) - \sum_{g=1}^m \lambda_{g2}^g (\mathcal{G}^g - 1) \\
 & - \sum_{g=1}^m \lambda_{\gamma 1}^g (-\gamma^g) - \sum_{g=1}^m \lambda_{\gamma 2}^g (\gamma^g - 1)
 \end{aligned} \tag{5.68}$$

Similarly by differentiating the Lagrangian function (5.68) with respect to  $\mathcal{G}^g$ , we can get

$$\begin{aligned}
 & \frac{1}{2} \int_{\Omega^g} \boldsymbol{\varepsilon}^T(\mathbf{u}) \frac{\partial \mathbf{D}^g}{\partial \mathcal{G}^g} \boldsymbol{\varepsilon}(\mathbf{u}) d\Omega - \int_{\Omega^g} \mathbf{u}^T \frac{\partial \mathbf{f}}{\partial \mathcal{G}^g} d\Omega \\
 & - \lambda (\gamma^g - 1) \Omega^g + \lambda_{g1}^g - \lambda_{g2}^g = 0, \quad (g = 1, 2, \dots, m)
 \end{aligned} \tag{5.69}$$

Differentiating the Lagrangian function (5.68) with respect to  $\gamma^g$ , we can get

$$\begin{aligned} & \frac{1}{2} \int_{\Omega^g} \boldsymbol{\varepsilon}^T(\mathbf{u}) \frac{\partial \mathbf{D}^g}{\partial \gamma^g} \boldsymbol{\varepsilon}(\mathbf{u}) d\Omega - \int_{\Omega^g} \mathbf{u}^T \frac{\partial \mathbf{f}}{\partial \gamma^g} d\Omega \\ & - \lambda(\mathcal{G}^g - 1)\Omega^g + \lambda_{\gamma_1}^g - \lambda_{\gamma_2}^g = 0, \quad (g = 1, 2, \dots, m) \end{aligned} \quad (5.70)$$

We define

$$\varphi = \frac{\frac{1}{2} \int_{\Omega^g} \boldsymbol{\varepsilon}^T(\mathbf{u}) \frac{\partial \mathbf{D}^g}{\partial \mathcal{G}^g} \boldsymbol{\varepsilon}(\mathbf{u}) d\Omega - \int_{\Omega^g} \mathbf{u}^T \frac{\partial \mathbf{f}}{\partial \mathcal{G}^g} d\Omega}{\lambda(1 - r^g)\Omega^g} \quad (5.71)$$

$$\psi = \frac{\frac{1}{2} \int_{\Omega^g} \boldsymbol{\varepsilon}^T(\mathbf{u}) \frac{\partial \mathbf{D}^g}{\partial \gamma^g} \boldsymbol{\varepsilon}(\mathbf{u}) d\Omega - \int_{\Omega^g} \mathbf{u}^T \frac{\partial \mathbf{f}}{\partial \gamma^e} d\Omega}{\lambda(1 - \mathcal{G}^g)\Omega^g} \quad (5.72)$$

We can update the design variables as following:

$$\begin{aligned} \mathcal{G}_{i+1}^g &= \begin{cases} \max\{(1-\eta)\mathcal{G}_i^g, 0\} & \text{if } \varphi_i \leq \max\{1-\eta, 0\} \\ \min\{(1+\eta)\mathcal{G}_i^g, 1\}, & \text{if } \varphi_i \geq \min\{1+\eta, 1\} \\ \mathcal{G}_i^g \cdot \varphi_i & \text{otherwise} \end{cases} \\ \gamma_{i+1}^g &= \begin{cases} \max\{(1-\eta)\gamma_i^g, 0\} & \text{if } \psi_i \leq \max\{1-\eta, 0\} \\ \min\{(1+\eta)\gamma_i^g, 1\}, & \text{if } \psi_i \geq \min\{1+\eta, 1\} \\ \gamma_i^g \cdot \psi_i & \text{otherwise} \end{cases} \end{aligned} \quad (5.73)$$

### Triangular one-material microstructure

For triangular model, the optimality conditions can be expressed as

$$\begin{aligned} & \underset{a^g, \theta^g (g=1, \dots, m)}{\text{Maximize}} \quad \Pi(\mathbf{u}) = \frac{1}{2} \sum_{g=1}^m \int_{\Omega^g} \boldsymbol{\varepsilon}^T(\mathbf{u}) \mathbf{D}^g \boldsymbol{\varepsilon}(\mathbf{u}) d\Omega - \sum_{g=1}^m \int_{\Omega^g} \mathbf{u}^T \mathbf{f} d\Omega - \sum_{g=1}^m \int_{\Omega^g} \mathbf{u}^T \mathbf{t} d\Gamma \\ & \text{Such that} \quad \sum_{g=1}^m (\sqrt{3} - \sqrt{3}(a^g)^2)\Omega^g - \Omega_s \leq 0 \\ & a^g - 1 \leq 0 \quad g = 1, 2, \dots, m \\ & -a^g \leq 0 \quad g = 1, 2, \dots, m \end{aligned} \quad (5.74)$$

Introducing multipliers  $\lambda_{a_1}^g, \lambda_{a_2}^g$  and  $\lambda$  ( $g = 1, 2, \dots, m$ ), the Lagrangian function  $L$  to the problem (5.74) can be expressed as

$$L = \Pi(\mathbf{u}) = \frac{1}{2} \sum_{g=1}^m \int_{\Omega^g} \boldsymbol{\varepsilon}^T(\mathbf{u}) \mathbf{D}^g \boldsymbol{\varepsilon}(\mathbf{u}) d\Omega - \sum_{g=1}^m \int_{\Omega^g} \mathbf{u}^T \mathbf{f} d\Omega - \sum_{g=1}^m \int_{\Omega^g} \mathbf{u}^T \mathbf{t} d\Gamma$$

$$- \lambda \left( \sum_{g=1}^m (\sqrt{3} - \sqrt{3}(a^g)^2 \Omega^g - \Omega_s) \right) - \sum_{g=1}^m \lambda_{a_1}^g (-a^g) - \sum_{g=1}^m \lambda_{a_2}^g (a^g - 1) \quad (5.75)$$

Differentiating the Lagrangian function (5.75) with respect to  $a^g$ , we can get

$$\frac{1}{2} \int_{\Omega^g} \boldsymbol{\varepsilon}^T(\mathbf{u}) \frac{\partial \mathbf{D}^g}{\partial a^g} \boldsymbol{\varepsilon}(\mathbf{u}) d\Omega - \int_{\Omega^g} \mathbf{u}^T \frac{\partial \mathbf{f}}{\partial a^g} d\Omega$$

$$+ 2\sqrt{3}\lambda a^g \Omega^g + \lambda_{a_1}^g - \lambda_{a_2}^g = 0, \quad (g = 1, 2, \dots, m) \quad (5.76)$$

If we define

$$\varphi = \frac{\frac{1}{2} \int_{\Omega^g} \boldsymbol{\varepsilon}^T(\mathbf{u}) \frac{\partial \mathbf{D}^g}{\partial a^g} \boldsymbol{\varepsilon}(\mathbf{u}) d\Omega - \int_{\Omega^g} \mathbf{u}^T \frac{\partial \mathbf{f}}{\partial a^g} d\Omega}{-2\sqrt{3}\lambda a^g \Omega^g} \quad (5.77)$$

We can update design variables as

$$a_{i+1}^g = \begin{cases} \min \{ (1+\eta)a_i^g, 1 \} & \text{if } \varphi_i \leq \max \{ 1-\eta, 0 \} \\ \max \{ (1-\eta)a_i^g, 0 \}, & \text{if } \varphi_i \geq \min \{ 1+\eta, 1 \} \\ a_i^g \cdot \varphi_i & \text{otherwise} \end{cases} \quad (5.78)$$

### Hexagon microstructure

For hexagon model, the optimality conditions can be expressed as

$$\begin{aligned}
 & \text{Maximize}_{a^g, \theta^g (g=1, \dots, m)} \quad \Pi(\mathbf{u}) = \frac{1}{2} \sum_{g=1}^m \int_{\Omega^g} \boldsymbol{\varepsilon}^T(\mathbf{u}) \mathbf{D}^g \boldsymbol{\varepsilon}(\mathbf{u}) d\Omega - \sum_{g=1}^m \int_{\Omega^g} \mathbf{u}^T \mathbf{f} d\Omega - \sum_{g=1}^m \int_{\Omega^g} \mathbf{u}^T \mathbf{t} d\Gamma \\
 & \text{Such that} \quad \sum_{g=1}^m 4\sqrt{3} \left(1 - \frac{\sqrt{3}}{2} a^{g2}\right) \Omega^g - \Omega_s \leq 0 \\
 & \quad a^g - 2\sqrt{3}/3 \leq 0 \quad \quad \quad g = 1, 2, \dots, m \\
 & \quad -a^g \leq 0 \quad \quad \quad g = 1, 2, \dots, m
 \end{aligned} \tag{5.79}$$

Introducing multipliers  $\lambda_{a_1}^e, \lambda_{a_2}^e$  and  $\lambda$  ( $g = 1, 2, \dots, m$ ), using Lagrangian function and defining

$$\varphi = \frac{\frac{1}{2} \int_{\Omega^g} \boldsymbol{\varepsilon}^T(\mathbf{u}) \frac{\partial \mathbf{D}^g}{\partial a^g} \boldsymbol{\varepsilon}(\mathbf{u}) d\Omega - \int_{\Omega^g} \mathbf{u}^T \frac{\partial \mathbf{f}}{\partial a^g} d\Omega}{-12\lambda a^g \Omega^g} \tag{5.80}$$

Updating design variable by:

$$a_{i+1}^g = \begin{cases} \min\{(1+\eta)a_i^g, 1\} & \text{if } \varphi_i \leq \max\{1-\eta, 0\} \\ \max\{(1-\eta)a_i^g, 0\}, & \text{if } \varphi_i \geq \min\{1+\eta, 1\} \\ a_i^g \cdot \varphi_i & \text{otherwise} \end{cases} \tag{5.81}$$

### Power-law one-material model

In the power-law one-material model, the optimality conditions can be expressed as

$$\begin{aligned}
 & \text{Maximize}_{\rho^g (g=1, \dots, m)} \quad \Pi(\mathbf{u}) = \frac{1}{2} \sum_{g=1}^m \int_{\Omega^g} \boldsymbol{\varepsilon}^T(\mathbf{u}) \mathbf{D}^g \boldsymbol{\varepsilon}(\mathbf{u}) d\Omega - \sum_{g=1}^m \int_{\Omega^g} \mathbf{u}^T \mathbf{f} d\Omega - \sum_{g=1}^m \int_{\Omega^g} \mathbf{u}^T \mathbf{t} d\Gamma \\
 & \text{Such that} \quad \sum_{g=1}^m \rho^g \Omega^g - \Omega_s \leq 0 \\
 & \quad \rho^g - 1 \leq 0 \quad \quad \quad g = 1, 2, \dots, m \\
 & \quad \rho_{\min} - \rho^g \leq 0 \quad \quad \quad g = 1, 2, \dots, m
 \end{aligned} \tag{5.82}$$

where  $\rho_{\min}$  is a lower bound vector on relative density.

Introducing multipliers  $\lambda_1^g, \lambda_2^g$  and  $\lambda$  ( $e=1,2,\dots,m$ ), the Lagrangian function L to the problem (5.82) may be expressed as

$$L = \Pi(\mathbf{u}) = \frac{1}{2} \sum_{g=1}^m \int_{\Omega^g} \boldsymbol{\varepsilon}^T(\mathbf{u}) \mathbf{D}^g \boldsymbol{\varepsilon}(\mathbf{u}) d\Omega - \sum_{g=1}^m \int_{\Omega^g} \mathbf{u}^T \mathbf{f} d\Omega - \sum_{g=1}^m \int_{\Omega^g} \mathbf{u}^T \mathbf{t} d\Gamma$$

$$- \lambda \left( \sum_{g=1}^m \rho^g \Omega^g - \Omega_s \right) - \sum_{g=1}^m \lambda_1^g (\rho_{\min} - \rho^g) - \sum_{e=1}^m \lambda_2^g (\rho^g - 1)$$
(5.83)

By differentiating the Lagrangian function (5.82) with respect to  $\rho^g$ , we can get

$$\frac{1}{2} \int_{\Omega^g} \boldsymbol{\varepsilon}^T(\mathbf{u}) \frac{\partial \mathbf{D}^g}{\partial \rho^g} \boldsymbol{\varepsilon}(\mathbf{u}) d\Omega - \int_{\Omega^g} \mathbf{u}^T \frac{\partial \mathbf{f}}{\partial \rho^g} d\Omega$$

$$- \lambda \rho^g \Omega^g + \lambda_1^g - \lambda_2^g = 0, \quad (g=1,2,\dots,m)$$
(5.84)

By defining

$$\varphi = \frac{\frac{1}{2} \int_{\Omega^g} \boldsymbol{\varepsilon}^T(u) \frac{\partial D^g}{\partial \rho^g} \boldsymbol{\varepsilon}(u) d\Omega - \int_{\Omega^g} u^T \frac{\partial f}{\partial \rho^g} d\Omega}{\lambda \rho^g \Omega^g}$$
(5.85)

We have

$$\varphi = 1 + \frac{1}{\lambda \rho^g \Omega^g} (\lambda_2^g - \lambda_1^g)$$
(5.86)

Updating design variables as

$$\rho_{i+1}^g = \begin{cases} \max \left\{ (1-\eta) \rho_i^g, \rho_{\min} \right\}, & \text{if } \varphi_i \leq \max \left\{ 1-\eta, \rho_{\min} / \rho_i^g \right\} \\ \min \left\{ (1+\eta) \rho_i^g, 1 \right\}, & \text{if } \varphi_i \geq \min \left\{ 1+\eta, 1 / \rho_i^g \right\} \\ \rho_i^g \cdot \varphi_i & \text{otherwise} \end{cases}$$
(5.87)

*Power-law bi-materials microstructure*

In the model of power-law bi-material microstructure model, the optimality conditions can be expressed as

$$\text{Maximize}_{\rho_1^g, \rho_2^g (g=1, \dots, m)} \Pi(\mathbf{u}) = \frac{1}{2} \sum_{g=1}^m \int_{\Omega^g} \boldsymbol{\varepsilon}^T(\mathbf{u}) \mathbf{D}^g \boldsymbol{\varepsilon}(\mathbf{u}) d\Omega - \sum_{g=1}^m \int_{\Omega^g} \mathbf{u}^T \mathbf{f} d\Omega - \sum_{g=1}^m \int_{\Omega^g} \mathbf{u}^T \mathbf{t} d\Gamma$$

$$\text{Such that } \sum_{g=1}^m \rho_1^g \rho_2^g \Omega^g - \Omega_{s1} \leq 0 \quad (5.88)$$

$$\sum_{g=1}^m \rho_1^g (1 - \rho_2^g) \Omega^g - \Omega_{s2} \leq 0$$

$$\rho_1^g - 1 \leq 0 \quad g = 1, 2, \dots, m$$

$$\rho_{\min} - \rho_1^g \leq 0 \quad g = 1, 2, \dots, m$$

$$\rho_2^g - 1 \leq 0 \quad g = 1, 2, \dots, m$$

$$-\rho_2^g \leq 0 \quad g = 1, 2, \dots, m$$

Introducing multipliers  $\lambda_{\rho_1}^{1g}, \lambda_{\rho_2}^{1g}, \lambda_{\rho_1}^{2g}, \lambda_{\rho_2}^{2g}$  and  $\lambda_1, \lambda_2$  ( $g = 1, 2, \dots, m$ ), the

Lagrangian function L to the problem (5.88) can be expressed as

$$L = \Pi(\mathbf{u}) = \frac{1}{2} \sum_{g=1}^m \int_{\Omega^g} \boldsymbol{\varepsilon}^T(\mathbf{u}) \mathbf{D}^g \boldsymbol{\varepsilon}(\mathbf{u}) d\Omega - \sum_{g=1}^m \int_{\Omega^g} \mathbf{u}^T \mathbf{f} d\Omega - \sum_{g=1}^m \int_{\Omega^g} \mathbf{u}^T \mathbf{t} d\Gamma$$

$$- \lambda_1 \left( \sum_{g=1}^m \rho_1^g \rho_2^g \Omega^g - \Omega_{s1} \right) - \lambda_2 \left( \sum_{g=1}^m \rho_1^g (1 - \rho_2^g) \Omega^g - \Omega_{s2} \right) \quad (5.89)$$

$$- \sum_{g=1}^m \lambda_{\rho_1}^{1g} (\rho_{\min} - \rho_1^g) - \sum_{g=1}^m \lambda_{\rho_1}^{2g} (\rho_1^g - 1) - \sum_{g=1}^m \lambda_{\rho_2}^{1g} (-\rho_2^g) - \sum_{g=1}^m \lambda_{\rho_2}^{2g} (\rho_2^g - 1)$$

Differentiating the Lagrangian function (5.88) with respect to  $\rho_1^g, \rho_2^g$  and

defining

$$\varphi = \frac{\frac{1}{2} \int_{\Omega^g} \boldsymbol{\varepsilon}^T(\mathbf{u}) \frac{\partial \mathbf{D}^g}{\partial \rho_1^g} \boldsymbol{\varepsilon}(\mathbf{u}) d\Omega - \int_{\Omega^g} \mathbf{u}^T \frac{\partial \mathbf{f}}{\partial \rho_1^g} d\Omega}{(\lambda_1 \rho_2^g - \lambda_2 \rho_2^g + \lambda_2) \Omega^g} \quad (5.90)$$

$$\psi = \frac{\frac{1}{2} \int_{\Omega^g} \boldsymbol{\varepsilon}^T(\mathbf{u}) \frac{\partial \mathbf{D}^g}{\partial \rho_2^g} \boldsymbol{\varepsilon}(\mathbf{u}) d\Omega - \int_{\Omega^g} \mathbf{u}^T \frac{\partial \mathbf{f}}{\partial \rho_2^g} d\Omega}{(\lambda_1 \rho_1^g - \lambda_2 \rho_1^g) \Omega^g}$$

Design variable are updated by:

$$\rho_{i+1}^g = \begin{cases} \max \left\{ (1-\eta)\rho_i^g, \rho_{\min} \right\} & \text{if } \varphi_i \leq \max \left\{ 1-\eta, \rho_{\min} / \rho_i^g \right\} \\ \min \left\{ (1+\eta)\rho_i^g, 1 \right\}, & \text{if } \varphi_i \geq \min \left\{ 1+\eta, 1 / \rho_i^g \right\} \\ \rho_i^g \cdot \varphi_i & \text{otherwise} \end{cases} \quad (5.91)$$

$$\rho_{2i+1}^g = \begin{cases} \max \left\{ (1-\eta)\rho_{2i}^g, 0 \right\} & \text{if } \psi_i \leq \max \{1-\eta, 0\} \\ \min \left\{ (1+\eta)\rho_{2i}^g, 1 \right\}, & \text{if } \psi_i \geq \min \left\{ 1+\eta, 1 / \rho_{2i}^g \right\} \\ \rho_{2i}^g \cdot \psi_i & \text{otherwise} \end{cases} \quad (5.92)$$

### Ranked layered bi-materials microstructures

The optimality conditions for rank-2 layered bi-material model can be expressed as

$$\text{Maximize}_{\mathcal{G}^g, \gamma_1^g, \gamma_2^g, \theta^g (g=1, \dots, m)} \Pi(\mathbf{u}) = \frac{1}{2} \sum_{g=1}^m \int_{\Omega^g} \boldsymbol{\varepsilon}^T(\mathbf{u}) \mathbf{D}^g \boldsymbol{\varepsilon}(\mathbf{u}) d\Omega - \sum_{g=1}^m \int_{\Omega^g} \mathbf{u}^T \mathbf{f} d\Omega - \sum_{g=1}^m \int_{\Omega^g} \mathbf{u}^T \mathbf{t} d\Gamma$$

$$\text{Such that } \sum_{g=1}^m (\mathcal{G}^g + (1-\mathcal{G}^g)\gamma_1^g \gamma_2^g) \Omega^g - \Omega_{s1} \leq 0$$

$$\sum_{g=1}^m \left[ (1-\mathcal{G}^g)(1-\gamma_1^g)\gamma_2^g \right] \Omega^g - \Omega_{s2} \leq 0$$

$$\mathcal{G}^g - 1 \leq 0 \quad \mathbf{g} = 1, 2, \dots, m$$

$$-\mathcal{G}^g \leq 0 \quad \mathbf{g} = 1, 2, \dots, m \quad (5.93)$$

$$\gamma_1^g - 1 \leq 0 \quad \mathbf{g} = 1, 2, \dots, m$$

$$-\gamma_1^g \leq 0 \quad \mathbf{g} = 1, 2, \dots, m$$

$$\gamma_2^g - 1 \leq 0 \quad \mathbf{g} = 1, 2, \dots, m$$

$$-\gamma_2^g \leq 0 \quad \mathbf{g} = 1, 2, \dots, m$$

Introducing multipliers  $\lambda_g^{1g}, \lambda_g^{2g}, \lambda_{\gamma_1}^{1g}, \lambda_{\gamma_2}^{1g}, \lambda_{\gamma_1}^{2g}, \lambda_{\gamma_2}^{2g}$  and  $\lambda_1, \lambda_2$  ( $g = 1, 2, \dots, m$ ), the Lagrangian function  $L$  to the problem (5.93) can be expressed as

$$\begin{aligned}
 L = \Pi(\mathbf{u}) = & \frac{1}{2} \sum_{g=1}^m \int_{\Omega^g} \boldsymbol{\varepsilon}^T(\mathbf{u}) \mathbf{D}^g \boldsymbol{\varepsilon}(\mathbf{u}) d\Omega - \sum_{g=1}^m \int_{\Omega^g} \mathbf{u}^T \mathbf{f} d\Omega - \sum_{g=1}^m \int_{\Omega^g} \mathbf{u}^T \mathbf{t} d\Gamma \\
 & - \lambda_1 \left( \sum_{g=1}^m (\mathcal{G}^g + (1 - \mathcal{G}^g) \gamma_1^g \gamma_2^g) \Omega^g - \Omega_{s1} \right) \\
 & - \lambda_2 \left( \sum_{g=1}^m [(1 - \mathcal{G}^g)(1 - \gamma_1^g) \gamma_2^g] \Omega^g - \Omega_{s2} \right) \quad (5.94) \\
 & - \sum_{g=1}^m \lambda_{\mu}^{1g} (-\mathcal{G}_1^g) - \sum_{g=1}^m \lambda_{\mu}^{2g} (\mathcal{G}_1^g - 1) - \sum_{g=1}^m \lambda_{\gamma_1}^{1g} (-\gamma_1^g) \\
 & - \sum_{g=1}^m \lambda_{\gamma_1}^{2g} (\gamma_1^g - 1) - \sum_{g=1}^m \lambda_{\gamma_2}^{1g} (-\gamma_2^g) - \sum_{g=1}^m \lambda_{\gamma_2}^{2g} (\gamma_2^g - 1)
 \end{aligned}$$

Differentiating the Lagrangian function (5.94) with respect to  $\mathcal{G}^g, \gamma_1^g, \gamma_2^g$  and defining

$$\begin{aligned}
 \varphi &= \frac{\frac{1}{2} \int_{\Omega^g} \boldsymbol{\varepsilon}^T(\mathbf{u}) \frac{\partial \mathbf{D}^g}{\partial \mathcal{G}^g} \boldsymbol{\varepsilon}(\mathbf{u}) d\Omega - \int_{\Omega^g} \mathbf{u}^T \frac{\partial \mathbf{f}}{\partial \mathcal{G}^g} d\Omega}{\left[ \lambda_1 (1 - \gamma_1^g \gamma_2^g) - \lambda_2 (1 - \gamma_1^g) \gamma_2^g \right] \Omega^e} \\
 \psi &= \frac{\frac{1}{2} \int_{\Omega^g} \boldsymbol{\varepsilon}^T(\mathbf{u}) \frac{\partial \mathbf{D}^g}{\partial \gamma_1^g} \boldsymbol{\varepsilon}(\mathbf{u}) d\Omega - \int_{\Omega^g} \mathbf{u}^T \frac{\partial \mathbf{f}}{\partial \gamma_1^g} d\Omega}{(\lambda_1 - \lambda_2) (1 - \mathcal{G}^g) \gamma_2^g \Omega^g} \quad (5.95) \\
 \omega &= \frac{\frac{1}{2} \int_{\Omega^g} \boldsymbol{\varepsilon}^T(\mathbf{u}) \frac{\partial \mathbf{D}^g}{\partial \gamma_2^g} \boldsymbol{\varepsilon}(\mathbf{u}) d\Omega - \int_{\Omega^g} \mathbf{u}^T \frac{\partial \mathbf{f}}{\partial \gamma_2^g} d\Omega}{\left[ \lambda_1 (1 - \mathcal{G}^g) \gamma_1^g + \lambda_2 (1 - \mathcal{G}^g) (1 - \gamma_1^g) \right] \Omega^e}
 \end{aligned}$$

The design variables are updated as

$$\mathcal{G}_{i+1}^g = \begin{cases} \max \{ (1 - \eta) \mathcal{G}_i^g, 0 \} & \text{if } \varphi_i \leq \max \{ 1 - \eta, 0 \} \\ \min \{ (1 + \eta) \mathcal{G}_i^g, 1 \}, & \text{if } \varphi_i \geq \min \{ 1 + \eta, 1 \} \\ \mathcal{G}_i^g \cdot \varphi_i & \text{otherwise} \end{cases} \quad (5.96)$$

$$\gamma_{ii+1}^g = \begin{cases} \max\{(1-\eta)\gamma_{ii}^g, 0\} & \text{if } \psi_i \leq \max\{1-\eta, 0\} \\ \min\{(1+\eta)\gamma_{ii}^g, 1\}, & \text{if } \psi_i \geq \min\{1+\eta, 1\} \\ \gamma_{ii}^g \cdot \psi_i & \text{otherwise} \end{cases} \quad (5.97)$$

$$\gamma_{2i+1}^g = \begin{cases} \max\{(1-\eta)\gamma_{2i}^g, 0\} & \text{if } \omega_i \leq \max\{1-\eta, 0\} \\ \min\{(1+\eta)\gamma_{2i}^g, 1\}, & \text{if } \omega_i \geq \min\{1+\eta, 1\} \\ \gamma_{2i}^g \cdot \omega_i & \text{otherwise} \end{cases} \quad (5.98)$$

## 5.2 Principal Stress Based Optimal Orientation

In the homogenization method, the formulation of the material distribution is based on the material with periodically repeated micro-voids. The composites with cell symmetry described above are orthotropic, and the angle of rotation of the material axes of this material will influence the value of the compliance of the structure. The optimal rotation of an orthotropic material is very important for the setting of topology design and the design of composite structures.

The optimal rotation can be found analytically (Cheng, 1988) and this is of great importance for computations. The general elasticity tensor  $E_{ijkl}^G$  can be calculated by

$$\mathbf{D}^G(x_i^g, \theta^g) = \mathbf{E}_{ijkl}^G(x_i^g, \theta^g) = \sum_{p=1}^2 \sum_{q=1}^2 \sum_{r=1}^2 \sum_{s=1}^2 \mathbf{a}_{ip}(\theta^g) \mathbf{a}_{jq}(\theta^g) \mathbf{a}_{kr}(\theta^g) \mathbf{a}_{ls}(\theta^g) E_{ijkl}^H(x_i^g) \quad (5.99)$$

where  $x_i^g$  is design variable,  $i=1, 2, \dots, n$ ,  $E_{ijkl}^H(x_i^g) = \mathbf{D}^H(x_i^g)$

In the plane stress/strain problems, the rotation  $\mathbf{a}(\theta^g)$  can be defined by

$$\mathbf{a}(\theta^g) = \begin{vmatrix} \cos \theta^g & -\sin \theta^g \\ \sin \theta^g & \cos \theta^g \end{vmatrix} \quad (5.100)$$

To determine the parameter  $\theta^g$ , the principal stress method is used which takes the principal stress directions as the optimal orientation.

The principal stress method was used by Suzuki and Kikuchi in 1991. Diaz and Bendsøe extended this method for multiple load cases in 1992. In their approach, for different load cases, the principal stress directions are determined first and then by considering the equation from stationarity of the Lagrangian with respect to  $\theta^g$ , a combined equation is obtained. By solving this equation, the optimal orientation was determined. Hassani and Hinton (1998) also used the principal stress method in their topology optimization program and provided quite good results for artificial and rectangular model by using the PLATO software. In this thesis, the optimal value of orientation of each cell is given by the solution data; it is not represented on the graphical optimal layout.

### **5.3 Convergence Criterion**

In the HDM program (*Homogenization with Different Microstructures*) developed in this research, the criterion of convergence is stated as following: By checking the objective function for every design variable including the orientation variable, if the difference between its value in step  $n+1$  and in step  $n$  divided by the value in step  $n$  is less than a small value  $\Delta$ , then an optimum

solution is reached.  $\Delta$  is called convergence tolerance. By testing with topology optimization process and considering convergence speed and accuracy of optimization layout, we suggest the value  $\Delta$  between 0.01 and 0.05.

#### 5.4 Measures to Control Checkerboard Pattern

The checkerboard pattern is a region where solid and void elements distribute in an alternating manner (Figure 5.2(b)). Designs with checkerboard patterns are unrealistic and undesirable in practice. Patches of checkerboard patterns appear often in the solutions obtained by the homogenization method that use the displacement based finite element method. It was earlier believed that these regions represented some sort of optimal microstructure, but later research results showed that the checkerboard patterns are due to bad numerical modelling of the stiffness of the checkerboard region.

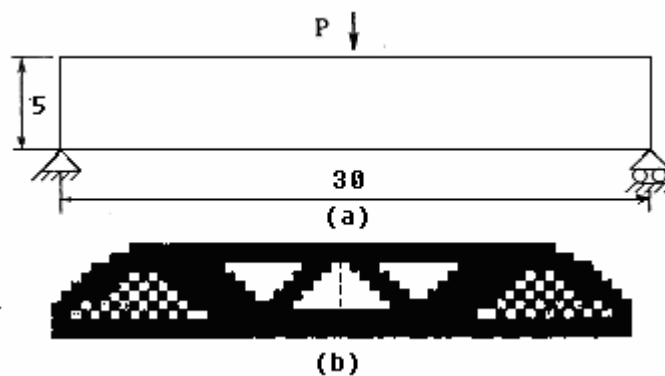


Figure 5.2 Checkerboard problem

One way to suppress it is to use higher-order finite elements for the

displacement function to avoid the checkerboard problem. Diaz and Sigmund (1995) and Jog and Haber (1996) show that checkerboards are mostly prevented when using 8 or 9-node finite elements for the homogenization approach. For the SIMP approach, however, checkerboards are only prevented using 8 or 9-node elements if the penalization power is small enough. However, a drawback of using higher-order finite elements is the substantial increase of computing (Bendsøe and Sigmund, 2002).

Another effective way to control the checkerboard pattern is using filter technique. Bendsøe and Sigmund (2002) classified the filter techniques into *Filtering the density* and *Filtering the sensitivities*.

The *Filtering the density* technique imposes explicit limitations on the allowable density distributions that can appear in the optimal design, and as such these limits have to be catered for as constraints in the optimization formulation. An alternative to this is to directly limit the variations of the densities that appear in the set of admissible stiffness tensor  $E_{ad}$  by only admitting filtered densities in the stiffness.

In the *Filtering the sensitivities*, the filter makes the design sensitivity of a specific element depend on a weighted average over the element itself and its eight direct neighbours. Such a filter is purely heuristic, but research results show that it is very efficient in removing checkerboards (Bendsøe and Sigmund, 2002).

In our computer program, a similar method with *Filter the sensitivities* is used. We use a modified **average**  $\varphi'$  instead of original  $\varphi$  for one design variable and  $\varphi', \psi', \omega', \phi'$  instead of  $\varphi, \psi, \omega, \phi$  for four design variables, which are described in Section 5.1

First, we assign  $\varphi$  to each node by

$$\varphi_k^{node} = \frac{\sum_i^{m1} x_i^g \varphi}{\sum_i^{m1} x_i^g} \quad i=1,2,\dots,m1 \quad (5.101)$$

where  $x_i^g$  is the design variable,  $m1$  is the maximum number of elements sharing the node  $k$ , which is generally equal to the number of sides or surfaces of the employed finite element.

Next, the  $\varphi_k^{node}$  is assigned back to the updated element by:

$$\varphi' = \frac{\sum_k^{m2} \varphi_k^{node}}{m2} \quad k=1,2,\dots,m2 \quad (5.102)$$

where  $m2$  is the number of nodes in each element.

## 5.5 Computer Program Implementation

The topology optimization procedure by using homogenization method consists

of three different modules: homogenization, structural analysis and optimization.

In the homogenization module, first we need to establish a model of microstructure. Then our aim is to develop the relationship between effective material properties and the geometrical shape parameters of the microstructure. One way to achieve this goal is to carry out a series of finite element analysis for the different geometrical shape parameters of the microstructure. Subsequently, the polynomials for the elasticity matrix of the homogeneous solid are obtained. Most of microstructures can be calculated by this way. With high speed computer technology development, more and more calculations of microstructure properties will use numerical method. Another way is using analytical formulae method, such as in the case of ranked layered one-material and bi-material microstructures, the effective material properties generally can be derived analytically. In such an analytical approach, explicit expressions for the effective elastic tensor can be obtained by establishing the optimal upper and lower bounds for the complementary elastic energy density of the porous material. These microstructures are known as “extremal” microstructures in the sense that they achieve optimality in the Hashin-Shtrikman bounds on the effective properties of composite materials. This method can be applied to both two-dimensional and three-dimensional layered material cell of finite rank. The third way is using a simple formula and combining it with penalty method, for example, Power-law material microstructure (Bendsøe and Sigmund, 2002) and

artificial model (Hassani and Hinton, 1998).

In the structural analysis module, first a finite element model of microstructures needs to be established. It is common practice to use a regular mesh of elements, each element is a microstructure. Then for a given boundary and loading conditions, a finite element analysis is carried out based on the effective material properties that have been obtained by homogenization method. Stress, strains and displacements can be calculated.

In the optimization module, considering the shape parameters of the microstructure model in finite elements as design variables, the total potential energy as objective function, the volume of material as global constraint, by using optimality criteria method and filter technique, the topology optimization program can be implemented.

The HDM computer program developed in this research was built on a computer Pentium III, 128MB memory, 32MB DDR Nvidia GeForce2 GTS Graphics cards, using Windows 2000 Operating System. The visual graphic was developed by Delphi 5.0 software. The mesh development uses Strand 7 standard finite element software by G+D Computing Pty. Ltd. Australia, which permits user to build models, add loads and constraints very easily and quickly. The following facilities are available in strand7.

- Create, delete and manipulate elements with a comprehensive set of

tools, automatic meshing and unlimited undo.

- Organise a complicated model into a simple set of parts using the Group Tree.
- Define your own coordinate systems and beam cross-sections.
- Check mesh quality with aspect ratio and warping contours and free edge detection.

However, the solver of the finite element was developed and included in the optimization program by the author. Four and eight nodes elements are available. The optimization code is a combination of C<sup>++</sup> and FORTRAN 95. All the programs are finally controlled by a HDM.bat batch file. Typically, for a 496 nodes, 450 meshes, single load problem, the analysis time is 12 minutes for 200 numbers of iterations.

The topology optimization algorithm is as follows:

*Step 1* Program start and greeting

*Step 2* Draw a suitable reference domain and discretize the reference domain by generating a finite element mesh for analysis, define surface tractions, fixed boundaries, loads, and material properties, etc. by using Strand7 software.

*Step 3* Choose a microstructure model out of fifteen models available and optimization parameters.

*Step 4* Calculate the initial value of the design variables. The initial

orientation value  $\theta$  is set to zero.

*Step 5* Compute the effective material properties of the composite, using homogenization theory. This gives a functional relationship between the density of material in the composite (i.e. sizes of holes) and the effective material properties.

*Step 6* Carry out structure analysis to obtain stress, strain and displacement.

*Step 7* Evaluate the objective function.

*Step 8* Use filter technique to modify  $\varphi, \psi, \omega, \phi$  to  $\varphi', \psi', \omega', \phi'$

*Step 9* Resize the design variables and orientation value

*Step 10* Check the volume constraint, if it is active, continue, otherwise update it and go back to Step 9

*Step 11* Form a new design based on the new set of design variables for each element

*Step 12* Check if solution has converged; if it is, go to next step, otherwise update design variables and go back to step 5

*Step 13* Output the image layout of new design

The algorithm is illustrated in Figure 5.3 and a typical run of HDM software is presented in Appendix B.

## **5.6 Summary**

Based on the study of homogenization method and the properties of different

microstructure models, a computer program named HDM (Homogenization with Different Microstructures) has been developed. This program includes five new one-material microstructure models and four new bi-material microstructure models. The new one-material models are: *cross shape microstructure model*, *circular microstructure model*, *triangular multi-voids microstructure model*, *rectangular multi-voids microstructure model*, and *square multi-voids microstructure model*. The new bi-material models are: *cross shape bi-material model*, *square bi-material model*, *rectangular bi-material model* and *triangular bi-material model*.

The program also includes some existing microstructure models for which the microstructures optimization program codes are not available in the literature. These models are: *ranked layered model*, *triangular microstructure model*, *hexagon microstructure model*, *power-law one-material model*, *power-law bi-material model* and *ranked layered bi-material model*.

A filtering program for checkerboard pattern control was established. The filter method is very useful not only for checkerboard pattern control but also for mesh-dependence problem, which easily appeared in SIMP method.

The program uses optimality criteria method for updating design variable and principal stress method for updating orientation variable. A simple convergence criterion was used.

In the next chapter, we use the program developed in this chapter to investigate some benchmark problems of topology optimization.

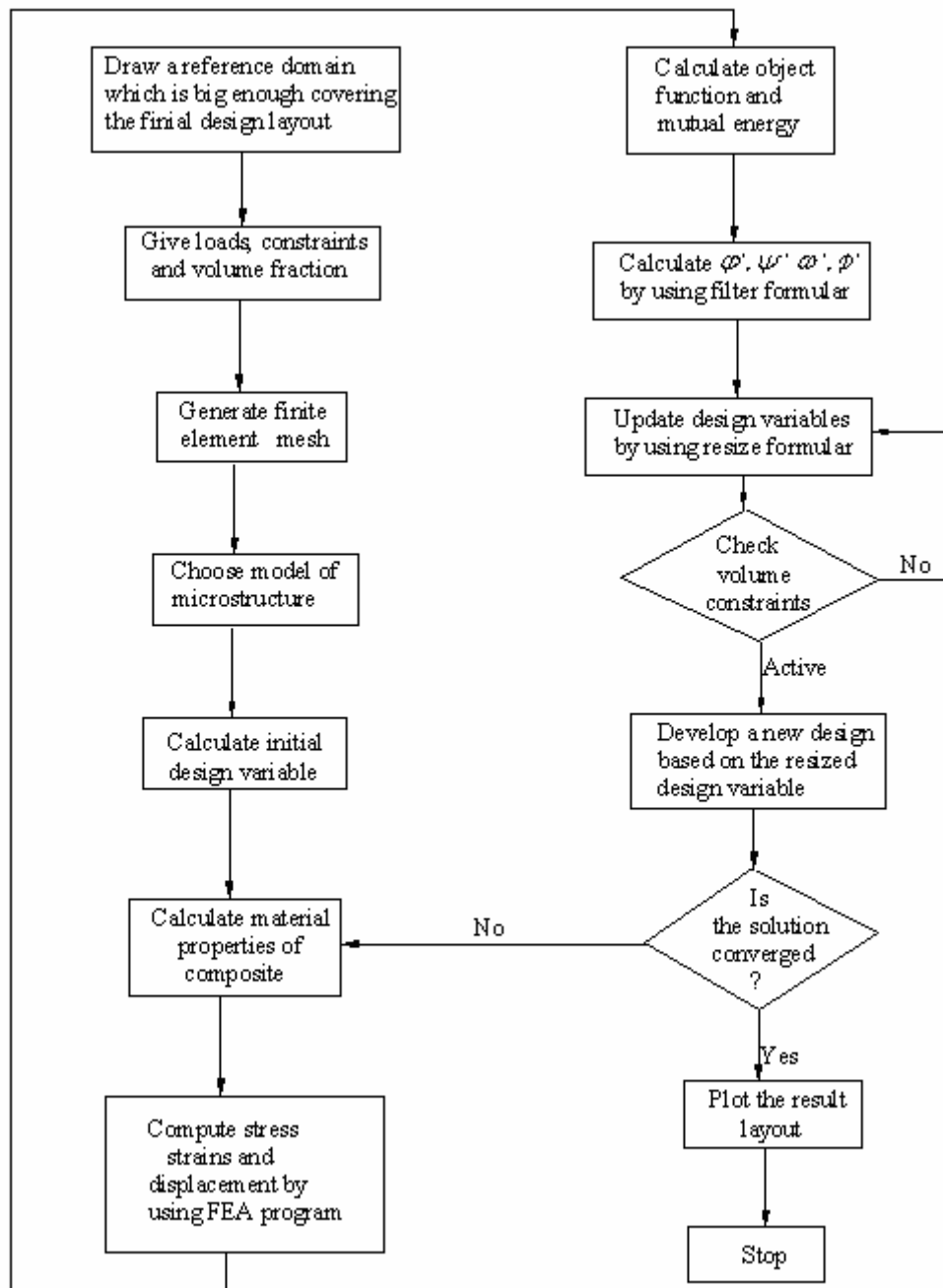


Figure 5.3 Topology optimization procedure using homogenization method

## **Chapter 6**

---

# **COMPARISONS BETWEEN ALGORITHMS USING BENCHMARK TOPOLOGY OPTIMIZATION PROBLEMS**

In this chapter, the HDM algorithm was evaluated by studying benchmark problems of topology optimization of cantilever beam made of isotropic material and comparing the results of the HDM algorithm for structural topology optimization with other solutions available in the literature. The study of HDM algorithm is divided into two parts: one-material models and bi-material models. In each section, benchmark problems are first described, followed by comparisons between the optimization solutions of HDM and other software packages in literature.

### **6.1 Algorithm Test by Deep Cantilever Beam Optimization Problem**

A deep cantilever beam with a single load and fixed constraint is shown in Figure 6.1. Modulus of elasticity of solid material  $E_a = 1 \times 10^5$  MPa, the Poisson's ratio  $\nu = 0.3$  and volume fraction  $V_s / V = 20\%$ .

The optimization criterion for the minimum compliance of this problem has been derived by Hassani and Hinton (1998) as shown in Appendix C. The optimum result for this problem should be a two bar truss feature running at  $\pm 45^\circ$  to the vertical direction shown in Figure 6.2.

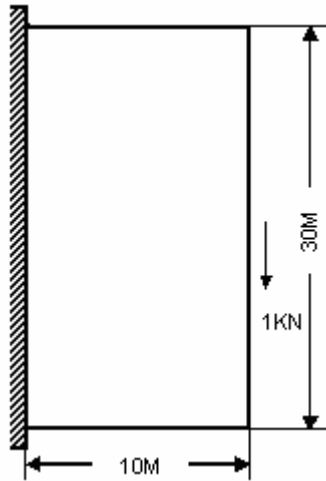


Figure 6.1 A deep cantilever beam

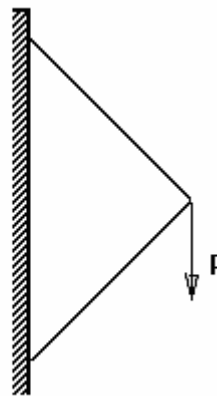
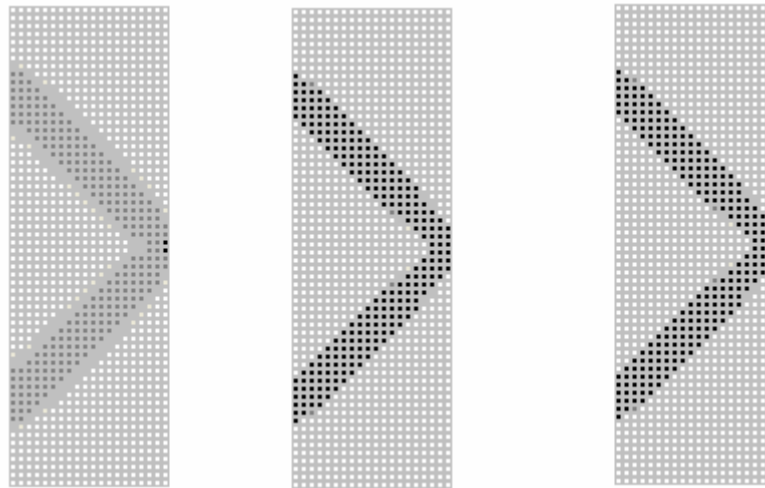


Figure 6.2 Optimum feature of the deep cantilever beam

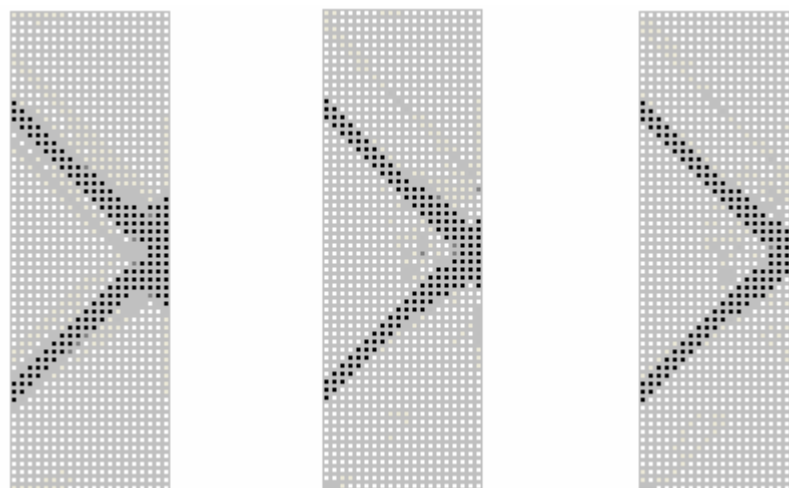
The optimum layouts of by HDM using nine different one-material models with the domain discretized to 1200 (20x60) eight-node finite elements and different convergence tolerance (a)  $\Delta_1 = 0.050$ , (b)  $\Delta_2 = 0.010$ , (c)  $\Delta_3 = 0.005$  are shown in Figures 6.3-6.11, in Figure 6.3, power-law one-material model; Figure 6.4, ranked layered material model; Figure 6.5, triangular material model; Figure 6.6, hexagon material model; Figure 6.7, cross shape material model; Figure 6.8, circular material model; Figure 6.9, triangular multi-void material model; Figure 6.10, rectangular multi-void material model; Figure 6.11, square multi-void material model.

It should be noted that in all result graphics, white areas mean no materials, black areas mean the areas taken up by solid material and the grey areas mean the areas taken up by mixture of material with void, the intensity of the grey shade reflects the density of the cell and one element represents one microcell.



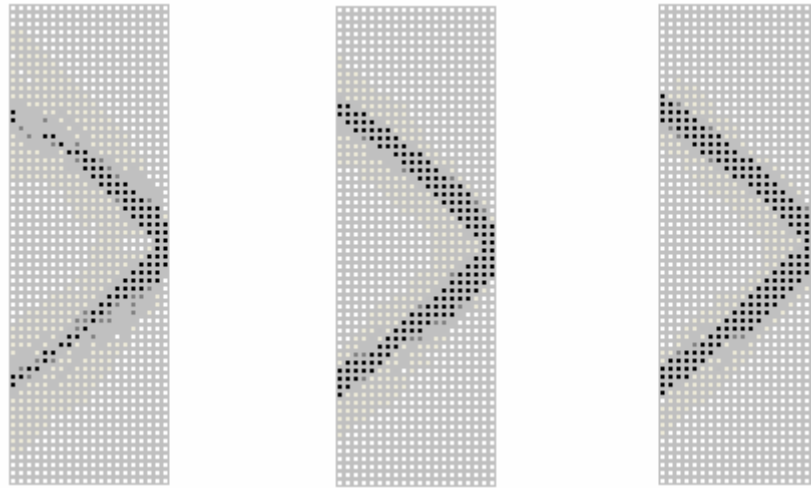
(a)  $\Delta_1 = 0.050$       (b)  $\Delta_2 = 0.010$       (c)  $\Delta_3 = 0.005$

Figure 6.3 Optimization layouts for power-law one-material model



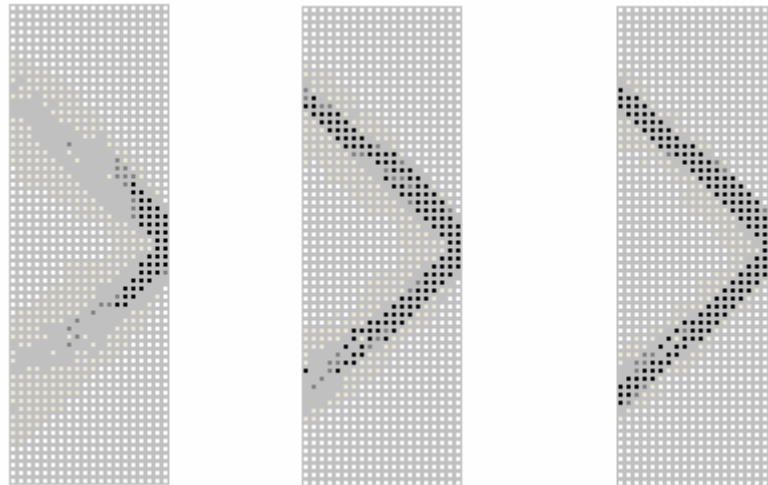
(a)  $\Delta_1 = 0.050$       (b)  $\Delta_2 = 0.010$       (c)  $\Delta_3 = 0.005$

Figure 6.4 Optimization layouts for ranked layered material model



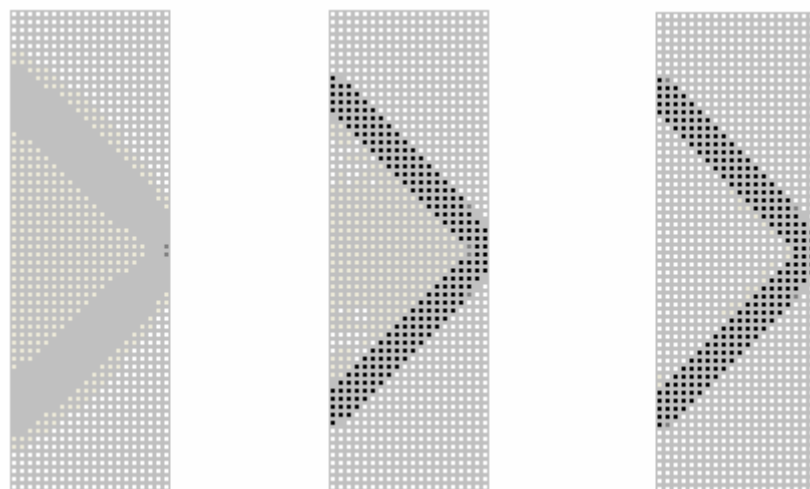
(a)  $\Delta_1 = 0.050$       (b)  $\Delta_2 = 0.010$       (c)  $\Delta_3 = 0.005$

Figure 6.5 Optimization layouts for triangular material model



(a)  $\Delta_1 = 0.050$       (b)  $\Delta_2 = 0.010$       (c)  $\Delta_3 = 0.005$

Figure 6.6 Optimization layouts for hexagon material model



(a)  $\Delta_1 = 0.050$       (b)  $\Delta_2 = 0.010$       (c)  $\Delta_3 = 0.005$

Figure 6.7 Optimization layouts for cross shape material model



(a)  $\Delta_1 = 0.050$



(b)  $\Delta_2 = 0.010$



(c)  $\Delta_3 = 0.005$

Figure 6.8 Optimization layouts for circular material model



(a)  $\Delta_1 = 0.050$

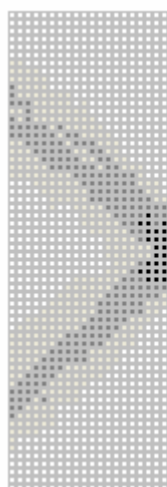


(b)  $\Delta_2 = 0.010$



(c)  $\Delta_3 = 0.005$

Figure 6.9 Optimization layouts for triangular multi-void material model



(a)  $\Delta_1 = 0.050$



(b)  $\Delta_2 = 0.010$



(c)  $\Delta_3 = 0.005$

Figure 6.10 Optimization layouts for rectangular multi-void material model

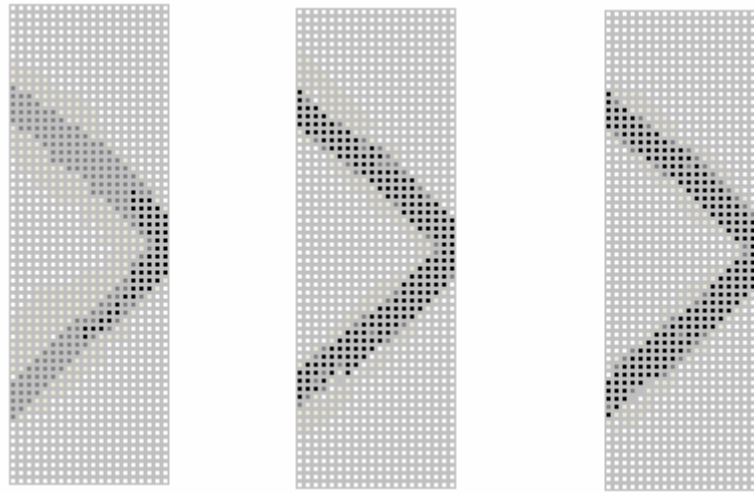
(a)  $\Delta_1 = 0.050$ (b)  $\Delta_2 = 0.010$ (c)  $\Delta_3 = 0.005$ 

Figure 6.11 Optimization layouts for square multi-void material model

The iteration numbers for different convergence tolerances are shown in Table 6.1.

Material model	convergence tolerance $\Delta_1 = 0.050$	convergence tolerance $\Delta_2 = 0.010$	convergence tolerance $\Delta_3 = 0.005$
Power-law	39	130	195
Ranked layered	43	168	233
Triangular	54	174	212
Hexagon	49	164	273
Cross shape	40	134	203
Circular	63	166	286
Triangular multi-void	53	203	395
Rectangular multi-void	52	166	231
Square multi-void	59	189	248

Table 6.1 Iteration numbers for different convergence tolerances

From the optimization results of different microstructure models we can see that all the one-material models using HDM software agree well with the optimization criterion for the minimum compliance of this problem derived by Hassani and Hinton (1998). We also noticed that initially the properties of the cell are periodically distributed throughout the domain, but the properties of the cells in the final results are no longer periodically distributed. Within these results, the ranked layered model shows a little difference. The power-law model performs the best. The optimization results also show that the convergence tolerances between 0.010 and 0.005 give similar layouts.

For bi-material cases, we choose the modulus of hard and soft materials elasticity  $E_a = 1 \times 10^5$  MPa,  $E_b = 1 \times 10^3$  MPa and Poisson's ratio  $\nu = 0.3$ .

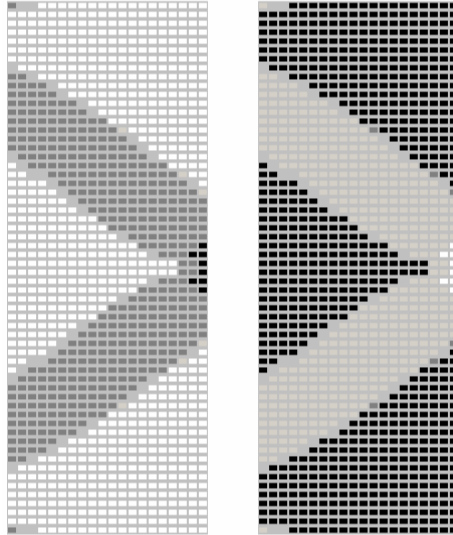
***Case a: bi-material without void***

The design domain was considered as a bi-material composite and it only contains the two materials, no voids. The aim of the optimization is to find the distribution of hard and soft materials in the given domain. In this case, the volume fractions of hard material  $V_H / V = 30\%$ , soft materials  $V_S / V = 70\%$ .

***Case b: bi-material with void***

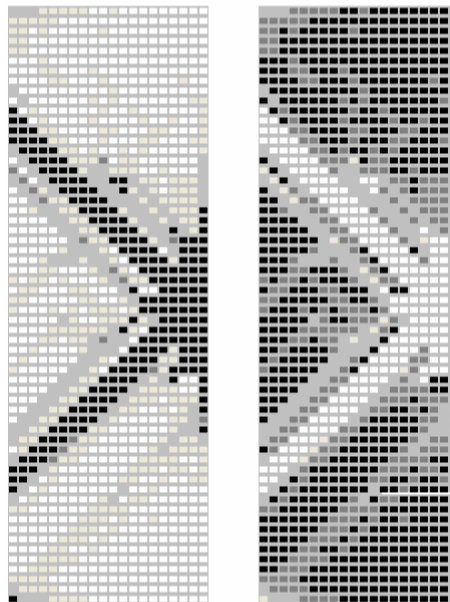
The design domain is considered as a bi-material composite with voids. The aim of the optimization is to find the distribution of hard and soft materials in the given domain. The volume fractions of hard material is  $V_H / V = 20\%$  and soft materials is  $V_S / V = 30\%$ .

In Case *a*, the results of using the six different material models are shown in Figure 6.12. In Figure 6.12, (a) power-law, (b) ranked layered, (c) square, (d) cross shape, (e) rectangular and (f) triangular bi-material model.



(a1) Hard material distribution      (a2) Soft material distribution

(a) Optimization layout for power-law bi-material model at  $\mu = 3$

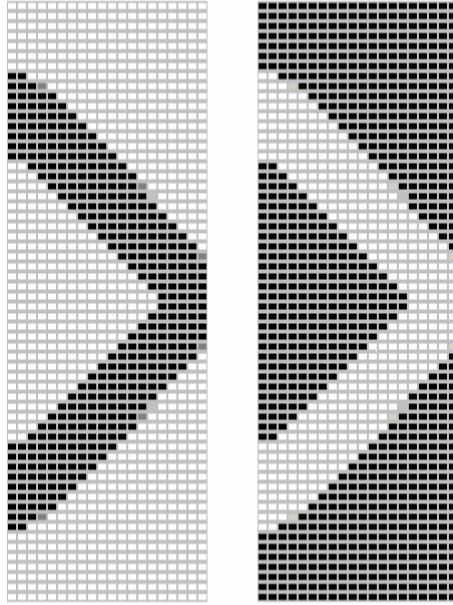


(b1) Hard material distribution      (b2) Soft material distribution

(b) Optimization layout for ranked layered bi-material model

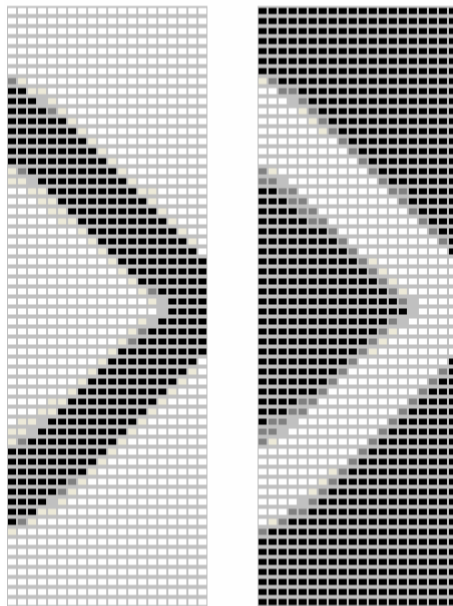
Figure 6.12 Optimization layouts of *Case a* (continued)

(Figure 6.12 continued)



(c1) Hard material distribution      (c2) Soft material distribution

(c) Optimization layout for square bi-material model

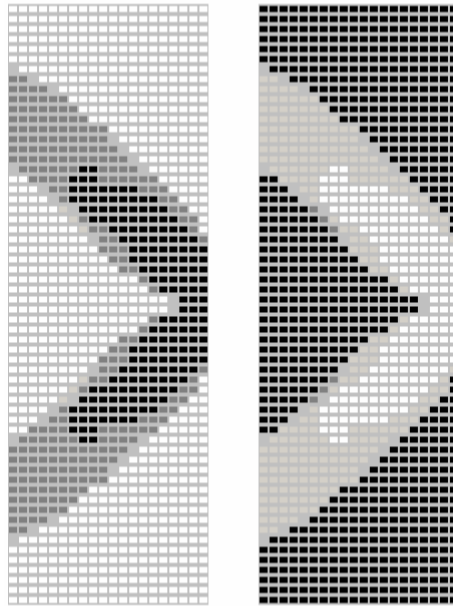


(d1) Hard material distribution      (d2) Soft material distribution

(d) Optimization layout for cross shape bi-material model

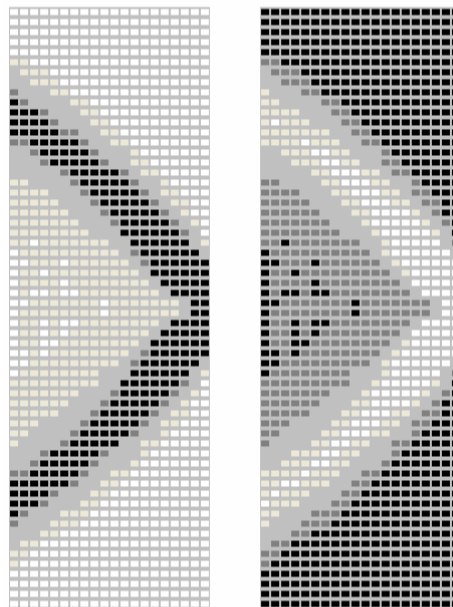
Figure 6.12 Optimization layouts of *Case a* (continued)

(Figure 6.12 continued)



(e1) Hard material distribution      (e2) Soft material distribution

(e) Optimization layout for double rectangular bi-material model

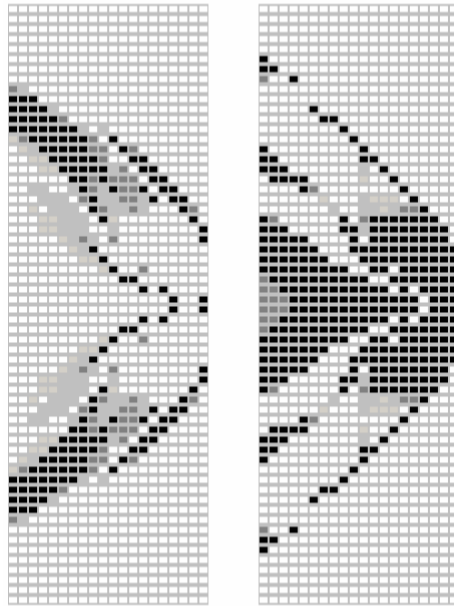


(f1) Hard material distribution      (f2) Soft material distribution

(f) Optimization layout for triangular bi-material model

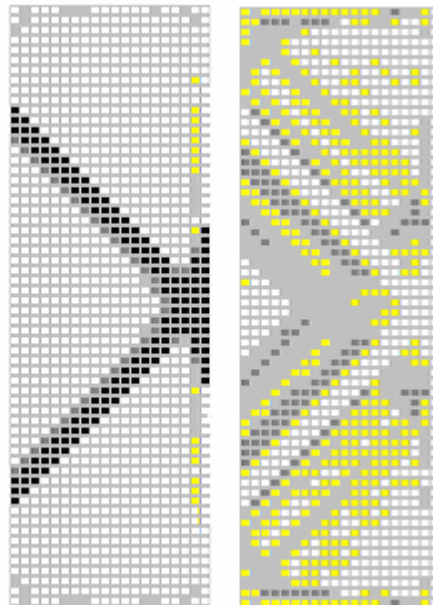
Figure 6.12 Optimization layouts of *Case a*

In Case *b*, the results of using the six different material models are shown in Figure 6.13.



(a1) Hard material distribution      (a2) Soft material distribution

(a) Optimization layout for power-law bi-material model at  $\mu = 3$

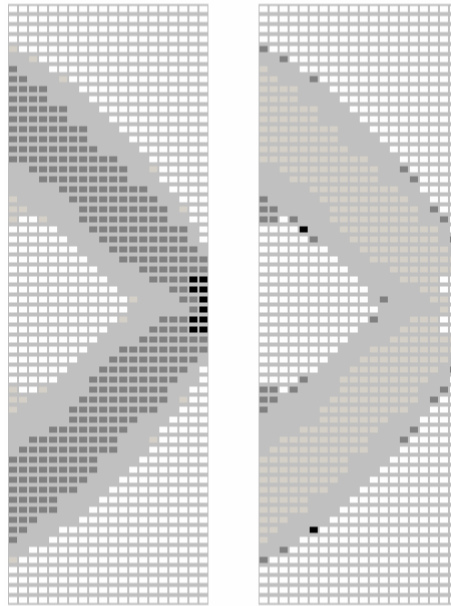


(b1) Hard material distribution      (b2) Soft material distribution

(b) Optimization layout for ranked layered bi-material model

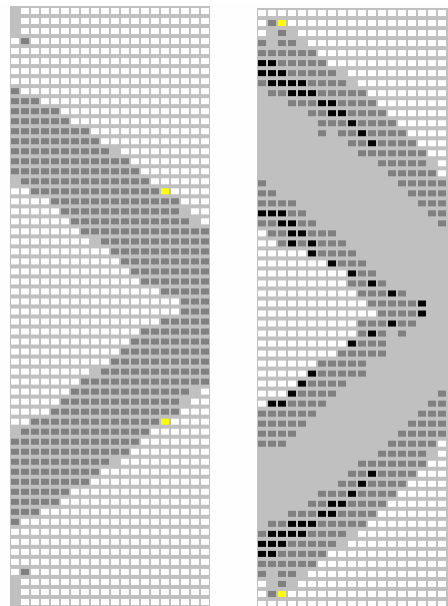
Figure 6.13 Optimization layouts of *Case b* (continued)

(Figure 6.13 continued)



(c1) Hard material distribution    (c2) Soft material distribution

(c) Optimization layout for square bi-material model

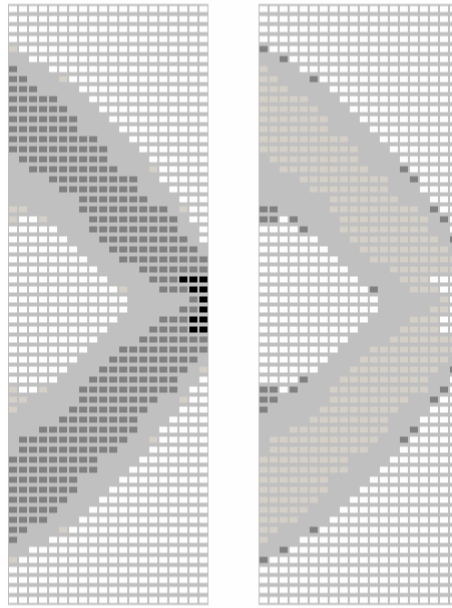


(d1) Hard material distribution    (d2) Soft material distribution

(d) Optimization layout for cross shape bi-material model

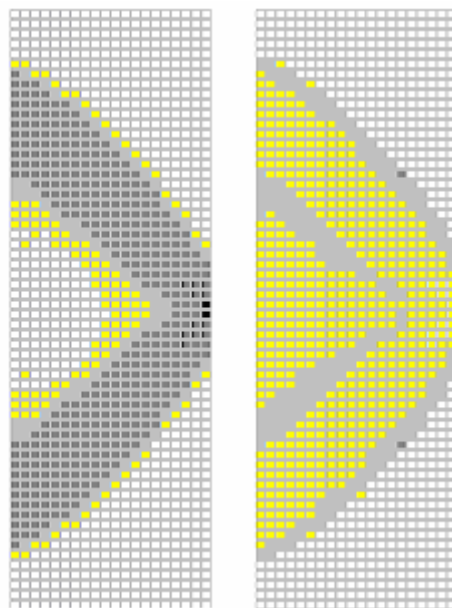
Figure 6.13 Optimization layouts of *Case b* (continued)

(Figure 6.13 continued)



(e1) Hard material distribution      (e2) Soft material distribution

(e) Optimization layout for double rectangular bi-material model



(f1) Hard material distribution      (f2) Soft material distribution

(f) Optimization layout for triangular bi-material model

Figure 6.13 Result layouts of **Case b**

From the layouts of *case a* and *case b* shown above, we can see that the hard material distributions in most bi-material models are concentrated on the high stress areas. Most of the optimization results are of a similar pattern but the optimization results of ranked layered bi-material models are very much different from the others in both *case a* and *case b*. This is because that in the rank-2 layered material model, any optimal microstructure is degenerated and the structure cannot sustain a non-aligned shear stress. This will result in the stiffness matrix of the structure becoming singular. To overcome the singularity problem, the measure adopted in the thesis is to use a very soft material instead of the voids. However, the minimum strain energy calculated during optimization process (commonly used for objective function which is equivalent with maximum total potential energy) is modified energy and the displacements between layers are larger than those found in other models. This leads the result shown much difference with others. In *case b*, the result of power-law model shows some difference with others. The reason is that the strain energy calculated in the optimization process for power-law model is not real; it does not necessarily converge to the true value of the optimal solution in some cases.

## **6.2 Comparing Algorithms for One-material Microstructure Models with Algorithms Found in Literature**

### ***6.2.1 Results of topology optimization available in literature***

The short cantilever beam shown in Figure 6.14 has been studied by many

authors. A point load of intensity  $P=1\text{kN}$  is applied midway down the right hand side of the beam. Modulus of elasticity is  $E = 10^5 \text{ MPa}$ , Poisson's ratio,  $\nu = 0.3$ .

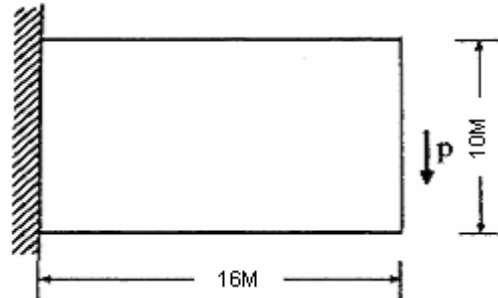


Figure 6.14 A short cantilever beam with a point load

Min, Nishiwaki and Kikuchi (1999) studied this benchmark problem by homogenization method. In their study, the design domain is discretized to 1440 (48 x 30) four-node finite elements with 1519 nodes as shown in Figure 6.15.

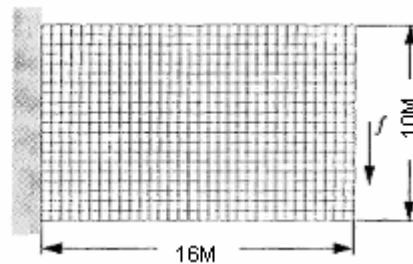


Figure 6.15 Discretized design domain (Min *et al.* 1999)

The design goal is to obtain the optimal topology of a structure with the maximum stiffness. The optimal structures of the stiffness optimization with different volume constraints  $\Omega_s = 0.2\Omega$ ,  $\Omega_s = 0.4\Omega$ ,  $\Omega_s = 0.6\Omega$  are shown in Figure 6.16.

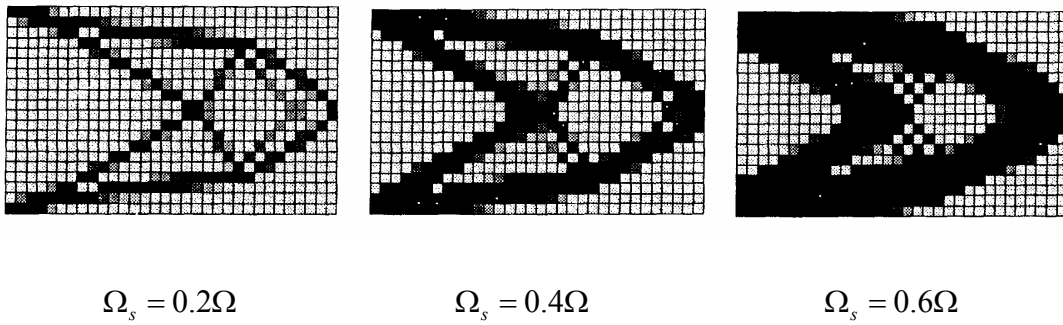
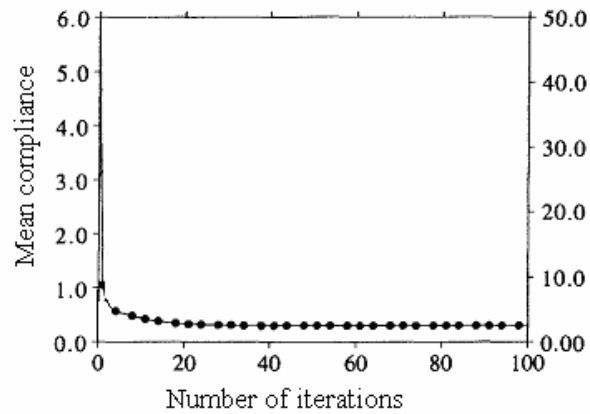
Figure 6.16 Optimal structure layouts (Min *et al.* 1999)

Figure 6.17 illustrates the iteration history in the case of volume constraint is 40%.

Figure 6.17 Convergence in the case of volume constraint 40% (Min *et al.* 1999).

Hassani and Hinton (1998) developed a topology optimization program named PLATO based on artificial and rectangular models and studied the topology optimization problems and the effect of the rectangular, artificial, and ranked layered material models. The following pictures are the part of their research results on the benchmark problem. Figure 6.18 shows a optimal layout using rectangular model with volume constraint of 40% and the iteration history.

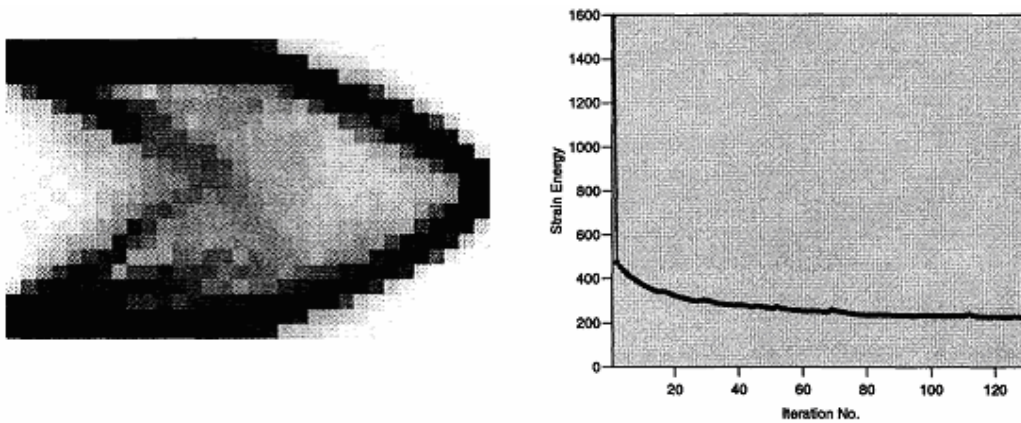


Figure 6.18 Optimal layout and iteration history (Hassani and Hinton, 1998)

The optimization results of using artificial model are shown in Figure 6.19.

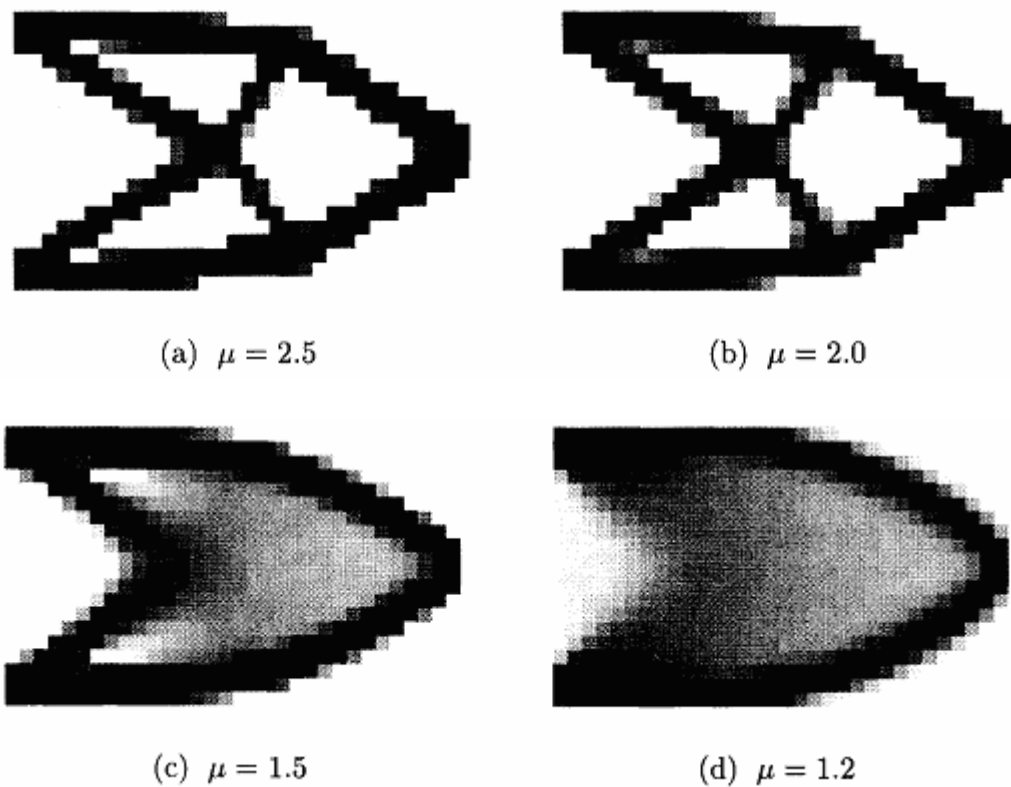


Figure 6.19 Optimal layouts of using artificial model with different penalties  $\mu$

(Hassani and Hinton, 1998)

The iteration histories are given in Figure 6.20.

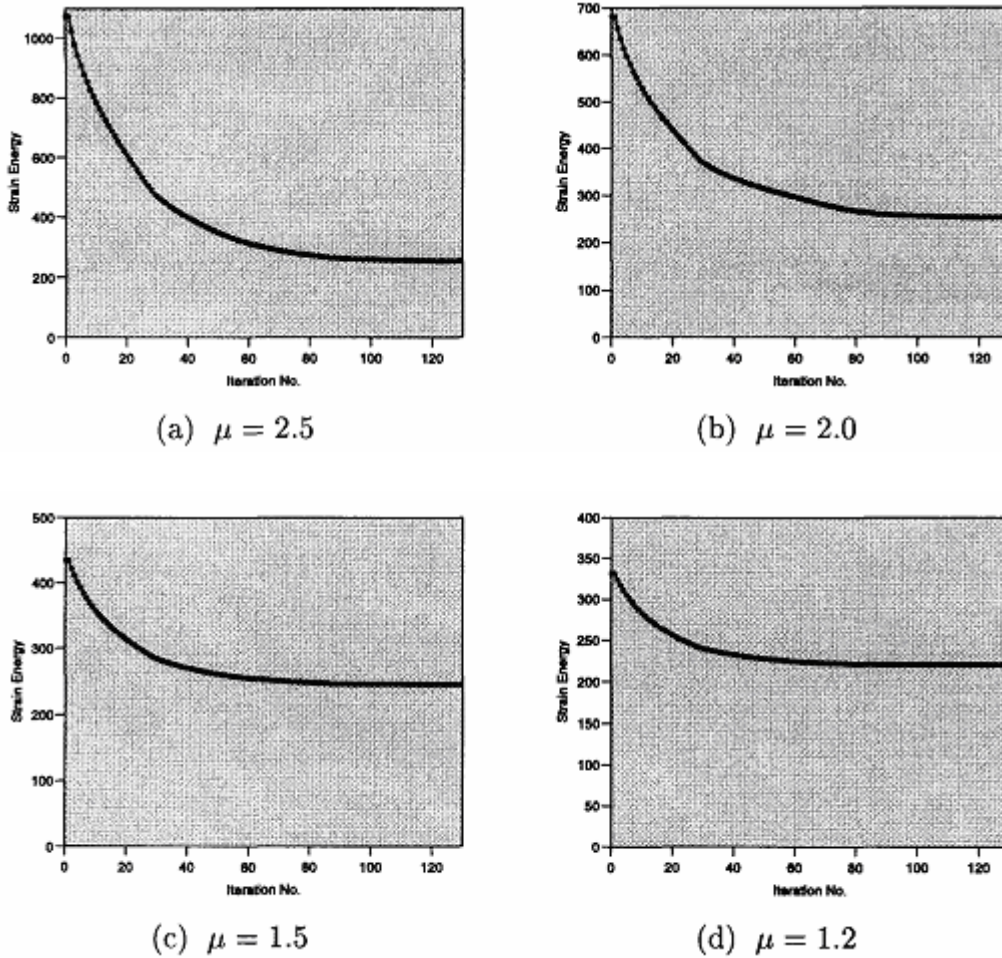


Figure 6.20 Iteration history of using artificial model with different penalties  $\mu$  (Hassani and Hinton, 1998)

They also gave the optimization results and iteration history of using ranked layered material model shown in Figure 6.21 and 6.22:

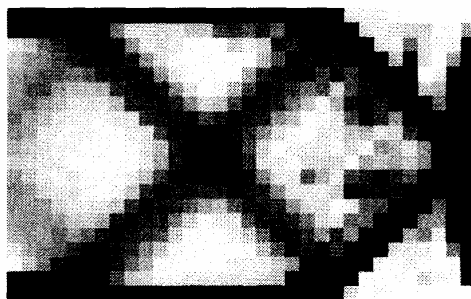


Figure 6.21 Optimization results of using ranked layered material model (Hassani and Hinton, 1998)

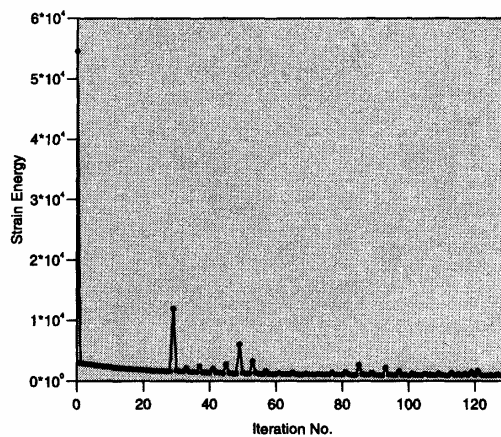
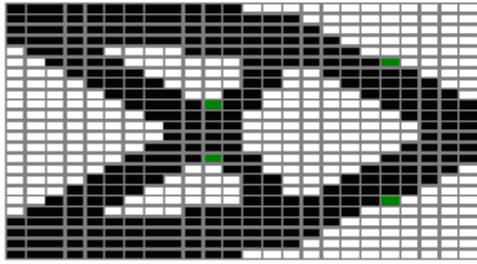


Figure 6.22 Iteration history of using ranked layered model (Hassani and Hinton, 1998)

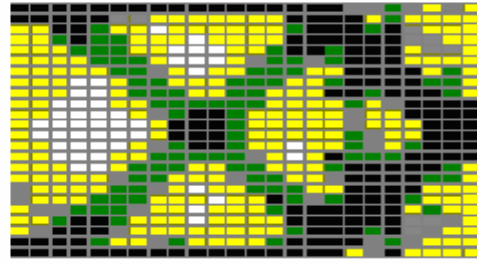
From the optimization layout and iteration history in literature, we can see that different software packages and using different microstructure models give similar results, as shown by the case of volume constraint of 40%, Figure 6.16 and 6.19,  $\mu = 2.5$ . From Figure 6.21 we can also see that the ranked layered model shows a different pattern with other models.

### 6.2.2. Results of HDM algorithm with different material models

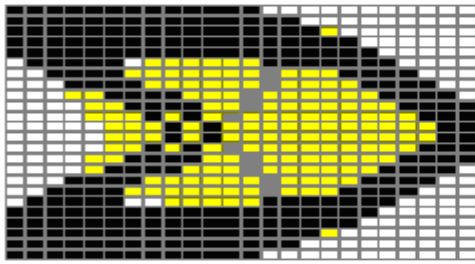
The same problem with the same volume constraint of 40% was solved by HDM. The optimization results of using HDM algorithm with different material models developed in Chapter 5 are shown in Figure 6.23: (a) power-law, (b) ranked layered (c) circular, (d) triangular, (e) hexagon, (f) cross shape, (g) triangular multi-void, (h) rectangular multi-void and (i) square multi-void material model.



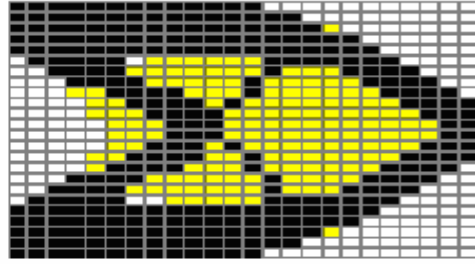
(a) Power-law one-material model.



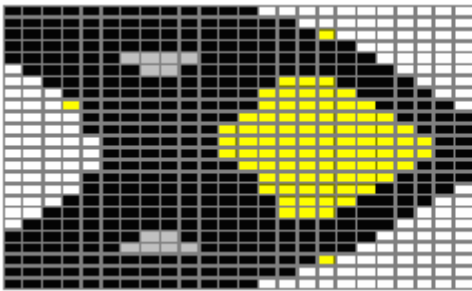
(b) Ranked layered material model.



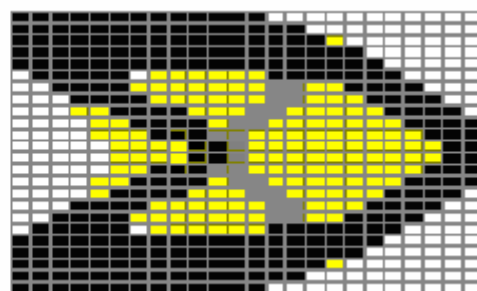
(c) Circular material model.



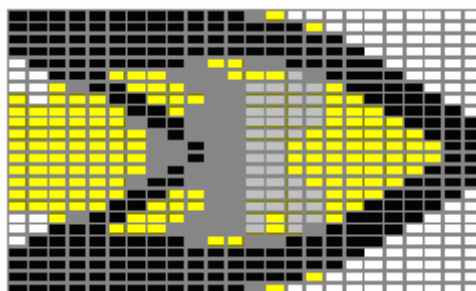
(d) Triangular material model.



(e) Hexagon material model.



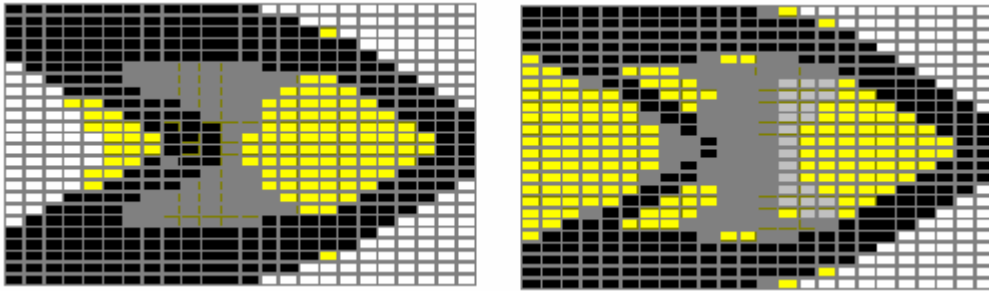
(f) Cross shape material model.



(g) Triangular multi-void model.

Figure 6.23 Optimization results with different microstructures (*continued*)

(Figure 6.23 continued)



(h) Rectangular multi-void model. (i) Square multi-void model.

Figure 6.23 Optimization results with different microstructures.

Compared to the optimization layout in literature, the layout of HDM using eight one-material models (except ranked layered model), can provide optimal topology of a design domain. The result layout pattern of the ranked layered microstructure model shows much difference from others, but similar to the result of the ranked layered model of PLATO. As discussed before, the difference of the results is because of the fact that ranked layered model does not take into account shear stress between layers. For the use of topology optimization technique at concept design stage at present, we can say that the algorithm of HDM is successful.

### ***6.2.3 Optimization layouts of the power-law model and the artificial model***

From the optimization results above, we can see that the optimization layout of using power-law model have a very similar layout pattern with artificial model with larger penalty value and results given by Min *et al.* (1999) results. To

investigate further, we solved the benchmark problem by using power values from 1 to 10. The effect on optimization layouts is shown in Figure 6.24.

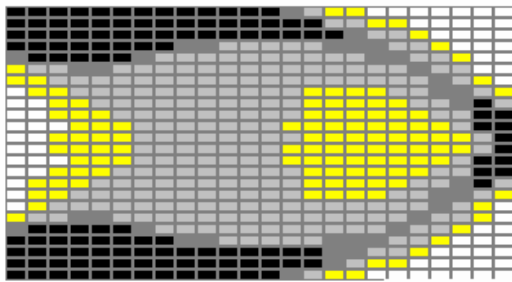
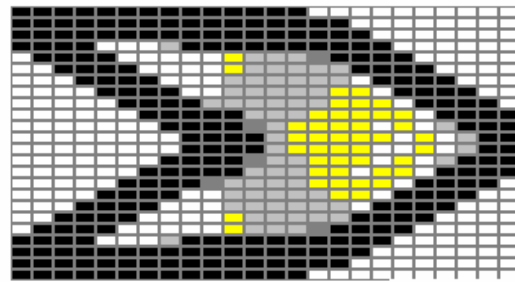
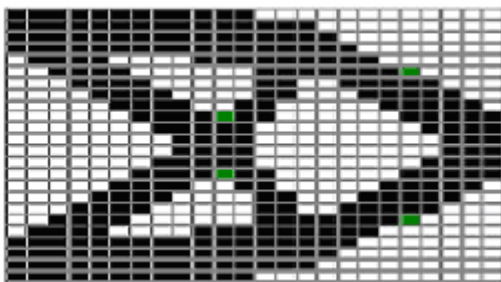
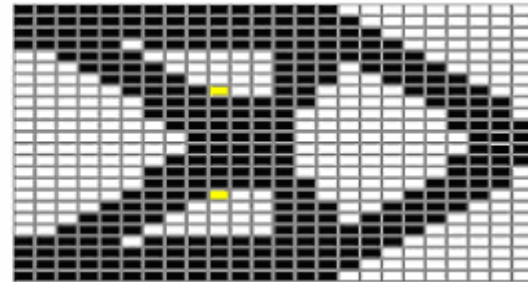
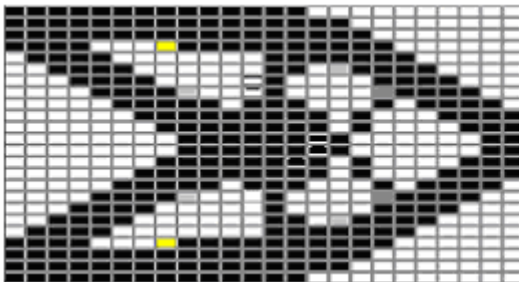
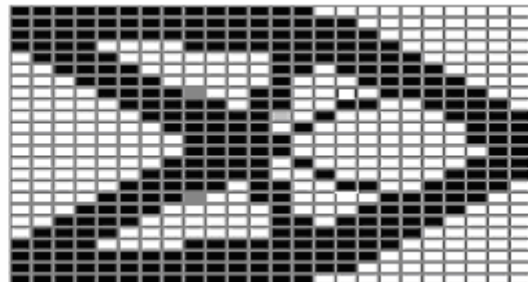
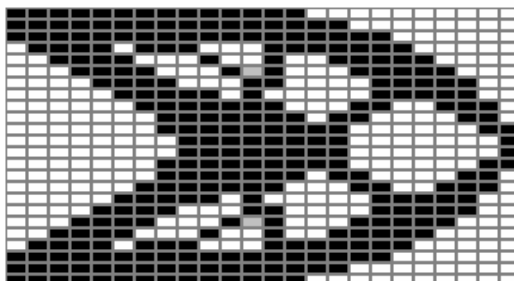
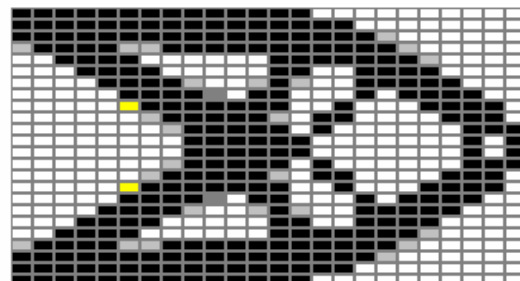
(a) Power value  $\mu = 1$ (b) Power value  $\mu = 2$ (c) Power value  $\mu = 3$ (d) Power value  $\mu = 4$ (e) Power value  $\mu = 5$ (f) Power value  $\mu = 6$ (g) Power value  $\mu = 7$ (h) Power value  $\mu = 8$ 

Figure 6.24 Optimization results for different power values (*continued*)

(Figure 6.24 continued)

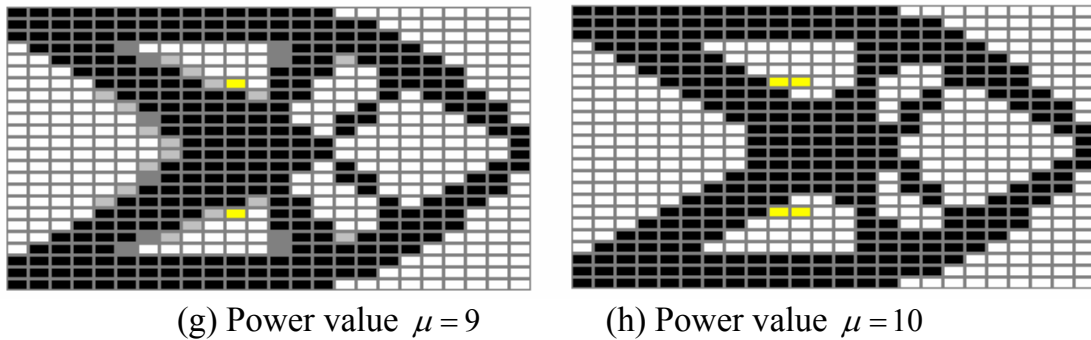
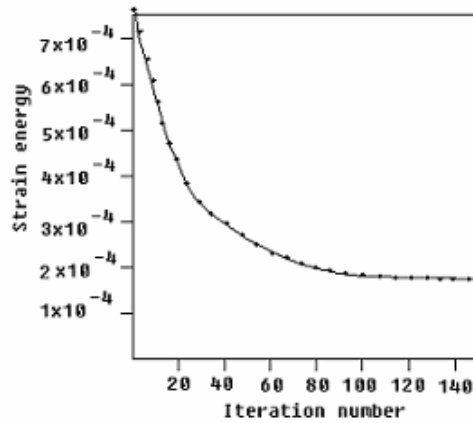


Figure 6.24 Optimization results for different power values.

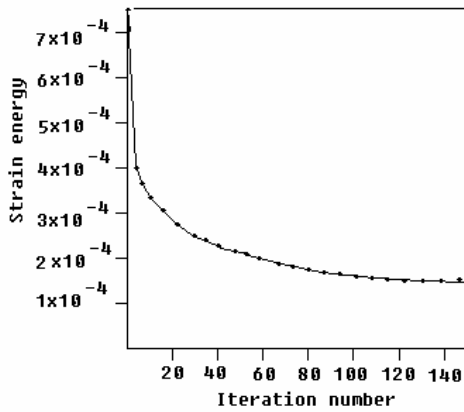
From the optimal layout patterns above, we can see that when  $\mu \leq 2$ , there are some grey shaded areas appearing on the optimal layouts. With increasing value of  $\mu$ , the grey shaded area is reduced. From the results we can also see that there are three similar patterns shown on the results,  $\mu \leq 2$ ,  $\mu = 3 \sim 4$  and  $\mu = 5 \sim 10$ . By comparison with other results in the literature, we can conclude that  $\mu = 3 \sim 4$  performs the best.

#### 6.2.4 Iteration history for different material models

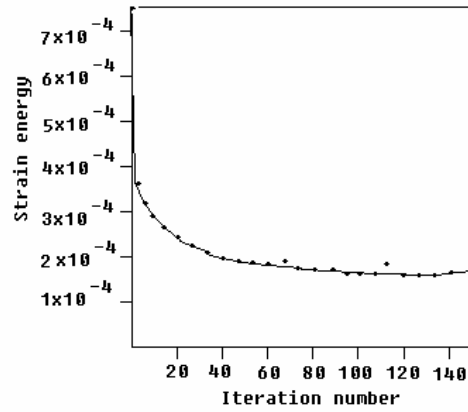
Figure 6.25 shows the iteration history for different material models. In Figure 6.25, (a) power-law one-material model with power value  $\mu = 3$ , (b) triangular material model, (c) hexagon material model, (d) cross shape material model, (e) circular material model, (f) triangular multi-void material model, (g) rectangular multi-void material model, (h) square multi-void material model, and (i) ranked layered material model.



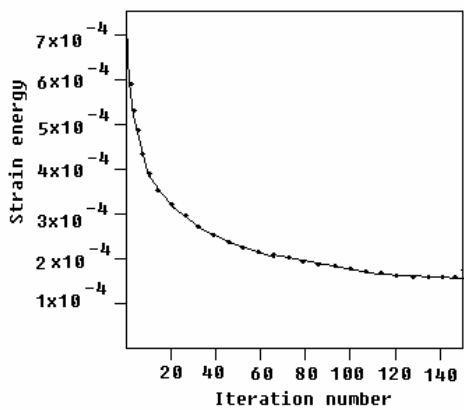
(a) Power-law one-material model.



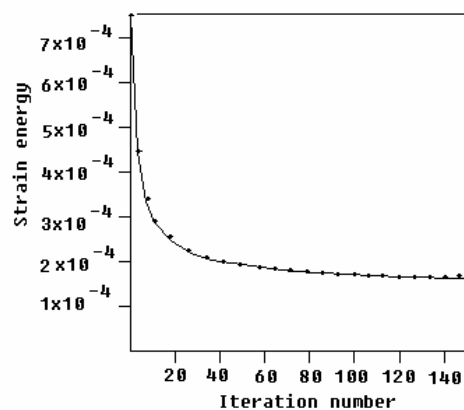
(b) Triangular material model.



(c) Hexagon material model.



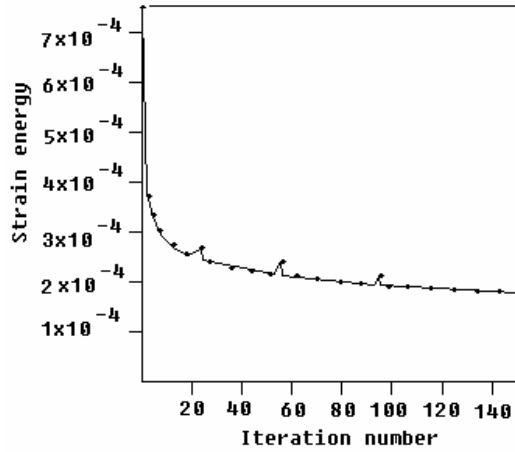
(d) Cross shape material model.



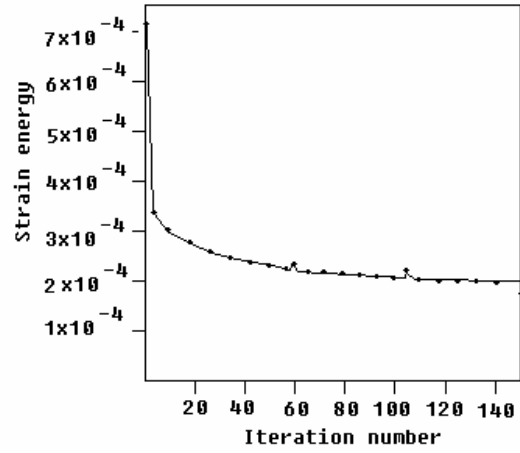
(e) Circular material model.

Figure 6.25 Iteration histories for different models (*continued*)

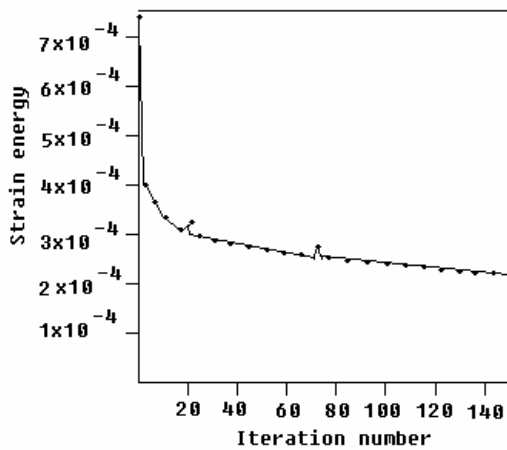
(Figure 6.25 continued)



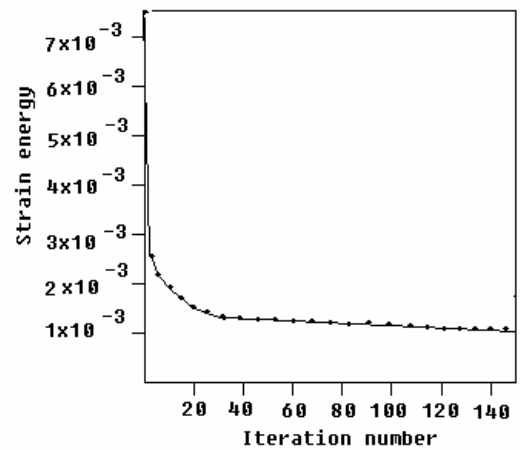
(f) Triangular multi-void model.



(g) Rectangular multi-void model.



(h) Square multi-void material model.



(i) Ranked layered material model.

Figure 6.25 Iteration histories for different material models

Table 6.2 shows iteration numbers and final strain energies at convergence tolerance  $\Delta = 0.05$  for the microstructures using HDM.

Microstructure Model	Iteration Number	Final Strain Energy
Power-law	203	0.00020
Cross shape	235	0.00019
Circular	211	0.000187
Hexagon	275	0.000198
Triangular	243	0.000189
Rectangular Multi-void	220	0.00021
Square Multi-void	243	0.00022
Triangular Multi-void	279	0.000189
Ranked layered	267	0.00128

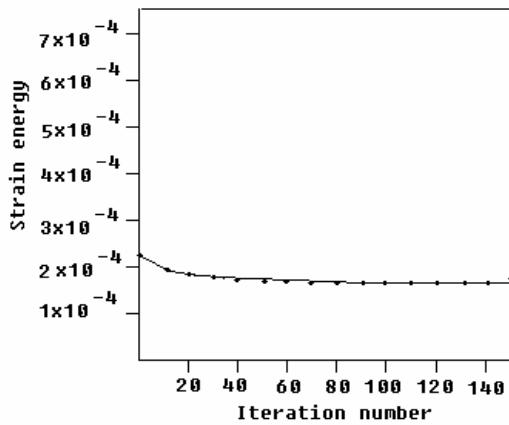
Table 6.2 Iteration numbers and final strain energies at convergence tolerance

$\Delta = 0.050$  for the microstructures using HDM

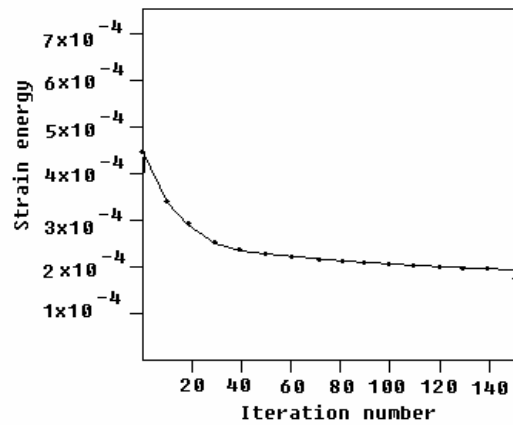
From the iteration histories and strain energies shown in Figure 6.25 and Table 6.2 and comparison with results from literature, the convergence speed by HDM is good. Among these material models, power-law, triangular, cross shape, circular and ranked layered one-material models perform with better convergence than others. The studies on the convergence criteria for the different models will be carried out in the next chapter.

### ***6.2.5 Comparisons of iteration history for the different power values in power-law model with artificial model***

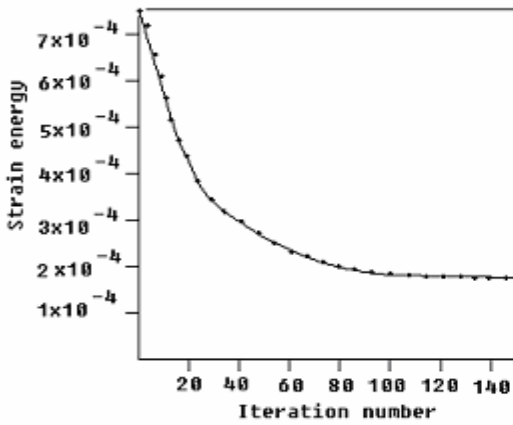
Figure 6.26 and Table 6.2 show the iteration histories and final strain energies for different power values of the power-law models.



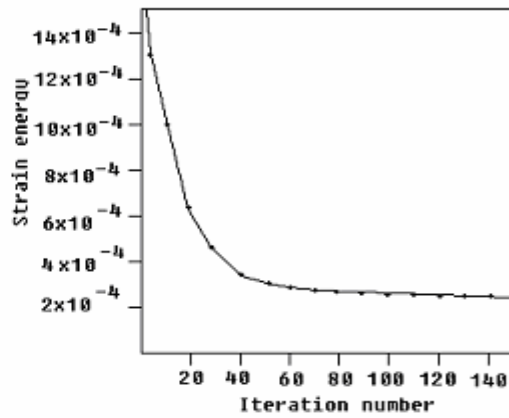
(a) Power value  $\mu = 1$



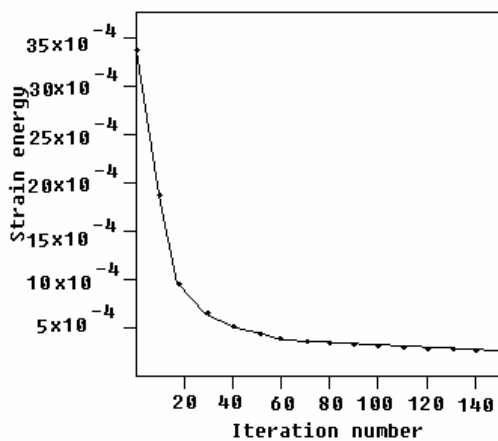
(b) Power value  $\mu = 2$



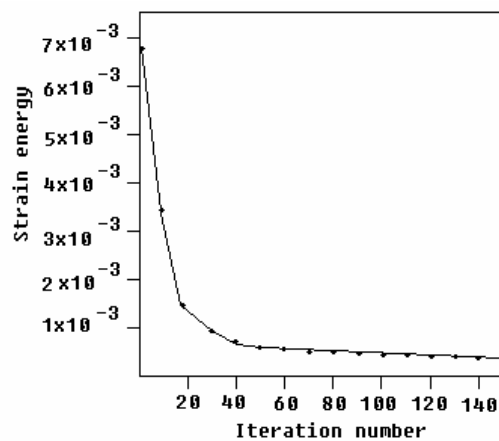
(c) Power value  $\mu = 3$



(d) Power value  $\mu = 4$



(e) Power value  $\mu = 5$



(f) Power value  $\mu = 6$

Figure 6.26 Iteration histories for different power values (*continued*)

(Figure 6.26 continued)

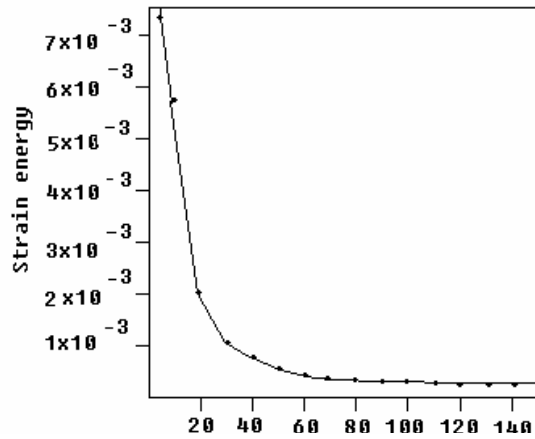
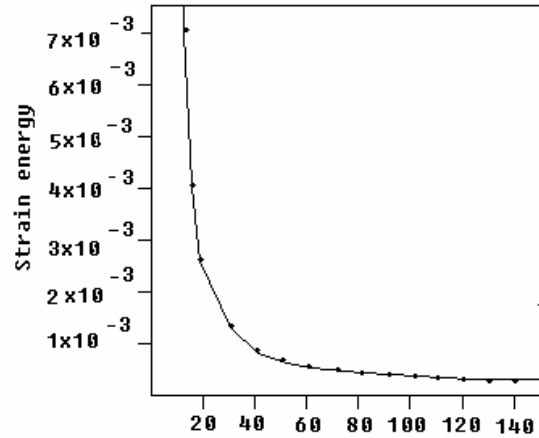
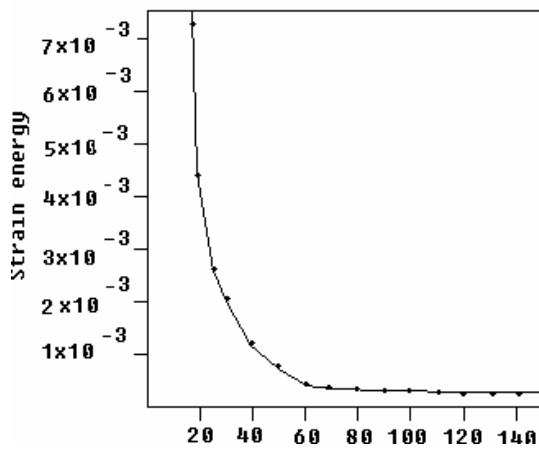
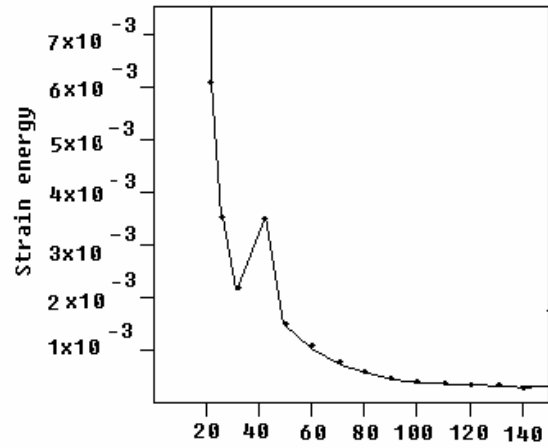
(g) Power value  $\mu = 7$ (h) Power value  $\mu = 8$ (i) Power value  $\mu = 9$ (j) Power value  $\mu = 10$ 

Figure 6.26 Iteration histories for different power values

Power value	Initial strain energy	Final strain energy
1	0.00022	0.00016
2	0.00044	0.00019
3	0.00087	0.00020
4	0.00174	0.00020
5	0.0034	0.00010
6	0.0069	0.00021
7	0.0138	0.00022
8	0.0276	0.000225
9	0.0536	0.00023
10	0.1107	0.00023

Table 6.2 Initial and final strain energy for different power values

It can be seen that the different power values greatly affect the initial strain energy value (increasing power value by 1 would double initial strain energy), but do not affect much the final strain energy. More studies of the effects on different power values will be presented in the next chapter.

### 6.3 Comparisons between Algorithms for Bi-material Microstructure Models

The cantilever beam was solved by Thomsen (1992) using bi-material model is shown in Figure 6.27. Point load of intensity  $P=1\text{kN}$  is applied midway down the right hand side of the beam.

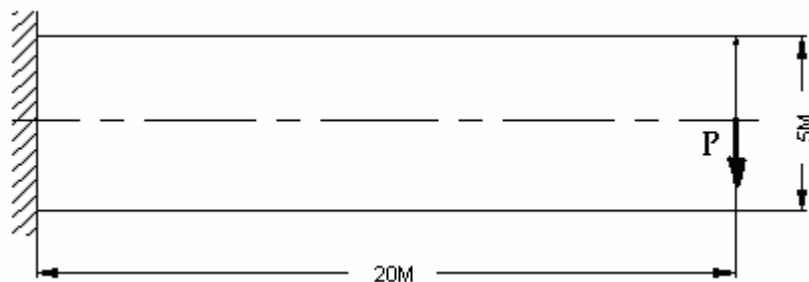
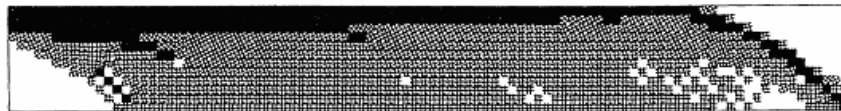


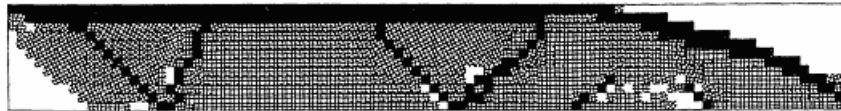
Figure 6.27 A cantilever beam with a point load

Thomsen (1992) studied this benchmark problem using ranked layered bi-material model. The material is modelled by one very soft material and two stiff materials. The stiffness ratios between "material 1" and "material 2" are set to be 10 and 75. The available amounts of "material 1" and "material 2" are set to be 20% and 65%, respectively, of the design domain volume. The structures have been discretized into 1152 (12 x 96) of four node elements.

The layout of optimal topologies of the upper half of the symmetrical layout of the beam is shown in Figure 6.28 and no iteration history was given by Thomsen. In this figure the distributions of isotropic "material 1" and "material 2" are illustrated by black and hatched domains, respectively, whereas white elements represent void. It appears that stiff "material 1" is distributed along the upper edge of the structure in order to carry the largest normal stresses, and that shear stresses are carried by softer "material 2" (Thomsen, 1992). The symmetrical layout of the upper half of the beam for two cases of stiffen ratio between 'material 1' and 'material 2' are shown in Figure 6.28



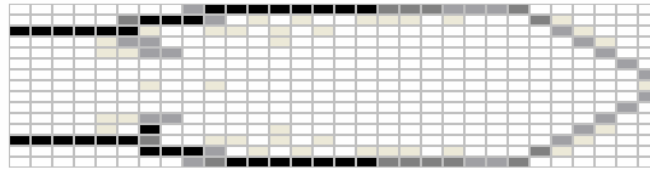
(a). Stiffness ratio between "material 1" and "material 2" was set to be 10



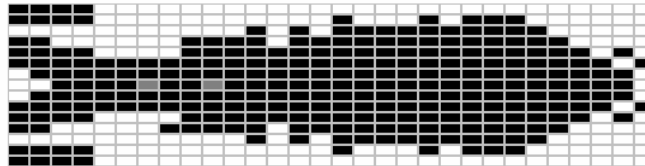
(b). Stiffness ratio between "material 1" and "material 2" was set to be 75

Figure 6.28 Optimal layout (Thomsen, 1992)

In this research, the structure was discretized into 1441 nodes and 450 elements. The stiffness ratios between "material 1" and "material 2" are set at 10. The optimization layout of using HDM with six bi-material microstructure models is illustrated in Figure 6.29.



(a1) Hard material distribution

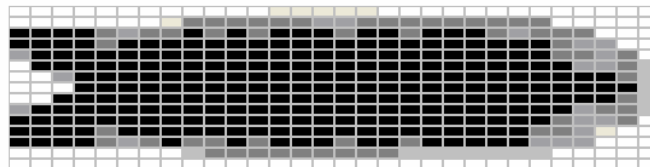


(a2) Soft material distribution

(a) Optimization layout for power-law bi-material model

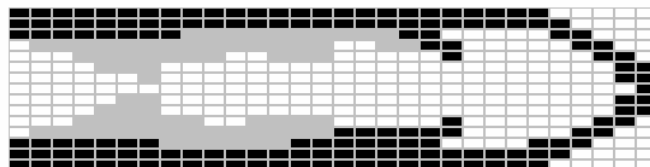


(b1) Hard material distribution



(b2) Soft material distribution

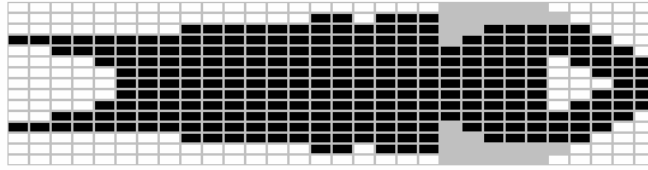
(b) Optimization layout for ranked layered bi-material model



(c1) Hard material distribution

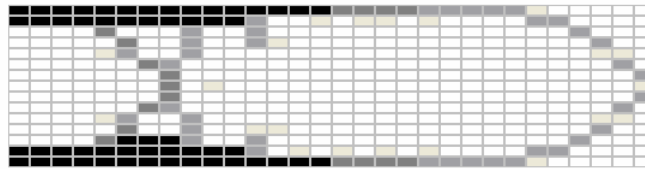
Figure 6.29 Optimization layouts using HDM (*continued*)

(Figure 6.29 continued)

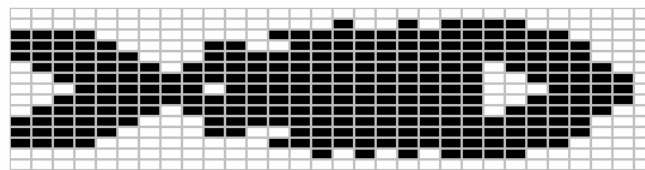


(c2) Soft material distribution

(c). Optimization layout for cross shape bi-material model

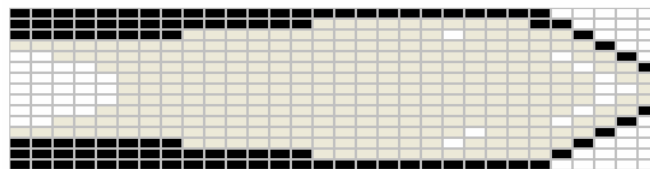


(d1) Hard material distribution



(d2) Soft material distribution

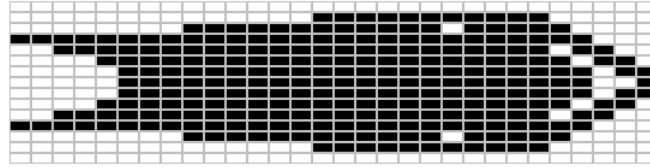
(d). Optimization layout for square bi-material model



(e1) Hard material distribution

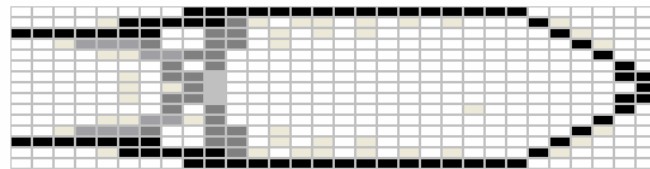
Figure 6.29 Optimization layouts using HDM (*continued*)

(Figure 6.29 continued)

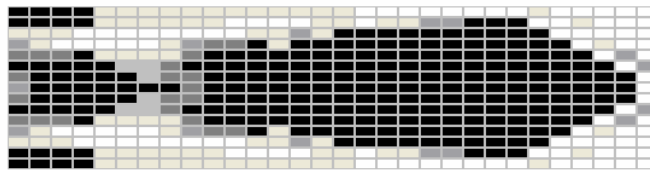


(e2) Soft material distribution

(e) Optimization layout for double rectangular bi-material model



(f1). Hard material distribution



(f2). Soft material distribution

(f). Optimization layout for triangular bi-material model

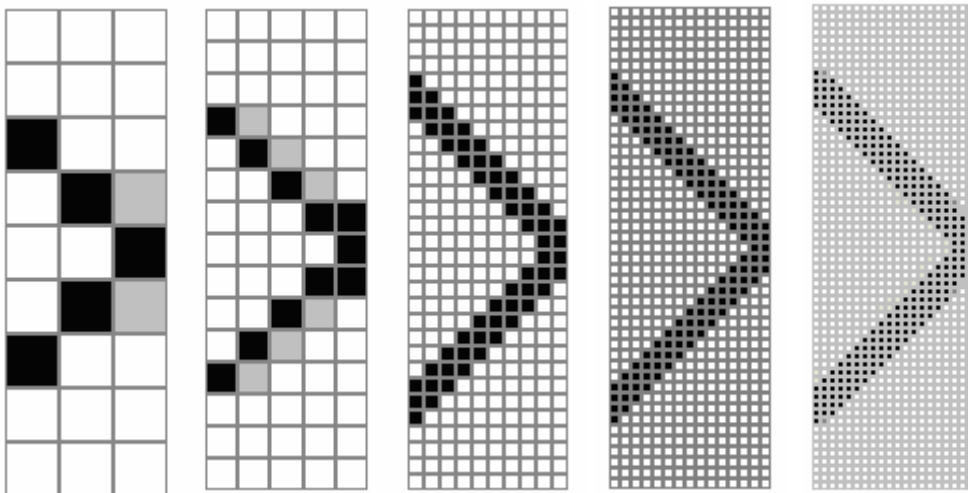
Figure 6.29 Optimization layouts using HDM

Figure 6.29 and 6.28 (a), show that the trends of the optimization layouts are identical, but not exactly the same. This is because those different microstructures have different layout geometrical patterns with different properties and these will affect the optimization solutions. The consistent tendency to optimum solution indicates that the HDM algorithm works well.

## 6.4 Effect of finite element discretization

To study the effect of finite element discretization on the results of topology optimization, the benchmark problem of Figure 6.1 (the deep cantilever beam with a single load and fixed constraint, Modulus of elasticity of solid material  $E_a = 1 \times 10^5$  MPa, the Poisson's ratio  $\nu = 0.3$  and volume fraction  $V_s/V = 20\%$ ) is studied by using one-material cross shape microstructure model. The domain is discretized to different meshing, from 27 elements to 1200 elements.

The optimum layouts with different finite element discretization are shown in Figure 6.30: (a) the domain is discretized to 27 (3x9) eight-node meshes, (b) the domain is discretized to 75 (5x15) eight-node meshes, (c) the domain is discretized to 300 (10x30) eight-node meshes, (d) the domain is discretized to 675 (15x45) eight-node meshes and (e) the domain is discretized to 1200 (20x60) eight-node meshes.



(a) 27 meshes (b) 75 meshes (c) 300 meshes (d) 675 meshes (e) 1200 meshes

Figure 6.30 Optimum layouts for different finite element discretizations.

Table 6.3 shows the history of iteration of strain energies for the different finite element discretizations, which are also plotted in Figure 6.31.

Iteration number	Strain energy for 27 meshes	Strain energy for 75 meshes	Strain energy for 300 meshes	Strain energy for 675 meshes	Strain energy for 1200 meshes
0	0.000258	0.000284	0.000352	0.000340	0.000270
10	0.000146	0.000161	0.000181	0.000180	0.000142
20	0.000067	0.000074	0.000087	0.000085	0.000075
30	0.000052	0.000055	0.000069	0.000063	0.000066
40	0.000048	0.000046	0.000053	0.000054	0.000057
50	0.000046	0.000043	0.000048	0.000047	0.000054
60	0.000046	0.000042	0.000046	0.000044	0.000050
70	0.000046	0.000042	0.000044	0.000043	0.000048
80	0.000046	0.000041	0.000044	0.000042	0.000046
90	0.000046	0.000041	0.000043	0.000042	0.000044
100	0.000046	0.000041	0.000043	0.000041	0.000044
110	0.000045	0.000041	0.000042	0.000040	0.000043
120	0.000045	0.000041	0.000042	0.000040	0.000043
130	0.000045	0.000041	0.000042	0.000039	0.000042
140	0.000045	0.000040	0.000042	0.000039	0.000042
150	0.000045	0.000040	0.000042	0.000039	0.000042

Table 6.3: Strain energies for the different finite element discretizations.

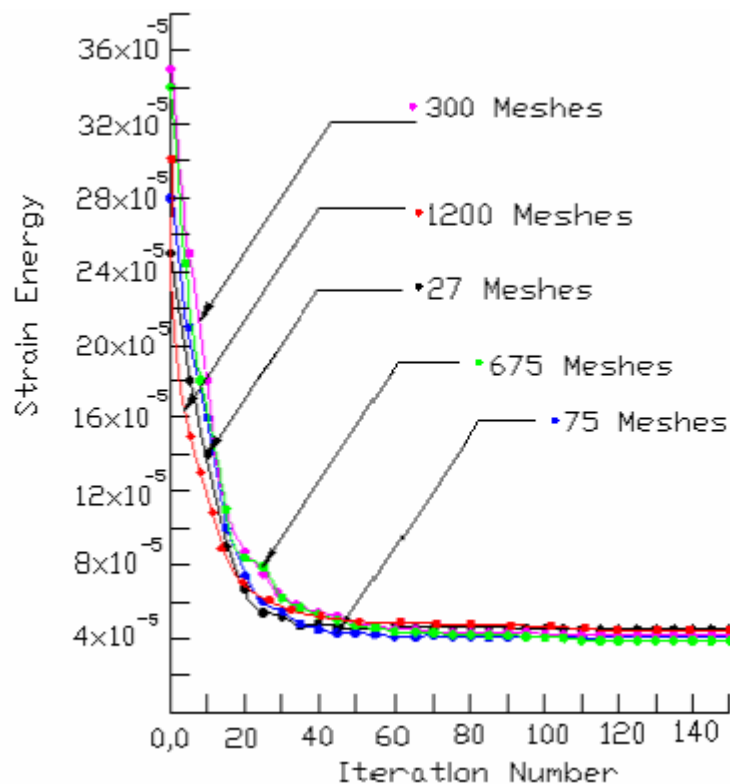


Figure 6.31 Iteration histories for different finite element discretizations.

From the results above, we can see that the optimization problem with either coarse meshes or fine meshes can converge quickly to the optimum layout. The final strain energies are also similar. It should be noted that the domain used for homogenisation throughout this research is one microstructure itself. These results also confirm that homogenisation works even when the average domain is just a single cell as noted by Manevitch et al (2002), page 11.

## **6.5 Conclusions**

The HDM algorithm was tested by investigating the cantilever beam problem and by comparing the optimization solutions of short cantilever beam problems given by the HDM algorithm with those given in literature. The results show that the HDM algorithm is effective and the solutions agree well with the solutions published in literature. Further studies of other problems are presented in the following chapters.

## **Chapter 7**

---

# **STUDY ON THE EFFECTS OF VARIOUS ONE-MATERIAL MICROSTRUCTURES ON TOPOLOGY OPTIMIZATION RESULTS**

To identify the influence of a microstructure model on optimization results will be very important to researchers in improving the homogenization method to make it more accessible for practical use. By solving a series of topology optimization problems for isotropic material, this chapter investigates the effects of different one-material microstructures on topology optimization. A range of examples of topological optimization problems and different loading cases are investigated. The loading cases considered here are single loading, surface loading, multiple loading and gravity loading. The factors that influence topology optimization results such as different material models, different power values for the power-law model are studied. The iteration and convergence characteristics for different microstructure models are also investigated. For each problem, first the PLATO software using rectangular model developed by Hassani and Hinton (1998), is used to find the topology optimum layout, then the HDM software using nine microstructure models is

used to search for the optimum layout. For the power-law model, different cases of power values from  $\mu = 1$  to 10 are also investigated to see the effects of  $\mu$  on the optimal layout.

In the study on effects of microstructures in this research, only a limited number of elements (300~1200 mesh, 8-node) was used. This is quite satisfactory in the strategically important concept design stage on which topology optimization mainly focuses. Other researchers also used small number of elements in topology optimization. For example, 640 (32 X 20) equal elements were used by Hassani and Hinton (1998) for rectangular and artificial models study. Min, Nishiwaki and Kikuchi (1999) studied the simply supported beam benchmark problem using homogenization method by discretizing the design domain into 1440 (48 x 30) four-node finite elements with 1519 nodes as shown in Figure 6.15.

## **7.1 Topology Optimizations with Single Load**

*Example 7.1 A simply supported beam with a single load*

A simply supported beam is shown in Figure 7.1. A point load of intensity  $P=1\text{kN}$  is applied midway down the top side of the beam. The modulus of elasticity  $E = 10^5 \text{ MPa}$ , Poisson's ratio,  $\nu = 0.3$  and volume fraction  $V_s/V=50\%$ .

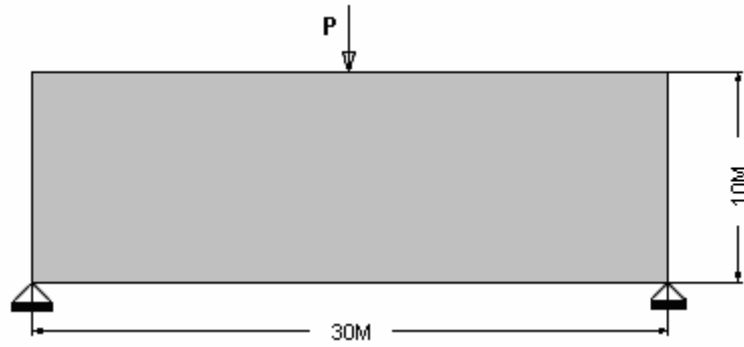


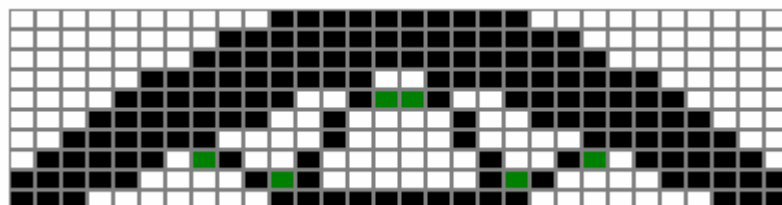
Figure 7.1 A simply supported beam

The result of using PLATO software (Hassani and Hinton, 1998) with rectangular microstructure carried out in this research is shown in Figure 7.2.



Figure 7.2 Optimization layout by PLATO software

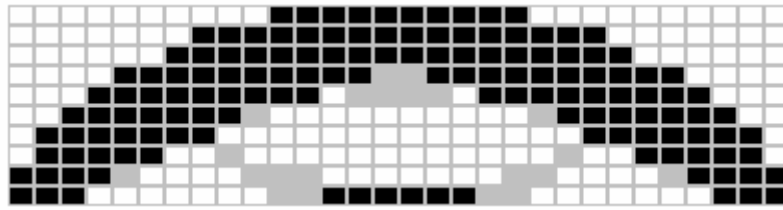
The layouts of using HDM with nine different material models are shown in Figure 7.3: (a) power-law, (b) triangular, (c) hexagon, (d) cross shape, (e) circular, (f) triangular multi-void, (g) rectangular multi-void, (h) square multi-void, and (i) ranked layered material model.



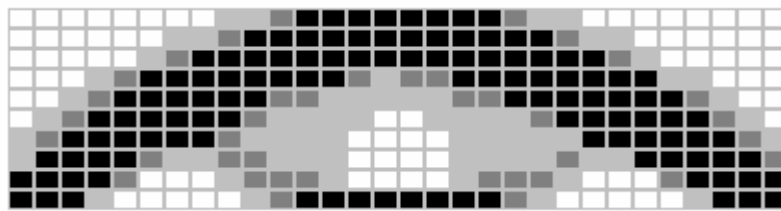
(a) Power-law one-material model

Figure 7.3 Optimization results for different microstructures by HDM with volume fraction 50% (continued)

(Figure 7.3 continued)



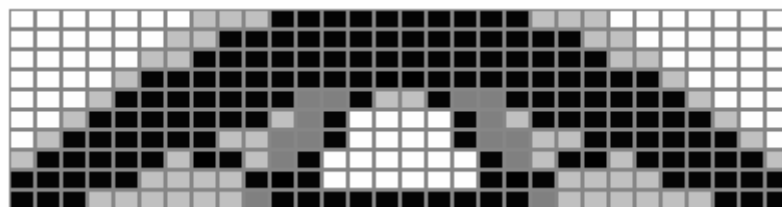
(b) Triangular material model



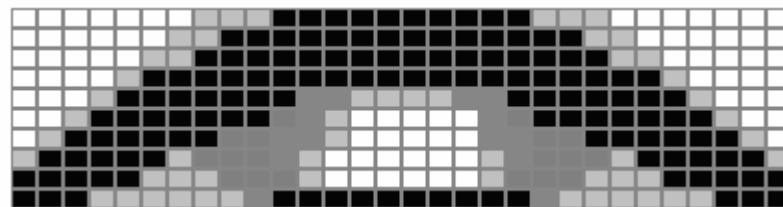
(c) Hexagon material model



(d) Cross shape material model



(e) Circular material model

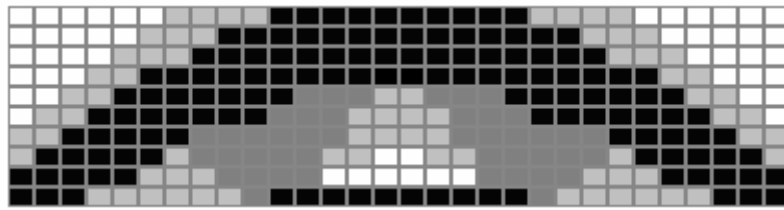


(f) Triangular multi-void material model.

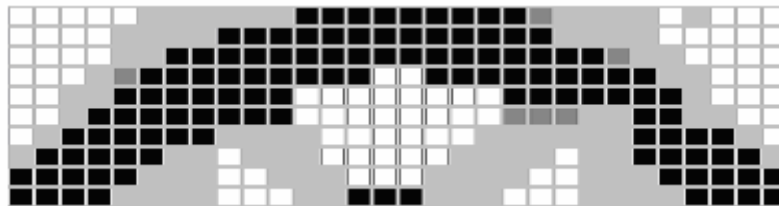
Figure 7.3 Optimization results for different microstructures by HDM with

volume fraction 50% (continued)

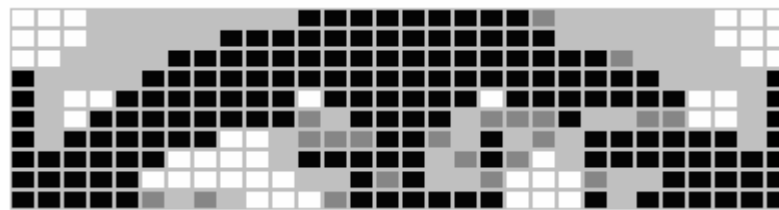
(Figure 7.3 continued)



(g) Rectangular multi-void material model.



(h) Square multi-void material model.



(i) Ranked layered material model.

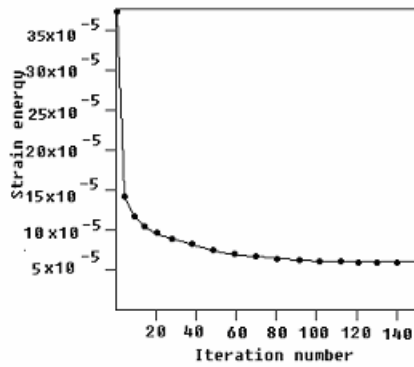
Figure 7.3 Optimization results for different microstructures by HDM with volume fraction 50%.

Figure 7.3 shows that except for the ranked layered model, all the rest eight one-material models provide optimal shapes similar to that given by the rectangular model using PLATO software. The power-law model (at  $\mu = 3$ ) gives the clearest image result. The optimal layout of the ranked layered model is different from the others, in that the material distribution is more complex, the layout is not as sharp and contrast, and material of high density is required at both left and right edges. The reason for this is as discussed in Chapter 6 that

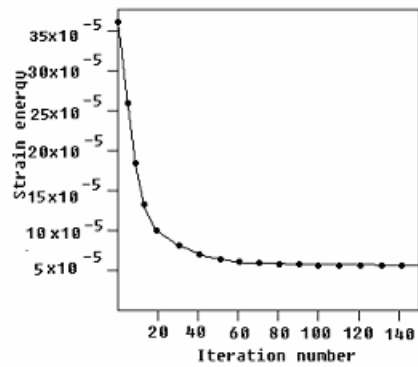
because the optimal microstructure is degenerated in the rank-2 layered material model and the structure cannot sustain a non-aligned shear stress. This will result in the stiffness matrix of the structure becoming singular. The technique used in the thesis to overcome the singularity problem is to use a very soft material instead of voids. However, the minimum strain energy calculated during optimization process (commonly used for objective function which is equivalent to maximum total potential energy) is only modified energy. This leads to the result shown much difference with others.

From the layouts above, we can also see that all the other results from different microstructures have a similar layout, but not exactly the same. The criterion of an optimal structure for this minimum compliance problem is to find the minimum strain energy (maximum total potential energy). Among these microstructure models, the strain energy can be calculated during the optimization process for the triangular, hexagon, cross shape, circular, triangular multi-void, rectangular multi-void and square multi-void material models. But the strain energy is modified during the optimization process for ranked layered and power-law models. For ranked layered and power-law models, Finite Element Method can be used for calculating the true value at the final stage of optimization.

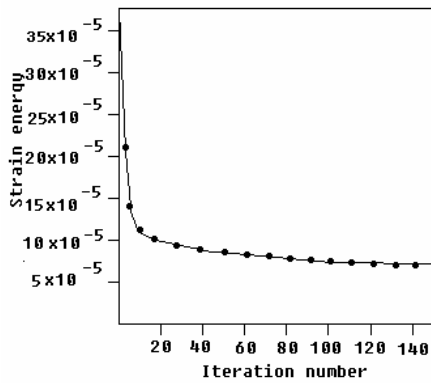
Figure 7.4 shows the iteration histories for different material models.



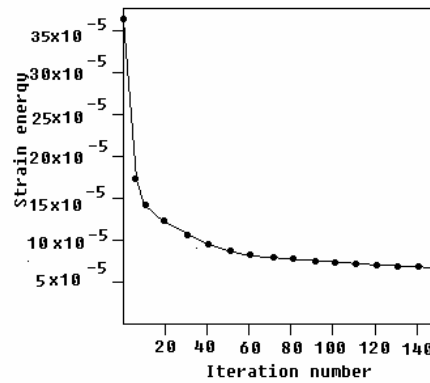
(a) Rectangular model (using PLATO)



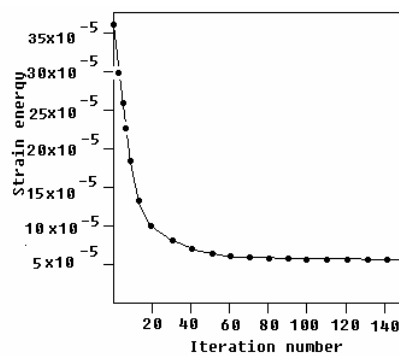
(b) Power-law model



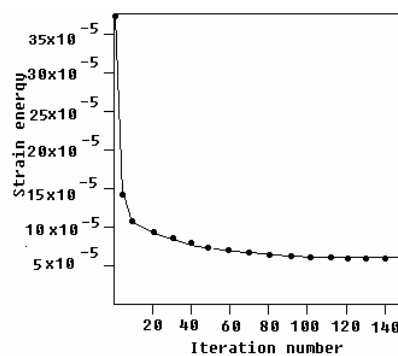
(c) Triangular material model.



(d) Hexagon material model.



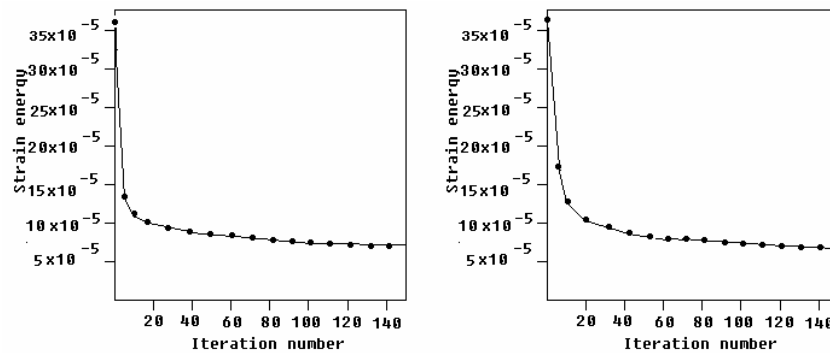
(e) Cross shape material model.



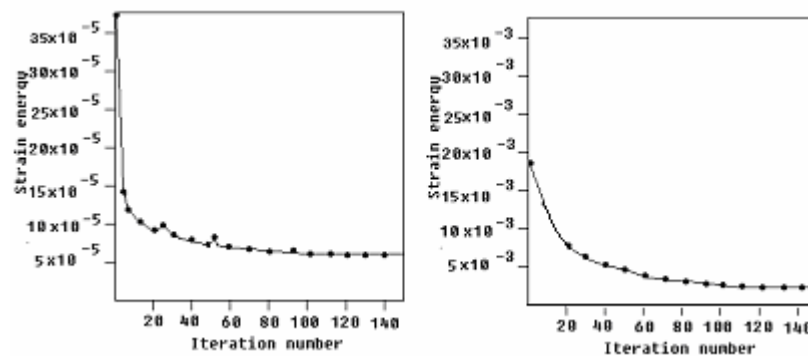
(f) Circular material model.

Figure 7.4 Iteration histories for different models (*continued*)

(Figure 7.4 continued)



(g) Triangular multi-void model. (h) Rectangular multi-void model.



(i) Square multi-void material model. (j) Ranked layered material model.

Figure 7.4 Iteration histories for different material models

In Figure 7.4, (a) rectangular material model by using PLATO software, (b) power-law, (c) triangular, (d) hexagon, (e) cross shape, (f) circular, (g) triangular multi-void, (h) rectangular multi-void, (i) square multi-void and (j) ranked layered material model.

Figure 7.5 shows all the iterations on the same graphic for comparison of the iteration histories given by the microstructure models (except ranked layered) using HDM.

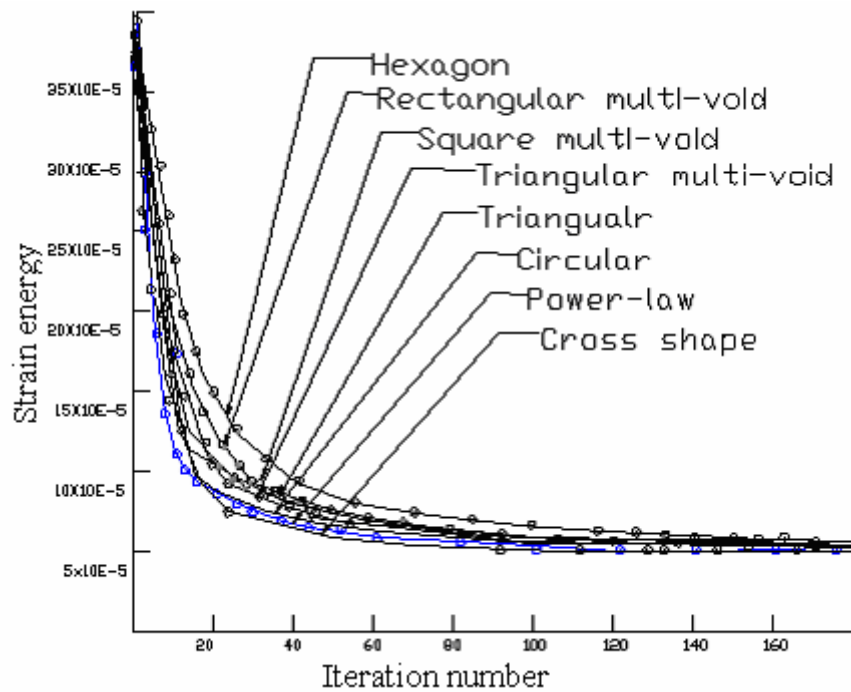


Figure 7.5 Comparison of iteration histories

Table 7.1 shows iteration numbers and final strain energies at convergence tolerance  $\Delta = 0.050$  for the microstructures using HDM.

Microstructure Model	Iteration Number	Final Strain Energy
Power-law	197	0.000065
Cross shape	233	0.000062
Circular	245	0.000064
Hexagon	267	0.000067
Triangular	229	0.000066
Rectangular Multi-void	220	0.000066
Square Multi-void	243	0.000067
Triangular Multi-void	279	0.000069
Ranked layered	267	0.0019

Table 7.1 Iteration numbers and final strain energies at convergence tolerance

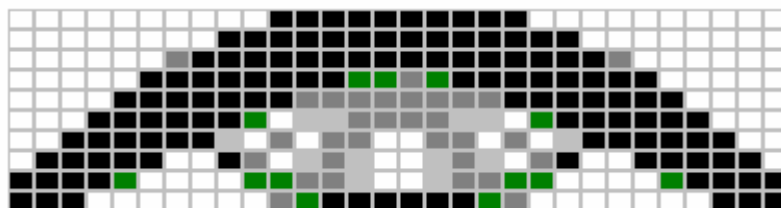
$\Delta = 0.050$  for the microstructures using HDM

From the iteration histories illustrated in Figure 7.4, Figure 7.5 and Table 7.1, we can see that all the microstructures give very good convergence, among them the power-law, cross shape and circular models have better convergence. The strain energy of the ranked layered material model is much higher than other material models. This is because the ranked layered model can not resist shear stress; displacement due to loading has to be greater, hence larger strain energy. In this case, the optimum value of strain energy of this material model is much more than those of other models.

For the power-law model, we investigate further the effect of changing the power value  $\mu$  on the optimum layout. Figure 7.6 shows the optimization layouts for different power values of the power-law models from one to ten.



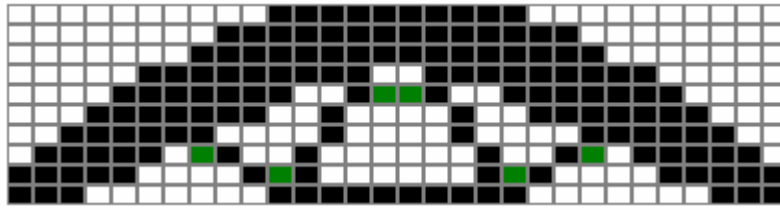
(a) Power value  $\mu = 1$



(b) Power value  $\mu = 2$

Figure 7.6 Optimization results for different power values (*continued*)

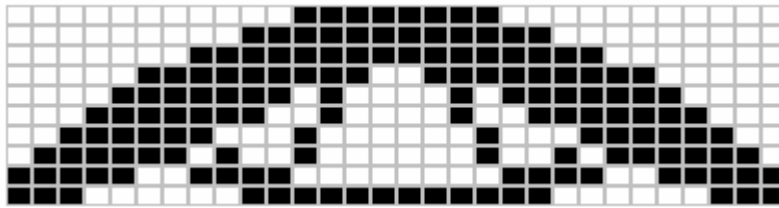
(Figure 7.6 continued)



(c) Power value  $\mu = 3$



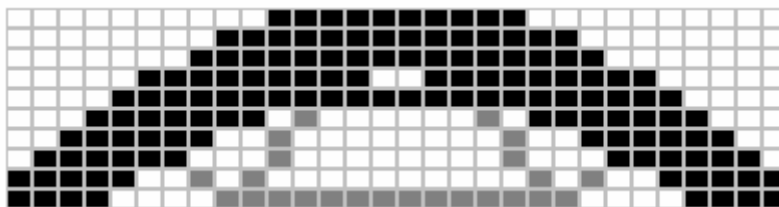
(d) Power value  $\mu = 4$



(e) Power value  $\mu = 5$



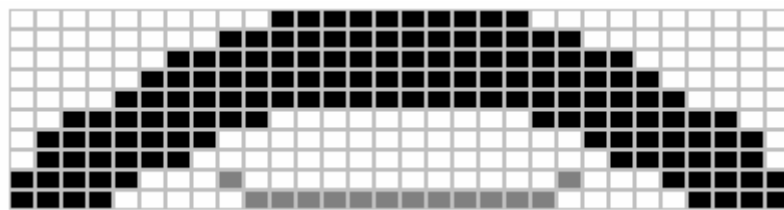
(f) Power value  $\mu = 6$



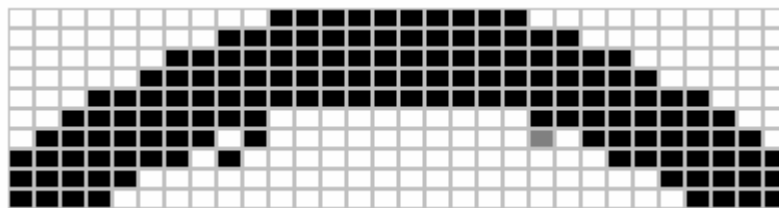
(g) Power value  $\mu = 7$

Figure 7.6 Optimization results for different power  $\mu$  (continued)

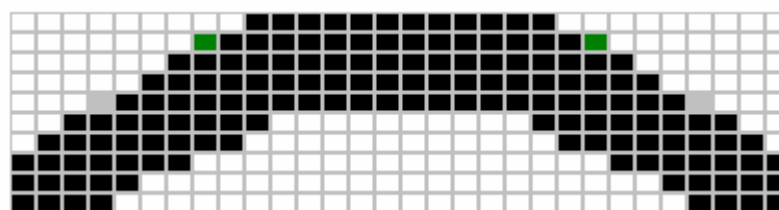
(Figure 7.6 continued)



(h) Power value  $\mu = 8$



(i) Power value  $\mu = 9$



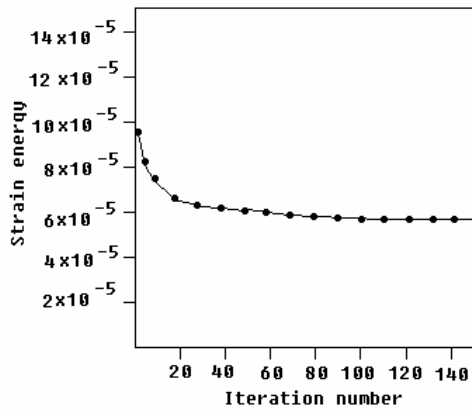
(j) Power value  $\mu = 10$

Figure 7.6 Optimization results for different power values

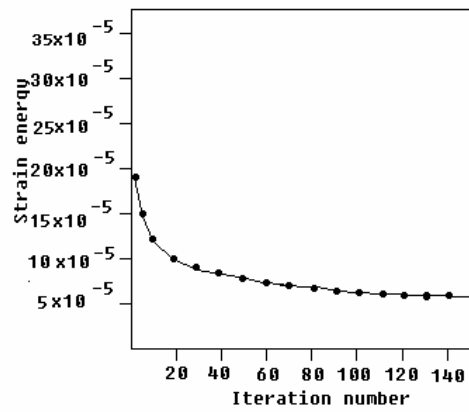
From the optimal layout given by Figure 7.6, we can see that for a small value of  $\mu$ , a grey area is appears in the solution at the central bottom area, however with the value of  $\mu$  increasing, the supporting from the central bottom area is gradually reduced. When  $\mu > 9$ , all the supports from the central area disappear. By comparison with other model results, the solutions of the power value between 2 and 7 agree well with other models.

Figure 7.7 shows the iteration histories for different power values in the

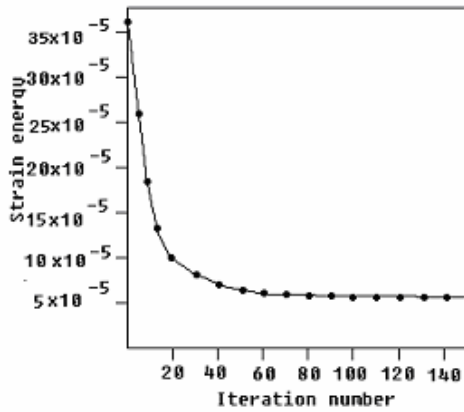
power-law one-material model.



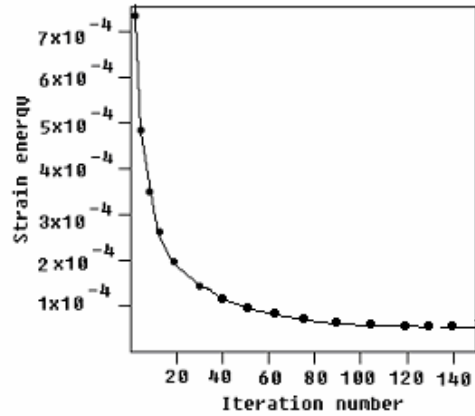
(a) Power value  $\mu = 1$



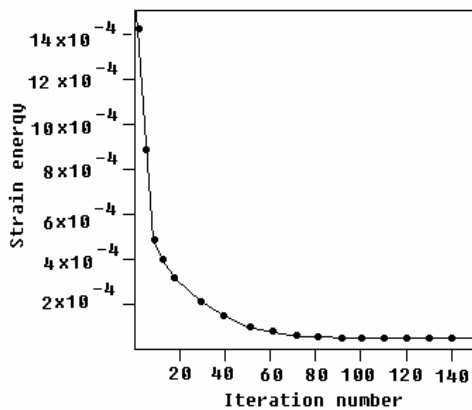
(b) Power value  $\mu = 2$



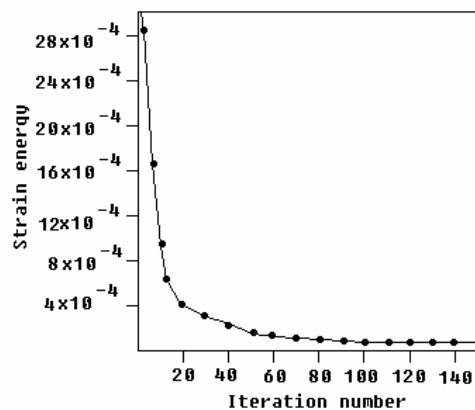
(c) Power value  $\mu = 3$



(d) Power value  $\mu = 4$



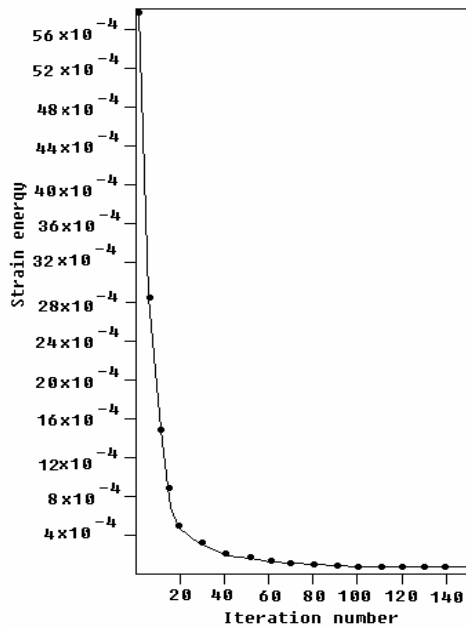
(e) Power value  $\mu = 5$



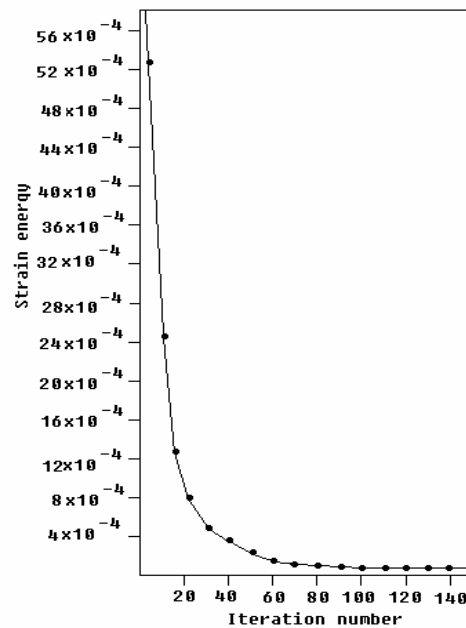
(f) Power value  $\mu = 6$

Figure 7.7 Iteration histories for different power values (*continued*)

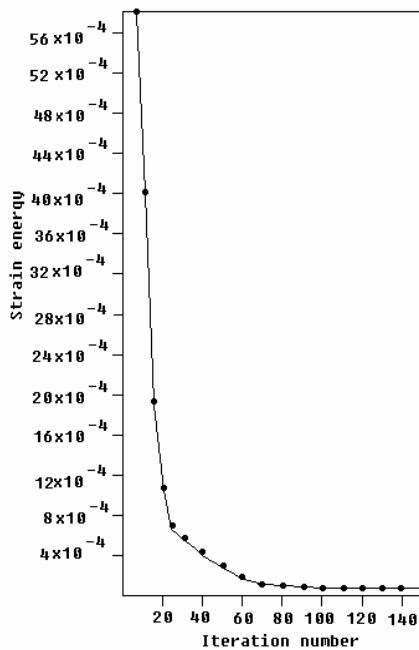
(Figure 7.7 continued)



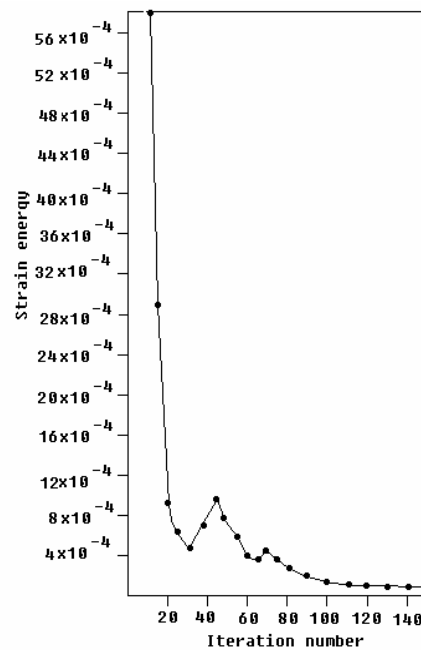
(g) Power value  $\mu = 7$



(h) Power value  $\mu = 8$



(i) Power value  $\mu = 9$



(j) Power value  $\mu = 10$

Figure 7.7 Iteration histories for different power values

Table 7.2 below shows the initial and final strain energy for different power values calculated by HDM.

Power value	Initial strain energy	Final strain energy
1	0.000091	0.000059
2	0.00018	0.000065
3	0.00036	0.000065
4	0.00073	0.000066
5	0.00146	0.000066
6	0.0029	0.000068
7	0.00583	0.000069
8	0.01166	0.000068
9	0.0233	0.000067
10	0.04667	0.000071

Table 7.1 The initial and final strain energy for different power values.

From the results above, we can see that the power-law models have very good convergence character for the power value between 1 and 9. Although the initial strain energy increases very rapidly with the value of power increasing, the final strain energy upon convergence is very similar.

On the simply supported beam problem, we can see that all the microstructure models (apart from the ranked layered model) agree well with the solution using PLATO software and have similar convergence histories. For the concept design stage, we can say the most of the layouts reach similar topological optimal layouts. By comparison of the value of the objective function of

optimization, the cross shape has the lowest strain energy. It also has the best convergence characteristics. From a manufacturing point of view, a solution with contrast and sharp image (black and white image) is easy to implement, their layouts given by power-law model with  $\mu = 3 : 5$  are the best. Ranked layered model gives a different layout pattern. The reason for this, as discussed before, is that there is no shear strength in this model and it would lead to a larger displacements between layers.

*Example 7.2 Square domain with a single corner load*

Figure 7.8 shows a square domain with boundary constraints on the top left corner and the bottom edge. A point load of intensity  $P = 1\text{kN}$  is applied at the left bottom corner of the square domain. The modulus of elasticity  $E = 10^5\text{ MPa}$ , Poisson's ratio,  $\nu = 0.3$  Two cases, **Case a** : the volume constraint  $V_s / V = 50\%$  and **Case b** : the volume constraint  $V_s / V = 20\%$ , are considered.

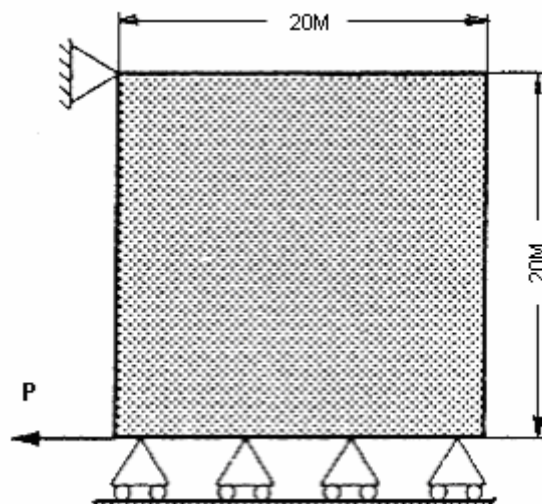


Figure 7.8 A Square domain with a point load

**Case a** : Volume constraint  $V_s / V = 50\%$  :

The optimum layout given by the PLATO software using rectangular material model calculated by the author is shown in Figure 7.9.

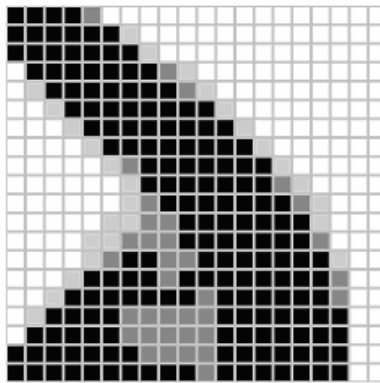
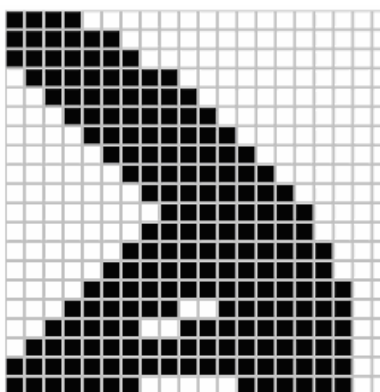


Figure 7.9 Optimum layout of using the PLATO software

The optimum layouts of using HDM with other nine different material models are shown in Figure 7.10: (a) power-law, (b) ranked layered, (c) triangular, (d) hexagon, (e) cross shape, (f) circular, (g) triangular multi-void, (h) rectangular multi-void, and (i) square multi-void material model.

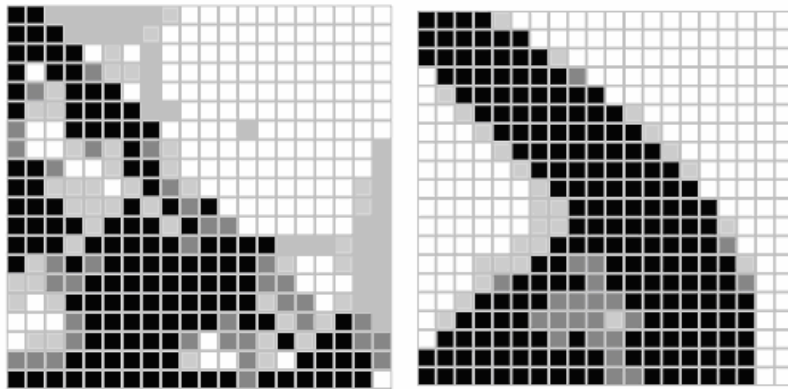


(a) Power-law one-material model  $\mu = 3$

Figure 7.10 Optimization results for different microstructures for Case **a**

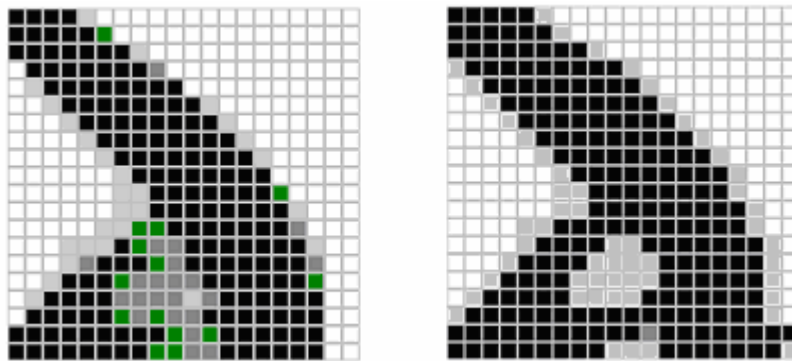
*(continued)*

(Figure 7.10 continued)



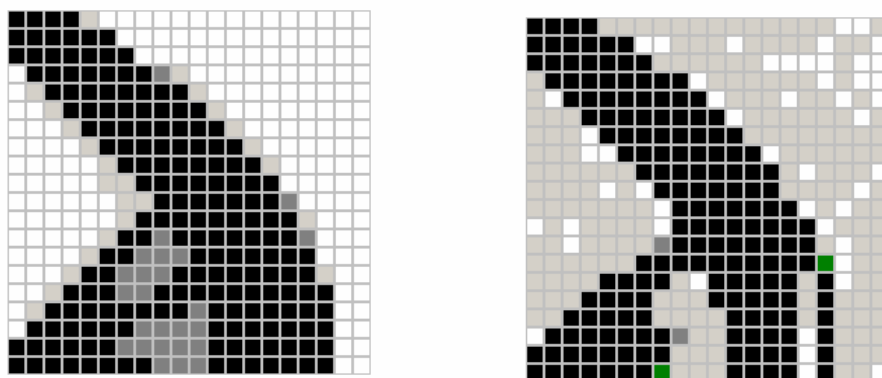
(b) Ranked layered material model.

(c) Triangular material model.



(d) Hexagon material model.

(e) Cross shape material model.



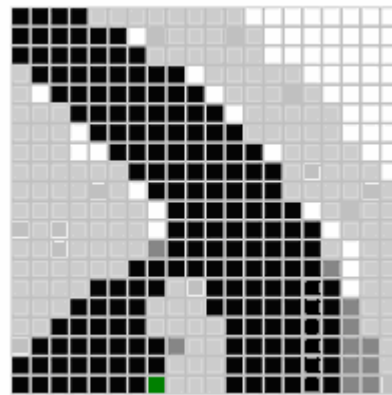
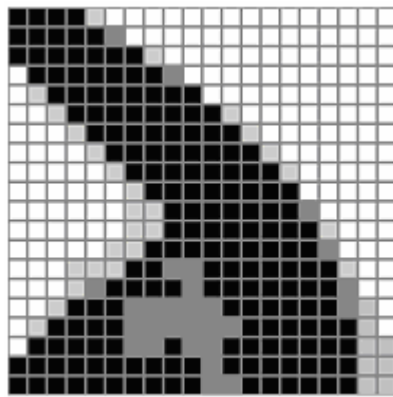
(f) Circular material model.

(g) Triangular multi-void model.

Figure 7.10 Optimization results for different microstructures for Case *a*

(continued)

(Figure 7.10 continued)



(h) Rectangular multi-void model.      (i) Square multi-void model.

Figure 7.10 Optimization results for different microstructures for Case *a*.

The results above show that all the microstructure models except the ranked layered model agree well with the results given by PLATO software using rectangular microstructure. The result of ranked layered model is again not as good as that given by the other eight models, because of its complex distribution of material, a high concentration of solid material in the middle of the left edge would not be sensible from an engineering point of view. The power-law and circular model gives the clearest and sharp images, which have good properties for manufacture.

**Case b** : Volume constraint  $V_s / V = 20\%$

The optimum layout by PLATO with rectangular material model calculated in this project is shown in Figure 7.11.

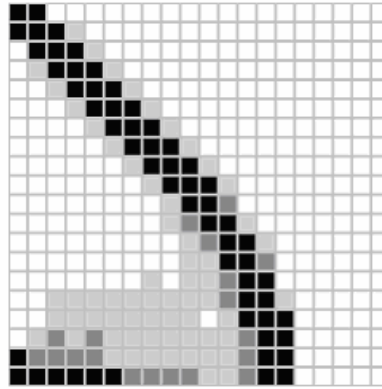
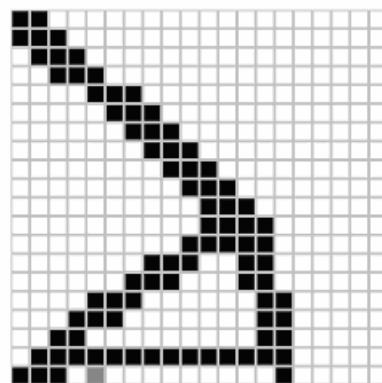
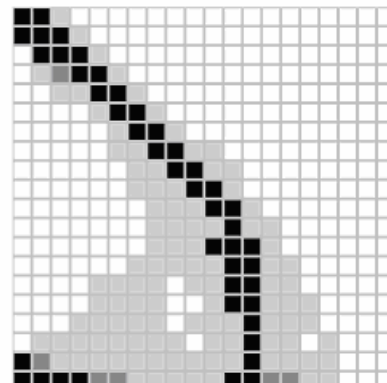
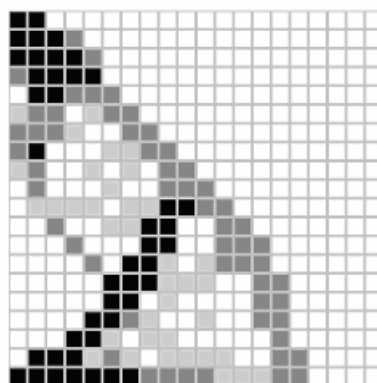


Figure 7.11 Optimum layout of using PLATO based on rectangular model

The optimum layouts of using HDM with nine different material models are shown in Figure 7.12. In Figure 7.12, (a) power-law, (b) ranked layered, (c) triangular, (d) hexagon, (e) cross shape, (f) circular, (g) triangular multi-void, (h) rectangular multi-void, and (i) square multi-void material model.

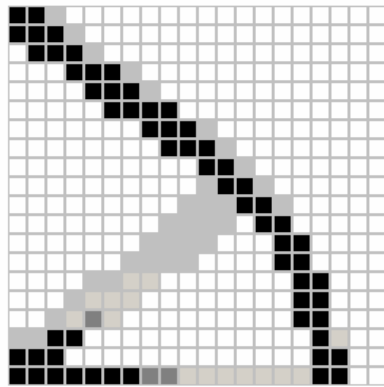


(a) Power-law model  $\mu = 3$ .

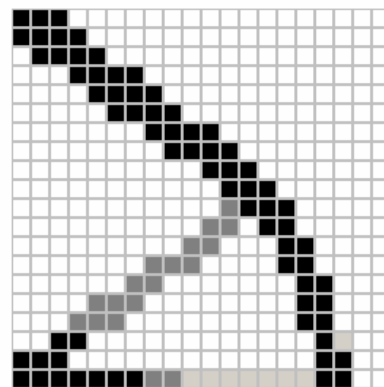


(b) Ranked layered material model. (c) Triangular material model. Figure 7.12 Results for different models for Case **b** (continued)

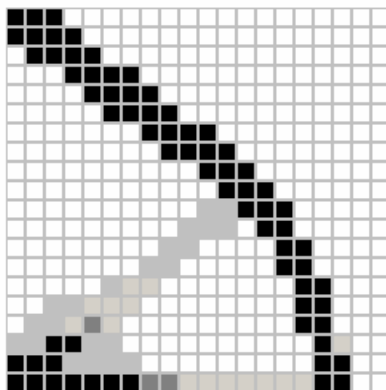
(Figure 7.12 continued)



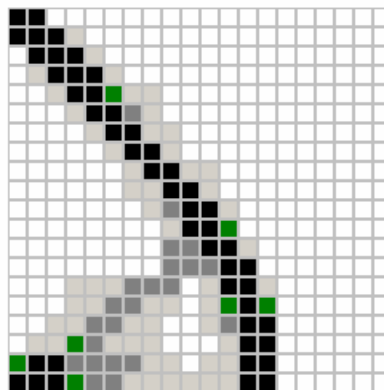
(d) Hexagon material model.



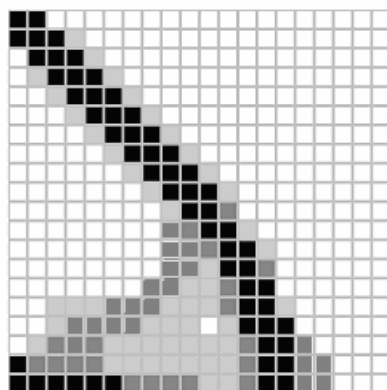
(e) Cross shape material model.



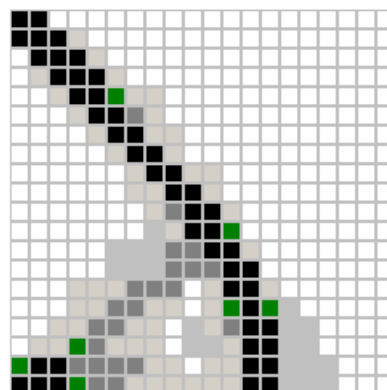
(f) Circular material model.



(g) Triangular multi-void model.



(h) Rectangular multi-void model.



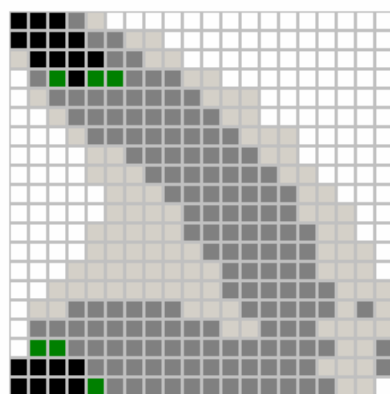
(i) Square multi-void model.

Figure 7.12 Optimization results of HDM with different microstructures

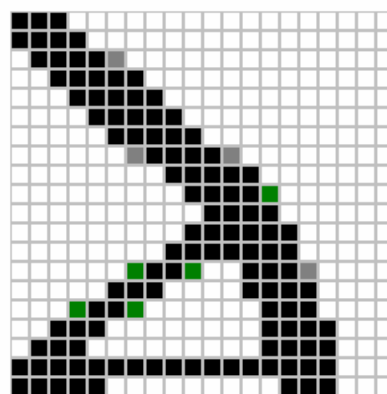
The results above show that all the microstructure models agree well with the results of the rectangular model obtained by PLATO. The power-law and cross

shape models give the sharpest image of the layouts. It can be seen that in the case of  $V_s / V = 20\%$ , the layout of the ranked layered model bears more resemblance to others, even though its distribution of material is still the most complicated. The triangular, rectangular and square multi-void models have more grey areas.

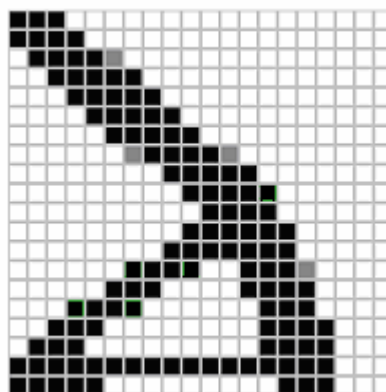
The effects of power values of the power-law model were further investigated. Figure 7.13 shows the optimization layouts for different power values from one to ten of the power-law one-material model with the volume fraction  $V_s/V=40\%$ .



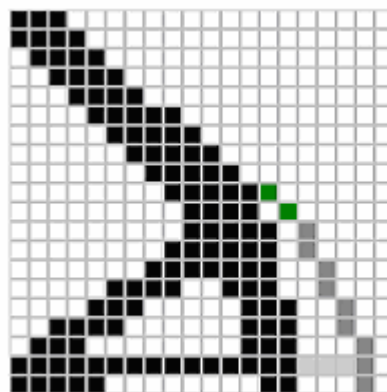
(a) Power value  $\mu = 1$



(b) Power value  $\mu = 2$



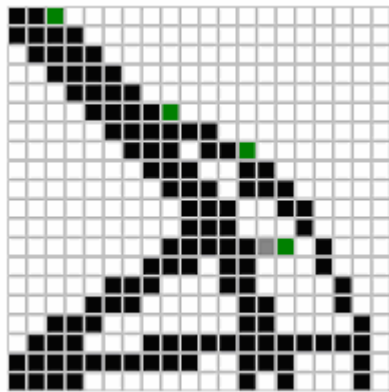
(c) Power value  $\mu = 3$



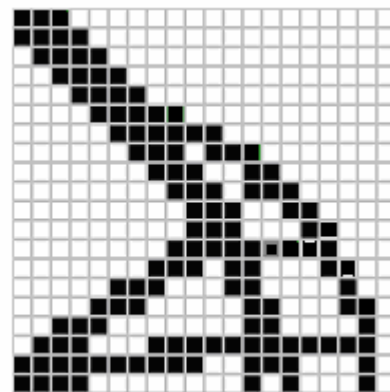
(d) Power value  $\mu = 4$

Figure 7.13 Optimization results with different power values (*continued*)

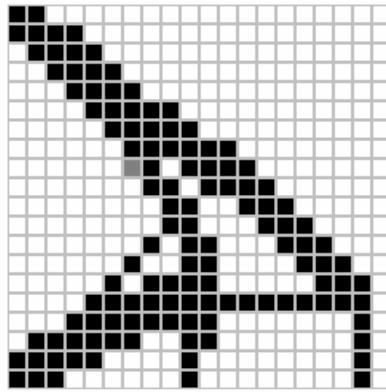
(Figure 7.13 continued)



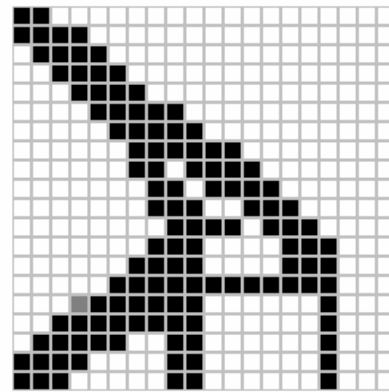
(e) Power value  $\mu = 5$



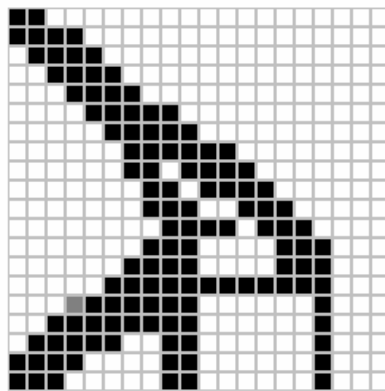
(f) Power value  $\mu = 6$



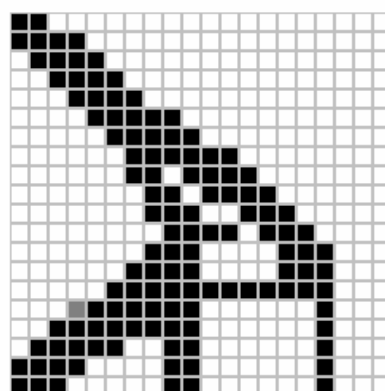
(g) Power value  $\mu = 7$



(h) Power value  $\mu = 8$



(i) Power value  $\mu = 9$



(j) Power value  $\mu = 10$

Figure 7.13 Optimization results with different power values

From the layout for different values of power-law model, we can see that for  $\mu$  from 2 to 10, all the images are sharp and of high contrast, but only the solutions of  $\mu$  equal to 2 and 3 agree well with other models. The layout is complex for  $\mu = 1$ .

From this example we can see that the power-law model with  $\mu$  equal to 2 and 3 perform the best. The cross shape and circular models also give good results. again, the ranked layered model shows a relatively different solution.

*Example 7.3 Rectangular design domain with two sides fixed under central single load.*

Figure 7.14 shows a design domain with fixed boundary constraint on the left and right side. A point load of intensity  $P = 1\text{kN}$  is applied midway on the top side of the beam. The modulus of elasticity  $E = 10^5 \text{ MPa}$ , Poisson's ratio,  $\nu = 0.3$  and volume fraction  $V_s / V = 50\%$ .

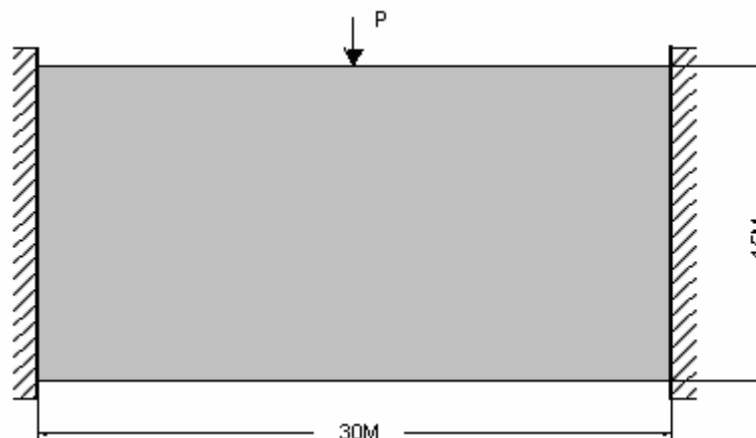


Figure 7.14 A domain with fixed side boundary constraints

The optimum layout of using PLATO with rectangular material model calculated in this research is shown in Figure 7.15.

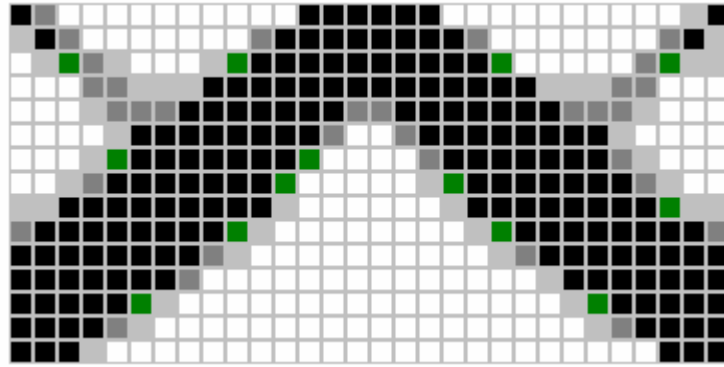
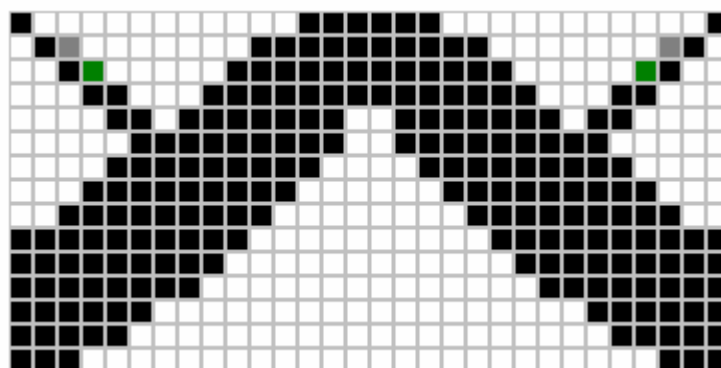


Figure 7.15 Optimum layout of using PLATO with rectangular material model.

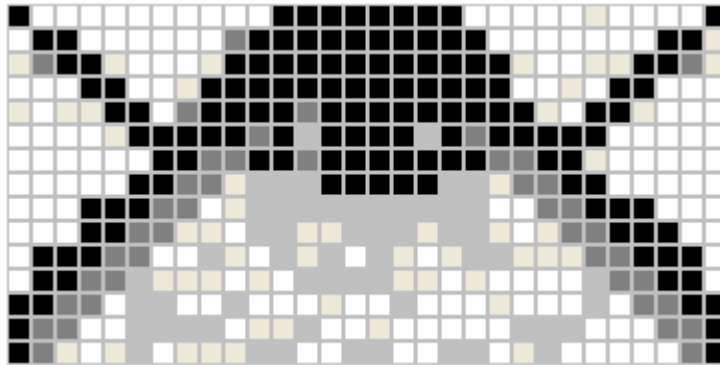
The optimum layouts of using HDM with nine different material models are shown in Figure 7.16: (a) power-law, (b) ranked layered, (c) triangular, (d) hexagon, (e) cross shape, (f) circular, (g) triangular multi-void, (h) rectangular multi-void, and (i) square multi-void material model.



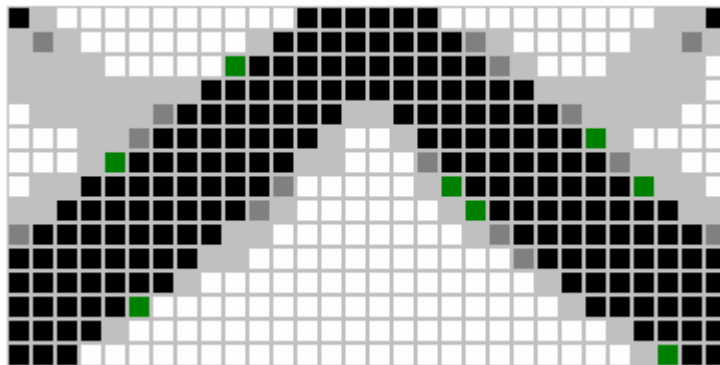
(a) Layout of power-law one-material model.

Figure 7.16 Optimization layouts for different microstructures (*continued*)

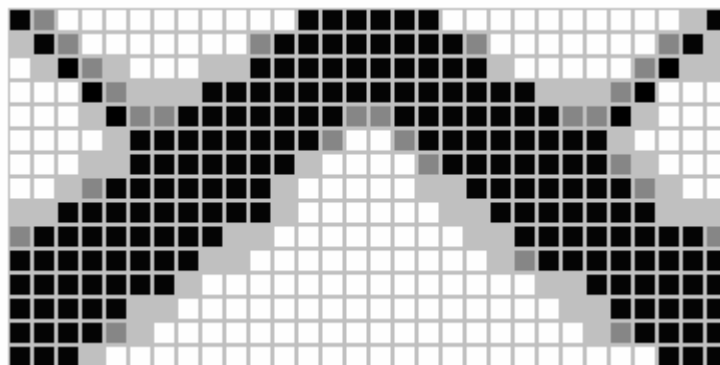
(Figure 7.16 continued)



(b) Layout of ranked layered material model.



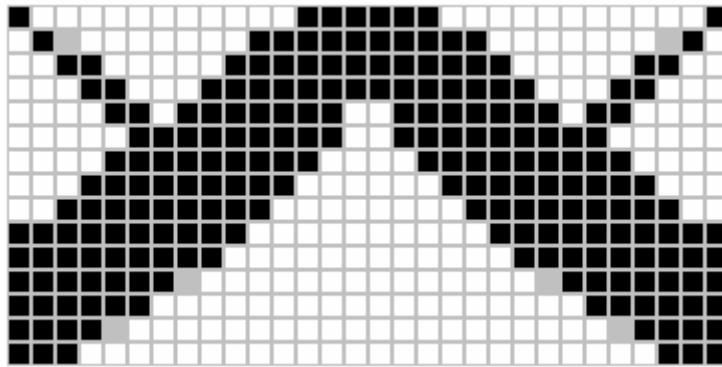
(c) Layout of triangular material model.



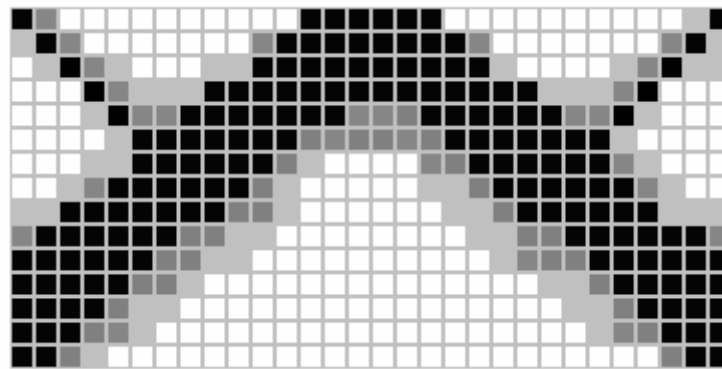
(j) Layout of hexagon material model.

Figure 7.16 Optimization layouts for different microstructures (*continued*)

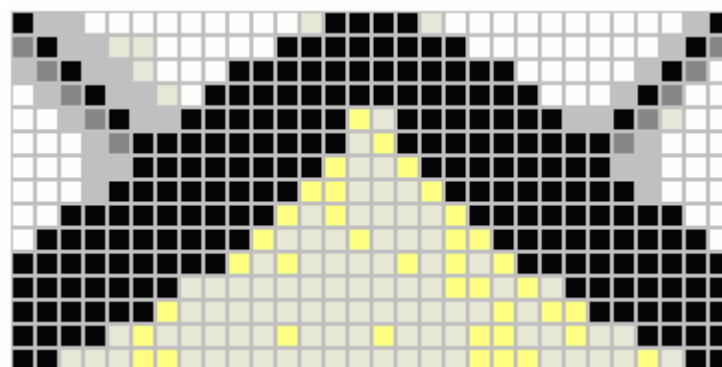
(Figure 7.16 continued)



(e) Layout of cross shape material model.



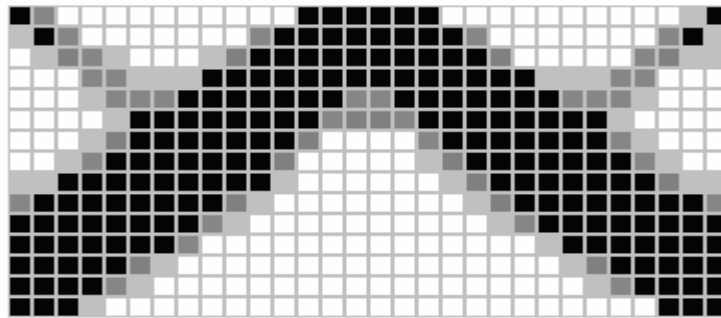
(f) Layout of circular material model.



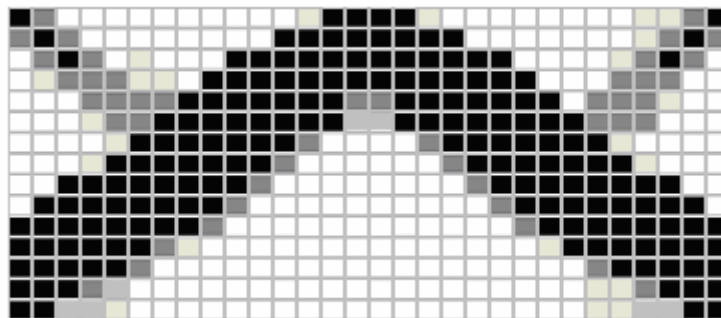
(g) Layout of triangular multi-void material model.

Figure 7.16 Optimization layouts for different microstructures (*continued*)

*(Figure 7.16 continued)*



(f) Layout of rectangular multi-void material model.



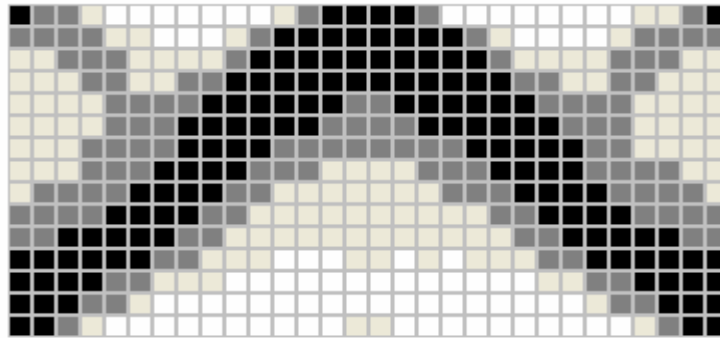
(i) Layout of square multi-void material model.

Figure 7.16 Optimization layouts for different microstructures

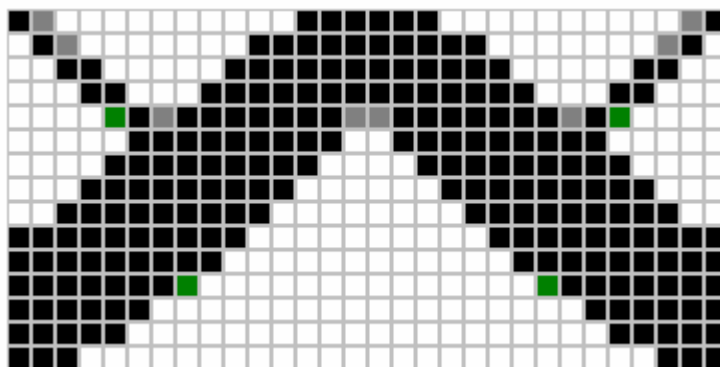
All the solutions using different models above give very similar layouts and agree well with that of the rectangular model given by PLATO software. Again the ranked layered material model layout shows more complicated distribution of material which would make it hard to implement. The cross shape and power-law models give the clearest layout.

The effects of power values on results of the power-law models were further investigated.

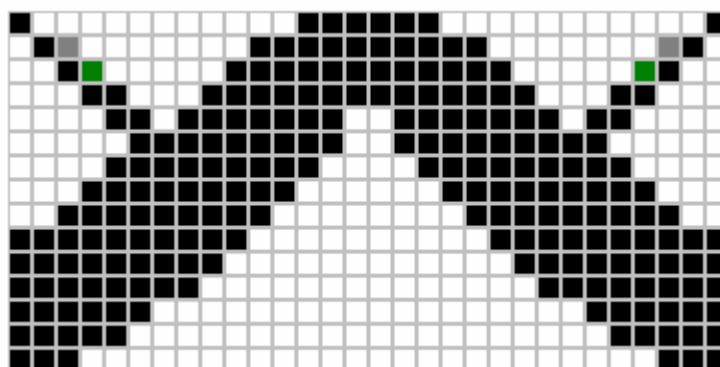
Figure 7.17 shows the optimization layouts for different power values from one to ten for the volume fraction  $V_s / V = 50\%$ .



(a) Power value  $\mu = 1$



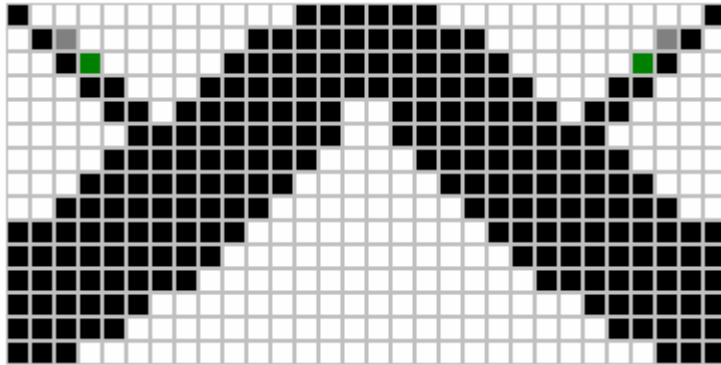
(b) Power value  $\mu = 2$



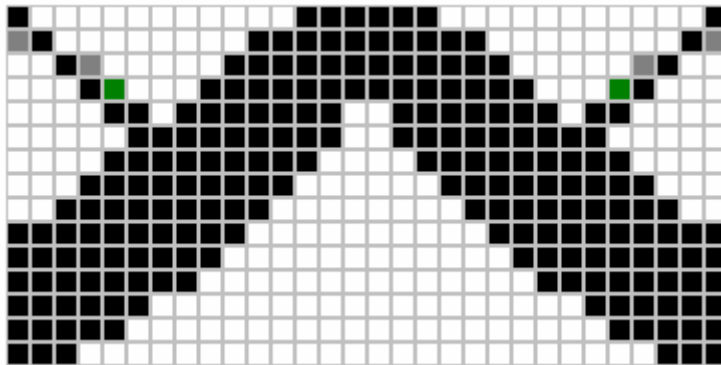
(b) Power value  $\mu = 3$

Figure 7.17 Optimization results for different power values (*continued*)

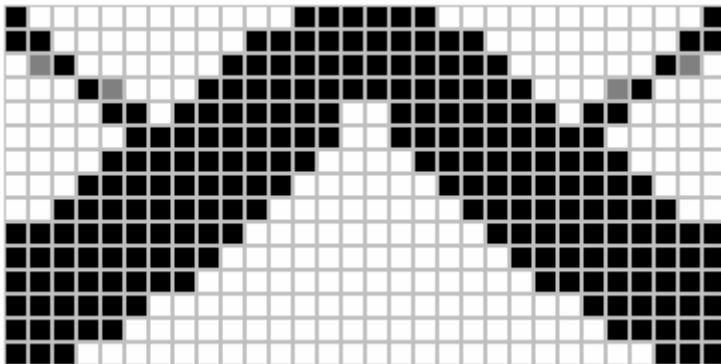
(Figure 7.17 continued)



(d) Power value  $\mu = 4$



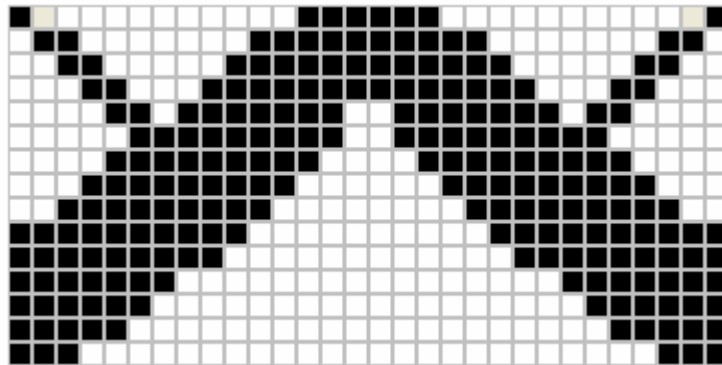
(e) Power value  $\mu = 5$



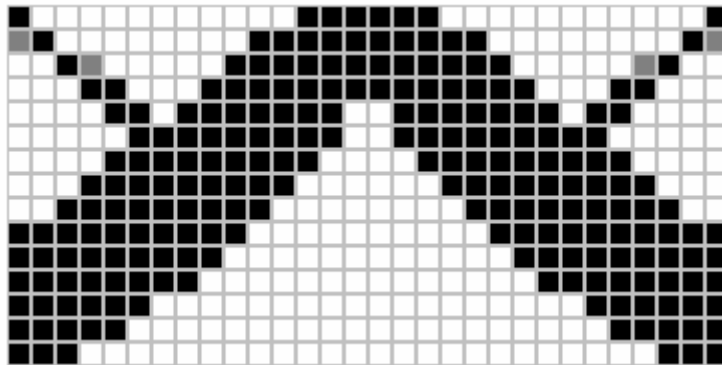
(f) Power value  $\mu = 6$

Figure 7.17 Optimization results for different power values (*continued*)

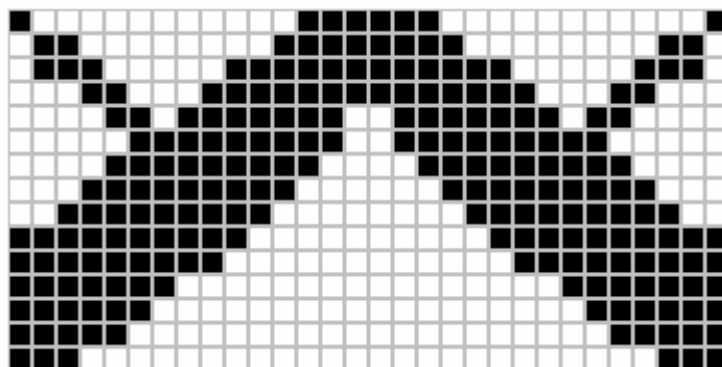
(Figure 7.17 continued)



(g) Power value  $\mu = 7$



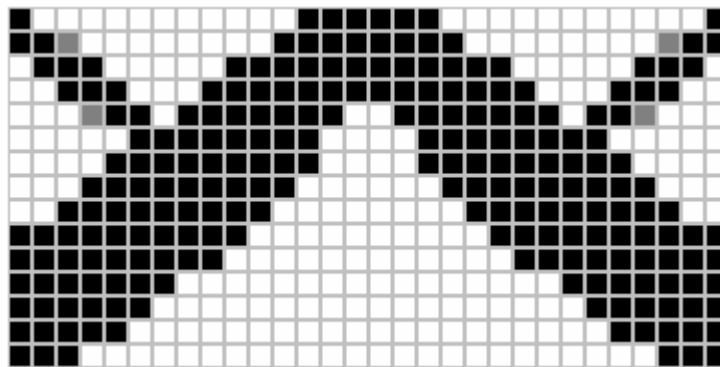
(h) Power value  $\mu = 8$



(i) Power value  $\mu = 9$

Figure 7.17 Optimization results for different power values (*continued*)

*(Figure 7.17 continued)*



(j) Power value  $\mu = 10$

Figure 7.17 Optimization results for different power values

The results above show that all values of power from 1 to 10 give similar layouts, among them those given by  $\mu = 2$  to 10 are very clear layout image and would be easy to implement. Even the power value  $\mu = 1$  also gives a good layout.

From the calculations for the single load cases, we can see that the power-law model with  $\mu = 2 \sim 3$  always performs well. While the ranked layered model shows a different and more complicated solution pattern.

## **7.2 Topology Optimization with Surface Load**

Many structures in the real environment are subjected to surface loading cases such as wind loads, traffic loads and so on. Such loads are pressure applied to a subdomain surface, which connects some defined points or points allowed to

move along some described direction. The pressure is then converted to consistent nodal loads at each element.

*Example 7.4 A model of bridge*

The design domain is a model of a bridge shown in Figure 7.18. The pressure load of intensity  $p = 1\text{kN}$ . Modulus of elasticity  $E = 10^5\text{ MPa}$ , Poisson's ratio,  $\nu = 0.3$  and volume fraction  $V_s / V = 30\%$ .

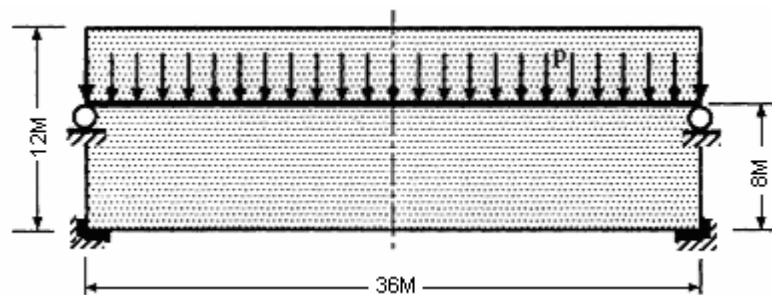


Figure 7.18 A bridge model

The result of using PLATO with rectangular material model calculated in this research is shown in Figure 7.19

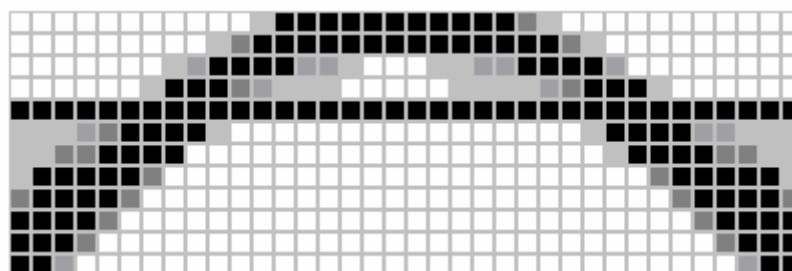
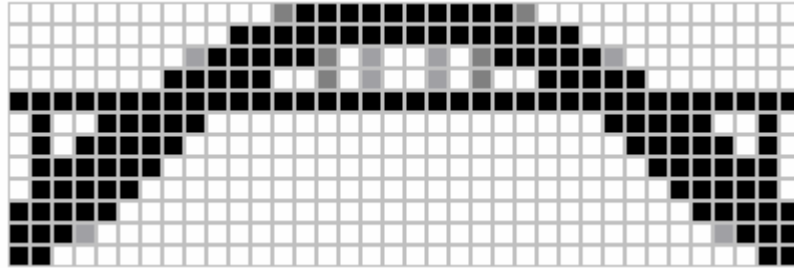


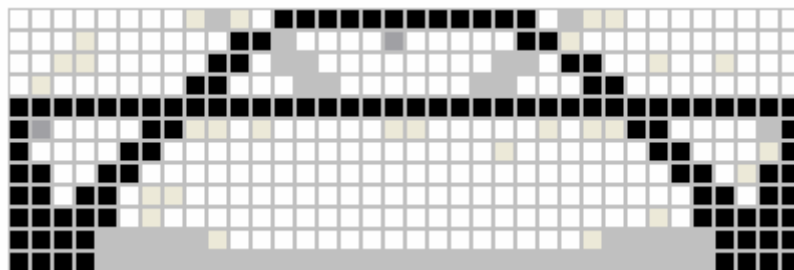
Figure 7.19 Result of using PLATO software

The results of using HDM with nine different material models are shown in Figure 7.20: (a) power-law, (b) ranked layered, (c) triangular, (d) hexagon, (e)

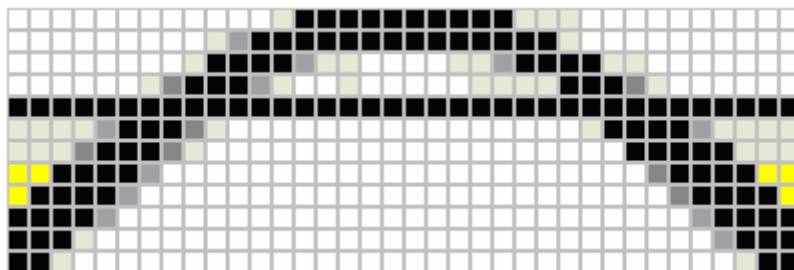
cross shape, (f) circular, (g) triangular multi-void, (h) rectangular multi-void, and (i) square multi-void material model.



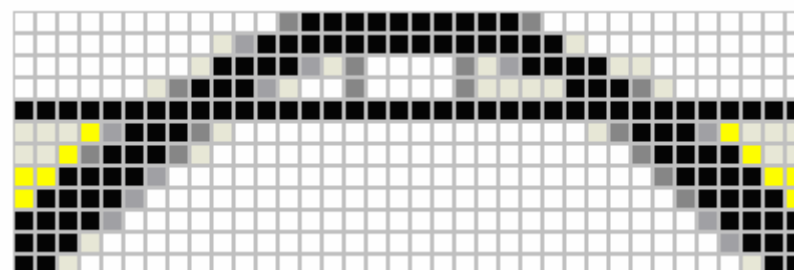
(a) Result layout for power-law one-material model



(b) Result layout for ranked layered material model



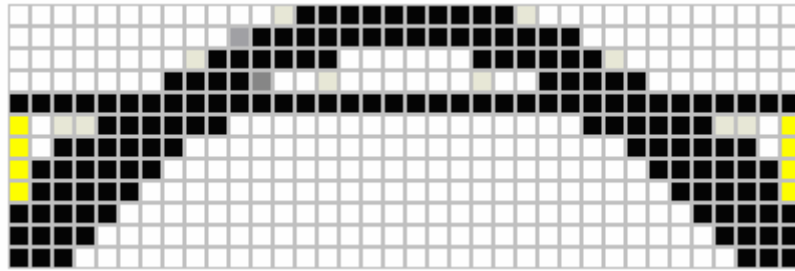
(c) Result layout for triangular material model.



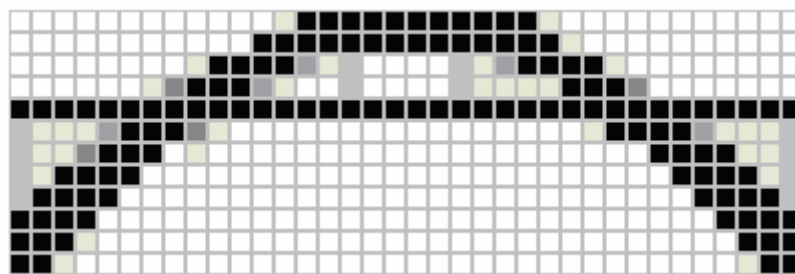
(c) Result layout for hexagon material model.

Figure 7.20 Optimization layouts for different microstructures (*continued*)

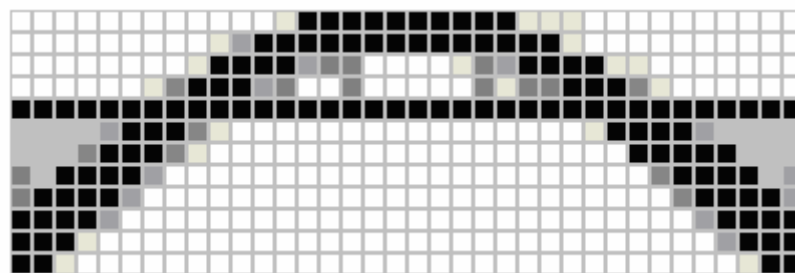
(Figure 7.20 continued)



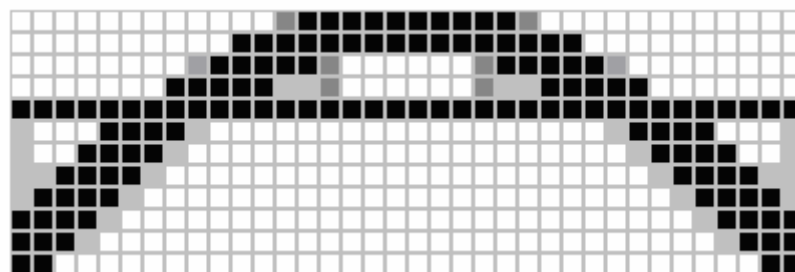
(e) Result layout for cross shape material model.



(f) Result layout for circular material model.



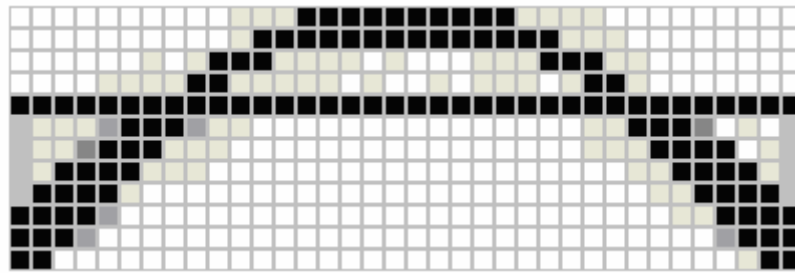
(g) Result layout for triangular multi-void material model.



(h) Rectangular multi-void material model.

Figure 7.20 Optimization layouts for different microstructures (*continued*)

*(Figure 7.20 continued)*



(i) Layout for square multi-void material model.

Figure 7.20 Optimization layouts for different microstructures

From the layout above, we can see that all the models give similar solutions, even in the case of ranked layered model. This is because in the pressure load case, the distribution of shear stress is more gradual compared to the single load case. From the point of view of practical implementation of layout, the ranked layered model still fares least favorable because of its complex material distribution and the requirement of considerable material at the bottom edge.

It should be noted here, the famous Sydney Harbor Bridge (In Figure 7.21) takes a very similar shape, indicating the ingenuity of the designers.

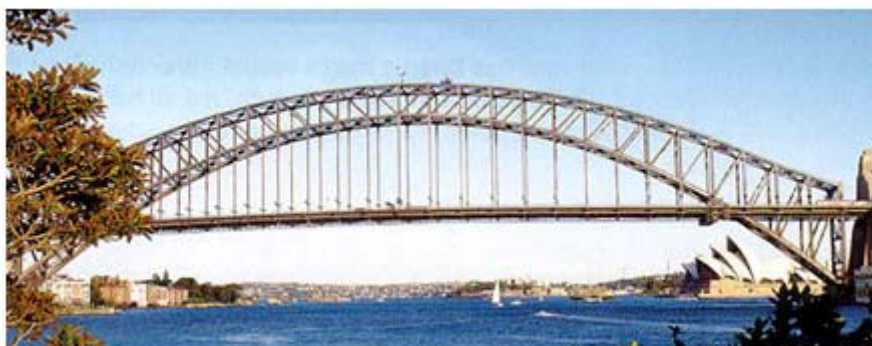
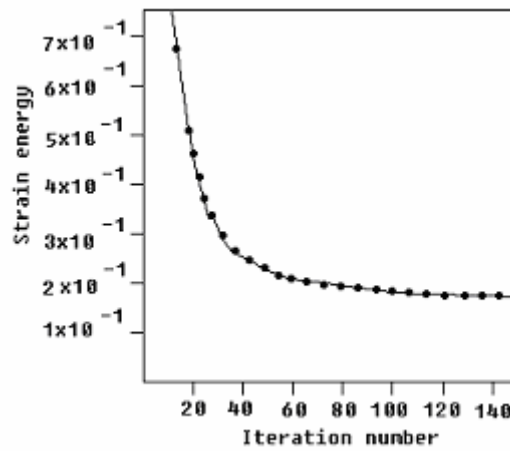
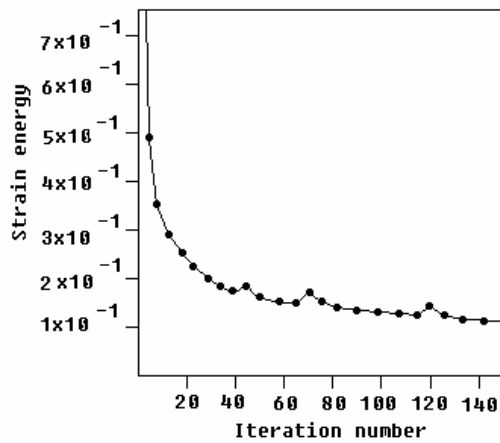


Figure 7.21 Sydney Harbor Bridge

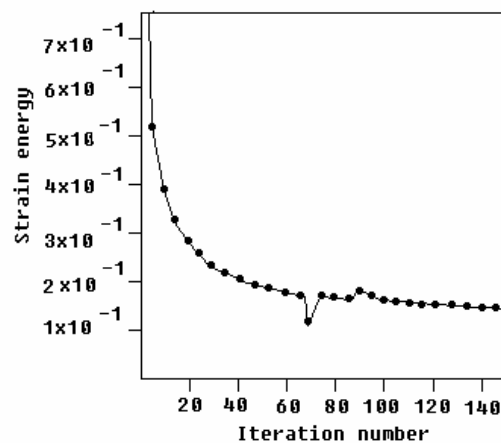
Figure 7.22 shows the iteration histories of HDM for different material models.



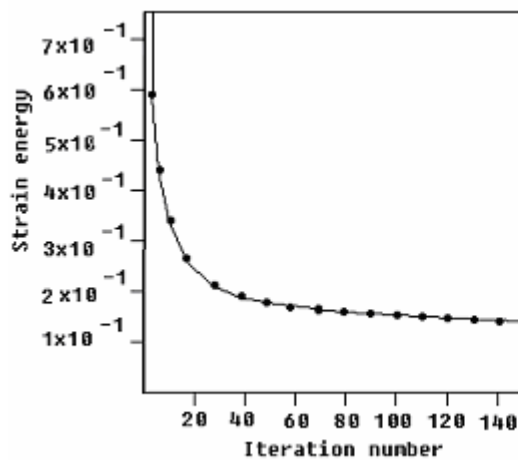
(a) Power-law one-material model



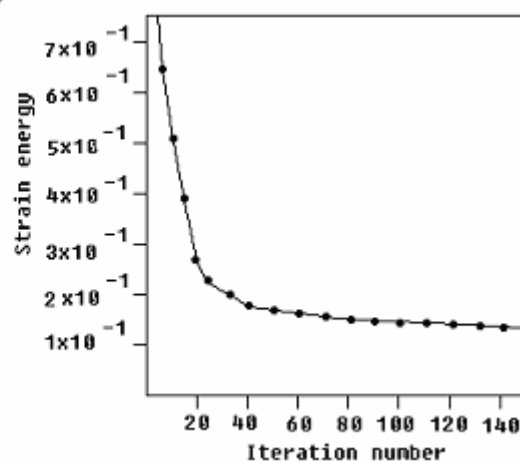
(b) Triangular material model.



(c) Hexagon material model.



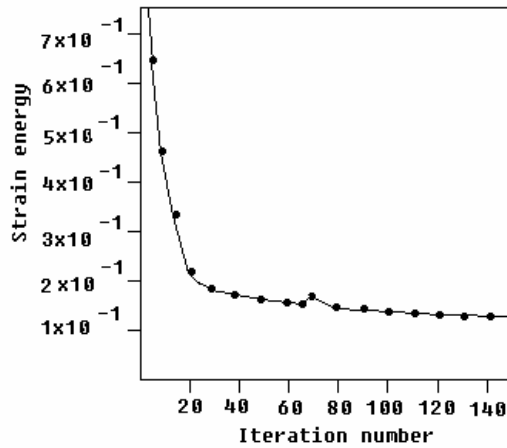
(d) Cross shape material model.



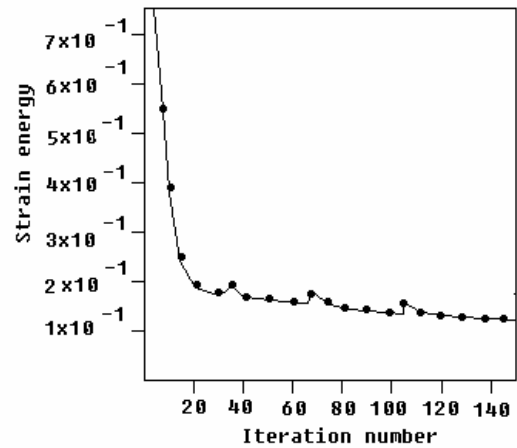
(e) Circular material model.

Figure 7.22 Iteration histories for different material models (*continued*)

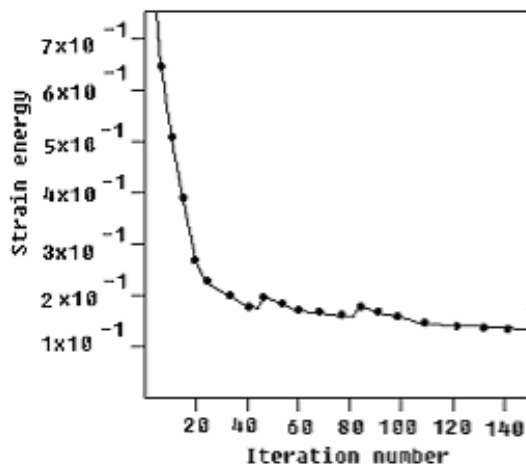
(Figure 7.22 continued)



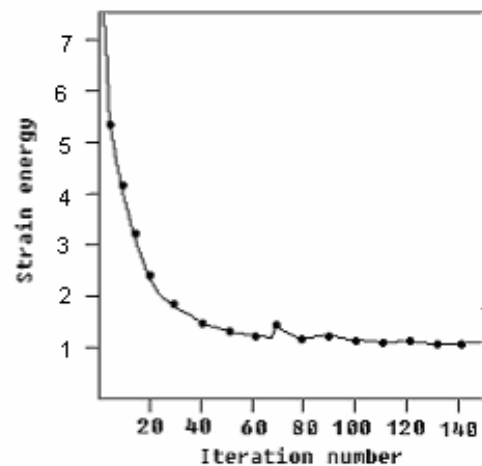
(f) Triangular multi-void model.



(g) Rectangular multi-void model.



(h) Square multi-void material model.



(i) Ranked layered material model.

Figure 7.22 Iteration histories for different material models

Table 7.3 shows iteration numbers and final strain energies upon convergence for convergence tolerance  $\Delta = 0.050$  for the microstructures using HDM.

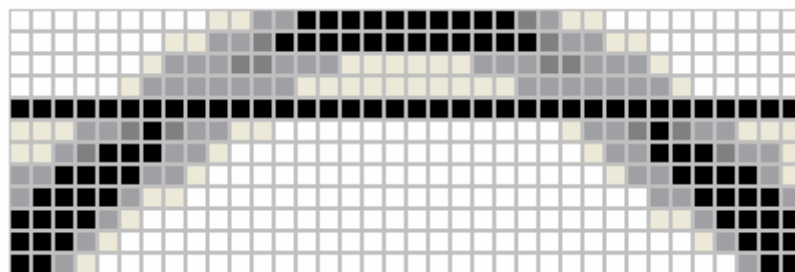
Microstructure Model	Iteration Number	Final Strain Energy
Power-law	232	0.1649
Cross shape	242	0.155
Circular	243	0.1567
Hexagon	274	0.1773
Triangular	257	0.1621
Rectangular Multi-void	264	0.1722
Square Multi-void	253	0.1823
Triangular Multi-void	266	0.1768
Ranked layered	273	1.2015

Table 7.3 Iteration numbers and final strain energies at convergence tolerance  $\Delta = 0.050$  for the microstructures using HDM

Figure 7.22 and Table 7.3 show that the cross shape, power-law, and circular models perform best in terms of convergence speed and final strain energy.

Further investigation of the effects of power values on optimization layouts.

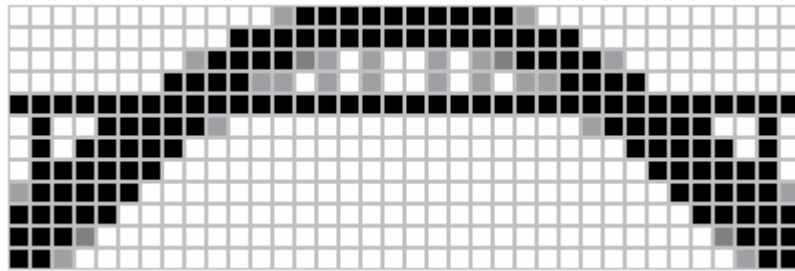
Figure 7.23 shows the optimization layouts for different power values from one to ten of the power-law model with the volume constraint  $V_s / V = 30\%$ .



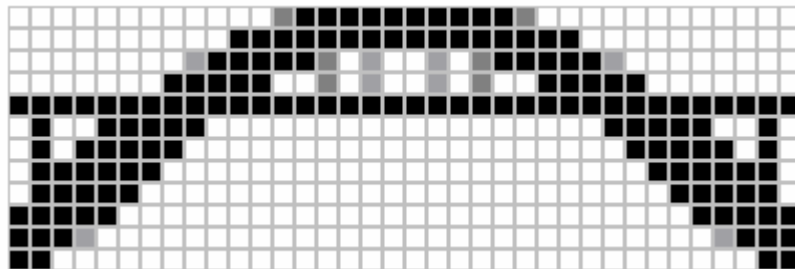
(a) Power value  $\mu = 1$

Figure 7.23 Optimization layouts for different power values (*continued*)

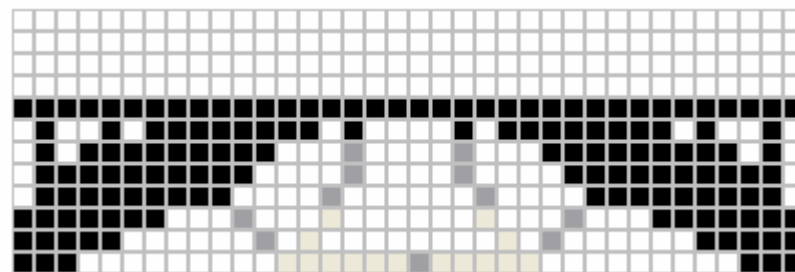
(Figure 7.23 continued)



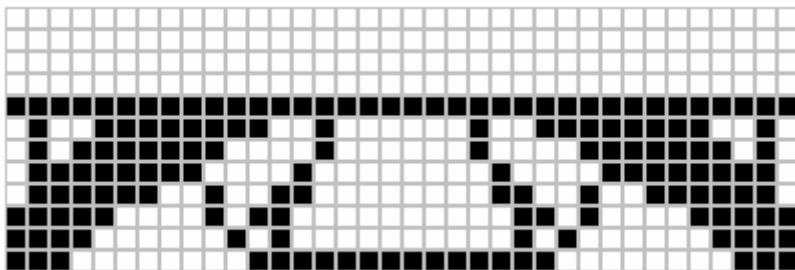
(b) Power value  $\mu = 2$



(d) Power value  $\mu = 3$



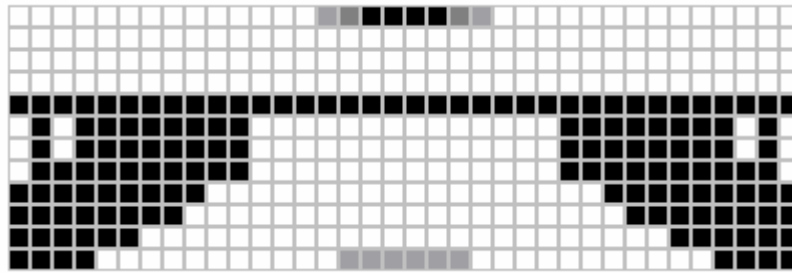
(d) Power value  $\mu = 4$



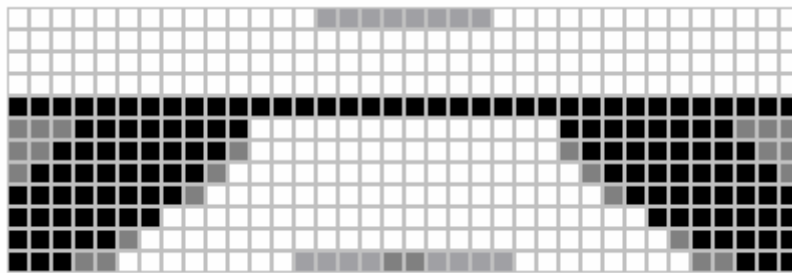
(e) Power value  $\mu = 5$

Figure 7.23 Optimization layouts for different power values (*continued*)

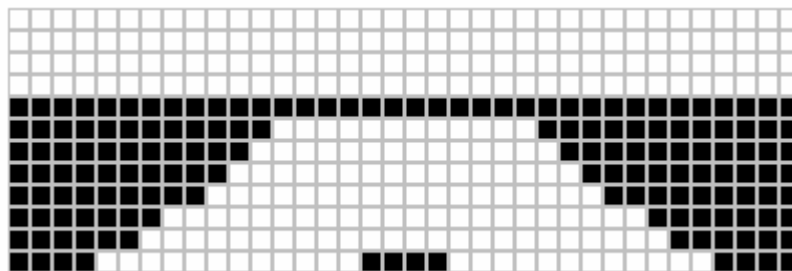
(Figure 7.23 continued)



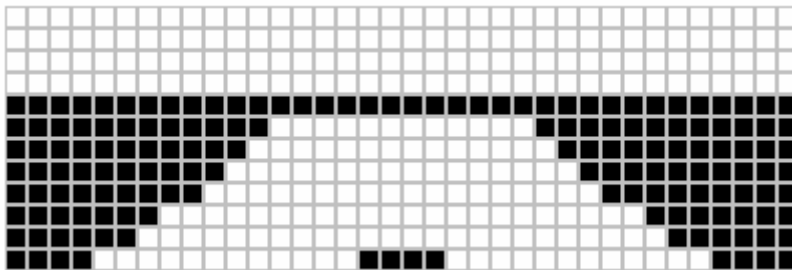
(f) Power value  $\mu = 6$



(g) Power value  $\mu = 7$



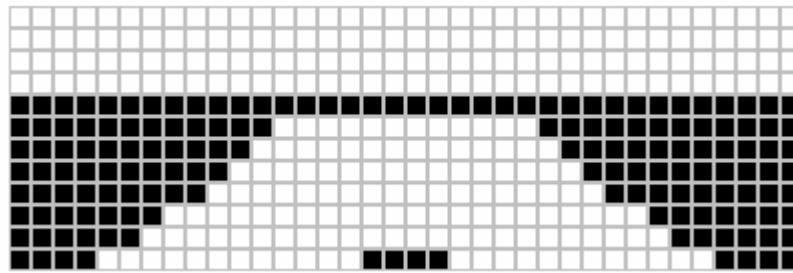
(h) Power value  $\mu = 8$



(j) Power value  $\mu = 9$

Figure 7.23 Optimization layouts for different power values (*continued*)

(Figure 7.23 continued)

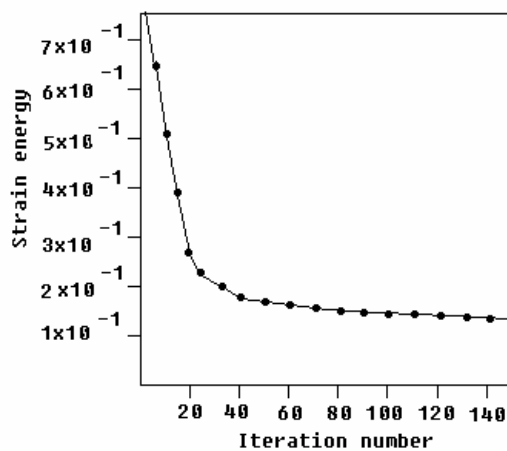


(j) Power value  $\mu = 10$

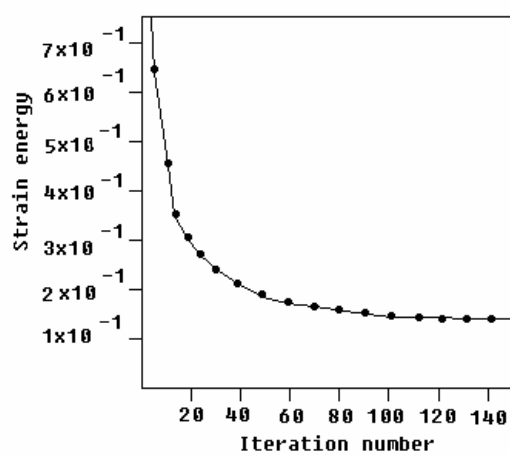
Figure 7.23 Optimization results for different power values

The results above show that the solutions of power value  $\mu$  between 1 and 3 agree well with other microstructure models. Those given by  $\mu \geq 4$  are very different, ranging from complicated layout for  $\mu = 4 \sim 5$  to not sensible for  $\mu = 6 \sim 9$ . In comparison with Sydney Harbor Bridge (Figure 7.21),  $\mu=2$  or  $\mu=3$  give the best layouts.

Figure 7.24 shows the iteration histories for different power values in the power-law material model.



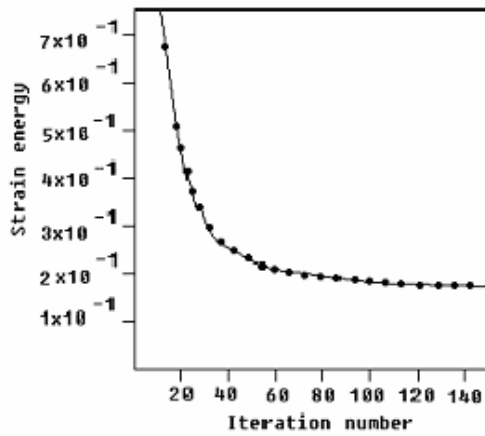
(a) Power value  $\mu = 1$



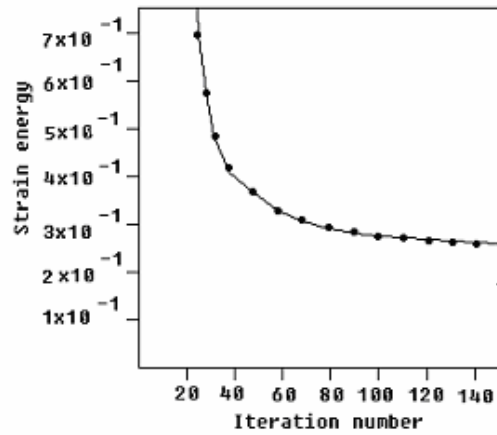
(b) Power value  $\mu = 2$

Figure 7.24 Iteration histories for different power values (continued)

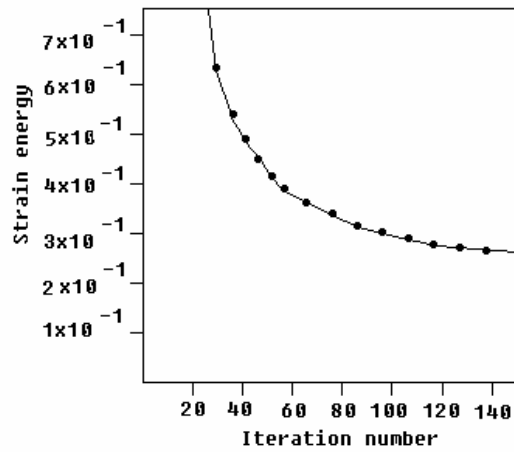
(Figure 7.24 continued)



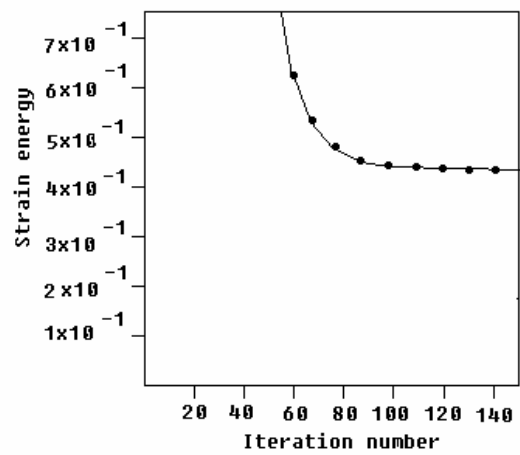
(c) Power value  $\mu = 3$



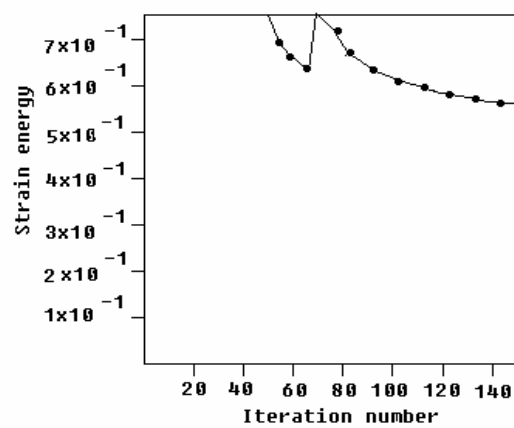
(d) Power value  $\mu = 4$



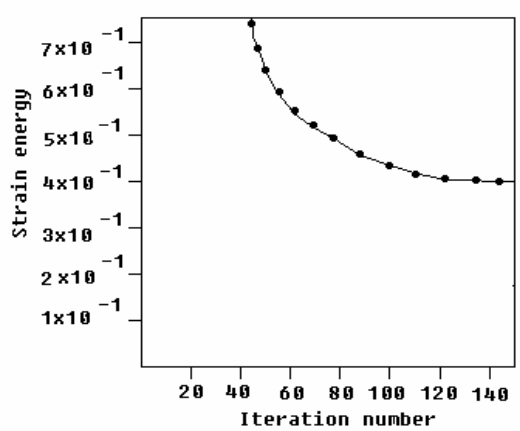
(e) Power value  $\mu = 5$



(f) Power value  $\mu = 6$



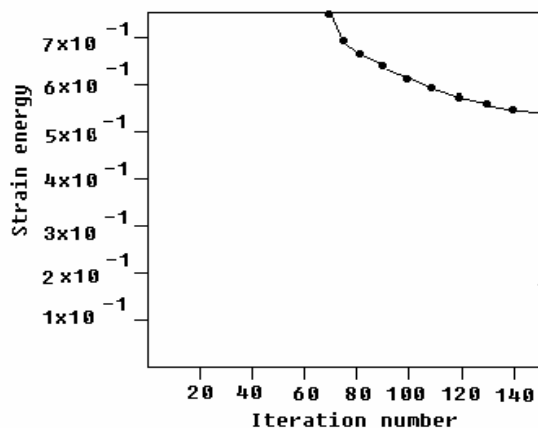
(g) Power value  $\mu = 7$



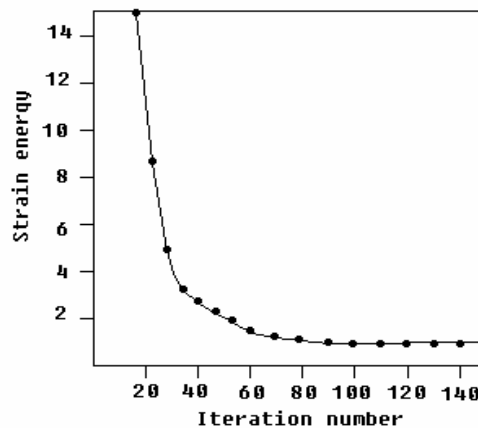
(h) Power value  $\mu = 8$

Figure 7.24 Iteration histories for different power values (continued)

(Figure 7.24 continued)



(i) Power value  $\mu=9$



(j) Power value  $\mu=10$

Figure 7.24 Iteration histories for different power values

Table 7.4 shows the initial and final strain energies for different power values.

Power value	Initial strain energy	Final strain energy
1	0.3313	0.1615
2	1.056	0.1619
3	3.390	0.1649
4	11.0125	0.269
5	35.6349	0.2801
6	113.0456	0.4718
7	200.727	0.5764
8	204.149	0.4485
9	205.688	0.5543
10	206.199	1.025

Table 7.4 Initial and final strain energies for different power values.

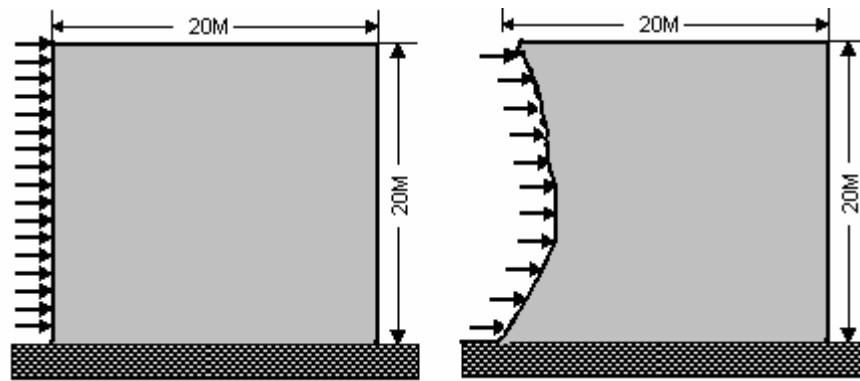
From the results shown in Figure 7.24 and Table 7.4, we can see that the power value  $\mu$  equals to 1, 2, 3 give the best convergence and  $\mu \geq 4$  converge to higher value of strain energy. The strain energy at power value  $\mu$  between 1 and 3 is lower than those of the value  $\mu \geq 4$ . This indicates that the layouts of the power value  $\mu \geq 4$  are not as good solutions.

Example 7.4 shows that all the models gave a very similar layout pattern, the cross shape, power-law, and circular models perform the best in terms of convergence speed and final strain energy. It should be reiterated that for power-law microstructure, power value  $\mu = 2 \sim 3$  gives the most desirable layout pattern.

#### *Example 7.5 Square domain with pressure load*

A square domain with supports and pressure load is shown in Figure 7.25. The pressure load of intensity  $p = 1\text{kN}$ . The modulus of elasticity  $E = 10^5\text{MPa}$ , Poisson's ratio,  $\nu = 0.3$  and volume fraction  $V_s / V = 30\%$ . In this example, we consider two loading cases:

- **(a)** Loading surface of the reference domain is fixed in the process of optimization.
- **(b)** Loading surface is allowed to conform to the boundary of the solid domain in the process of optimization.



- (a). Loading surface of the reference domain is fixed in the process of optimization.
- (b). Loading surface is allowed to conform to the domain boundary in the process of optimization.

Figure 7.25 A square domain with pressure load

**Case a:** Loading surface of the reference domain is fixed

The results of using PLATO with rectangular material model calculated in the research are shown in Figure 7.26.

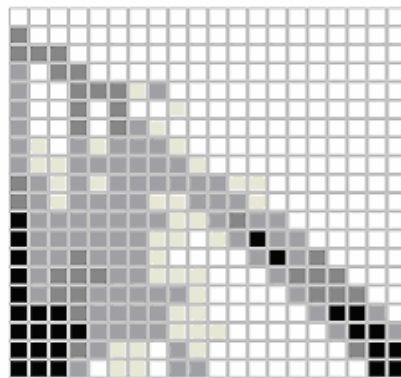
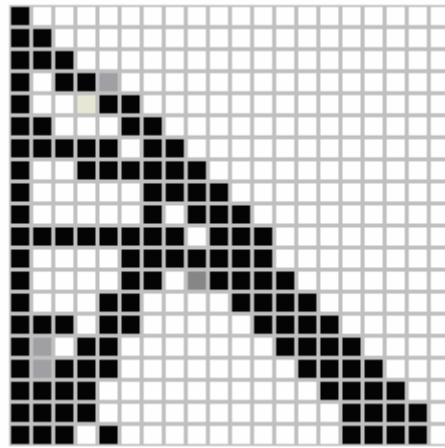
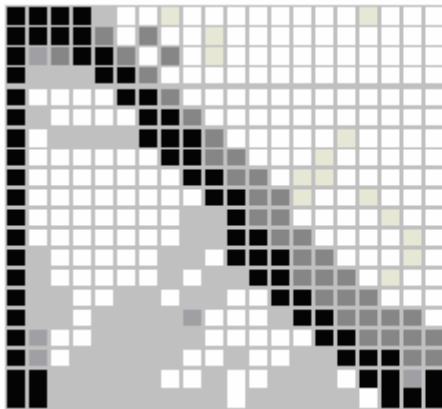


Figure 7.26 Results of using PLATO software

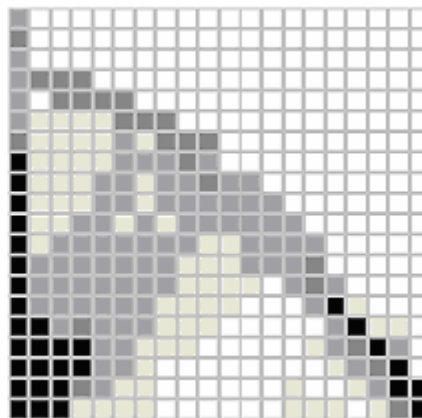
The results of using HDM with different material models are shown in Figure 7.27. In Figure 7.27, (a) power-law, (b) ranked layered, (c) triangular, (d) hexagon material model. (e) cross shape, (f) circular, (g) triangular multi-void, (h) rectangular multi-void, and (i) square multi-void material model.



(a) Power-law one-material model.



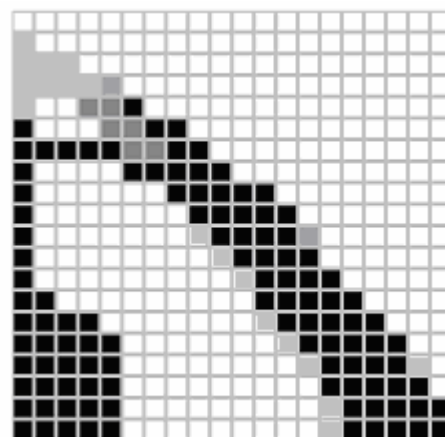
(b) Ranked layered material model.



(c) Triangular material model.



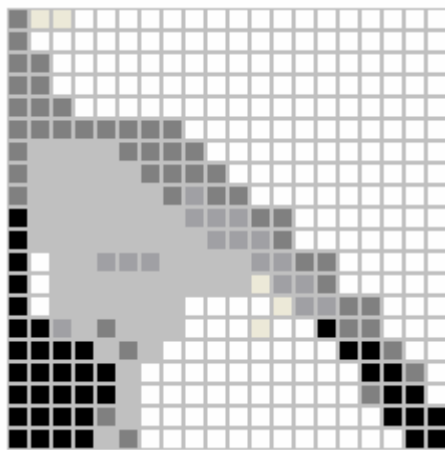
(d) Hexagon material model.



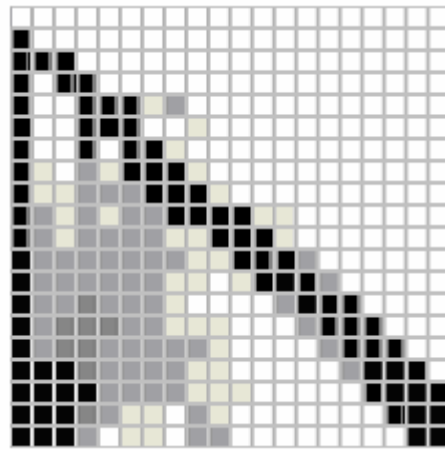
(e) Cross shape material model.

Figure 7.27 Optimization layouts for different microstructures (*continued*)

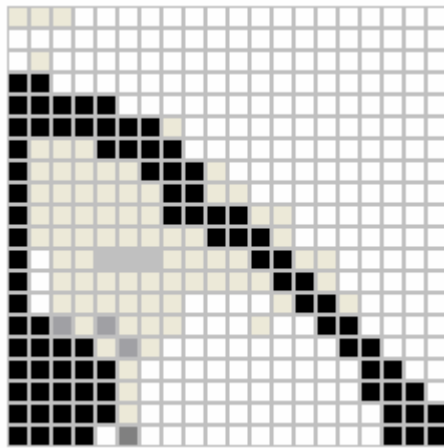
(Figure 7.27 continued)



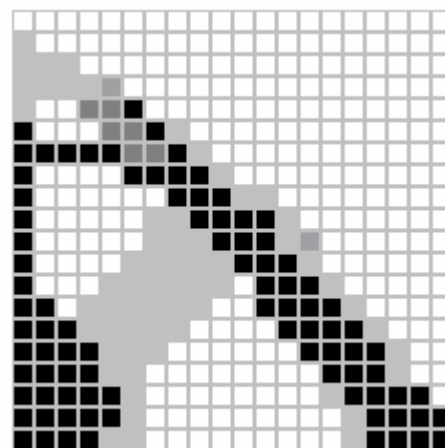
(f) Circular material model.



(g) Triangular multi-void material model.



(h) Rectangular multi-void model.



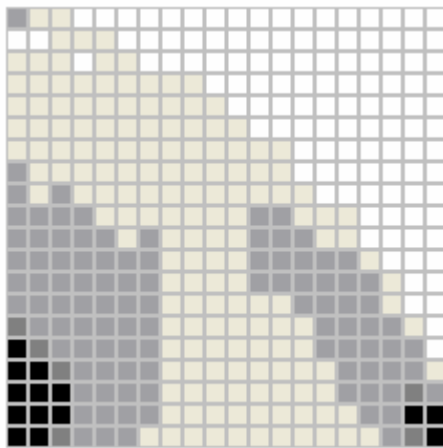
(i) Square multi-void material model.

Figure 7.27 Optimization layouts for different microstructures

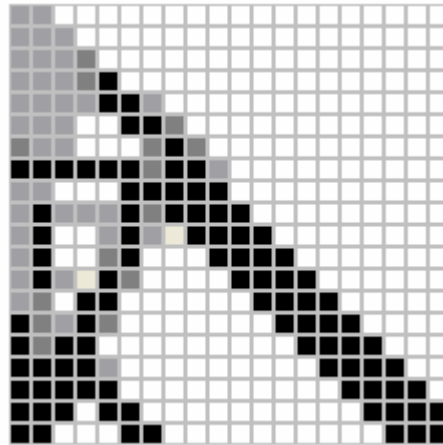
Similarly as above, all the solutions from the microstructures we developed give a similar layout pattern. As far as the requirement of the concept design stage is concerned, all the microstructure models are effective. From the point of view of implementation, cross shape and power-law microstructures offer the best solutions.

Figure 7.28 shows the optimization layouts for different power values from one

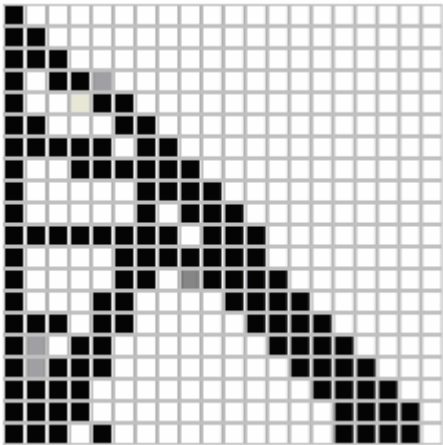
to ten of the power-law model for the volume fraction  $V_s / V = 30\%$ .



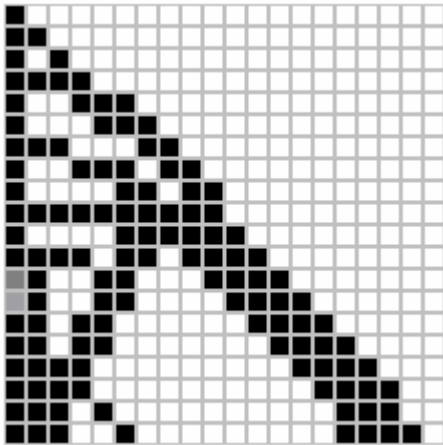
(a) Power value  $\mu = 1$



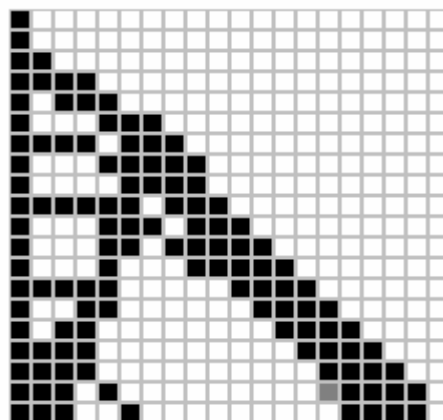
(b) Power value  $\mu = 2$



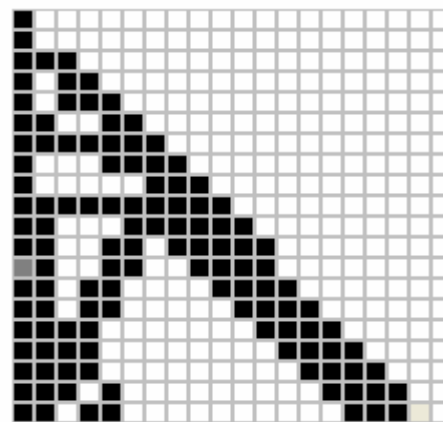
(c) Power value  $\mu = 3$



(d) Power value  $\mu = 4$



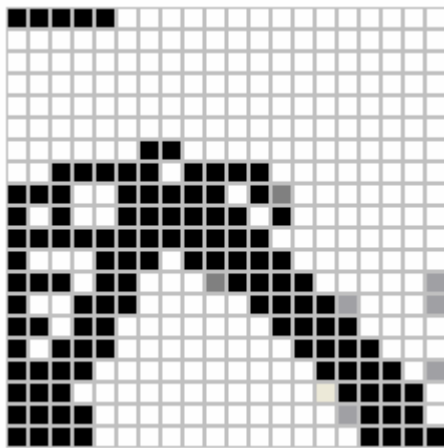
(e) Power value  $\mu = 5$



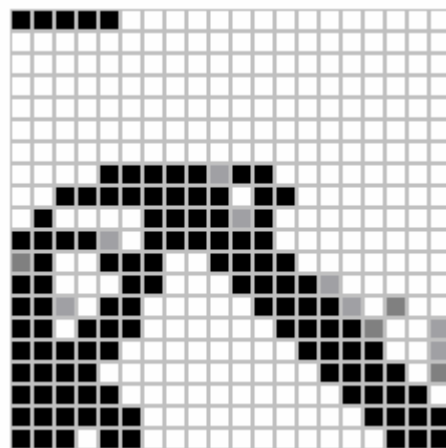
(f) Power value  $\mu = 6$

Figure 7.28 Optimization results for different power values (*continued*)

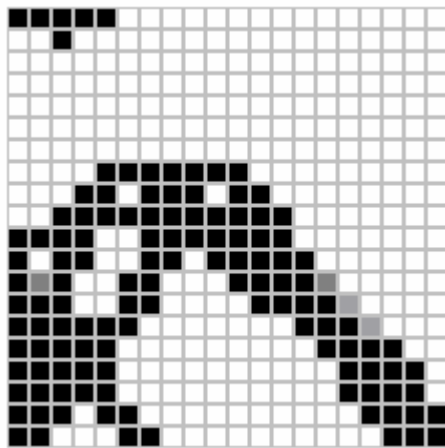
(Figure 7.28 continued)



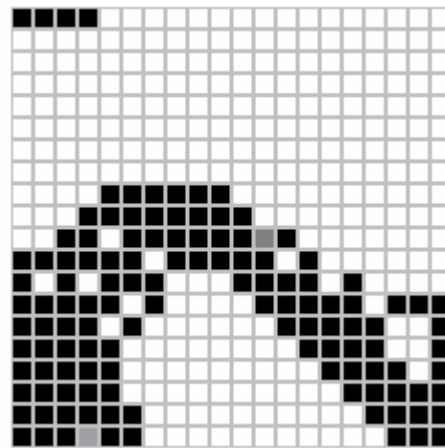
(g) Power value  $\mu = 7$



(h) Power value  $\mu = 8$



(i) Power value  $\mu = 9$



(j) Power value  $\mu = 10$

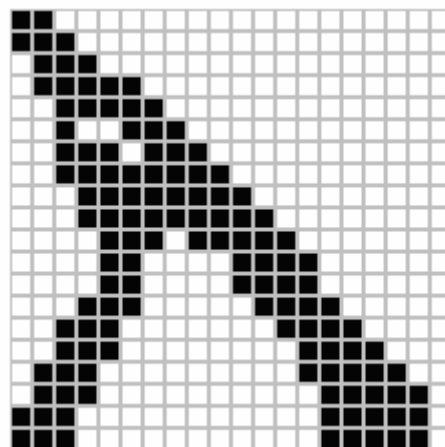
Figure 7.28 Optimization results for different power values

From the result layouts, we can see that the power values  $\mu$  between 2 and 6 agree well with other models giving the optimum layout that are easy to implement. The results are much different when the power value is either  $\mu = 1$  or  $\mu \geq 7$  for which the layout is either more complicated ( $\mu = 1$ ) or not sensible with solid material at the top edge and void at top part of the left edge ( $\mu \geq 7$ ).

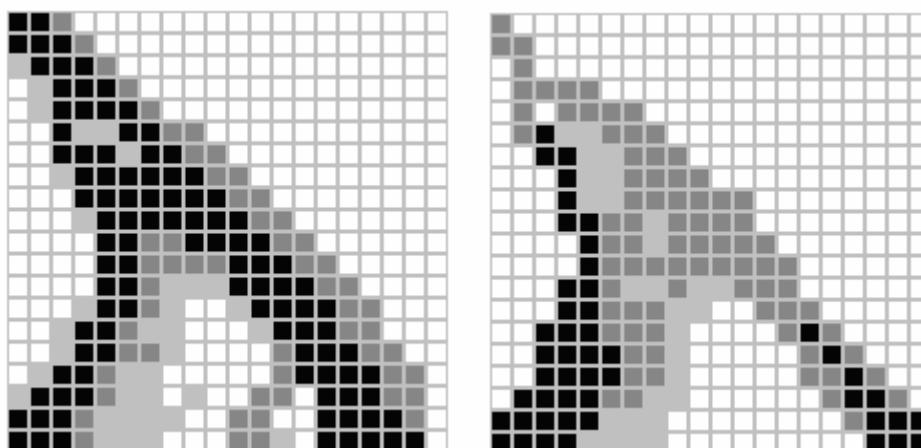
**Case b:** Loading surface of the reference domain is allowed to conform to the solid boundary.

In this problem, load points are allowed to translate along the loading action lines while keeping the same values. In this case, loading surface can be changed with the topology of the varying domain (see Figure 7.25 (b)).

The PLATO software does not have facilities to solve such problems. The results of using HDM with nine different models are shown in Figure 7.29.



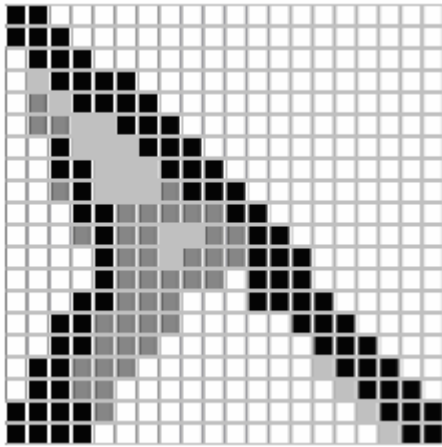
(a) Power-law one-material model.



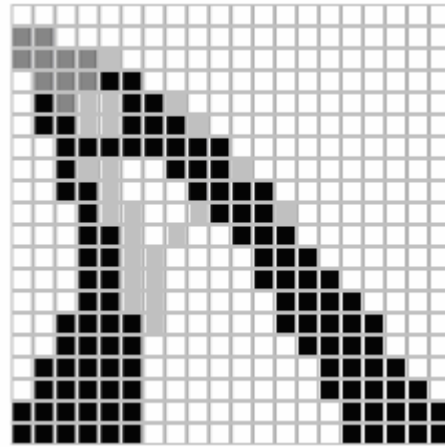
(b) Ranked layered material model. (c) Triangular material model.

Figure 7.29 Optimization layouts for different microstructures for the square domain with pressure load problem in Case b (continued)

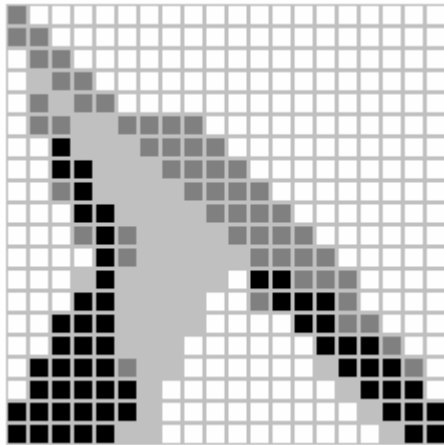
(Figure 7.29 continued)



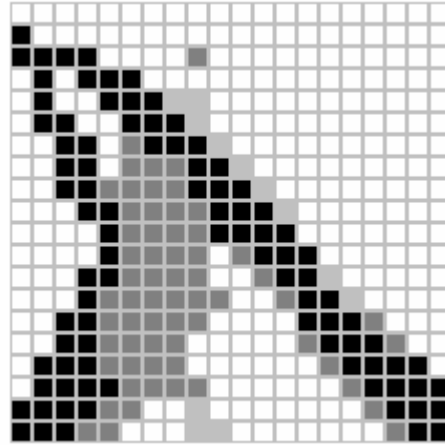
(d) Hexagon material model.



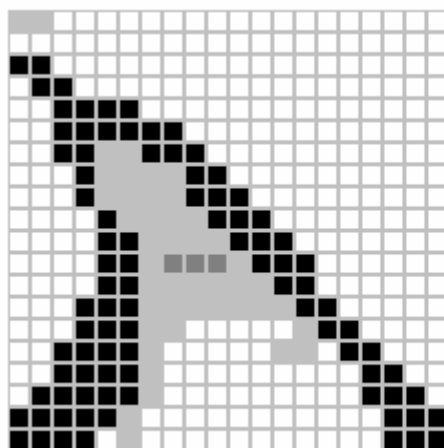
(e) Cross shape material model.



(f) Circular material model.



(g) Triangular multi-void material model.



(h) Rectangular multi-void model.



(i) Square multi-void material model.

Figure 7.29 Optimization layouts for different microstructures in *Case b*

From the optimal layouts obtained, we can see that all the solutions from different microstructures give a similar pattern. For the concept design stage, we can say that all nine microstructure models are effective for this problem. Among them, power-law model those microstructures with  $\mu = 2 \sim 3$  give the best solution.

### 7.3 Topology Optimizations with Multiple Loads

Many structures in the environment are subjected to a variety of load cases at the same time such as snow loads, traffic loads. In multiple loading cases, assume that there are  $n$  loads applied to the structure independently. The optimization problems can be redefined as

$$\begin{aligned} & \min_{u^i \in V, E} \sum_{i=1}^n w^i l^i(u^i) \\ & \text{subject } a_E(u^i, v) = l^i(v), \text{ for all } v \in V, I = 1, 2, \dots, n \\ & \quad E \in E_{ad} \end{aligned} \quad (7.1)$$

Where  $w^i$  is weighting coefficient, usually we can simply choose  $w^i = 1/n$ .

In the optimization processes, we need to change the  $\varphi', \psi'$  (Chapter 5, Section 5.4) for single loading cases to  $\varphi'' = \sum_{i=1}^n w^i \varphi^i$  and  $\psi'' = \sum_{i=1}^n w^i \psi^i$ .

*Example 7.6 A simply supported beam with multiple load*

A simply supported beam is shown in Figure 7.30. Three concentrated loads of

intensity  $p_1 = p_2 = p_3 = 1 \text{ kN}$  are applied downwards simultaneously at point of  $\frac{1}{4}$ ,  $\frac{1}{2}$ ,  $\frac{3}{4}$  of the bottom side of the beam. The modulus of elasticity  $E = 10^5 \text{ MPa}$ , Poisson's ratio,  $\nu = 0.3$  and volume fraction  $V_s / V = 40\%$ .

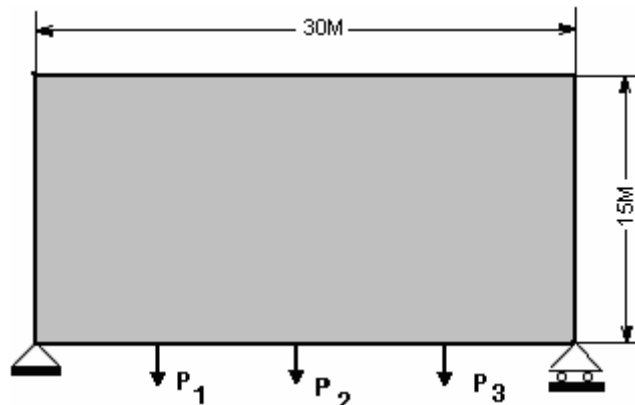
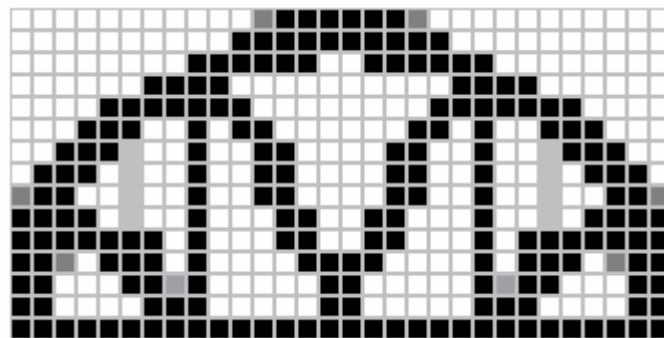


Figure 7.30 A simply supported beam with multiple load

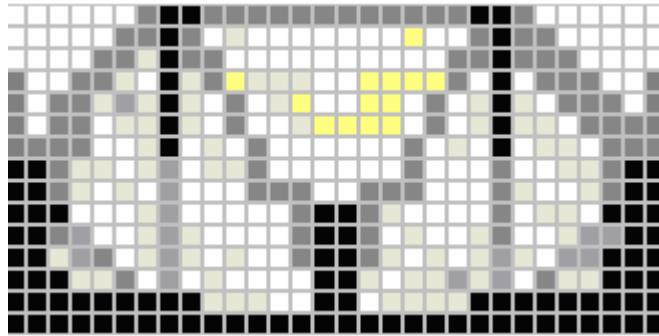
The results of using HDM with nine different material models are shown in Figure 7.31.



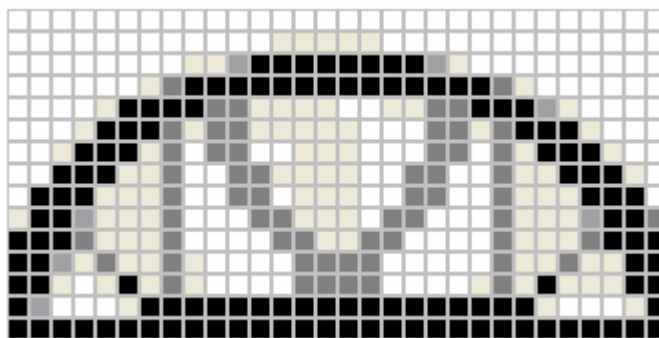
(a) Power-law one-material model

Figure 7.31 Optimization results for different microstructures (*continued*)

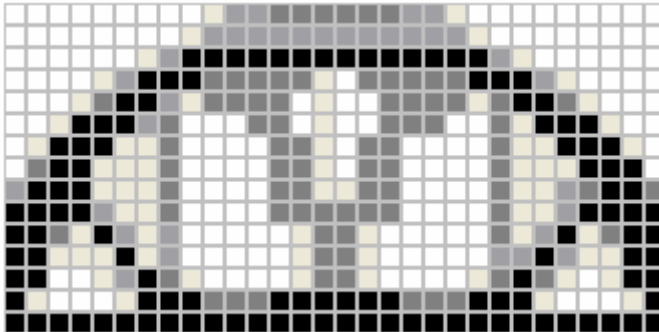
(Figure 7.31 continued)



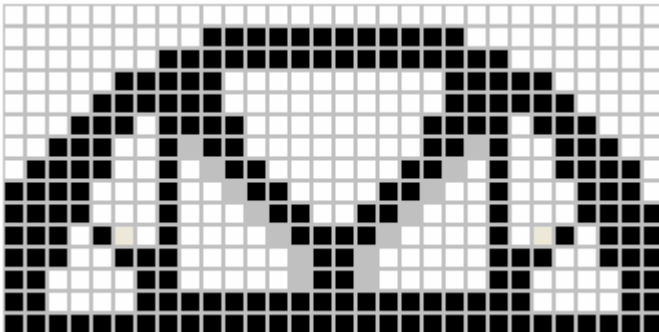
(b) Ranked layered material model.



(c) Triangular material model



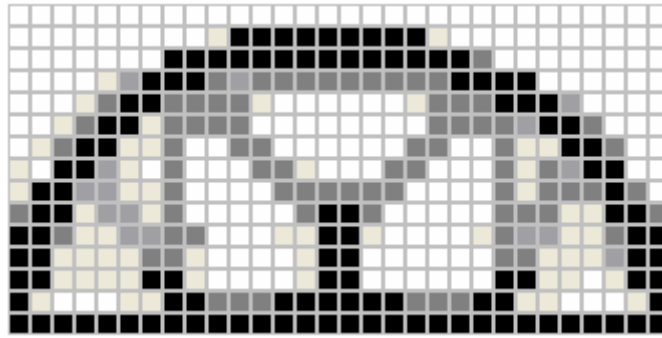
(d) Hexagon material model



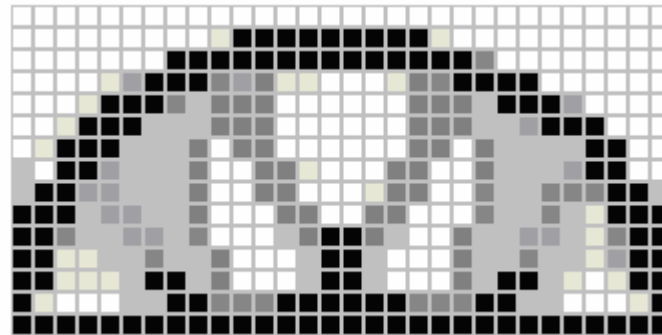
(d) Cross shape material model

Figure 7.31 Optimization results for different microstructures (*continued*)

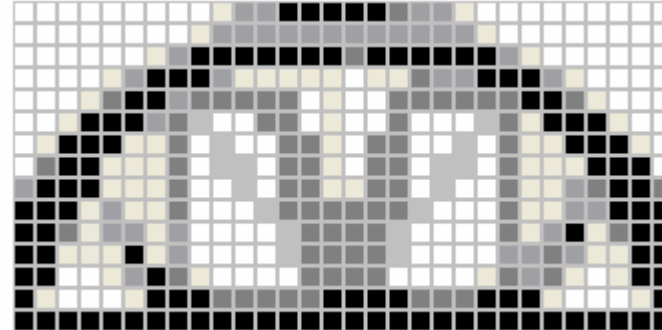
(Figure 7.31 continued)



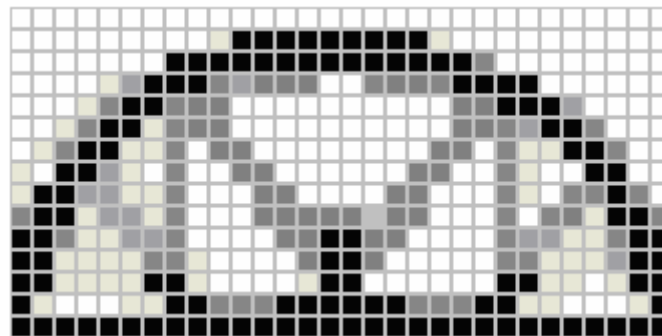
(k) Circular material model



(g) Triangular multi-void material model.



(h) Rectangular multi-void material model.



(i) Square multi-void material model.

Figure 7.31 Optimization results for different microstructures.

From the results obtained we can see that all the solutions from different microstructure models give very similar layouts while the ranked layered shows a little difference. This indicates that all the microstructure models are effective for this multiple loading problem. Among them the cross shape and power-law microstructures again give the clearest layouts.

### **7.4 Topology Optimizations with Gravity Load**

*Example 7.7 A simply supported beam with gravity load*

A simply supported beam is shown in Figure 7.32. The modulus of elasticity  $E = 10^5$  MPa, Poisson's ratio,  $\nu = 0.3$ . The design domain is a rectangular block with the dimensions of 30x10x1. Gravity load  $g = 1$  kN is assumed. The design objective is to minimise the mean compliance under gravity loading for a given volume fraction  $V_s / V = 20\%$ . This problem is related to the designing of a stone bridge in which the most considerable loading is self-weight.

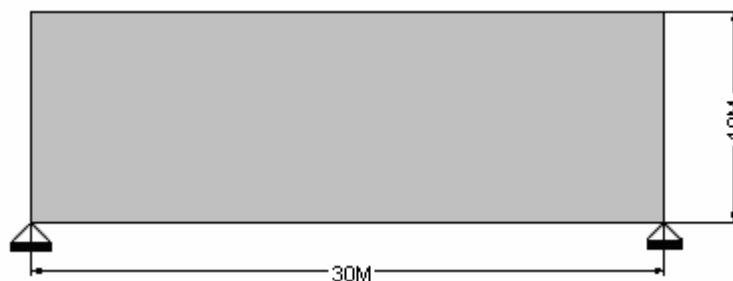
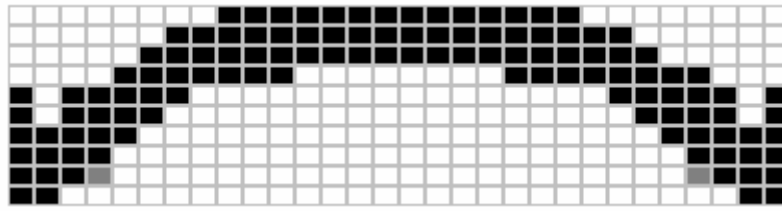
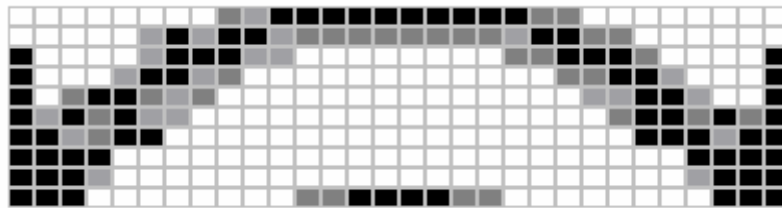


Figure 7.32 A simply supported beam under gravity loads

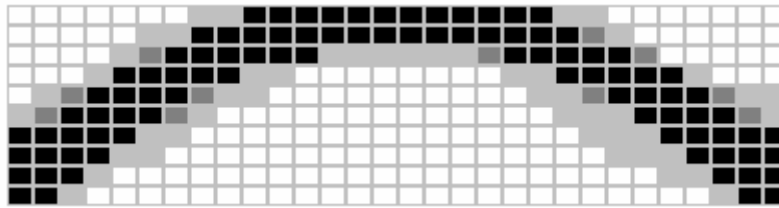
The results of using HDM with nine different material models are shown in Figure 7.33.



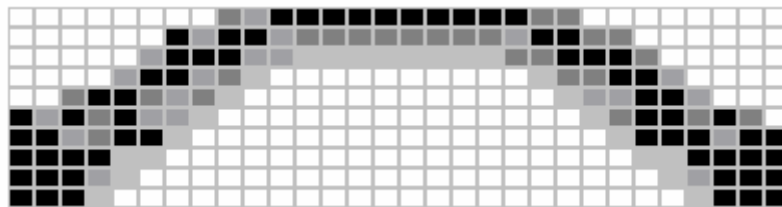
(a) Power-law one-material model.



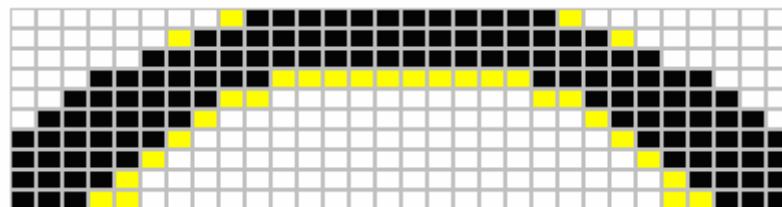
(b) Ranked layered material model.



(c) Triangular material model.



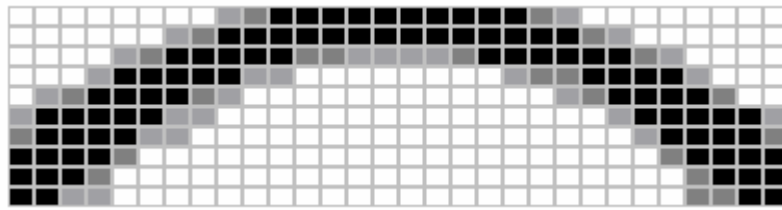
(d) Hexagon material model.



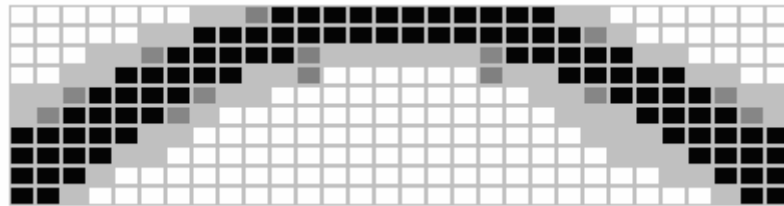
(e) Cross shape material model.

Figure 7.33 Optimization layouts for gravity load (*continued*)

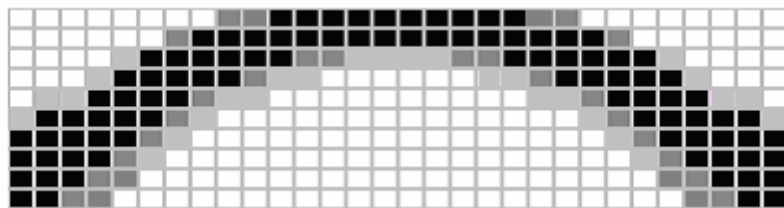
(Figure 7.33 continued)



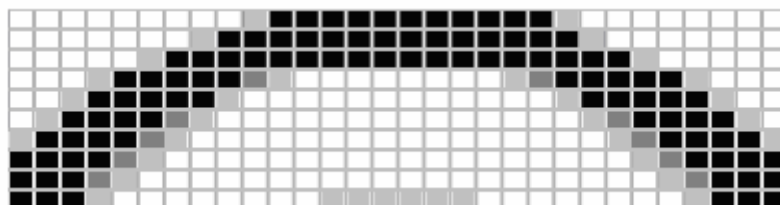
(l) Circular material model.



(g) Triangular multi-void material model.



(h) Rectangular multi-void material model.



(i) Square multi-void material model.

Figure 7.33 Optimization layouts for gravity load

The results above show that most microstructure models give similar patterns. The layouts of ranked layered, square multi-void, and power-law models show a little difference from others in that more material is required at the left and right edge or at the bottom edge. From the implementation point of view, the

cross shape model offers the best layout. The ranked layered, hexagon and square multi-void give much complicated patterns. At concept design stage, all the microstructure models are effective for this problem.

## **7.5 Effect of Microstructures on Topology Optimization**

As presented in the sections above, we tested the effects of microstructures on topology optimization with a series of problems. We can conclude that:

- ***Effects of the different material models on optimization layout***

Because of the complicated features of structural topology optimization, all the studies have aimed at the concept design. The studies of a series of topology optimization problems show that all nine new material models using HDM investigated in the thesis can converge to an optimal topology of a design domain. Overall, the cross shape model and the power-law model (with  $\mu = 3$ ) give the clearest image result. Compared to other models, the result layout pattern of the ranked layered microstructure model is very much different from others in some problems. This is because the ranked layered microstructure model does not cater for shear stress between the layers. This will result in the stiffness matrix of the structure almost becoming singular and large displacement leading to higher strain energy. It can be seen that for a structure has high shear stress throughout most of its domain, the ranked

layered model is not suitable for finding the optimum topology.

- ***Effects of power value for the power-law model on optimization solutions***

From the layout patterns of the benchmark problems, we can see that in most problems, different values of  $\mu$  give different layouts. Especially in the cases of surface loading that higher values of  $\mu$  do not perform well compared to lower value of  $\mu$ . For point load cases, high values of  $\mu$  perform comparatively as well as lower values of  $\mu$ . Compared to the optimization solution of other microstructure models, we suggest the power value  $\mu = 2 : 3$  for the power-law model.

- ***Effects of the different material models on convergence***

The iteration histories of optimization problems showed that the all the material models except ranked layered model using HDM have similar convergence. Among them the cross shape, power-law and circular microstructures performed best. This indicates the HDM program is stable. The final energy of the ranked layered material model is much larger than other material models. This is because the ranked layered material model does not have shear strength and we use very soft material instead of voids. In power-law models, with the power value increasing, the initial strain energy is larger than other models, however

the final value of strain energy upon reaching convergence are similar.

- ***Effects of different power values on convergence for power-law model***

With regard to the iteration histories, different power values greatly affect the initial strain energy value for power values. In the case of  $\mu < 4$ , the power value does not affect the final strain energy to a great extent. With the power value  $\mu$  increasing, the final strain energy increases slowly.

## **7.6 Conclusions**

The applications using the nine microstructures programmed by HDM to topology optimization problems with different loading cases show that the algorithm converges for all one-material microstructure models. The final optimum layouts are similar for different microstructures, with that of the ranked layered model shows a different layout from others, especially in the case of point loading. The final layout given by this model has much larger final strain energy and not suitable for problems in which shear stress is high.

Among these various microstructure models, the cross shape and the power-law models with  $\mu=3$  consistently perform better in terms of final strain energy value, convergence speed and ease of practical implementation. Higher values of  $\mu$  are not suitable for surface loading while most power

values give similar layout and final strain energies for point loading problems.

According to the studies carried out here, for power-law microstructures we suggest to choose the power value  $\mu=3$  for most of optimization problems.

## **Chapter 8**

---

# **STUDY OF THE EFFECT OF BI-MATERIAL MICROSTRUCTURES ON TOPOLOGY OPTIMIZATION RESULTS**

In bi-material microstructures, the material model contains two materials, one harder and the other softer, with or without void. A void implies that there is no material. If a portion of the medium consists only of voids, material is not placed over that area. On the other hand, if there is no porosity at some position, a solid structure needs to be placed at that location.

Bi-material optimization has significant practical importance and can be used in many engineering fields. For example, it can be used for the optimal design of steel reinforcement in concrete or metal fiber reinforcement in ceramic composites. At present there has been very little work done on the topology optimization problems by using bi-material microstructures and effects of different bi-material models on topology optimization solutions.

In this chapter, a range of examples of topological optimization problems are solved using different bi-material microstructures presented in Chapter 5 for

isotropic material. These models are power-law bi-material model, ranked layered bi-material model, cross shape bi-material model, square bi-material model, double rectangular bi-material model and triangular bi-material model. A study on the effects of the different bi-material microstructures on topology optimization problems is also carried out.

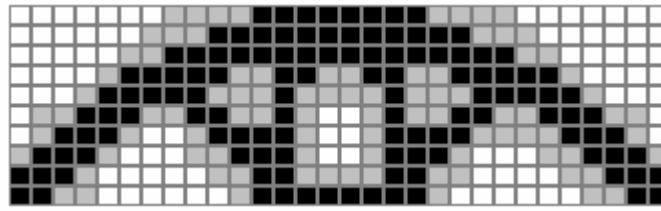
### **8.1 Topology Optimization Using Bi-material Models with Void**

First, we investigate the case of the design domain being treated as two-material composites with voids. The aim of the optimization is to find the distribution of hard and soft materials in the given domain.

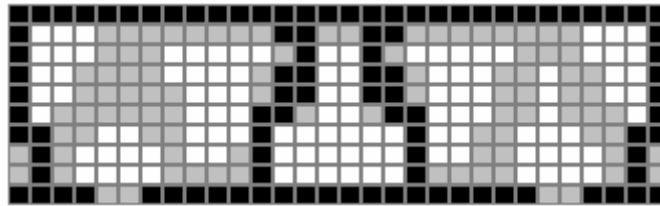
*Example 8.1 A simply supported beam with a single load*

Considering the optimization problem of simply supported beam shown previously in Figure 7.1, the modulus of hard and soft materials elasticity are given as  $E_a = 1 \times 10^5$  MPa,  $E_b = 1 \times 10^3$  MPa and the Poisson's ratio  $\nu = 0.3$ . The volume fraction of hard material is  $V_H / V = 20\%$  and the soft materials is  $V_S / V = 30\%$ , Void 50%.

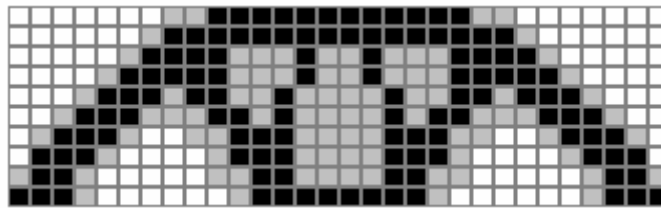
The results of using the six different bi-material models are shown in Figure 8.1. In the following graphics, the mesh with black color means hard material areas, grey means soft material areas, and white means no materials.



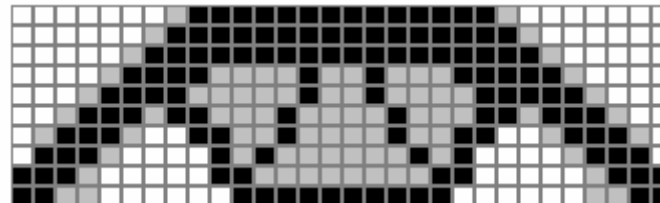
(a) Power-law bi-material model at  $\mu = 3$



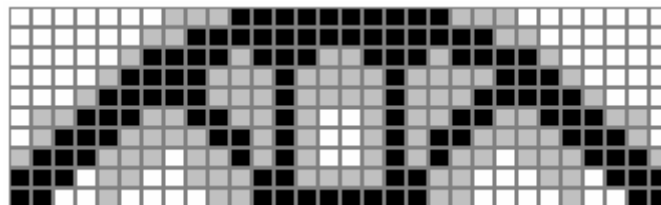
(b) Ranked layered bi-material model



(c) Square bi-material model



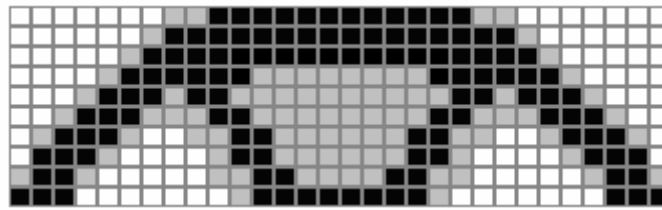
(d) Cross shape bi-material model



(e) Double rectangular bi-material model

Figure 8.1 Optimization layouts of bi-material models (*continued*)

(Figure 8.1 continued)



(F) Triangular bi-material model

Figure 8.1 Optimization layouts of bi-material models

Similar to the case of one-material model, the optimization layouts using bi-material models show that except for the ranked layered bi-material model, all models provide a similar optimum layout, although the triangular bi-material model shows a slight difference. The layout of ranked layered bi-material model is very different from others, because of its failure to account for shear stress.

Figure 8.2 shows the iteration history for ranked layered bi-material model.

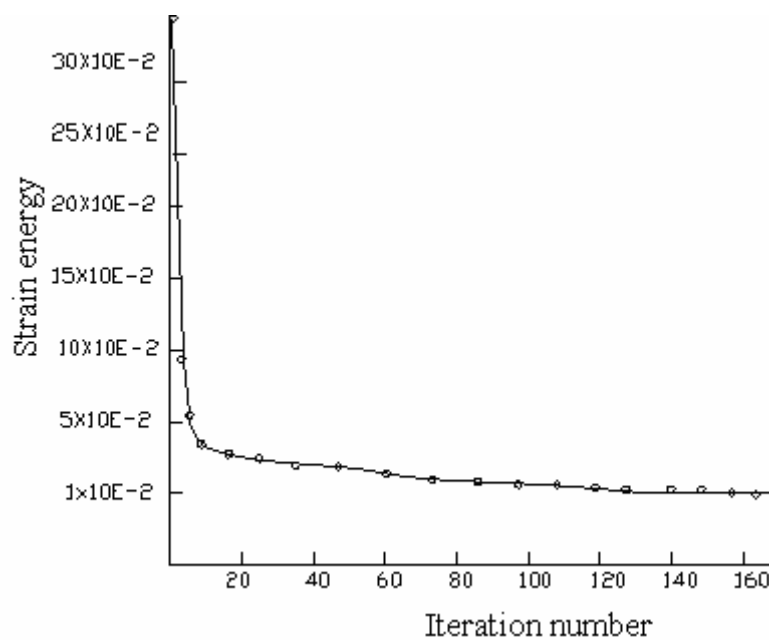


Figure 8.2 Iteration history for ranked layered bi-material model

Figure 8.3 shows the iteration histories for the rest of bi-material models.

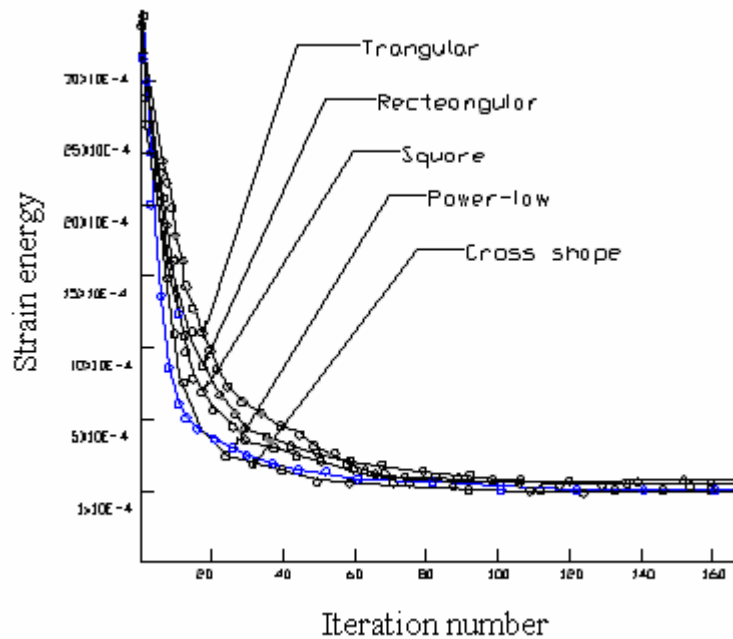


Figure 8.3 Iteration histories for the rest of bi-material models

Table 8.1 shows iteration numbers and final strain energies at convergence tolerance  $\Delta = 0.05$  for the bi-material microstructures using HDM.

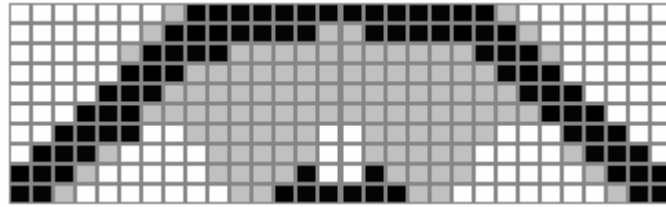
Microstructure Model	Iteration Number	Final Strain Energy
Power-law bi-material	234	0.000123
Cross shape bi-material	269	0.000117
Square bi-material	284	0.000152
Rectangular bi-material	294	0.000144
Triangular bi-material	304	0.000235
Ranked layered bi-material	344	0.0098

Table 8.1 Iteration numbers and final strain energies at convergence tolerance

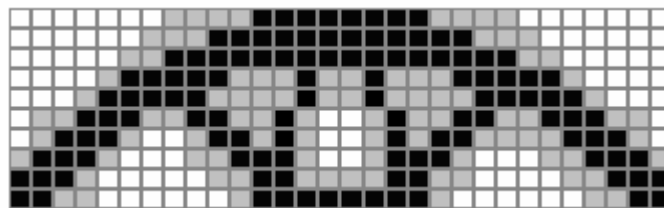
$\Delta = 0.05$  for the microstructures using HDM

From Figure 8.3 and Table 8.1, it can be seen all models show good convergence, among them the cross shape has the lowest strain energy.

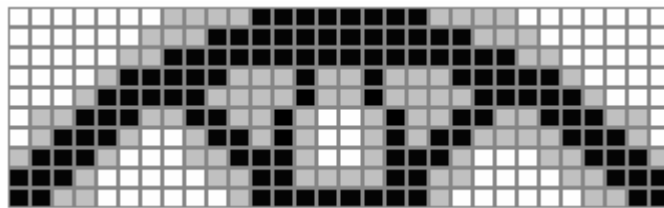
Figure 8.4 shows the optimization layout for different power values ( $\mu = 1 : 6$ ) in power-law bi-material model.



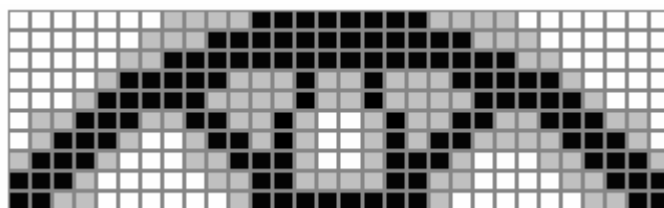
$\mu = 1$



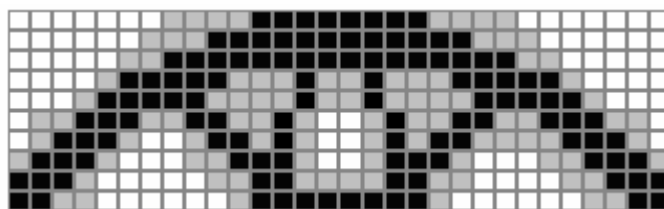
$\mu = 2$



$\mu = 3$



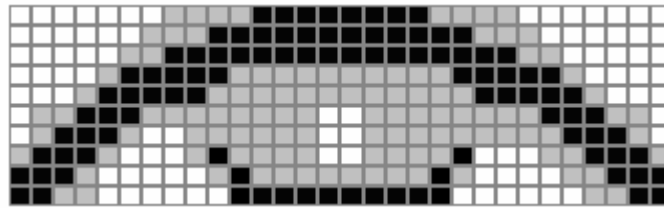
$\mu = 4$



$\mu = 5$

Figure 8.4 Optimization layouts for different power values (*continued*)

(Figure 8.4 continued)



$$\mu = 6$$

Figure 8.4 Optimization layouts for different power values

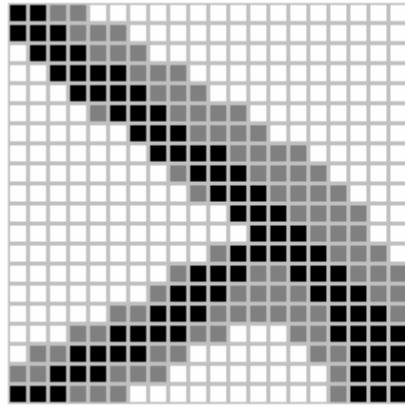
From the optimization layouts of power-law models above, we can see that the power value between 2 and 5 gives a very similar layout pattern. For the power value equals 1 or 6, the solution shows a little difference.

The optimization process of Example 8.1 shows similar result to the case of one-material model. Except for the ranked layered bi-material model, all models provide a similar optimum layout. The layout of ranked layered bi-material model is very different from others. This is because the structure cannot sustain a non-aligned shear stress. This results in more displacements between layers leading to the observed difference in layout pattern.

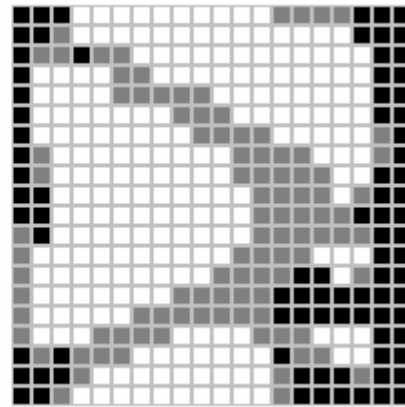
*Example 8.2 A square domain with single load*

Considering the problem of the square domain with a single corner load shown in Figure 7.8, Modulus of hard and soft materials elasticity are  $E_a = 1 \times 10^5$  MPa,  $E_b = 1 \times 10^3$  MPa and the Poisson's ratio  $\nu = 0.3$ . The volume fraction of hard material is  $V_H / V = 20\%$  and the soft material is  $V_S / V = 30\%$ , Void 50%.

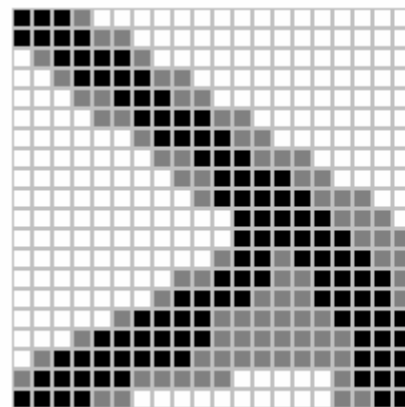
The results of using the six different material models are shown in Figure 8.5.



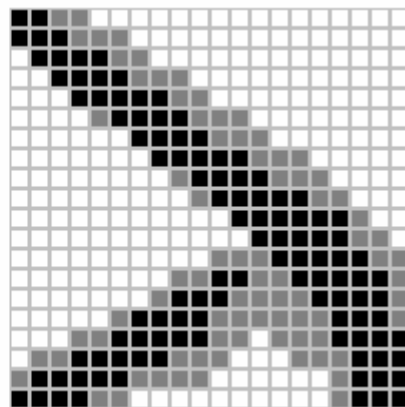
(a) Power-law at  $\mu = 3$



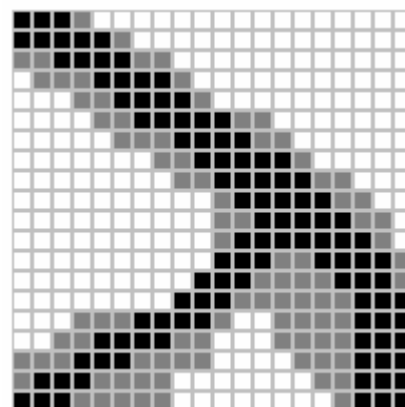
(b) Ranked layered bi-material



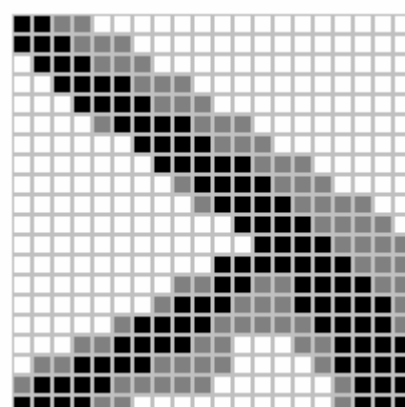
(c) Square bi-material model



(d) Cross shape bi-material model



(e) Double rectangular bi-material model



(f) Triangular bi-material model

Figure 8.5 Optimization layouts of six bi-material models

Table 8.2 shows iteration numbers and final strain energies at convergence tolerance  $\Delta = 0.050$  for the bi-material microstructures using HDM.

Microstructure Model	Iteration Number	Final Strain Energy
Power-law bi-material	245	0.00044
Cross shape bi-material	232	0.00032
Square bi-material	267	0.00037
Rectangular bi-material	287	0.00053
Triangular bi-material	378	0.00066
Ranked layered bi-material	400	0.14

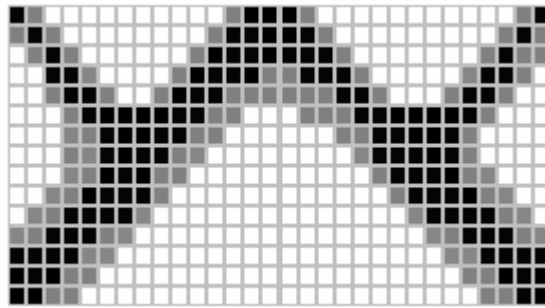
Table 8.2 Iteration numbers and final strain energies at convergence tolerance  $\Delta = 0.050$  for the microstructures using HDM

The layouts of Example 8.2 show similar results with those of Example 8.1, that all the solutions have similar patterns except the ranked layered bi-material model, the layout of which is far more complicated and has much more iteration numbers to reach convergence. It can be seen that again the cross shape model performs the best with lowest strain energy. The power-law and the square bi-material models are also good.

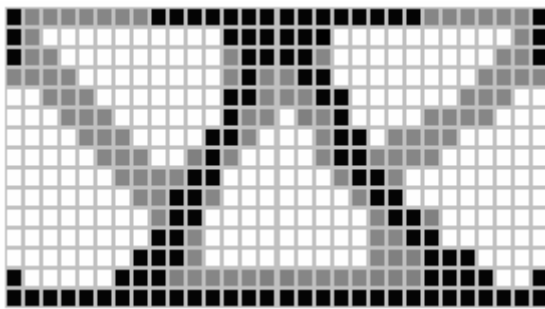
*Example 8.3 Double sides supported beam with both sides fixed under central single load*

Considering the previously studied design domain as shown in Figure 7.14, the modulus of hard and soft materials elasticity are  $E_a = 1 \times 10^5$  MPa,  $E_b = 1 \times 10^3$  MPa and the Poisson's ratio  $\nu = 0.3$ . The volume fraction of hard material is  $V_H / V = 20\%$  and the soft materials is  $V_S / V = 30\%$ , Void 50%.

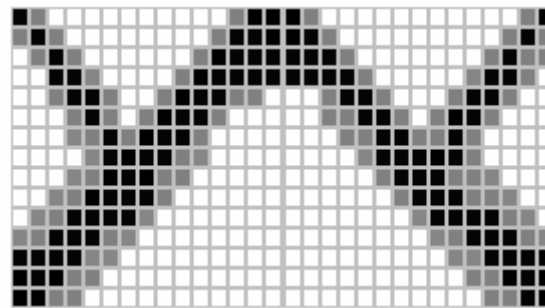
The results of using the six different material models are shown in Figure 8.6.



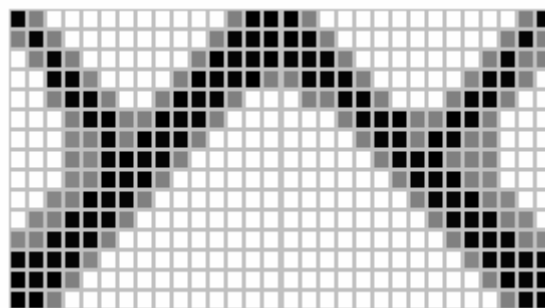
(a) Power-law bi-material model at  $\mu = 3$



(b) Ranked layered bi-material model



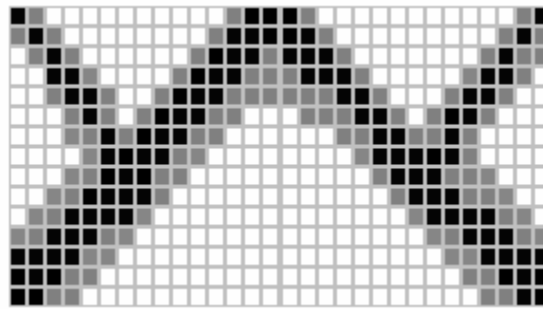
(c) Square bi-material model



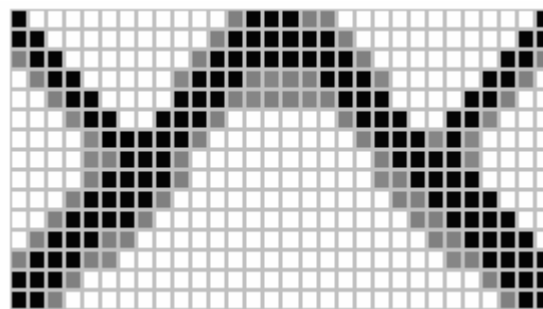
(d) Cross shape bi-material model

Figure 8.6 Result layouts of six bi-material models (*continued*)

(Figure 8.6 continued)



(e) Double rectangular bi-material model



(f) Triangular bi-material model

Figure 8.6 Optimization layouts of six bi-material models

The layouts given by the six bi-material models are very similar. Again, the ranked layered model shows a difference with distribution of material required at the bottom and top edges.

*Example 8.4 A model of a bridge with surface load*

The design domain is a model of a bridge shown in Figure 8.7. The pressure load of intensity  $p = 1\text{kN}$ . The modulus of hard and soft materials elasticity are  $E_a = 1 \times 10^5 \text{ MPa}$ ,  $E_b = 1 \times 10^3 \text{ MPa}$  and the Poisson's ratio  $\nu = 0.3$ . The volume fractions of hard material is  $V_H / V = 20\%$ , soft material is  $V_S / V = 30\%$ , Void 50%.

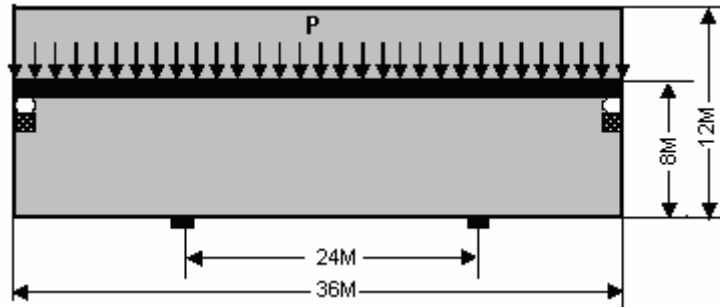
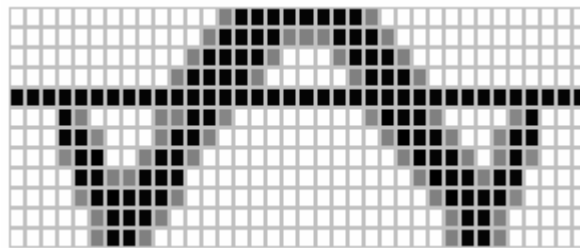
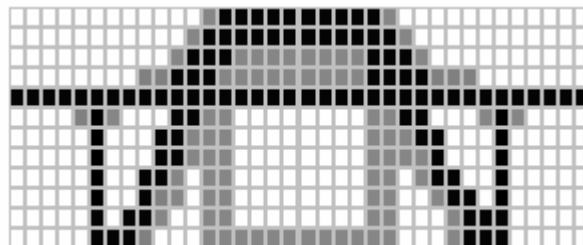


Figure 8.7 Design domain of a bridge model

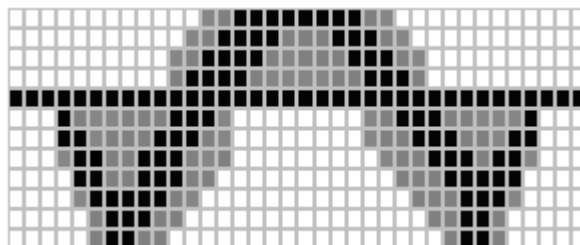
The results of using the six different material models are shown in Figure 8.8.



(a) Power-law bi-material model at  $\mu = 3$



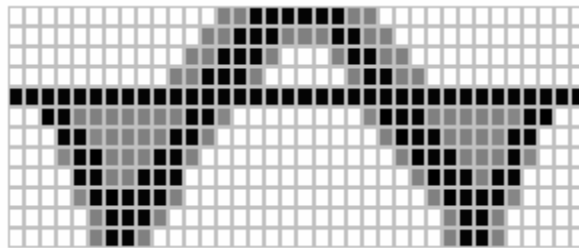
(b) Ranked layered bi-material model



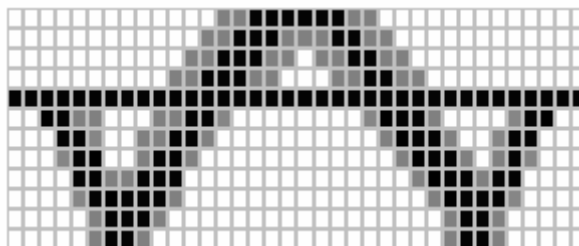
(b) Square bi-material model

Figure 8.8 Optimization layouts of six bi-material models (*continued*)

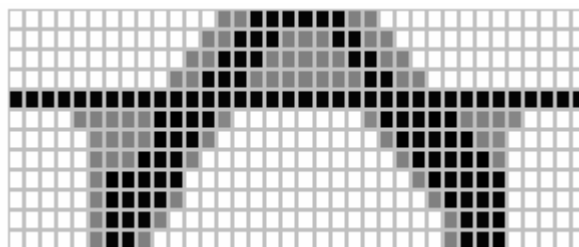
*(Figure 8.8 continued)*



(d) Cross shape bi-material model



(e) Double rectangular bi-material model



(f) Triangular bi-material model

Figure 8.8 Optimization layouts of six bi-material models

The optimization layouts obtained by six bi-material models are similar, again the solution of ranked layered model shows a little difference with material required at bottom edge and extra pillars required.

From the examples discussed above, we can see that for the topology optimization using bi-material model with voids cases, the cross shape

bi-material model performs the best with lowest strain energy and fewer iteration numbers. The optimal structure is also easy for implementation. The power-law bi-material model with  $\mu = 3$  is good compared with other models. The ranked layered bi-material model shows different results with higher strain energies and complicated layout patterns. This is because in this model optimal microstructure is degenerated and has no shear strength between layers. The strain energy calculated is a modified form of energy. All these make the optimal results different with others.

## **8.2 Topology Optimization Using Bi-material Models without Void**

In the following problems, we consider the design domain as consisting of a two material composites and each cell only contains the two materials, not any voids. The aim of the optimization is to find the distribution of hard and soft materials in the given domain.

### *Example 8.5 Short cantilever beam with single load*

The short cantilever beam is shown in Figure 8.9. A point load of intensity  $P = 10\text{kN}$  is applied at the right bottom corner of the beam. The modulus of hard and soft materials elasticity are  $E_a = 1 \times 10^5 \text{ MPa}$  and  $E_b = 1 \times 10^3 \text{ MPa}$ , Poisson's ratio,  $\nu = 0.3$ . The volume fractions of hard material  $V_H / V = 30\%$ , soft materials  $V_S / V = 70\%$ .

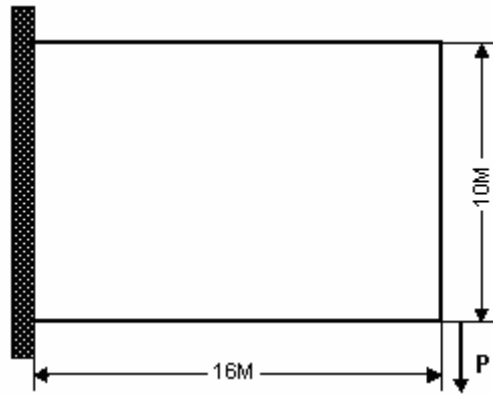
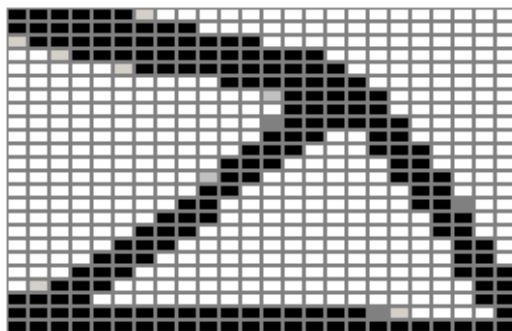
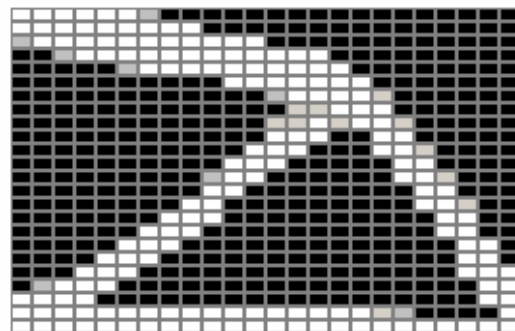


Figure 8.9 A short cantilever beam

The results of using the six different material models are shown in Figure 8.10. In the following graphics, we show the distributions of hard and soft material in separate pictures. The left side is hard material distributions and right side is soft material distributions.

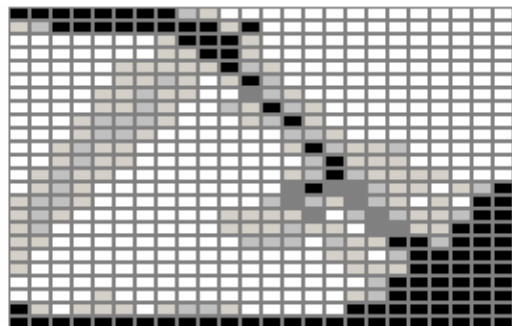


(a1) Hard material distribution

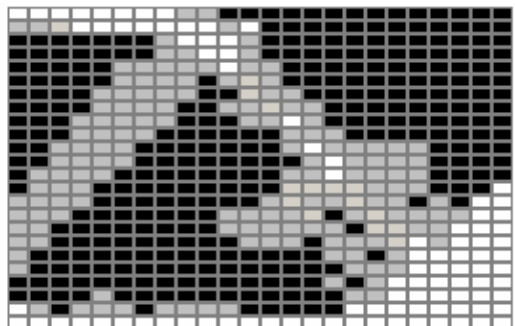


(a2) Soft material distribution

(a) Power-law bi-material model at  $\mu = 3$



(b1) Hard material distribution

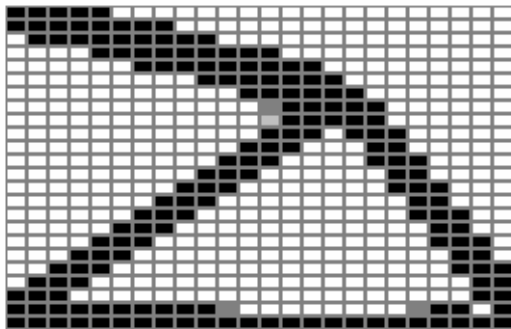


(b2) Soft material distribution

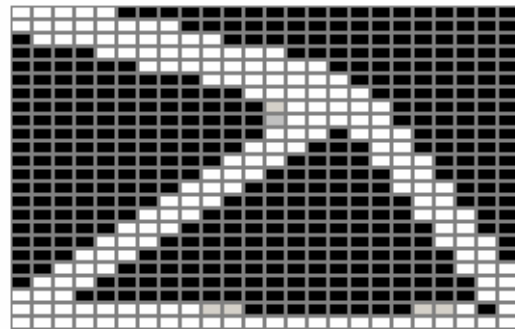
(c) Ranked layered bi-material model

Figure 8.10 Optimization layouts of six bi-material models (*continued*)

(Figure 8.10 continued)

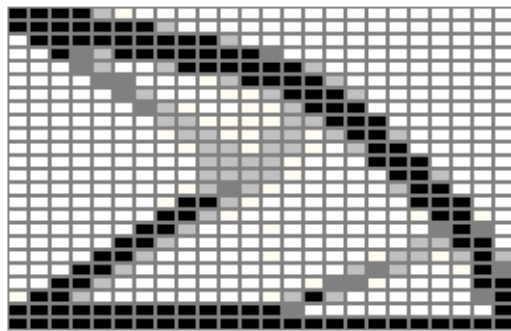


(c1) Hard material distribution

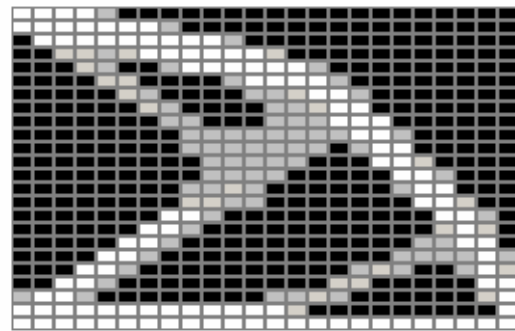


(c2) Soft material distribution

(c) Square bi-material model

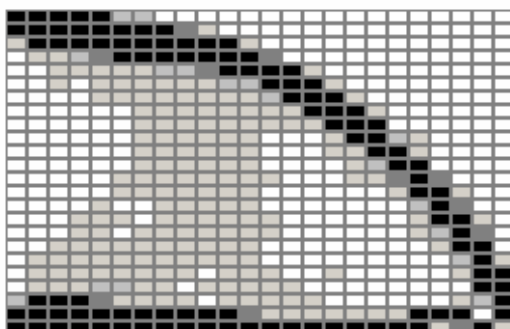


(d1) Hard material distribution

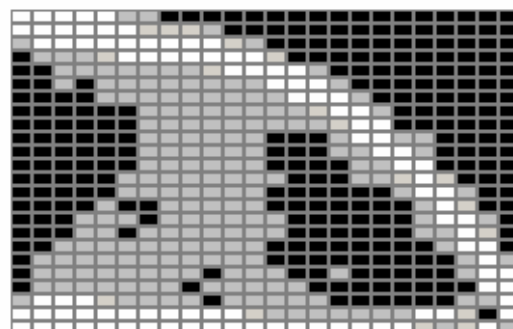


(d2) Soft material distribution

(d) Cross shape bi-material model



(e1) Hard material distribution



(e2) Soft material distribution

(d) Double rectangular bi-material model

Figure 8.10 Optimization layouts of six bi-material models (*continued*)

(Figure 8.10 continued)

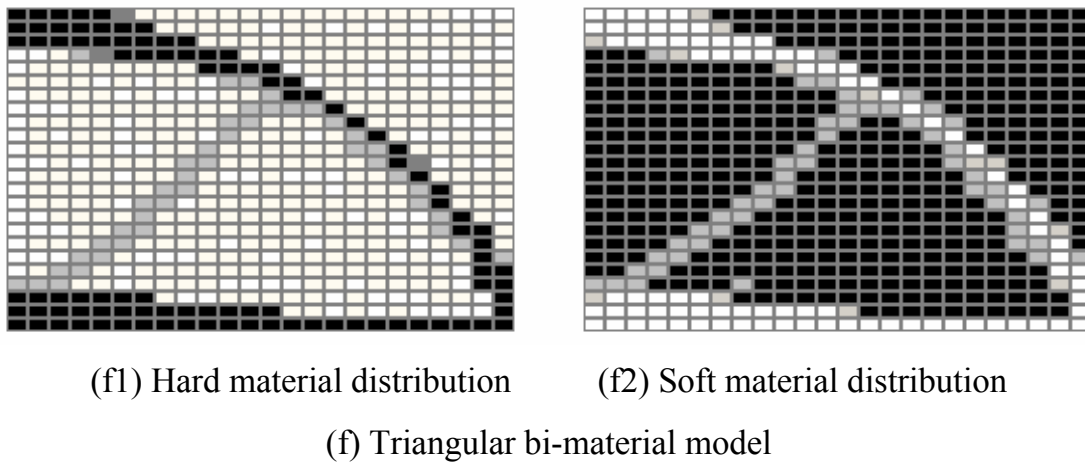


Figure 8.10 Optimization layouts of six bi-material models

The results above show that all the bi-material models yield similar patterns, with the layouts of ranked layered and double rectangular models slightly different. As far as implantation of the solution is considered, the square and the power-law bi-material models yield the best layouts.

*Example 8.6 A simply supported beam with two point loads*

A simply supported beam is shown in Figure 8.11. Two point loads of intensity  $P = 5\text{kN}$  are applied downwards simultaneously at point of  $1/3$  and  $2/3$  of the top side of the beam. The modulus of hard and soft materials elasticity are  $E_a = 1 \times 10^5 \text{ MPa}$  and  $E_b = 1 \times 10^3 \text{ MPa}$ , Poisson's ratio,  $\nu = 0.3$ , The volume fractions of hard material  $V_H / V = 30\%$ , soft materials  $V_S / V = 70\%$ .

The results of using the six different material models are shown in Figure 8.12.

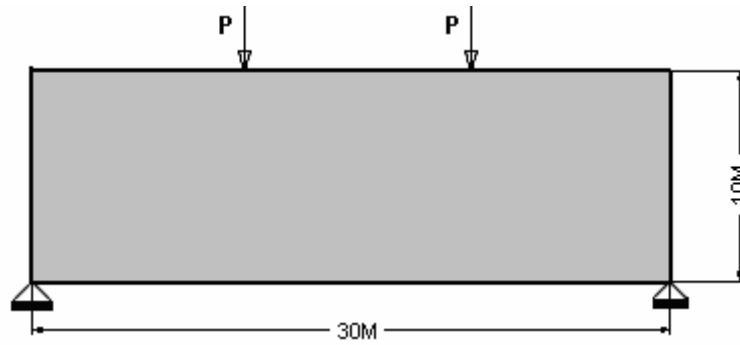
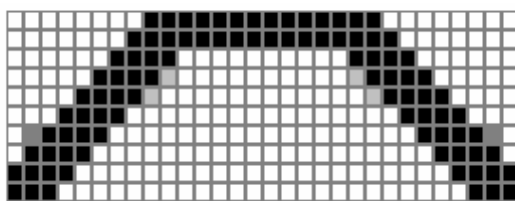
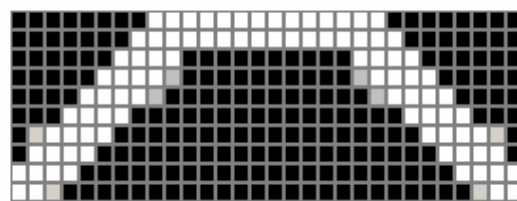


Figure 8.11 A supported beam

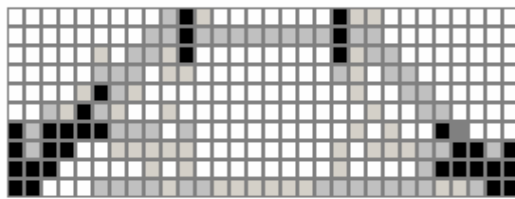


(a1) Hard material distribution

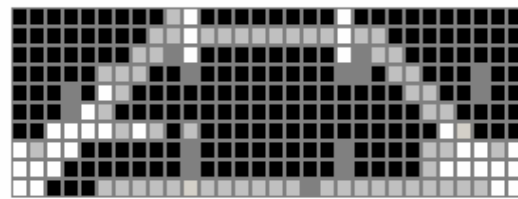


(a2) Soft material distribution

(a) Power-law bi-material model at  $\mu = 3$

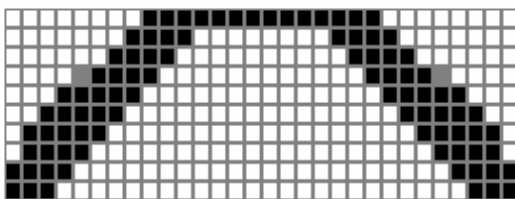


(b1) Hard material distribution

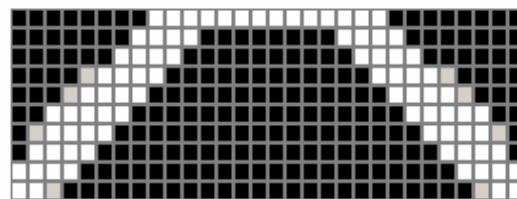


(b2) Soft material distribution

(b) Ranked layered bi-material model



(c1) Hard material distribution

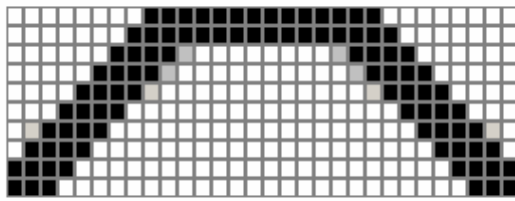


(c2) Soft material distribution

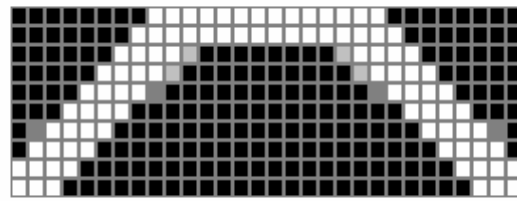
(c) Square bi-material model

Figure 8.12 Optimization layouts of six bi-material models (*continued*)

(Figure 8.12 continued)

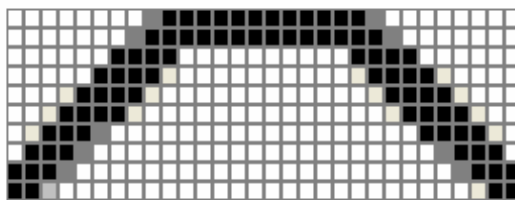


(d1) Hard material distribution

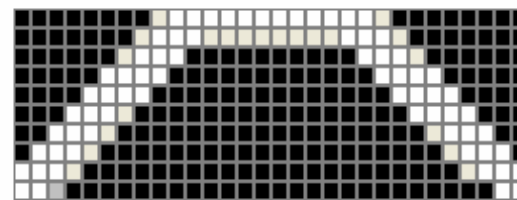


(d2) Soft material distribution

(d) Cross shape bi-material model

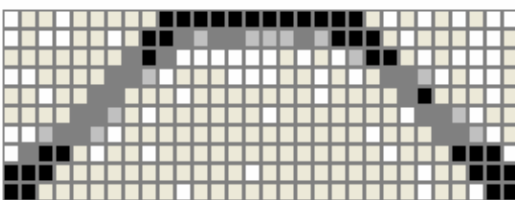


(e1) Hard material distribution

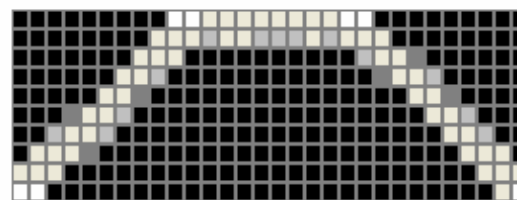


(e2) Soft material distribution

(e) Double rectangular bi-material model



(f1) Hard material distribution



(f2) Soft material distribution

(f) Triangular bi-material model

Figure 8.12 Optimization layouts of six bi-material models

Figure 8.12 shows that all the six material models discussed above can provide similar topology optimization solutions of the design domain. Compared to other models, the layout pattern of the ranked layered bi-material model shows more complex pattern and very much different from others. The layouts given by power-law, square, cross shape and double rectangular bi-material models are the easiest to implement.

Example 8.7 A beam with both ends built in with concentrated loads at top and bottom edges

A beam with both ends built in under concentrated loads is shown in Figure 8.13. Two point loads of intensity  $P = 10\text{kN}$  are applied at the middle point of the bottom side and the top side of the beam in opposite directions as shown. The modulus of hard and soft materials elasticity are  $E_a = 1 \times 10^5 \text{ MPa}$  and  $E_b = 1 \times 10^3 \text{ MPa}$ , Poisson's ratio,  $\nu = 0.3$ , The volume fractions of hard material  $V_H / V = 30\%$ , soft material  $V_S / V = 70\%$ .

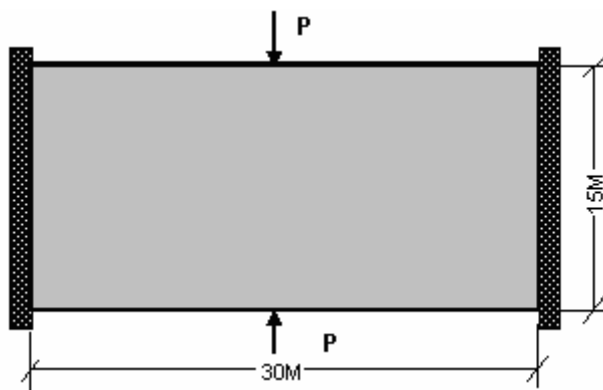
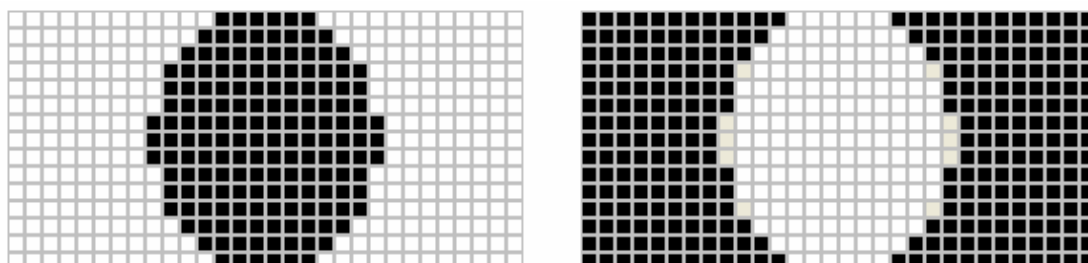


Figure 8.13 A two side's supported beam

The results of using the six different material models are shown in Figure 8.14.



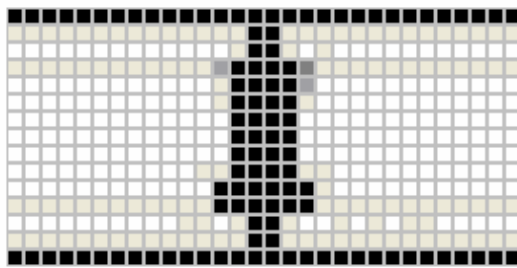
(a1) Hard material distribution

(a2) Soft material distribution

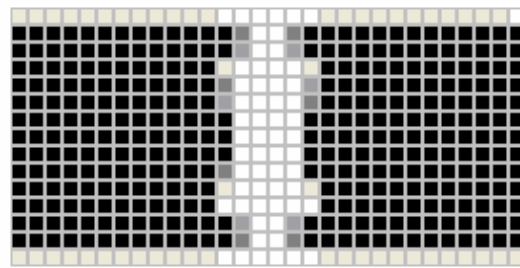
(a) Power-law bi-material model at  $\mu = 3$

Figure 8.14 Optimization layouts of bi-material models (*continued*)

(Figure 8.14 continued)

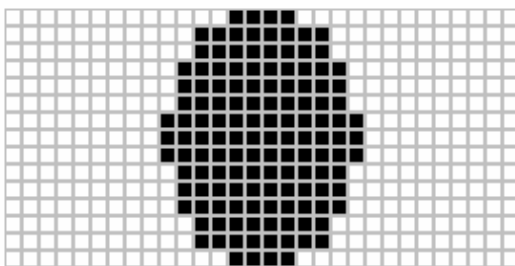


(b1) Hard material distribution

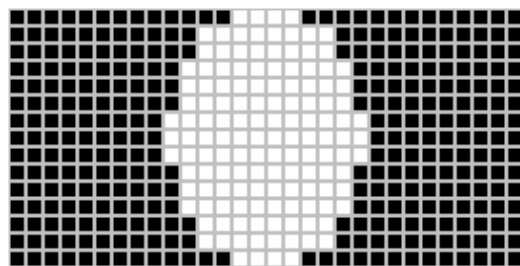


(b2) Soft material distribution

(b) Ranked layered bi-material model

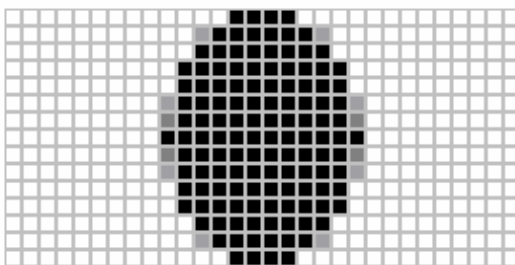


(c1) Hard material distribution

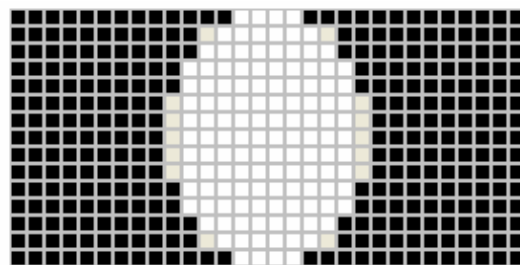


(c2) Soft material distribution

(c) Square bi-material model

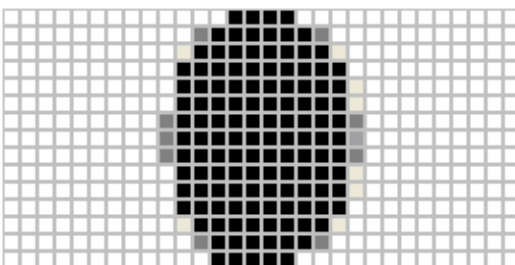


(d1) Hard material distribution

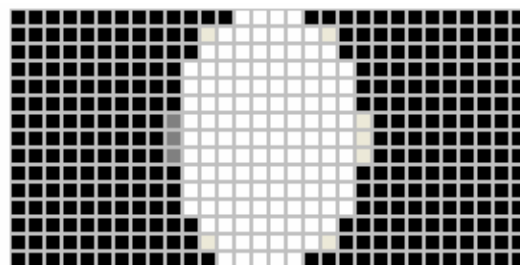


(d2) Soft material distribution

(d) Cross shape bi-material model



(e1) Hard material distribution

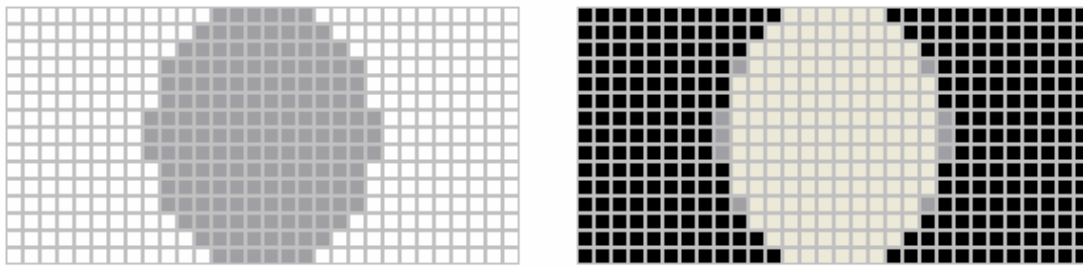


(e2) Soft material distribution

(e) Double rectangular bi-material model

Figure 8.14 Optimization layouts of bi-material models (continued)

(Figure 8.14 continued)



(f1) Hard material distribution

(f2) Soft material distribution

(f) Triangular bi-material model

Figure 8.14 Optimization layouts of six bi-material models

It can be seen that even with a small added resistance to shear, the ranked layered model still yields a pattern very different from other models. Its layout is more complicated. All other models show a very similar layout patterns. While the triangular bi-material model shows a mixtures of material pattern at central area.

*Example 8.8 A model of the frame of a press machine*

A model of a press machine frame is shown in Figure 8.15. Pressure loads of intensity  $P = 100\text{kN}$  are applied as shown. The modulus of hard and soft materials elasticity are  $E_a = 1 \times 10^5 \text{ MPa}$  and  $E_b = 1 \times 10^3 \text{ MPa}$ , Poisson's ratio,  $\nu = 0.3$ , The volume fractions of hard material  $V_H / V = 30\%$ , soft materials  $V_S / V = 70\%$ .

The results of using the six different material models are shown in Figure 8. 16.

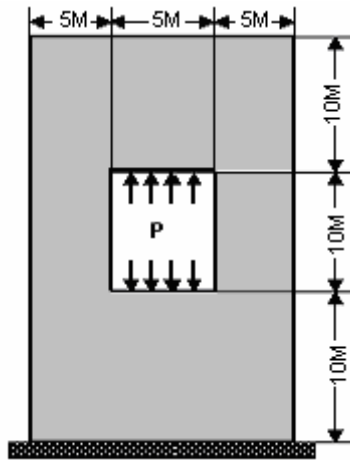
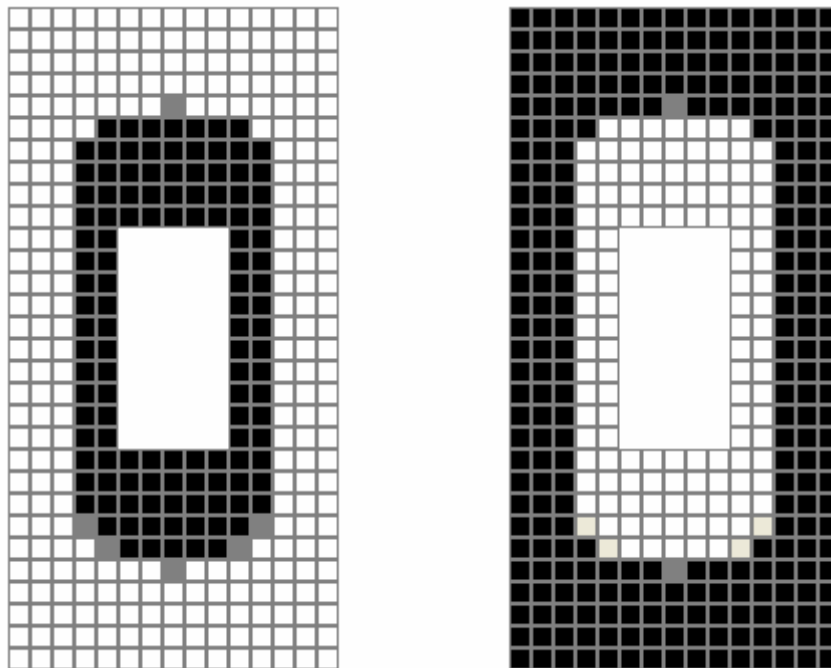


Figure 8.15 Press machine frame model



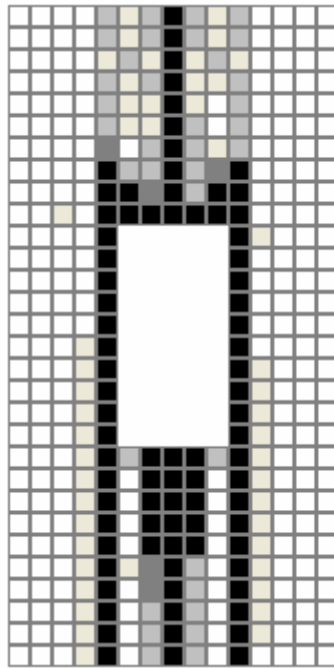
(a1) Hard material distribution

(a2) Soft material distribution

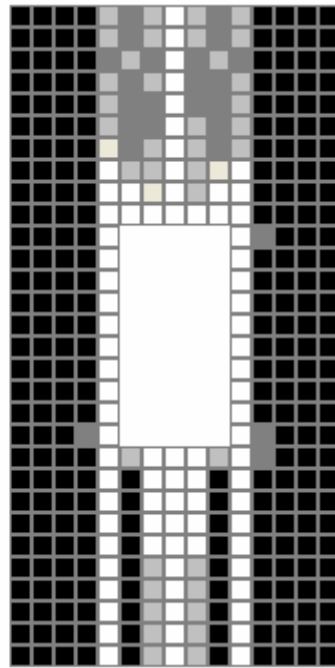
(a) Power-law bi-material model at  $\mu = 3$

Figure 8.16 Optimization layouts of six bi-material models (*continued*)

(Figure 8.16 continued)

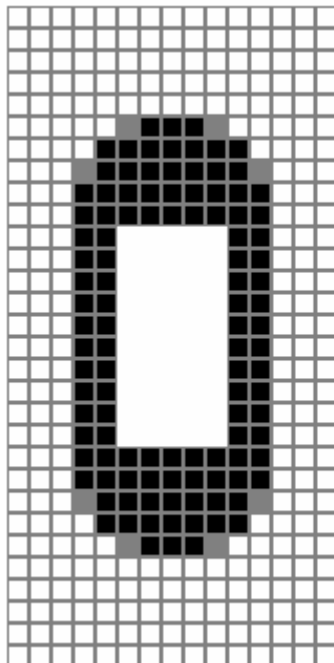


(b1) Hard material distribution

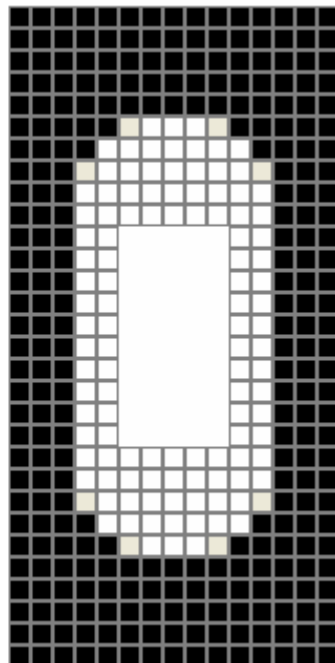


(b2) Soft material distribution

(b) Ranked layered bi-material model



(c1) Hard material distribution

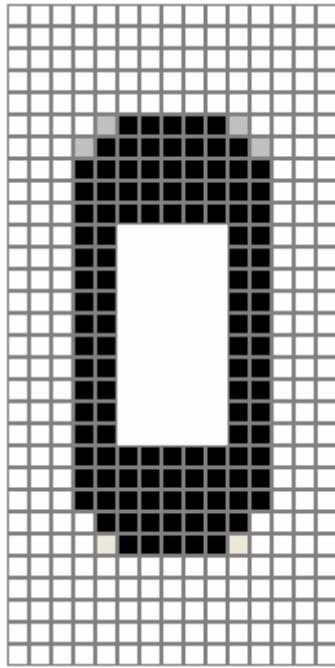


(c2) Soft material distribution

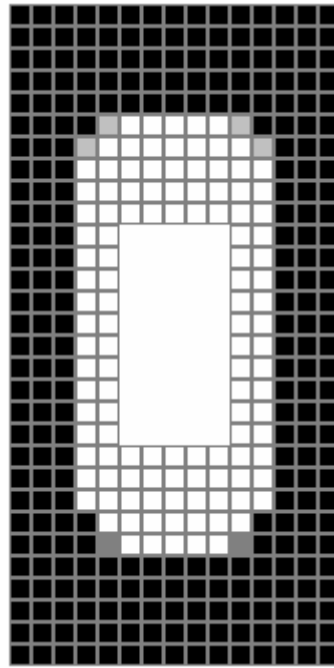
(c) Square bi-material model

Figure 8.16 Optimization layouts of six bi-material models (continued)

(Figure 8.16 continued)

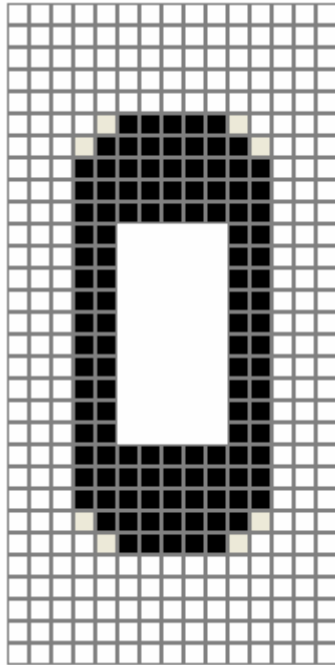


(d1) Hard material distribution

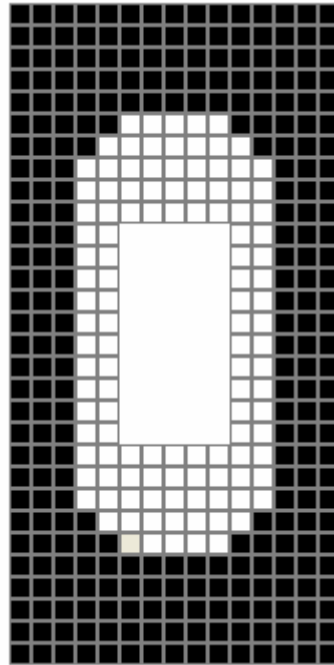


(d2) Soft material distribution

(d) Cross shape bi-material model



(e1) Hard material distribution

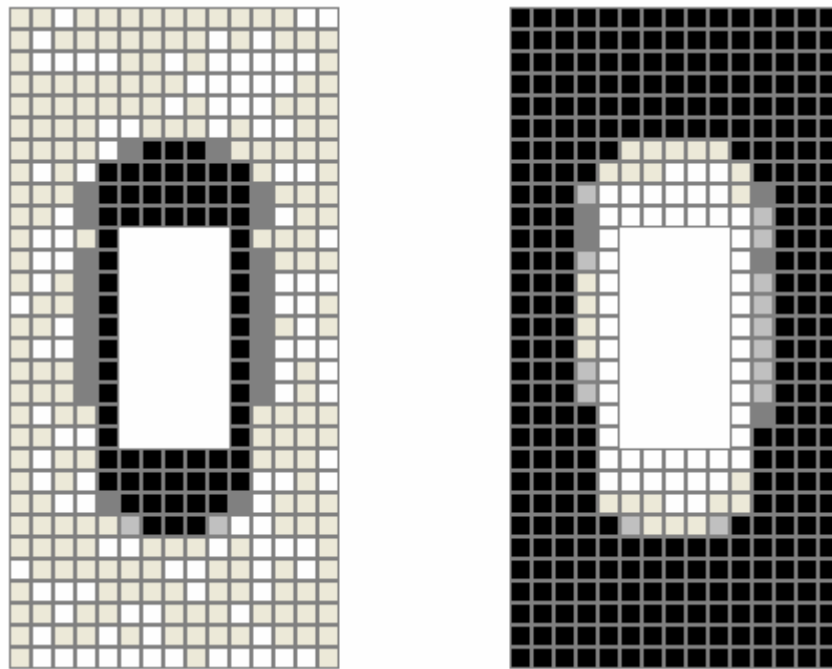


(e2) soft material distribution

(e) Double rectangular bi-material model

Figure 8.16 Optimization layouts of six bi-material models (continued)

(Figure 8.16 continued)



(f1) Hard material distribution      (f2) Soft material distribution  
 (f) Triangular bi-material model

Figure 8.16 Optimization layouts of six bi-material models

Similarly as in previous examples, apart from ranked layered model, all the other models provide similar optimum layouts.

From the discussion for the problems of topology optimization using bi-material models without void cases, we can see that all the bi-material models can supply a similar layout pattern except ranked layered model. The reason is the same as the case of bi-material models with voids, because in the rank-2 layered material model, any optimal microstructure is degenerated and the structure cannot sustain a non-aligned shear stress. This will result in the stiffness matrix of the structure becoming singular. To overcome the singularity problem, we use a very soft material instead of the voids. However, the

minimum strain energy calculated during optimization process (commonly used for objective function which is equivalent with maximum total potential energy) is modified energy and the displacements between layers are larger than other models. All these lead to the result of ranked layered bi-material model showing much difference with others.

### **8.3 Effects of Different Models on Topology Optimization**

Based on the results from different optimization problems considered in this chapter, the following effects have been observed.

- ***Effects of the different material models on optimization layout***

The results of using the six bi-material models show that all the bi-material models give similar layout patterns. The layout pattern of the ranked layered microstructure model is very much different from the rest. This is because the ranked layered microstructure model does not bear shear stress between the layers. With regard to speed of convergence and the ease of implementation, the cross shape and the power-law bi-material models perform best

- ***Effects of power values for power-law bi-material models***

The calculation results show that different power values affect slightly the optimization result layout for the power-law bi-material model by choosing

the value between 2 and 5 as shown in Figure 8.4. All optimal layouts have patterns that are easy to implement.

- ***Effects of different bi-material models on iteration history***

As shown in Figure 8.3, Table 8.1 and Table 8.2 that power-law, cross shape models take less iteration to get convergence than other models. Among these six bi-material models, ranked layered bi-material model has much high strain energy at convergence.

## **8.4 Conclusions**

In this chapter, a series of benchmark problems are presented to investigate of the performance of the different bi-material microstructure models. The results show that the six bi-material microstructure models presented in Chapter 5 can be used in the topology optimization problems. It can be said that all the six bi-material microstructure models are effective for a range of structural topology optimization problems.

Similarly to previous finding for one-material models in Chapter 7, the ranked layered microstructure model gives a layout that is very different from others. This is because the ranked layered microstructure model does not account for the shear stress between the layers. All the other models give similar topology optimization layouts. The difference between these optimum layouts is due to

different geometry shapes of microstructures which will give rise to different relative distribution parameters and angles of orientation in the microstructures leading to different searching directions for the optimum. Among the six bi-material microstructures, the cross shape, power-law bi-material microstructures perform the best in terms of convergence and ease of practical implementation of the optimum layout.

## **Chapter 9**

---

### **CONCLUSIONS AND RECOMMENDATIONS**

The objective of this research was to investigate the use of homogenization method for topology structural optimization problem with an emphasis on the study of different microstructures and their effects on the topology optimization results. The following objectives have been achieved:

- The properties of different microstructure models were investigated (Chapter 3).
- The strengths and weaknesses of each type of microstructures were discussed (Chapter 3).
- New microstructure models were established and new methods to define microstructures were proposed permitting using shape optimization method to find optimum microstructures (Chapter 4).
- Optimality criteria and schemes of updating design variables were formulated for these new microstructures and for existing microstructures, the information of which is not available in the literature (Chapter 5).

- A general computer software package, which incorporates fifteen existing and newly developed microstructure models for two-dimensional structural topology optimization, is developed (Chapter 5).
- Some benchmark structural topological optimization problems and a series of problems with different loading cases were solved (Chapters 6~8).
- Results from different microstructure models were compared (Chapters 6~8).
- The program for controlling checkerboard problem was developed (in Chapter 5).

Based on the research above, we can draw the following conclusions and further developments required in the area:

## **9.1 Conclusions**

### ***9.1.1 Comparison of microstructure models***

#### ***9.1.1.a Existing microstructure models***

##### *Power-law (SIMP) model*

The advantages of SIMP or Power-law models are: these types of models do not require homogenization of the microstructure. Therefore, the algorithm does not require higher mathematics for derivations and are easy to be understood. Due to the penalty power used, the optimization solutions are

clearer than other microstructures. These make the optimal solution easy to be implemented in practice. The disadvantage of SIMP (Power-law) is the solution depends on the value of penalization.

Our research shows that the power-law models give the clearest solution images among all the microstructures used and the resulting optimization layouts are the easiest to implement. But for some problems different power values may give different solutions. Therefore, choosing suitable power values is very important in using power-law model. According to our studies, we suggest choosing the power value  $\mu = 3$  for one-material microstructure and between 2 and 5 for bi-material microstructure model (Chapters 6~8).

#### *Ranked layered model*

The advantage in using ranked layered microstructure model is that the effective material properties of the microstructures can be derived by analytical method which shows that they achieve optimality in the well-known Hashin-Shtrikman bounds on the effective properties of composite materials. Therefore, ranked layered microstructures are also called optimal microstructures in this sense. The disadvantage is that the rank layered material cells provide no resistance to shear stress between the layers. This will result in the stiffness matrix of the structure becoming singular. One-way of “avoiding” the singularity problem is to use a very soft material instead of the voids. On the other hand, the combination of a very soft material with a solid material will cause numerical problems due to ill conditioning of the global stiffness matrix.

Our calculation results show that the results from the ranked layered model are much different from the solutions of other microstructure models. Their optimal layout are complicated and would be difficult to implement in practice, especially when shear stress is high throughout most of the structure as in the case of simply supported beam or cantilever beam under concentrated loads. (Chapter 3, Chapters 6~8).

### *Triangular and Hexagon microstructure models*

The advantage of the triangular and hexagon microstructure models is that they give real calculated energy. The disadvantages of triangular microstructures are: comparing to rectangular microstructure model, these two models have more complicated shapes and this will increase computation time and cost, the homogenization equation has to be solved by numerical techniques. A series of topology optimization results obtained in this research show that the triangular and hexagon microstructure models give similar optimization solutions to those of the rectangular model (Chapters 6~7).

#### **9.1.1.b New microstructure models**

##### *SIB microstructure models*

In the thesis, we proposed a new method to define microstructures. Two types: circular and cross shape microstructures, were developed. The results show that

the optimization solutions of these two microstructure models are similar to those using rectangular microstructure (Section 4.1.1, Chapters 6~7).

#### *Multi-void microstructure model*

Three types of multi-void microstructures were presented and compared: rectangular multi-void model, triangular multi-void model and square multi-void model. The difference between the single void microstructures and multi-void microstructures is that for the same volume of solid material, the multi-void microstructures have more internal boundary. This will result in different stiffness in unit cell. But the calculation results show that the optimization solutions by using multi-void microstructures are similar to those given by single void microstructures (Section 4.1.2, Chapters 6~7).

#### *Bi-material models*

Four new bi-material models were developed and programmed: cross shape bi-material model, square bi-material model, double rectangular bi-material model and triangular bi-material models. All these new bi-material models give similar patterns of optimum layouts (Section 4.1.3, Chapter 6, Chapter 8).

### ***9.1.2 Optimization results given by HDM***

Firstly, by testing with benchmark problems and compared with other software package, it can concluded that the optimization results by HDM for different microstructure models largely converge to solutions of similar final strain

energy value. This demonstrates the effectiveness of the algorithms and computer program in finding the optimum solution (Chapters 6~7).

Secondly, for two-dimensional continuum structures investigated in this thesis, the computer program incorporating different microstructure models is effective in solving stiffness optimization problems. For one-material model, the loading cases considered include single loading, surface loading, multiple loading and gravity loading. For bi-material optimization problems, we consider the material without void and with void under concentrated loading and surface loading cases. It can be said that all the fourteen microstructure models are effective for a range of structural topology optimization problems.

### ***9.1.3 Optimal layout criteria***

From the study in Chapter 6, Chapter 7 and Chapter 8 we can see that all the results from different microstructures give similar layouts, but not exactly the same. The reason is that the different geometry shape for different microstructures will provide different relative distribution parameters and angle of orientation in the microstructure and these will lead to different searching directions for optimum. The criterion for finding the optimal layout is very important. In the thesis we use the final value of strain energy of the layout for minimum compliance problems. The solution with the minimum strain energy is regarded as optimal structure. From the point of view of computation, speed of convergence would also be a factor. It was shown that HDM using fifteen

microstructures converges in all cases. Another criterion is the ease of manufacturing, the optimum layout that requires simple, clear, sharp contrast solutions would be more desirable. Among these microstructures, the cross shape and power-law with  $\mu = 3$ , for both one-material and bi-material models, perform the best in terms of convergence and ease of implementation of the optimum layouts. The ranked layered model gives more complicated layouts in most cases.

#### ***9.1.4 Checkerboard control***

By using a modified average  $\varphi'$  instead of the original  $\varphi$  for problems with one design variable in a microstructure, or up to  $\varphi', \psi', \omega', \phi'$  instead of  $\varphi, \psi, \omega, \phi$  for problems of up to four design variables in a microstructure, as described in section 5.1, the checker board patterns in the optimization process are efficiently eliminated (Section 5.4).

## **9.2 Recommendations for further investigations**

Further research needs to be carried out in the following areas to study microstructures of homogenization for topology optimization:

### ***A. Optimal microstructures study***

- The newly developed microstructures did not consider the optimal bounds of the optimization problems such as Hashin-Shtrikman and

further studies need to be carried out for optimal bounds of the optimization problem in using the microstructure models proposed here.

- The new definition of microstructures proposed here points to the use of shape optimization method to find optimum microstructures, avoiding the use of the more complicated topology optimization method. More case studies need to be investigated to develop simple shape but optimum microstructures.

### ***B. Investigation of other optimization problems***

Although extensive work has been conducted by using the newly developed microstructures for a range of optimization problems, much more work is still needed to look into topics; such as mesh dependency problems, natural frequency problems, structures with multiple constraints, plate and shell structures. Further research should also be extended to three-dimensional microstructures design.

## APPENDIX A

---

### *The homogenization formulas in elastic composite materials with a periodic structure*

Let us consider non-homogeneous, elastic solid, which occupies a domain  $\Omega$  in the space  $\mathbf{R}^3$  with a smooth boundary  $\Gamma$  comprising  $\Gamma_d$  (where displacements are prescribed) and  $\Gamma_t$  (the traction boundary), body force  $\mathbf{f}$  and traction  $\mathbf{t}$  applied (Figure A1).

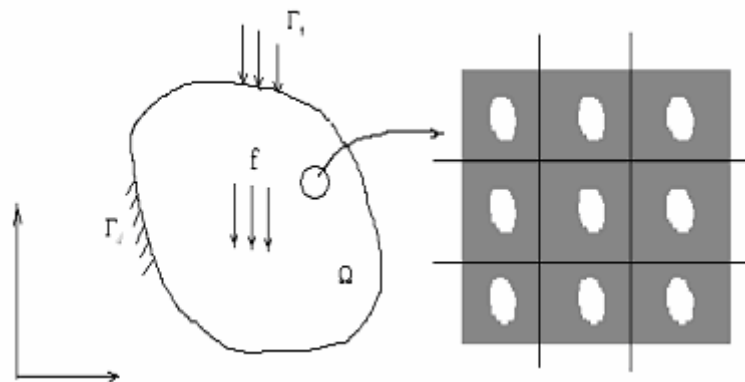


Figure A1 A structure with cellular microstructure

Let  $\mathbf{u}$  to be the displacement field that defines equilibrium of elastic structure and  $\mathbf{v}$  to be the kinematically admissible virtual displacement field.

Let  $a(\mathbf{u}, \mathbf{v})$  be the energy bilinear form

$$a(\mathbf{u}, \mathbf{v}) = \int_{\Omega} E_{ijkl}(\mathbf{x}) \varepsilon_{ij}(\mathbf{u}) \varepsilon_{kl}(\mathbf{v}) d\Omega \quad (\text{A1})$$

with strain-displacement relations

$$\varepsilon_{ij}(\mathbf{u}) = \frac{1}{2} \left( \frac{\partial u_i}{\partial x_j} + \frac{\partial u_j}{\partial x_i} \right) \quad (\text{A2})$$

and the load bilinear form for external work

$$L(\mathbf{v}) = \int_{\Omega} \mathbf{f} \cdot \mathbf{v} d\Omega + \int_{\Gamma_T} \mathbf{t} \cdot \mathbf{v} ds \quad (\text{A3})$$

The linear problem of elasticity for such a body can be formulated in the following way:

- equilibrium equations  $\frac{\partial \sigma_{ij}}{\partial x_j} + f_i = 0$  in  $\Omega$  (A4)

- loading conditions  $\sigma_{ij} n_j = t_i$  on  $\Gamma_t$ ,  $u_i = 0$  on  $\Gamma_d$  (A5)

- linear elasticity relationship  $\sigma_{ij} = E_{ijkl} \varepsilon_{kl}$  (A6)

The coefficients of elasticity  $\{ E_{ijkl} \}$  of a non-homogeneous body are functions of the spatial coordinates  $\mathbf{x} = (\mathbf{x}_1, \mathbf{x}_2, \mathbf{x}_3)$ , and are assumed to satisfy the following conditions (Kalamkarov and Kolpakov 1997, Bendsøe 1995):

$$\mathbf{C1.} \quad E_{ijkl} = E_{jikl} = E_{ijlk} = E_{klij}, \quad (\text{A7})$$

$$\mathbf{C2} \quad E_{ijkl}(\mathbf{x}) \in E_{ad}(\Omega) \text{ and } \|E_{ijkl}\|_{E_{ad}(\Omega)} \leq M, \quad (\text{A8})$$

$$\mathbf{C3.} \quad E_{ijkl}(\mathbf{x}) \varepsilon_{ij} \varepsilon_{kl} \geq m \varepsilon_{ij} \varepsilon_{kl} \quad (\text{A9})$$

Where the constants  $0 < m$  and  $M < \infty$  do not depend on  $\mathbf{x}$ ,  $E_{ad}(\Omega)$  is admissible elasticity tensors which is allowed to vary over the domain of the body.  $\|E_{ijkl}\|$  is norm of coefficient of elasticity  $\{ E_{ijkl} \}$ .

Let us further consider the case when a non-homogeneous elastic material has a periodic structure in the coordinates  $x_1, x_2, x_3$ , . The rectangular base cell of the cellular body  $Y$  is illustrated in Figure A2. The boundary of the hole  $H$  is

defined by  $S$  ( $\partial H = S$ ) and is assumed to be smooth and the tractions  $\mathbf{p}$  may exist inside the holes.

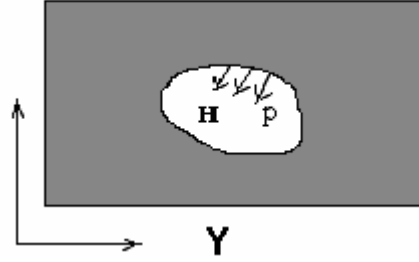


Figure A2 Base cell

The virtual displacement equation can be constructed as:

$$\int_{\Omega^e} E_{ijkl} \frac{\partial u_k^e}{\partial x_l} \frac{\partial v_i}{\partial x_j} d\Omega = \int_{\Omega^e} f_i^e v_i d\Omega + \int_{\Gamma_t} t_i v_i d\Gamma + \int_{S^e} p_i^e v_i dS \quad \forall \mathbf{v} \in \mathbf{V}^e, \mathbf{u}^e \in \mathbf{V}^e \quad (\text{A10})$$

where  $e$  as a superscript indicates dependency to the cell of periodicity and  $\mathbf{V}^e$  is a space of admissible displacements.  $t_i$  and  $p_i$  are components of traction  $\mathbf{t}$  and pressure  $\mathbf{p}$ .

Introducing the following properties:

If  $\Psi = \Psi(\mathbf{x}, \mathbf{y})$  and  $\mathbf{y}$  depends at least on  $\mathbf{x}$ , then

$$\frac{d\Psi}{d\mathbf{x}} = \frac{\partial\Psi}{\partial\mathbf{x}} + \frac{\partial\Psi}{\partial\mathbf{y}} \frac{\partial\mathbf{y}}{\partial\mathbf{x}} \quad (\text{A11})$$

In this case, as  $\mathbf{y} = \mathbf{x}/\zeta$  so

$$\frac{d\Psi}{d\mathbf{x}} = \frac{\partial\Psi}{\partial\mathbf{x}} + \frac{1}{\zeta} \frac{\partial\Psi}{\partial\mathbf{y}} \quad (\text{A12})$$

By using the above properties and Einstein summation convention, we can explore (A10) as

$$\int_{\Omega^e} E_{ijkl} \left\{ \frac{1}{\zeta^2} \frac{\partial u_k^0}{\partial y_l} \frac{\partial v_i}{\partial y_j} + \frac{1}{\zeta} \left[ \left( \frac{\partial u_k^0}{\partial x_l} + \frac{\partial u_k^1}{\partial y_l} \right) \frac{\partial v_i}{\partial y_j} + \frac{\partial u_k^0}{\partial y_l} \frac{\partial v_i}{\partial x_j} \right] \right\} +$$

$$\left[ \left( \frac{\partial u_k^0}{\partial x_l} + \frac{\partial u_k^1}{\partial y_l} \right) \frac{\partial v_i}{\partial x_j} + \left( \frac{\partial u_k^1}{\partial x_l} + \frac{\partial u_k^2}{\partial y_l} \right) \frac{\partial v_i}{\partial y_j} \right] + \zeta(\dots) \Bigg\} d\Omega \quad (\text{A13})$$

$$= \int_{\Omega^\zeta} f_i^\zeta v_i d\Omega + \int_{\Gamma_l} t_i v_i d\Gamma + \int_{S^\zeta} p_i^\zeta v_i ds \quad \forall \mathbf{v} \in \mathbf{V}_{\Omega \times \Psi}$$

where  $u^0, u^1$  and  $u^2$  are terms in the asymptotic expansion of  $\mathbf{u}$  in (3.3)

$$\mathbf{V}_{\Omega \times \Psi} = \{ \mathbf{v}(\mathbf{x}, \mathbf{y}); (\mathbf{x}, \mathbf{y}) \in \Omega \times \Psi \mid \mathbf{v}(\cdot, \mathbf{y}) \} \text{ Y-periodic};$$

$$\mathbf{V}_\Omega = \{ \mathbf{v}(\mathbf{x}) \text{ defined in } \Omega \mid \mathbf{v} \text{ smooth enough and } \mathbf{v}|_{\Gamma_d} = 0 \}$$

$$\mathbf{v}_\Psi = \{ \mathbf{v}(\mathbf{y}) \text{ defined in } \Psi \mid \mathbf{v}(\mathbf{y}) \}, \text{ Y-periodic and smooth enough}$$

$\Psi$  indicates solid part of the cell;

$$\mathbf{v} \text{ smooth enough and } \mathbf{v}|_{\Gamma_d} = 0$$

For a Y-periodic function  $\Phi(y)$ , when  $\zeta \rightarrow 0$ , the  $\Phi(\frac{\mathbf{x}}{\zeta})$  slowly changes with  $\mathbf{x}$

and  $\Phi(\frac{\mathbf{x}}{\zeta}) \rightarrow \Phi(\mathbf{y})$  in any case.  $\Phi(\frac{\mathbf{x}}{\zeta})$  can be defined by microscopic averaging

domain cell Y. The following functions are exist (Manevith, Andrianov and Oshmyan, 2002).

$$\Phi(\frac{\mathbf{x}}{\zeta}) = \frac{1}{|Y|} \int_{\Psi} \Phi(\mathbf{y}) dY \quad (\text{A14})$$

$$\Phi(\frac{\mathbf{x}}{\zeta}) = \frac{1}{\zeta|Y|} \int_S \Phi(\mathbf{y}) dS \quad \text{on } \mathbf{S} \quad (\text{A15})$$

where  $|Y|$  is volume of Y,  $\Psi$  is solid part of domain cell Y and  $\mathbf{S}$  denotes boundary of the hole in domain cell Y.

Therefore we have

$$\int_{\Omega^\zeta} \Phi(\frac{\mathbf{x}}{\zeta}) d\Omega = \frac{1}{|Y|} \int_{\Omega} \int_{\Psi} \Phi(\mathbf{y}) dY d\Omega, \quad (\text{A16})$$

$$\int_{dS} \Phi\left(\frac{\mathbf{x}}{\zeta}\right) d\Omega = \frac{1}{\zeta|Y|} \int_{\Omega} \int_S \Phi(\mathbf{y}) dS d\Omega, \quad (\text{A17})$$

By equating the terms with the same power of  $\zeta$  in equation (A13), we have

$$\frac{1}{|Y|} \int_{\Omega} \int_{\Psi} E_{ijkl} \frac{\partial u_k^0}{\partial y_l} \frac{\partial v_i}{\partial y_j} dY d\Omega = 0 \quad \forall \mathbf{v} \in \mathbf{V}_{\Omega \times \Psi} \quad (\text{A18})$$

$$\int_{\Omega} \left\{ \frac{1}{|Y|} \int_{\Psi} E_{ijkl} \left[ \left( \frac{\partial u_k^0}{\partial x_l} + \frac{\partial u_k^1}{\partial y_l} \right) \frac{\partial v_i}{\partial y_j} + \frac{\partial u_k^0}{\partial y_l} \frac{\partial v_i}{\partial x_j} \right] dY \right\} d\Omega = \int_{\Omega} \left( \frac{1}{|Y|} \int_S p_i v_i ds \right) d\Omega$$

$$\forall \mathbf{v} \in \mathbf{V}_{\Omega \times \Psi} \quad (\text{A19})$$

$$\int_{\Omega} \left\{ \frac{1}{|Y|} \int_{\Psi} E_{ijkl} \left[ \left( \frac{\partial u_k^0}{\partial x_l} + \frac{\partial u_k^1}{\partial y_l} \right) \frac{\partial v_i}{\partial x_j} + \left( \frac{\partial u_k^1}{\partial x_l} + \frac{\partial u_k^2}{\partial y_l} \right) \frac{\partial v_i}{\partial y_j} \right] dY \right\} d\Omega$$

$$= \int_{\Omega} \left( \frac{1}{|Y|} \int_{\Psi} f_i v_i dY \right) d\Omega + \int_{\Gamma_i} t_i v_i d\Gamma \quad \forall \mathbf{v} \in \mathbf{V}_{\Omega \times \Psi} \quad (\text{A20})$$

Now, if we choose  $\mathbf{v} = \mathbf{v}(\mathbf{x})$  from (A19), we can get

$$\int_{\Omega} \left( \frac{1}{|Y|} \int_S p_i dS \right) v_i(\mathbf{x}) d\Omega = 0 \quad (\text{A21})$$

$$\int_S p_i(\mathbf{x}, \mathbf{y}) dS = 0 \quad (\text{A22})$$

*This implies that the applied tractions on the boundary of the hole are self-equilibrating.*

Let us choose  $\mathbf{v} = \mathbf{v}(\mathbf{y})$ . By integrating by parts and applying the divergence theorem to the integral in  $\Psi$ , and using periodicity from (A18) we can get:

$$\frac{1}{|Y|} \int_{\Omega} \left\{ \int_S E_{ijkl} \frac{\partial u_k^0}{\partial y_l} n_j v_i dS - \int_{\Psi} \left[ \frac{\partial}{\partial y_j} \left( E_{ijkl} \frac{\partial u_k^0}{\partial y_l} \right) \right] v_i dY \right\} d\Omega = 0 \quad \forall \mathbf{v} \in \mathbf{V}_{\Omega}. \quad (\text{A23})$$

Therefore, we have

$$\frac{\partial}{\partial y_j} \left( E_{ijkl} \frac{\partial u_k^0}{\partial y_l} \right) = 0 \quad \forall \mathbf{y} \in \Psi \quad (\text{A24})$$

$$E_{ijkl} \frac{\partial u_k^0}{\partial y_l} n_j = 0 \quad \text{on } S. \quad (\text{A25})$$

It can be concluded that

$$u^0(\mathbf{x}, \mathbf{y}) = u^0(\mathbf{x}) \quad (\text{A26})$$

*This implies that the first term of the asymptotic expansion only depends on the macroscopic scale  $\mathbf{x}$ .*

Now, introducing (A26) into (A19), we can get

$$\int_{\Psi} E_{ijkl} \left( \frac{\partial u_k^0}{\partial x_l} + \frac{\partial u_k^1}{\partial y_l} \right) \frac{\partial v_i(\mathbf{y})}{\partial y_j} dY = \int_s p_i v_i dS \quad \forall \mathbf{v} \in \mathbf{V}_{\Psi} \quad (\text{A27})$$

Upon integrating by parts, using the divergence theorem and applying the periodicity conditions on the opposite faces of  $Y$ , (A27) becomes

$$\begin{aligned} \int_s E_{ijkl} \left( \frac{\partial u_k^0(x)}{\partial x_l} + \frac{\partial u_k^1}{\partial y_l} \right) v_i n_j dS - \int_{\Psi} \frac{\partial}{\partial y_j} \left[ E_{ijkl} \left( \frac{\partial u_k^0(x)}{\partial x_l} + \frac{\partial u_k^1}{\partial y_l} \right) \right] v_i dY \\ = \int_s p_i v_i dS \quad \forall \mathbf{v} \in \mathbf{V}_{\Psi} \end{aligned} \quad (\text{A28})$$

Therefore, we have:

$$\frac{\partial}{\partial y_j} \left( E_{ijkl} \frac{\partial u_k^1}{\partial y_l} \right) + \frac{\partial}{\partial y_j} \left( E_{ijkl} \frac{\partial u_k^0(x)}{\partial x_l} \right) = 0 \quad \text{on } \Psi, \quad (\text{A29})$$

$$E_{ijkl} \frac{\partial u_k^1}{\partial y_l} + E_{ijkl} \frac{\partial u_k^0(x)}{\partial x_l} n_j = p_i \quad \text{on } S \quad (\text{A30})$$

Now considering (A18) by choosing  $\mathbf{v} = \mathbf{v}(\mathbf{x})$ , we have

$$\int_{\Omega} \left[ \frac{1}{|Y|} \int_{\Psi} E_{ijkl} \left( \frac{\partial u_k^0}{\partial x_l} + \frac{\partial u_k^1}{\partial y_l} \right) dY \right] \frac{\partial v_i(\mathbf{x})}{\partial x_j} d\Omega$$

$$= \int_{\Omega} \left( \frac{1}{|Y|} \int_{\Psi} f_i dY \right) v_i(\mathbf{x}) d\Omega + \int_{\Gamma_i} t_i v_i(\mathbf{x}) d\Gamma \quad \forall \mathbf{v} \in \mathbf{V}_{\Omega}. \quad (\text{A31})$$

Now considering (A20) by choosing  $\mathbf{v} = \mathbf{v}(\mathbf{y})$  we have

$$\begin{aligned} & \int_{\Omega} \left[ \frac{1}{|Y|} \int_{\Psi} E_{ijkl} \left( \frac{\partial u_k^1}{\partial x_l} + \frac{\partial u_k^2}{\partial y_l} \right) \frac{\partial v_i(\mathbf{y})}{\partial y_j} dY \right] d\Omega \\ &= \int_{\Omega} \left( \frac{1}{|Y|} \int_{\Psi} f_i v_i(\mathbf{y}) dY \right) d\Omega \quad \forall \mathbf{v} \in \mathbf{V}_{\Psi} \end{aligned} \quad (\text{A32})$$

Eliminating  $\frac{1}{|Y|}$ , we can get the following formula:

$$\int_{\Psi} E_{ijkl} \left( \frac{\partial u_k^1}{\partial x_l} + \frac{\partial u_k^2}{\partial y_l} \right) \frac{\partial v_i(\mathbf{y})}{\partial y_j} dY = \int_{\Psi} f_i v_i(\mathbf{y}) dY \quad \forall \mathbf{v} \in \mathbf{V}_{\Psi} \quad (\text{A33})$$

*This implies equilibrium of the base cell in the microscopic level.*

Our aim is to construct the homogenized elastic constants, which reflect the mechanical behavior of the microstructure, in macroscopic coordinate systems and without explicitly using the parameter  $\zeta$ . Therefore, we consider using (A27) again.

Let  $(\chi_p)_{kl} \in V_{\Psi}$  is the solution of following equation (Hassani and Hinton, 1998, Bendsøe, 1995 and Bendsøe and Sigmund, 2002):

$$\int_{\Psi} E_{ijkl} \frac{\partial (\chi_p)_{kl}}{\partial y_q} \frac{\partial v_i(\mathbf{y})}{\partial y_j} dY = \int_{\Psi} E_{ijkl} \frac{\partial v_i(\mathbf{y})}{\partial y_j} dY \quad \forall \mathbf{v} \in \mathbf{V}_{\Psi} \quad (\text{A34})$$

and  $\beta_k \in V_{\Psi}$ , is a Y- periodic function being the solution of

$$\int_{\Psi} E_{ijkl} \frac{\partial \beta_k}{\partial y_l} \frac{\partial v_i(\mathbf{y})}{\partial y_j} dY = \int_{\Psi} p_i v_i(\mathbf{y}) dY \quad \forall \mathbf{v} \in \mathbf{V}_{\Psi} \quad (\text{A35})$$

The solution  $u^1$  will be

$$u_i^1 = \vartheta_i^k(\mathbf{x}) - \chi_i^{kl}(\mathbf{x}, \mathbf{y}) \frac{\partial u_k^0(\mathbf{x})}{\partial x_l} - \beta_i(\mathbf{x}, \mathbf{y}) \quad (\text{A36})$$

Where  $\vartheta_i^k$  are arbitrary constants of integration in  $y$ .

Now takes (A36) into (A31), we can get

$$\begin{aligned} \int_{\Omega} \left[ \frac{1}{|Y|} \int_{\Psi} \left( E_{ijkl} - E_{ijpq} \frac{\partial \chi_p^{kl}}{\partial y_q} \right) dY \right] \frac{\partial u_k^0(\mathbf{x})}{\partial x_l} \frac{\partial v_i(\mathbf{x})}{\partial x_j} d\Omega = \int_{\Omega} \left( \frac{1}{|Y|} \int_{\Psi} E_{ijkl} \frac{\partial \beta_k}{\partial y_l} dY \right) \frac{\partial v_i(\mathbf{x})}{\partial x_j} d\Omega \\ + \int_{\Omega} \left( \frac{1}{|Y|} \int_{\Psi} f_i dY \right) v_i(\mathbf{x}) d\Omega + \int_{\Gamma_i} t_i v_i(\mathbf{x}) d\Gamma \quad \forall \mathbf{v} \in \mathbf{V}_{\Psi} \end{aligned} \quad (\text{A37})$$

Now, if we define that

$$E_{ijkl}^H = \frac{1}{|Y|} \int_{\Psi} \left( E_{ijkl} - E_{ijpq} \frac{\partial (\chi_p)_{kl}}{\partial y_q} \right) dY \quad (\text{A38})$$

$$\bar{\sigma}_{ij}(\mathbf{x}) = \int_{\Psi} E_{ijkl} \frac{\partial \beta_k}{\partial y_l} dY \quad (\text{A39})$$

$$\bar{f}_i(\mathbf{x}) = \frac{1}{|Y|} \int_{\Psi} f_i dY \quad (\text{A40})$$

(A35) can be written as

$$\begin{aligned} \int_{\Omega} E_{ijkl}^H \frac{\partial u_k^0(\mathbf{x})}{\partial x_l} \frac{\partial v_i(\mathbf{x})}{\partial x_j} d\Omega = \int_{\Omega} \bar{\sigma}_{ij}(\mathbf{x}) \frac{\partial v_i(\mathbf{x})}{\partial x_j} d\Omega \\ + \int_{\Omega} \bar{f}_i(\mathbf{x}) v_i(\mathbf{x}) d\Omega + \int_{\Gamma_i} t_i v_i(\mathbf{x}) d\Gamma \quad \forall \mathbf{v} \in \mathbf{V}_{\Psi} \end{aligned} \quad (\text{A41})$$

It should be noted that the formula above is very similar to the equation of virtual displacement (A10).  $E_{ijkl}^H$  defined by (A38) is the homogenized elastic constant.  $\bar{\sigma}$  are average ‘residual’ stresses within the cell due to the tractions  $p$  inside the holes and  $\bar{f}$  are the average body forces.

The solution of the elastic composite material with a periodic structure problem by homogenization method can be summarized as:

- a. Solving the integral equations (A34) and (A35) in the base cell and get  $\chi$  and  $\Phi$  .
- b. Using (A38), (A39) and (A40) get  $E_{ijkl}^H$ ,  $\bar{\sigma}$  and  $\bar{f}$
- c. In macroscopic coordinates  $x$ , construct and solve the equation (A41).

## APPENDIX B

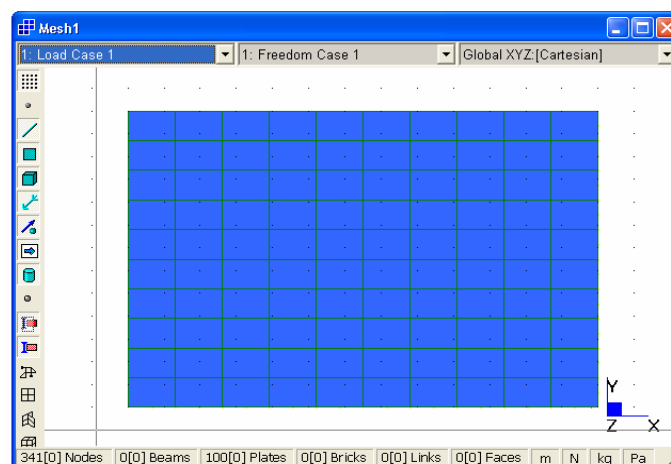
---

### *A typical run of the HDM software*

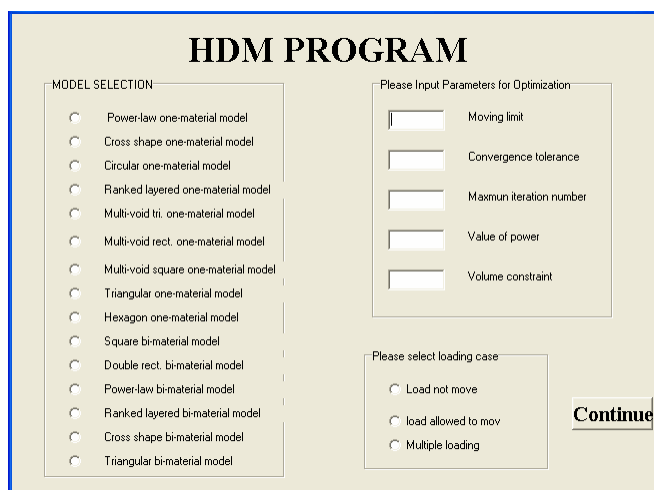
**Step 1:** Start HDM.bat batch file, the following picture will appear



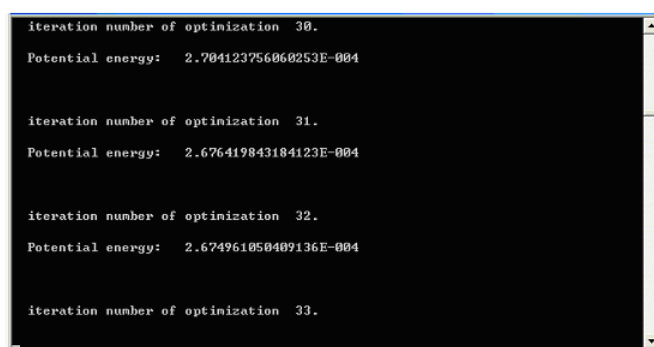
**Step 2:** On clicking **START** button the program will start Strand7 program. Discretize the reference domain and generate a finite element mesh, boundary conditions, loading case and material properties and save the output file as Data.txt. Then close Strand7 program.



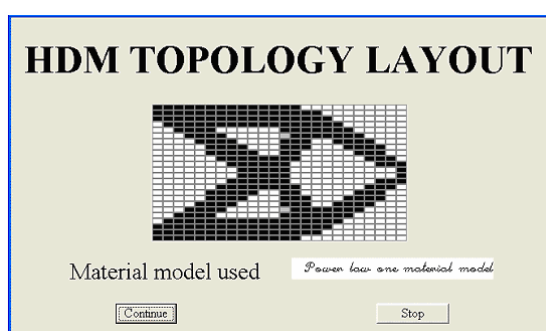
**Step 3:** The following picture will appear to let you choose material model and optimization parameters.



**Step 4:** Click **Continue** button, the computer will automatically start HDM.exe calculation procedure.



**Step 5:** When the calculation finished, the output image will appear, for example, the optimum solution for power-law one-material model as following:



**Step 6:** Click **Continue** button, the picture of step 3 will appear and let you choose material model and optimization parameters again. Click **Stop** button will stop the program.

## APPENDIX C

---

### *Optimality criteria for deep cantilever beam with a single load*

The deep cantilever beam with a single load and fixed constraint is shown in Figure C1. The optimization criterion for the minimum compliance (maximum stiffness) with upper side volume constraint for this problem has been derived by Hassani and Hinton (1998). Here we give a brief review as following:

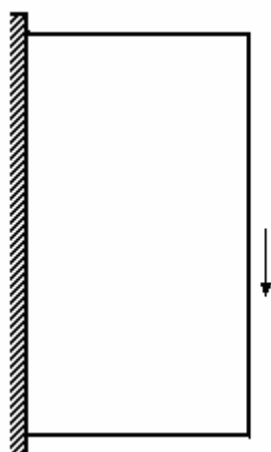


Figure C1 Deep cantilever beam

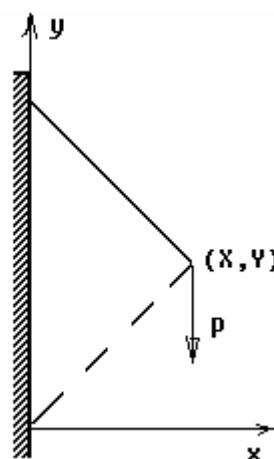


Figure C2 Truss structure

Firstly, a finite number of truss elements with lower side constraints for the cross sectional area of elements are considered. The optimization problem can be written as (Hassani and Hinton, 1998):

$$\begin{aligned}
 & \text{Minimize } \sum_{i=1}^n \frac{f_i^2 l_i}{a_i E_i} \\
 & \text{subject to } a_i^0 l_i^0 - a_i l_i \leq 0 \quad i = 1, 2, \dots, n \\
 & \sum_{i=1}^n a_i l_i - V \leq 0
 \end{aligned} \tag{C1}$$

where  $f_i$  is internal force in element  $i$ ,  $a_i$ ,  $l_i$  and  $E_i$  are cross section area, length and modulus of elasticity of member  $i$  of the truss,  $V$  is volume limitation and  $a_i^0$  is the lower bound of the cross section area.

The Lagrange function can be written as

$$L = \sum_{i=1}^n \frac{f_i^2 l_i}{a_i E_i} + \sum_{i=1}^n \lambda_i (a_i^0 l_i^0 - a_i l_i) + \lambda (\sum_{i=1}^n a_i l_i - V) \quad (C2)$$

where  $\lambda_i$  and  $\lambda$  are Lagrange multipliers.

Differentiating the Lagrange function of (C2) with respect to  $a_i$ , we have

$$-\frac{f_i^2 l_i}{a_i^2 E_i} - \lambda_i l_i + \lambda l_i = 0 \quad (C3)$$

From (C3), the cross section area  $a_i$  can be obtained as

$$a_i = \sqrt{\frac{f_i^2}{(\lambda - \lambda_i) E_i}} \quad (C4)$$

From Kuhn-Tucker conditions, we know that if  $a_i > a_i^0$ , the constraint

$a_i^0 l_i^0 - a_i l_i \leq 0$  not active, so  $\lambda_i = 0$ ; we have

$$a_i = \sqrt{\frac{f_i^2}{\lambda E_i}} \quad (C5)$$

if  $a_i > a_i^0$ , then  $\lambda_i \geq 0$ , we have

$$a_i \leq \sqrt{\frac{f_i^2}{\lambda E_i}} \quad (C6)$$

Using the definition of strain  $\varepsilon = \frac{f_i}{a_i E_i}$  and substituting into (C5) and (C6)

results in

$$\begin{aligned} \sqrt{\frac{E_i}{\lambda}} \varepsilon &= 1 & \text{for } a_i > a_i^0 \\ \sqrt{\frac{E_i}{\lambda}} \varepsilon &\leq 1 & \text{for } a_i = a_i^0 \end{aligned} \quad (C7)$$

By defining a criterion function  $\varphi$  as

$$\varphi = \sqrt{\frac{E_i}{\lambda}} \varepsilon \quad (C8)$$

Then (C7) can be reduced to

$$\begin{aligned} \varphi &= 1 & \text{for } a_i > a_i^0 \\ \varphi &\leq 1 & \text{for } a_i = a_i^0 \end{aligned} \quad (C9)$$

Secondly we extend the criteria by letting cross section  $a_i \rightarrow 0$ . In this case, we still have  $\lambda > 0$ , for if  $\lambda = 0$ , the truss will have infinite rigidity. So (C9) can be written as

$$\begin{aligned} \varphi &= 1 & \text{for } a_i > 0 \\ \varphi &\leq 1 & \text{for } a_i = 0 \end{aligned} \quad (C10)$$

Now, we can extend the result to the structure of the deep cantilever beam which can be thought as an infinite number of elements, i.e. to a continuum comprising infinite number of truss-like elements in all potential direction. In these cases, at each point  $(x, y)$  of the domain of interest a potential truss member passing through that point, can be represented by the coordinates of the point and orientation  $\theta$  of the member, the strain in each element can be written as  $\varepsilon(x, y, \theta)$ . The (C10) can be changed to

$$\begin{aligned} \varphi(x, y, \theta) &= 1 & \text{for } a(x, y, \theta) > 0 \\ \varphi(x, y, \theta) &\leq 1 & \text{for } a(x, y, \theta) = 0 \end{aligned} \quad (C11)$$

According to the Hassani and Hinton (1998), at each point  $(x, y)$  there exists an optimal passing member in the direction  $\theta^*$  only if

$$|\varepsilon(x, y, \theta^*)| = \max_{\theta} |\varepsilon(x, y, \theta)| \quad (C12)$$

where  $\theta^*$  is a specific value of  $\theta$ .

From (C10), the optimality criteria function is proposed to be the strain and choosing  $\lambda = E_i$ , we can conclude that the condition for optimal member is the principal strain

$$|\varepsilon_1| = 1 \quad (C13)$$

Now we consider the problem of Figure C2, the boundary conditions are

$$u(0, y) = v(0, y) = 0 \quad (C14)$$

Where  $u$  and  $v$  are displacement in  $x$  and  $y$  direction.

The optimal layout can be defined as a set of points which belong to the half plane (all  $(x, y)$ , which  $x > 0$ ) that satisfy (C14) and optimality criteria (C13).

Therefore the displacement field should be (Rozvary *et al*, 1995):

$$u(x, y) = 0 \quad \text{and} \quad v(x, y) = 2x \quad (C15)$$

Apply to the condition of (C14), we have:

$$\varepsilon_x = 0, \quad \varepsilon_y = 0, \quad \varepsilon_{xy} = 2 \quad (C16)$$

where  $\varepsilon_x$ ,  $\varepsilon_y$  and  $\varepsilon_{xy}$  are strain in  $x$ ,  $y$  direction and share strain

Results in

$$\varepsilon_1 = 1, \quad \varepsilon_2 = -1, \quad \text{and} \quad \alpha = 45^\circ \quad (C17)$$

where the  $\varepsilon_1$ ,  $\varepsilon_2$ , and  $\alpha$  are principal strain, orthogonal strain to the direction of the major principal strain and the direction of principal strain.

This result indicates that the optimal bar must run at  $\pm 45^\circ$  to the vertical. By removing the potential members with zero force, the optimum result should be a two bar truss feature running at  $\pm 45^\circ$  to the vertical. Figure C2 shows the optimal layout.

## **REFERENCES**

---

- Aboudi, J., Pindera, M. and Arnold, S. (2001), Linear thermo elastic high-order theory for multiphase materials, *Journal of Applied Mechanics*, Vol.68, pp. 697-707.
- Allare, G. and Aubry, S. (1999), On optimal microstructures for a plane shape optimization problem, *Structural Optimization*, Vol.17, pp. 86-94.
- Arora, J.S. (1993), Sequential linearization and quadratic programming techniques. in: Kamat M. (Ed.), *Structural Optimization: Status and Promise*, AIAA, Washington DC, USA, pp. 71-102.
- Auster, P. (1988), *The invention of solitude*. London: Faber and Faber Ltd.
- Babuska, I. (1976 a), Solution of interface problems by homogenization I, *Journal of Mathematical Analysis*, Vol. 7, pp. 603-634.
- Babuska, I. (1976 b), Solution of interface problems by homogenization II, *Journal of Mathematical Analysis*, Vol. 7, pp. 635-645.
- Babuska, I. (1977), Solution of interface problems by homogenization III, *Journal of Mathematical Analysis*, Vol. 8, pp. 923-937.
- Banichuk, N. V. (1992), Optimal design of anisotropic structural element, *Proceedings of IUTAM Symposium on Optimal Design with Advanced Materials, 18-20 August, 1992, Lyngby, Denmark*.
- Beckers, M. (1999), Topology optimization using a dual method with discrete

- variables, *Structural Optimization* 17, pp. 14-24.
- Bendsøe, M.P. (1986), Generalized plate models and optimal design, in *Homogenization and effect moduli of materials and media, The IMA Volumes in Mathematics and Its Applications*, Editor: J.L. Eriksen, D. Kinderlehrer, R. Kohn and J.-L. Lions, Springer, Berlin, pp. 1-26.
- Bendsøe, M.P. (1995), *Optimization of structural topology, shape, and material*, Springer-Verlag, Berlin.
- Bendsøe, M.P. and Kikuchi, N. (1988), Generating optimal topologies in structural design using a homogenization method, *Computer Methods in Applied Mechanics and Engineering*, Vol. 71, pp. 197-224.
- Bendsøe, M.P. and Sigmund, O. (2002), *Topology Optimization*, Springer, Berlin.
- Bendsøe, M.P. and Kikuchi, N. (1989), Optimal shape design as a material distribution problem, *Structural Optimization*, Vol. 1, pp. 193-202.
- Bendsøe, M.P. and Diaz, A.R. (1998), A method for treating damage related criteria in optimal topology design of continuum structures, *Structural Optimization*, Vol. 16, pp. 108-115.
- Bennett, J.A. and Botkin, M.E. (Eds.) (1986), *The Optimum Shape, Automated Structural Design*, Plenum, New York.
- Buhl, T., Pedersen, C.B.W. and Sigmund, O. (2000), Stiffness design of geometrically nonlinear structures using topology optimization, *Struct Multidisc Optim.* Vol.19, pp. 93-104.

- Bulman, S., Sienz, J. and Hinton, E., (2001), Comparisons between algorithms for structural topology optimization using a series of benchmark studies, *Computers & Structures*, Vol. 79, pp. 1209-1218.
- Chan, C.M., Sherbourne, A.N. and Grierson, D.E. (1994), Stiffness optimization technique for 3D tall steel building frameworks under multiple lateral loadings, *Engineering Structures*, Vol. 16 (8), pp. 570-576.
- Chen, K.T. and Olhoff, N. (1981), An investigation concerning optimal design of solid elastic plate, *International Journal of Solids and Structures* 16 (3), pp. 305-323.
- Chu, D.N. (1997), *Evolutionary Structural Optimization Method for Systems with Stiffness and Displacement Constraints*. PhD thesis, Dept. of Civil and Building Engineering, Victoria University of Technology, Melbourne, Australia.
- Cioranescu, D. and Paulin, J.S.J. (1979), Homogenization in open sets with holes, *Journal of Math. Analysis and Appl.*, Vol. 71, pp. 590-607.
- Coupez, T., Digonnet, H. and Ducloux, R. (2000), Parallel meshing and remeshing, *Applied Mathematical Modelling*, Vol. 25, pp. 153-175.
- Diaz, A and Lipton, R (1997), Optimal material layout for 3D elastic structures, *Structural Optimization*, Vol. 13, pp. 60-64.
- Diaz, A.R. and Bendsoe, M.P. (1992), Shape Optimization of structures for multiple loading conditions using a homogenization method, *Structural Optimization*, Vol. 4, pp. 17-22.
- Ding, Y. (1986), Shape Optimization of structures: a literature review.

- Computers and Structures*, Vol. 24, pp. 985-1004.
- Dobbs, M.W.; Felton, L.P. (1969), Optimization of truss geometry, *J. Struct. Div.*, ASCE 100 (ST1), pp. 2105-1118
- Dorn, W.C.; Gomory, R.E.; Greenberg, H.J. (1964), Automatic design of optimal structures, *J. de Mecanique* Vol. 3, pp. 25-52
- Duana, B. Y., Templemanb, A. B. and Chena, J.J. (2000), Entropy-based method for topological optimization of truss structures, *Computers & Structures*, Vol. 75, pp. 539-550.
- Fernandes, P. Guedes, J.M. and Rodrigues, H. (1999), Topology optimization of three-dimensional linear elastic structures with a constraint on ‘perimeter’, *Computers and Structures*, Vol. 73, pp. 583-594.
- Fiacco, A.V. and McCormick, G.P. (1968), *Nonlinear Programming: Sequential Unconstrained Minimization Techniques*, Wiley, New York.
- Fleury, C. (1979), Structural weight Optimization by dual methods for convex programming, *International Journal for Numerical Methods in Engineering*, Vol. 14, pp. 1761-1783.
- Folgado, J., Rodrigues, H. and Guedes, J.M. (1995), Layout design of plate reinforcements with a buckling load criterion, *WCSSMO-I Proceedings of the First World Congress of Structural and Multidisciplinary Optimization*, 28 May - 2 June 1995, Goslar, Germany.
- Fuchs, M.B., Paley, M., Miroshnik, E. (1999), The Aboudi micro-mechanical model for shape design of structures, *Computer and Structures*, Vol. 73, pp. 355-362

- Fuch, M.B and Moses, E (2000), Optimal structural topologies with transmissible loads, *Struct Multidisc Optim.* Vol.19, pp. 263-273.
- Gellatly, R.A. and Berke, L. (1971), Optimal Structural Design, *USAF AFFDL-TR-70-165*.
- Gibiansky1, L. V. and Sigmund, O. (2000), Multiphase composites with extremal bulk modulus, *Journal of the Mechanics and Physics of Solids*, Vol. 48, pp. 468-491.
- Grandhi, R.V., Bharatram, G. and Venkayya, V.B. (1992), Optimum design of plate structures with multiple frequency constraint, *Mechanics of Solids*, Vol. 12(1), pp. 29-136.
- Haftka, R.T. and Grandhi, R.V. (1986), Structural optimization-a survey, *Computer Methods in Applied Mechanics and Engineering*, Vol. 57, pp. 91-106.
- Haftka, R.T., Gurdal, Z. and Kamat, M.P. (1992), *Elements of Structural Optimization*, 3rd revised edition, Kluwer Academic Publishers, Dordrecht.
- Hassani, B. and Hinton, E. (1998), *Homogenization and Structural Topology Optimization*, Springer-Verlag, Berlin.
- Haug, E. J. and Arora, J. S. (1979), *Applied optimal design*, John wiley and Sons, New York.
- Heyman, J. (1951), Plastic design of beams and frames for minimum material consumption, *Quarterly of Applied Mathematics*, Vol. 8, pp. 373-381.

- Hinton, E., Bulman, S. Sienz, J. and Ghasemi, M.R. (1998), Fully intergrated design optimization, *Proceedings of Australasian Conference on Structural Optimization, February 11-13, 1998, Sydney, Australia*, pp. 3-30.
- Holland, J.H. (1975), *Adaptation in natural and artificial systems*, University of Michigan Press, Ann Arbor, USA.
- Hornung, U. (1997), *Homogenization and Porous Media*, Springer, New York.
- Jacobsen, J. B., Olhoff, N. and Rønholt, E. (1998), Generalized shape optimization of three-dimensional structures using materials with optimum microstructures, *Mechanics of Materials*, Vol. 98, pp. 207-225.
- Jakiela, M. J., Chapman, C., Duda, J., Adewuya, A. and Saitou, K. (2000), Continuum structural topology design with genetic algorithms, *Computer Methods in Applied Mechanics and Engineering*, Vol. 186, pp. 339-356.
- Jog, C. S., Haber, R.B. and Bendsøe, M.P. (1992), Topology design using a material with self-optimizing microstructure, *Proceedings of IUTAM Symposium on Optimal Design with Advanced Materials, 18-20 August, 1992, Lyngby, Denmark*.
- Kalamkarov, A. L. and Kolpakov, A. G. (1997), *Analysis, Design and Optimization of Composite Structures*, John Wiley & Sons, England.
- Khan, M.R. and Willmert, K.D. (1981), An efficient optimality criterion

- method for natural frequency constrained structures, *Computers and Structures*, Vol. 14, pp. 501-507.
- Kim, H., Querin, O.M., Steven, G.P. and Xie, Y.M. (1998), Development of an intelligent cavity creation (ICC) algorithm for evolutionary structural structures, *Computer Methods in Applied Mechanics and Engineering*, Vol. 121, pp. 259-280.
- Kirsch, U. (1989), Optimal topologies of Structures. *Appl. Mech. Rev.* Vol. 42, pp. 223-239.
- Kirsch, U. (1993), *Structural optimization*, Springer, Berlin.
- Krog, L. A. and Olhoff, N. (1999), Optimum topology and reinforcement design of disk and plate structures with multiple stiffness and eigen frequency objectives, *Computers & Structures*, Vol.72, pp. 535-563.
- Lin, C. Y. and Chou, J. N. (1999), A two-stage approach for structural topology optimization, *Advances in Engineering Software* , Volume 30, pp. 261-271.
- Lurie, K.A., Fedorov, A.V. and Cherkaev, A.V. (1982 a), Regularization of optimal design problems for bars and plates, Parts I, *J. Optim. Theory Appl.* 37(4), pp. 499-521.
- Lurie, K.A., Fedorov, A.V. and Cherkaev, A.V. (1982 b), Regularization of optimal design problems for bars and plates, Parts II, *J. Optim. Theory Appl.* 37(4), pp. 523-543.
- Ma, Z.D., Kikuchi, N. and Cheng, H. C. (1995), Topology design for vibrating structures, *Computer Methods in Applied Mechanics and*

- Engineering*, Vol. 121, pp. 259-280.
- Manevitch, L. I., Andrianov, I. V. and Oshmyan, V. G., (2002), *Mechanics of Periodically Heterogeneous Structures*, Springer-Verlag, Great Britain.
- Manickarajah, D., Xie, Y.M., Steven, G.P. (1998), An evolutionary method for Optimization of plate buckling resistance, *Finite Elements in Analysis and Design*, Vol. 29, pp. 205-230.
- Mattheck, C. (1997), *Design in Nature: Learning from Trees*, Springer-Verlag, Berlin.
- Maxwell, C. (1895), *Scientific Papers II.*, Cambridge University Press, pp. 175.
- Michell, A.G.M. (1904), The limit of economy of material in frame-structures, *Phil. Mag.*, Vol. 8, pp. 589-597.
- Milton, G.W. (1986), Modelling the properties of composites by laminates, in *Homogenization and Effective Moduli of Materials and Media*, Editor: J. L. Ericksen, Springer-Verlag, New York, pp. 151-174.
- Min, S., Nishiwaki, S. and Kikuchi, N. (2000), Unified topology design of static and vibrating structures using multiobjective optimization, *Computers and Structures* 75, pp. 93-116.
- Misra, A. (1993), A homogenization method for effective moduli of randomly packed grains, ASME, 1993, AMD-Vol. 166, pp63-74.
- Morris, A.J. (Ed.) (1982), *Foundation of Structural Optimization: A Unified Approach*, John Wiley & Sons, New York.
- Nagendra, S., Haftka, R.T. and Giirdal, Z. (1993). Design of blade stiffened

- composite panels by a genetic algorithm approach, *Proceedings of the 34th AIAA/ASME/AHS SDM Conference*, La Jolla, USA, pp. 2418-2436.
- Neves, M.M., Rodrigues, H and Guedes, J.M. (2000), Optimum design of periodic linear elastic microstructures, *Computers and Structures* 76, pp. 421-429.
- Olhoff, N., Bendsoe, M.P., Rasmussen, J. (1991), On CAD-integrated structural topology and design optimization, *Comp. Meth. Appl. Mech. Engrg.* 89, pp. 259-279
- Olhoff, N., Jacobson, J.B., Ronholt, E. (1997), Three-dimensional structural topology and layout optimization based on optimum microstructures, *WCSSMO-2 Second World Congress of Structural and Multidisciplinary Optimization, Extended Abstracts (held in Zakopane)*, pp. 198-199.
- Olhoff, N., Ronholt, E. and Scheel, J. (1998), Topology optimization of plate-like structures using 3-D elasticity and optimum 3-D microstructures, *Structural Optimization*, Vol. 16, pp. 1-18.
- Pedersen, P. (1995), Material optimizations – an engineering view, in *Advances in Structural Optimization*, Editor: J. Herskovits, Kluwer Academic Publishers, Netherlands, pp. 223-261.
- Pedersen, P. (1993), Optimal orientation of anisotropic material, Optimal distribution of anisotropic material, Optimal shape design with anisotropic material, Optimal design for a class of non-linear elasticity, in *Optimization of Large Structural Systems*, Editor: G.I.N. Rozvany, Kluwer Academic Publishers, Netherlands, pp. 649-682.

- Pedersen, P. and Taylor, J. E. (1992), Optimal design based on power-law non-linear elasticity, *Proceedings of IUTAM Symposium on Optimal Design with Advanced Materials, 18-20 August, 1992, Lyngby, Denmark.*
- Prager, W. and Shield, R.T. (1968), Optimal design of multi-purpose structures, *Int. J. Solids and Structures*, Vol. 4, pp. 469-475.
- Prager, W. and Taylor J.E. (1968), Problems of optimal structural design, *Journal of Applied Mechanics*, Vol. 35, pp. 102-106.
- Prager, W. and Rozvany, G.I.N. (1977), Optimization of structural geometry, In *Dynamic Systems*, Editor: A.R. Bednarek, and L. Cesari, Academic Press, New York, pp. 265-293.
- Querin, O.M., Steven G.P. and Xie Y.M. (1996), Topology optimization of structures with material and geometric nonlinearities, *5th AIAA/USAF/NASA/ISSMO Symposium on Multidisciplinary Analysis and Optimization*, Bellevue Washington, USA, pp. 1812-1818.
- Rasmussen, J. (1990), The structural Optimization system CAOS, *Structural Optimization*, Vol. 2(2), pp. 109-115.
- Ringerts, U.T. (1988), On methods for discrete structural optimization, *Engineering Optimization*, Vol. 13, pp. 47-64.
- Rizzi, D. (1976), Optimization of multi-constrained structures based on optimality criteria. *Proceedings of AIAA/ASME/SAE 17th Structures, Structural Dynamics and Materials Conference*, King of Prussia, USA, pp. 448-462.

- Rong, J.H., Xie, Y.M., Yang, X.Y. and Liang, Q.Q., (2001), Topology optimization of structures under dynamic response constraints, *Sound & Vibration*, 23(4), pp. 177-189.
- Rosen, J.B. (1961), The gradient projection method for nonlinear programming, *Journal of the Society for Industrial and Applied Mathematics*, Vol. 8, pp. 181-217.
- Rozvany, G.I.N., Ong, T.G., Szeto, W.T., Olhoff, N. and Bendsøe, M.P. (1987 a), Least-weight design of perforated plates I, *Internal. J. Solids and Structures* Vol. 23, pp. 521-536.
- Rozvany, G.I.N., Ong, T.G., Szeto, W.T., Olhoff, N. and Bendsøe, M.P. (1987 b), Least-weight design of perforated plates II. *Internal. J. Solids and Structures* Vol. 23, pp. 537-550.
- Rozvany, G.I.N. (1995), What is meaningful in topology design? An engineer's viewpoint, *Advances in Structural Optimization*, edited by J. Herskovits, Kluwer Academic Publishers, Netherlands, pp. 149-188.
- Rozvany, G.I.N. (1998), Topology optimization of multipurpose structures, *Proceedings of Australasian Conference on Structural Optimization, February 11-13, 1998, Sydney, Australia*, pp. 31-41.
- Rozvany, G.I.N. (2001), Aim, scope, method, history and unified terminology of computer-aided topology optimization in structural mechanics, *Struct Multidisc Optim.*, Vol. 21, pp. 90-108.
- Rozvany, G.I.N., Sigmund, O. and Birker, T. (1992), Optimal design of

- composite and fibre-reinforced plate, *Proceedings of IUTAM Symposium on Optimal Design with Advanced Materials, 18-20 August, 1992, Lyngby, Denmark.*
- Rozvany, G.I.N. (1989), *Structural Design via Optimality Criteria*, Kluwer, Dordrecht.
- Rozvany, G.I.N. (1993), Layout theory for grid-type structures, in *Topology Design of Structures*, Editor: M.P. Bendsoe, and C.A. Mota Soares, Kluwer, Dordrecht, pp. 251-271.
- Rozvany, G.I.N., Bendsoe, M.P. and Kirsch, U. (1995), Layout optimization of structures, *Appl. Mech. Rev.* 48, pp. 41-119
- Rozvany, G.I.N. (1998), Exact analytical solutions for some popular benchmark problems in topology optimization, *Structural Optimization*, Vol. 15, pp. 42-48.
- Sandgren, E. (1990), Nonlinear integer and discrete programming in mechanical design optimization, *Journal of Mechanical Design, ASME*, Vol. 112, pp. 223-229.
- Schmit, L.A. (1960), Structural design by systematic synthesis, *Proceedings of the 2nd conference on Electronic Computation*, ASME, New York, pp. 105-122.
- Sheng, P. (1986), Macrostructures and physical properties of composites, in *Homogenization and Effective Moduli of Materials and Media*, Editor: J.L. Ericksen, Springer-Verlag, New York, pp. 196-213.
- Sigmund, O. (1994), Materials with prescribed constitutive parameters: An

- inverse homogenization problem, *Int. J. Solids Struct.*, 31, pp. 2313-2329.
- Sigmund, O. (2000), A new class of extremal composites, *Journal of the Mechanics and Solids*, 48, pp. 397-428.
- Sigmund, O. and Petersson, J. (1998), Numerical instabilities in topology optimization: A survey on procedures dealing with checkerboards, mesh-dependencies and local minima, *Structural Optimization*, Vol. 16, pp. 68-75.
- Sigmund, O. (2001 a), Systematic design of mechanical systems using topology optimization, *Engineering Design Optimization Proceeding of the 2<sup>nd</sup> ASMO UK/ISSMO Conference*, 10-11 July 2000, Swansea, UK.
- Sigmund, O. (2001 b), A 99 line topology optimization code written in Matlab, *Struct Multidisc Optim.* Vol. 21, pp. 120-127.
- Sigmund, O. (2001 c), Design of multi-physics actuators using topology optimization-Part II : Two-material structures, *Comput. Methods Appl. Mech. Engrg.* 190, pp. 6605-6627.
- Soto, C. A. and Diaz, A. R. (1992), A model for layout optimization of okate structures, *Proceedings of IUTAM Symposium on Optimal Design with Advanced Materials, 18-20 August, 1992, Lyngby, Denmark.*
- Suzuki K. and Kikuchi N. (1991), A homogenization method for shape and topology optimization, *Comp. Meth. Appl. Mech. Eng.*, 93, pp. 291-318
- Suzuki, K. and Kikuchi, N. (1993), Layout optimization using the homogenization method, in *Optimization of Large Structural Systems*, Editor: G.I.N Rozvany, Kluwer Academic Publishers, Netherlands, pp.

157-175.

Strand7 Program, *G+D Computing Pty. Ltd.* Australia.

Tartar, L. (1986), Remark on Homogenization, in *Homogenization and Effective Moduli of Materials and Media*, Editor: J.L. Ericksen, Springer-Verlag, New York, pp. 228-246.

Taylor J.E. (1977), Optimal truss design based on an algorithm using optimality criteria, *Int. J. Solids Struct.* Vol.13, pp. 913-923

Tenek, L. H. and Hagiwara, I. (1993), Static and vibrational shape and topology optimization using homogenization and mathematical programming, *Computer Methods in Applied Mechanics and Engineering*, Vol. 109, pp.143-154.

Thomsen, J. (1992), Topology optimization of structures composed of one or two materials, *Structural Optimization*, Vol. 5, pp. 108-115.

Topping, B.H.V. (1993). Topology design of discrete structures. In *Topology Design of Structures*, Editor: M.P. Bendsøe, and C.A. Mota Soares, Kluwer Academic Publishers, Netherlands.

Tortorelli, D.A., Tiller, M. M. and Dantzig, J. A. (1992), Optimal design of advanced materials, *Proceedings of IUTAM Symposium on Optimal Design with Advanced Materials, 18-20 August, 1992, Lyngby, Denmark.*

Yang, X.Y. (1999), *Bi-directional Evolutionary Method for Stiffness and Displacement Optimization*. Master thesis, Dept. of Civil and Building Engineering, Victoria University of Technology, Melbourne, Australia.

- Youn, S. K. and Park, S. H. (1997), A study on the shape extraction process in the structural topology optimization using homogenized material, *Computers and Structures*, Vol 62, pp. 527-538.
- Venkayya, V.B., Khot, N.S. and Reddy, V.S (1968), Optimization of structures based on the study of strain energy distribution, *AFFDL-TR-68-150*.
- Xie, Y.M. and Steven, G.P. (1993), A simple evolutionary procedure for structural Optimization, *Computers and Structures*, Vol. 49, pp. 885-896.
- Xie, Y.M. and Steven, G.P. (1994), Optimal design of multiple load case structures using an evolutionary procedure, *Engineering Computations*, Vol. 11, pp. 295-302.
- Xie, Y.M. and Steven, G.P. (1997), *Evolutionary Structural Optimization*, Springer-Verlag, Berlin.
- Yang, R.J. and Chahande, A.I. (1995), Automotive applications of topology optimization , *Structural Optimization*, Vol. 9, pp. 245-249.
- Yang, R.J. and Chuang, C.H. (1994), Optimal topology design using linear programming, *Computers and Structures*, Vol. 52, pp. 265-275.
- Yi, Y.M., Park, S. H. and Youn, S. K. (2000), Design of microstructures of viscoelastic composites for optimal damping characteristics, *International Journal of Solids and Structures*, Vol.37, pp. 4791-4810.
- Young, V., Querin, O.M., Steven, G.P. and Xie, Y.M. (1998), 3D bi-directional evolutionary structural optimization, *Proceedings of the Australasian Conference on Structural Optimization, Sydney, Australia*, pp.

275-282.

Zacharopoulos, A., Willmert, K.D. and Khan, M.R. (1984), An optimality criterion method for structures with stress, displacement and frequency constraints. *Computers and Structures*, Vol. 19, pp. 621-629.

Zhou, M.; Rozvany, G.I.N. (1991), The COG algorithm, Part II: Topological, geometrical and general shape optimization, *Comp. Meth. Appl. Mech. Eng.* Vol. 89, pp. 309-336.

Zienkiewicz, O.C. (1977), *The Finite Element Method*, McGraw-Hill, London.

Zoutendijk, G. (1960), *Methods for Feasible Direction*, Elsevier, Amsterdam.